A Methodology for Spreading Codes Radio-Frequency Compatibility Assessment

Dipl.-Ing. Diana Fontanella

Vollständiger Abdruck der von der Fakultät für Luft- und Raumfahrt der Universität der Bundeswehr München zur Erlangung des akademischen Grades eines

Doktor Ingenieurs (Dr.-Ing.)

genehmigten Dissertation.

Gutachter:

1. Prof. (i. R.) Dr.-Ing. Bernd Eissfeller

2. Prof. Dr. Fabio Dovis

Die Dissertation wurde am 15.02.2019 bei der Universität der Bundeswehr München eingereicht und durch die Fakultät für Luft- und Raumfahrt am 04.09.2020 angenommen. Die mündlichen Prüfung fand am 15.10.2020 statt.

Kurzfassung

Diese Arbeit gibt einen vollständigen Überblick über Pseudo-Random Noise (PRN)-Codes und deren für den Einsatz in der Satellitennavigation relevante Eigenschaften.

Zunächst wird ein theoretischer Rahmen für das Verständnis der Rolle von Spreizcodes als Bestandteil von Navigationssignalen geschaffen. Es werden verallgemeinerte Ausdrücke zur Beschreibung heutiger Navigationssignale abgeleitet und der Einfluss von PRN-Codes auf die Spektren dieser Signale erklärt. Das Konzept von kurzen und langen Codes wird eingeführt, um zwischen Signalen zu unterscheiden, die mit einem Linienspektrum modelliert werden müssen beziehungsweise mit einem kontinuierlichen Spektrum modelliert werden können.

Ausgehend von der mathematischen Darstellung von Navigationssignalen werden Ausdrücke für die Auto- und Kreuzkorrelation zwischen Spreizcodes als Grundlage für das Verständnis von Leistungskennzahlen von PRN-Codes wie dem Korrelationshistogramm und den Korrelationsperzentilen abgeleitet. Die vorgenannten Ausdrücke werden dann erweitert und verallgemeinert, um Sekundärcodes, Unterträgerkomponenten, Chipform und Integrationszeit berücksichtigen zu können. Sensitivitätsanalysen basierend auf den eingeführten Kennzahlen werden in Bezug auf die wesentlichen Designparameter der Signale, den Dopplerfrequenz-Offsets zwischen den Signalen verschiedener Satelliten und die Empfänger-Integrationszeit durchgeführt. Ergebnisse und Schlussfolgerungen hinsichtlich der Eigenschaften von PRN-Codes werden skizziert.

Als Hauptbeitrag wird eine neue Hochfrequenzkompatibilitäts-Methodik zur Bewertung der Selbst- und Kreuzinterferenz von Spreizcodes vorgeschlagen. Ziel ist es, die ITU-Empfehlung ITU-R M.1831 zu ergänzen, die ausschließlich auf der Abschätzung der aggregierten Störleistungspegel basiert. Die neue Methodik gilt grundsätzlich für Navigationssysteme, die auf der Code Division Multiple Access (CDMA)-Technologie basieren und sich das gleiche Funkfrequenzband teilen. Die auf PRN-Codes basierende RFC-Analyse ist allgemeingültig, ihre Relevanz ist jedoch vor allem für Signale mit kurzen PRN-Codes von Bedeutung. Die beschriebenen Bewertungskriterien liefern ein Maß für die CDMA-Isolationseigenschaften von PRN-Codesätzen.

Umfangreiche Simulationsergebnisse belegen die Gültigkeit der vorgeschlagenen Methodik. Die Analysen zu spezifischen PRN-Codesätzen zeigen relevante Aspekte in Bezug auf die Kompatibilität von PRN-Codes und damit auf die gegenseitige Beeinflussung von Satellitensignalen auf.

A Methodology for Spreading Codes Radio-Frequency Compatibility Assessment

Diana Fontanella

A Thesis submitted to the Faculty of Aerospace Engineering of Universität der Bundeswehr München in fulfilment of the requirements for the degree of

Doctor of Engineering (Dr.-Ing.).

Reviewer:

1. Prof. (i. R.) Dr.-Ing. Bernd Eissfeller
2. Prof. Dr. Fabio Dovis

The Thesis was submitted on 15.02.2019 to the Universität der Bundeswehr München and accepted by the Faculty of Aerospace Engineering on the 04.09.2020. The oral examination took place on the 15.10.2020.

Abstract

This thesis provides a complete overview on Pseudo-Random Noise (PRN) codes and their performance figures in the context of satellite navigation.

First, a theoretical framework for understanding the role of spreading codes into navigation signals' structure is provided. Generalised expressions to describe nowadays navigation signals are derived and the impact of PRN codes onto the signals' spectral content is explained. The concept of short codes and long codes is introduced to distinguish between signals that can be modelled respectively with the line spectrum and continuous spectrum approach.

Starting from the mathematical representation of navigation signals, expressions for the auto- and cross-correlation between spreading codes are given as a basis to understand PRN codes performance figures such as the correlation histogram and correlation percentiles. The aforementioned expressions are then extended and generalised to take into account for secondary codes, sub-carrier components, chip shape, and integration time. Sensitivity analyses based on the introduced figures of merit are carried out with respect to the main signals' design parameters, Doppler frequency offset, and receiver integration time. Results and conclusions on the behaviour of PRN codes are outlined.

As main contribution, a new radio-frequency compatibility methodology for the assessment of spreading codes self- and cross-interference is proposed. The objective is to complement the ITU Recommendation ITU-R M.1831 which is based solely on the estimation of aggregate interference power levels. The new methodology strictly applies to navigation systems based on Code Division Multiple Access (CDMA) technology that share the same radio-frequency band. The validity of the PRN codes based RFC analysis is general, however its relevance is mostly significant for short-code signals. The assessment criteria described provide a measure of the CDMA isolation properties of PRN code sets in the service volume.

Extensive simulation results prove the validity of the proposed methodology. The analyses on specific PRN code sets allow observing relevant aspects related to the PRN codes compatibility.

Acknowledgments

When I started working at the Institute of Space Technology and Space Applications back in 2010 the last thing I wanted to do was a PhD. I have always had passion for technical matters and a scientific research position was right for me, but I was tired of learning theory: all I wanted to do was to start the 'real' work.

During the time at Universität der Bundeswehr I had the opportunity to work on very interesting projects and to grow technical experience on satellite navigation systems. But I also learned to cherish the challenges of scientific research, the academic environment, the world of conferences and publications. When I left the Institute in 2014 I felt like losing the chance to acquire a formal recognition for all the scientific work performed and I committed myself to completing this PhD.

I would like to express my deep and sincere gratitude to my supervisor, Professor Bernd Eissfeller, who first gave me the great occasion to work for the Institute and later the chance to pursue my personal goal of earning a doctorate degree despite my time at the university was over.

Warm thanks also to my ex-colleagues and friends Matteo Paonni, Roland Bauernfeind, and Elias Gkougkas for the amazing time spent together at the Institute. In particular I would like to express my gratitude to Matteo for his support as a mentor and for the countless technical discussions from which I have so much profited.

On a more personal note, I am very grateful to Giorgio, for all the Sundays and bank holidays he spent on my side while I was writing this PhD thesis. The achievement of this goal has been possible also thanks to his patience and support.

Finally, my most gratitude goes to my mother, who has taught me the value of academic education – beyond an enabler for professional success – and the importance of perseverance in achieving personal goals. I am thankful for all her support, love and understanding.

Table of Contents

List of Tables

List of Figures

List of Acronyms

ACF	Auto-Correlation Function
ADC	Analog-to-Digital Conversion
AGC	Automatic Gain Control
AltBOC	Alternative Binary Offset Carrier
AM	Amplitude Modulation
ARNS	Aeronautical Radio-Navigation Service
ATV	Amateur Television
BB	Base-Band
BPSK	Binary Phase Shift Keying
BOC	Binary Offset Carrier
C/N_0	Carrier-to-Noise Density Ratio
CAF	Cross-Ambiguity Function
CCF	Cross-Correlation Function
CBOC	Composite Binary Offset Carrier
CD	Code Delay
CDMA	Code Division Multiple Access
CI	Cross-Interference
CIT	Coherent Integration Time
CMCU	Clock Management and Control Unit
CP	Correlation Percentile
CS	Commercial Service
DAC	Digital-to-Analog Conversion
DFT	Discrete Fourier Transform
DGD	Differential Group Delay
DLL	Delay Lock Loop
DFMC	Dual-Frequency Multi-Constellation
DSP	Digital Signal Processing
DSSS	Direct-Sequence Spread Spectrum
ECEF	Earth-Centred, Earth-Fixed

EIRP	Effective Isotropically Radiated Power
EL	Early-Late
EWF	Evil Wave-Form
EU	European Union
FFT	Fast Fourier Transform
FGMU	Frequency Generation and Modulation Unit
FIR	Finite Impulse Response
FM	Frequency Modulation
FT	Fourier Transform
GD	Group Delay
GEO	Geostationary Equatorial Orbit
GNSS	Global Navigation Satellite System
GSO	Geosynchronous Orbit
ICG	International Committee on Global Navigation Satellite Systems
IDFT	Inverse Discrete Fourier Transform
IF	Intermediate Frequency
IGSO	Inclined Geosynchronous Orbit
i.i.d.	independent and identically distributed
ITU	International Telecommunication Union
I/Q	In-phase/Quadrature
LOS	Line-Of-Sight
LNA	Low-Noise Amplifier
LTI	Linear Time-Invariant
MAI	Multiple Access Interference
MBOC	Multiplexed Binary Offset Carrier
MCS	Multi-level Coded Symbol
MEO	Medium Earth Orbit
MMS	Mobile Satellite Services
MTR	Master Timing Reference
NB	Narrow-Band
NSGU	Navigation Signal Generation Unit
OMUX	Output Multiplexer

OOB	Out-Of-Band
OS	Open Service
PDF	Probability Density Function
PR	Pseudorange
PRN	Pseudo-Random Noise
PSD	Power Spectral Density
PSWF	Prolate Spheroidal Wave Functions
PVT	Position, Velocity and Time
QZSS	Quasi-Zenith Satellite System
RF	Radio-Frequency
RFC	Radio-Frequency Compatibility
RNSS	Radio-Navigation Satellite Service
SBAS	Space Based Augmentation System
SCB	S-Curve Bias
SI	Self-Interference
SIS	Signal-In-Space
SQM	Signal Quality Monitoring
SRRC	Square-Root Raised Cosine
SV	Satellite Vehicle
TDMA	Time Division Multiple Access
TMBOC	Time Multiplexed Binary Offset Carrier
US	United States of America
WB	Wide-Band
w.r.t.	with respect to

1. Introduction

1.1 Objective and Motivation

Over the last years it is observed a significant growth in number and power of Global Navigation Satellite System (GNSS) and Satellite-Based Augmentation System (SBAS) signals transmitted in the Radio-Navigation Satellite Service (RNSS) frequency bands. Aggregate interference levels need to be carefully assessed and regulated for ensuring that legacy and new-generation GNSS receivers will work properly within defined coverage areas and can achieve desired performance.

With the European Union decision in the 1990s to set up Galileo as own Code Division Multiple Access (CDMA) based navigation system, the need to assure compatibility with the American Global Positioning System (GPS) grew in importance as it was planned to use the same centre frequencies of GPS for Galileo signals. One of EU main objectives was in fact to set up a system not only compatible with GPS but also interoperable.

After lengthy negotiations between EU and US, the agreement on the common use of L1/E1 frequency band was signed on June 9th, 2004. In the context of this agreement a methodology for the computation of the Radio Frequency Compatibility (RFC) between GPS and Galileo was established [31]. The method is based on the computation of the Carrier-to-Noise Density Ratio (C/N_0) of the desired signal transmitted by the reference system in the presence of in-band interference generated by an interfering system. The methodology quantifies the degree of radio frequency compatibility among RNSS signals through two criteria:

- The Effective C/N_0 observed by a reference receiver processing the desired signal when different sources of interference are accounted for, i.e. intra-system interference, inter-system interference and external interference.
- The C/N_0 Degradation caused by the presence of a new interfering system onto the effective C/N_0 observed by a reference receiver processing the desired signal.

In the evolving GNSS scenario, compatibility assessments on a multilateral base are gaining more and more importance. In order to regulate this complex scenario a specific International Telecommunication Union (ITU) recommendation called Rec.

ITU-R M.1831 was issued later in 2007 [32]. In this document a coordination methodology for RNSS inter-system interference estimation was established, mostly following the approach described in [31].

Later, other RFC assessment criteria have been proposed to complement and possibly improve Rec. ITU-R M.1831. Among these, a presentation from the European Commission in the framework of the ICG activities ([33], [34]) suggested to assess the noise floor increase caused by the current/planned transmitted GNSS signals in order to agree on a maximum interference level and to limit the contributions from each GNSS provider.

An important aspect to take into account for RFC assessments is the frequency representation of the navigation signals. The analytical approach described in [31], [32] approximates the power spectral densities of the received signals as a continuous spectrum, where the fine structures of individual signal spectra are averaged together into a smooth shape. However real spectra of signals with periodic spreading codes are characterized by a fine structure of spectral lines, whose frequency and magnitude depends on the specific spreading code sequence, chip rate, presence of secondary codes and/or navigation data.

The near-continuous noise-like spectral density modelling is valid for long-code signals but for short-code signals this assumption is not appropriate as the signal power is significantly concentrated into spectral lines. Since most modernized GNSS signals belong to the category of long-code signals, the analytical approach of Rec. ITU-R M.1831 is the most employed in ITU coordination activities for RNSS inter-system interference estimation. Nevertheless it is believed in the navigation community that this approach has shortfalls when it comes to the GPS L1 C/A self-interference and in general to GNSS signals that belong to the category of the so-called short-code signals.

From a first look, the inadequacy of the RFC methodology to assess the degradation caused by short-code signals could be neglected as the C/A code is the only short-code currently transmitted and it is also since the beginning of satellite navigation. On the other hand, the risk is twofold:

- An underestimation of the C/A code self-interference could lead to ITU multi-lateral agreements that do not protect the GPS L1 C/A users and expected performance. Models have been developed to reflect the qualitative

characteristics of L1 C/A self-interference and to assess its effects on receiver performance ([35], [36], and [37]), but no such model is recognised as standard reference and adopted for compatibility assessments.

- An incomplete or inaccurate RFC methodology could allow the design and transmission of new short-code signals that significantly degrade the performance of other navigation services. As a matter of fact, while the effects of intra-system interference are under control of the navigation system provider, the same cannot be ensured for the inter-system interference.

The main limitation of the RFC methodology discussed above consists of considering only the aggregate interfering power levels. The cross-correlation interference between desired and interfering spreading codes also plays an important role, especially when it comes to short-code signals. Every navigation system provider needs to ensure for each service not only a good isolation of the selected Pseudo-Random Noise (PRN) code set with it-self (self-interference, SI) but also with all other PRN code sets transmitted in the same radio frequency band (cross-interference, CI).

Until recently, GPS signals along with a few low-power SBAS signals were the only signals occupying L-band and investigation on PRN code correlation properties for the evaluation of self- and cross-interference was primarily of academic interest for the following reasons:

- the power of individual navigation signals is far less than the noise power in a receiver front-end;
- the aggregate power of interfering navigation signals is comparable to the receiver noise floor and the aggregate smooth spectrum is used for interference computation as described in the abovementioned methodologies [31], [32];
- the assumption of aggregate smooth spectrum is justified for most GNSS signals.

Nevertheless, future signals' design and choice of the spreading codes should be based on criteria that minimise not only the self-interference but also the cross-interference with legacy GNSS signals. GPS L1 C/A currently represents the most relevant case of short-code signal for global systems but other system providers may

plan new services for fast acquisition based on short codes. The ITU methodology shall be ready to assess not only the compatibility between transmitted power levels but also between PRN code sets.

The main objective of this thesis is to investigate the nature of short-code signals and to propose a new methodology complementary to Rec. ITU-R M.1831 for assessing the effects of self- and cross-correlation interference between spreading codes.

1.2 Thesis Outline

This thesis is organised as follows:

- Chapter 2 provides a review of GNSS signal structures focussing on the expression of the different signal components such as chip shape, modulation, spreading codes, overlay codes, presence or absence of data. The mathematical model for a generic GNSS base-band signal is introduced both at transmitter side and at receiver side in the time and frequency domain. An overview on the transmit chain for a typical navigation payload and a high-level description of a typical receiver chain are also included.
- Chapter 3 focuses on spreading codes and starts with an overview of all publicly known PRN code families currently (or planned to be) transmitted by GNSS providers. It follows a summary of the measures of randomness for a spreading code set, i.e. the three Golomb's postulates [25]. The auto- and cross-correlation formulas at the basis of spreading codes performance figures are derived and well recognized figures of merit for PRN codes design are presented. The concepts of self-interference and cross-interference are introduced as respectively the interference caused by a PRN codes set on it-self or onto a different PRN codes set. A sensitivity study, based on the figure of merits previously introduced, explores the PRN codes self-interference with respect to some signal design parameters (secondary codes, sub-carrier, chip shape) as well as Doppler frequency and receiver integration time. The analysis is then extended to the cross-interference case.
- Chapter 4 is the core of the thesis and propose a new methodology, complementary to the Rec. ITU-R M.1831, based on the spreading codes cross-correlation interference. The new proposed method combines the PRN codes performance figures described in Chapter 3 with both the simulation

and analytical approaches in [32] to provide an overall PRN spreading codes performance figure. Extensive simulation results for the new methodology are provided.

- Chapter 5 draws the conclusions of this thesis and provides the author's recommendations for future work.
- Appendix A shows the power spectral densities of the Galileo signals baseline (E1 OS, E6 CS, E5) as computed with the spectral line model described in Chapter 2.
- Appendix A investigates the concept of nominal and non-nominal signal distortions for the Galileo signals. This topic is complex and quite controversial: substantial literature is available on the subject but no common understanding has been reached up to now in the scientific community. The Galileo system provider is still investigating the nature, effects, modelling, and detectability of such distortions. The content of this Appendix reflects only the author's view.

1.3 Thesis Contributions

The main contributions of this thesis are summarised in the following:

- A new radio-frequency compatibility methodology for the assessment of spreading codes self- and cross-interference is proposed. The objective is to complement Rec. ITU-R M.1831 which is based solely on the estimation of aggregate interference power levels. The assessment criteria described provide a measure of the CDMA isolation properties of PRN code sets in the service volume.
- Extensive simulation results prove the validity of the proposed methodology. The analyses on specific PRN code sets allow observing some relevant aspects related to the PRN codes compatibility among signals.
- A complete overview and description of spreading codes performance figures is provided as well as a sensitivity analysis with respect to the main design parameters (secondary codes, sub-carrier, chip shape), Doppler frequency and receiver integration time.
- A general representation for current GNSS signal structures is provided, which allows expressing contributions from the different signal components

separately, accounting for various chip shapes, modulations, spreading codes, overlay codes, presence or absence of data. The mathematical formulation proposed is used to better explain the frequency representation of navigation signals and the spectral line model.

- The concept of nominal and non-nominal signal distortions affecting navigation signals is investigated and a threat model for Galileo baseline modulations is proposed.

1.4 Glossary of Terms

Scope of this section is to provide fundamental definitions in the domain of satellite navigation for better understanding the topics analysed in the following chapters.

GNSS – Global Navigation Satellite System (GNSS) is a term commonly used for indicating satellite navigation systems that provide autonomous geo-spatial positioning with global coverage. This term includes e.g. the GPS, GLONASS, Galileo, and Beidou.

SBAS – A Satellite-Based Augmentation System (SBAS) is a civil aviation safety-critical system that supports regional augmentation through the use of geostationary satellites which broadcast the augmentation information (integrity and error corrections). Currently there are some SBAS systems already operational, such as WAAS (USA), EGNOS (Europe), SDCM (Russia), and GAGAN (India).

RNSS – According to ITU Radio Regulations, Section IV. Radio Stations and Systems – Article 1.43, a Radio-Navigation Satellite Service (RNSS) is "a radiodetermination-satellite service used for the purpose of radionavigation. This service may also include feeder links necessary for its operation". GNSS and SBAS signals belong to the category of RNSS services and their frequency band allocation is regulated by the ITU.

Spread Spectrum Technology – Method by which a radio-frequency signal generated with a particular bandwidth is artificially spread in the frequency domain to result in a signal with a wider bandwidth. Different Spread Spectrum (SS)

techniques are available, but they all have one thing in common: they perform the spreading and de-spreading operation by means of a pseudo random noise (PRN) code attached to the communication channel. The ratio (in dB) between the spread baseband and the original signal is called processing gain. Several advantages result from the use of this technology:

- Resistance to interception: the power level drops below the radio-frequency noise floor, which makes the SS signal invisible for unauthorized users.
- Resistance to interference: narrow-band interference degradation is reduced by the de-spreading operation in the receiver processing.
- Resistance to fading. The broad bandwidth resulting from the spreading operation offer more robustness to channel propagation effects such as multipath fading.
- Multiple access capability: multiple users can transmit simultaneously in the same frequency band as long as they use different PRN codes.

Frequency-hopping spread spectrum (FHSS), direct-sequence spread spectrum (DSSS), time-hopping spread spectrum (THSS), chirp spread spectrum (CSS), and combinations of these techniques are forms of spread spectrum. Most of nowadays GNSS systems are based on DSSS signalling. More details are provided in Chapter 3.

When it comes to sharing the same frequency band resource among several transmitters, there are only few fundamental types of channel access schemes available:

- **CDMA** – Code Division Multiple Access (CDMA) is a channel access method where multiple transmitters can send information simultaneously over a single communication channel. To minimise the interference between channels, CDMA employs spread spectrum technology and a special coding scheme (where each transmitter is assigned a code). GPS and Galileo are two very significant examples of CDMA in which every satellite is assigned a different code. This enables the receiver to determine the satellite from which each signal is coming and, consequently, to help the receiver calculate its position by simultaneous ranging to multiple satellites.

- **FDMA** –Frequency Division Multiple Access (FDMA) is a channel access method where multiple transmitters can send information simultaneously by dividing the bandwidth of the channel into separate non-overlapping frequency sub-channels and allocating each sub-channel to a separate transmitter. The number of different users is limited to the number of sub-channels in the frequency spectrum. FDMA is the least efficient in term of frequency-band usage. GLONASS is the only satellite navigation system using FDMA.
- **TDMA** –Time Division Multiple Access (TDMA) is a channel access method where several transmitters share the same frequency channel by dividing the signal into different time slots. Thus, different communication channels can be established for a unique carrier frequency. Nowadays no GNSS makes use of TDMA for satellite transmission. Examples of TDMA systems are GSM, DECT, TETRA, and IS-136.

PRN Code – A Pseudo-Random-Noise code (PRN code) is a binary sequence that has a spectrum similar to a random sequence of bits but is deterministically generated.

Compatibility – General definition from [30]:
"Compatibility refers to the ability of space-based positioning, navigation, and timing services to be used separately or together without interfering with each individual service or signal.

- Radiofrequency compatibility should involve thorough consideration of detailed technical factors, including effects on receiver noise floor and cross-correlation between interfering and desired signals. The International Telecommunications Union (ITU) provides the framework for discussions on radiofrequency compatibility.
- Compatibility should also involve spectral separation between each system's authorized service signals and other systems' signals.
- Any additional solutions to improve compatibility are encouraged."

The definition of criteria together with binding thresholds that would assure compatibility in line with the above definition cannot be absolutely determined. Currently, the compatibility among RNSS services is regulated through the methodology described in Recommendation ITU-R M.1831 [32]. A comprehensive description of ITU-R M.1831 and its limitations is provided in Chapter 4.

The concept of interoperability is strictly related to the one of compatibility. In particular, compatibility can be considered as a pre-requisite of interoperability.
Interoperability – General definition from [30]:
"Interoperability refers to the ability of open global and regional satellite navigation and timing services to be used together to provide better capabilities at the user level than would be achieved by relying solely on one service or signal.

- Ideal interoperability allows navigation with signals from at least four different systems with no additional receiver cost or complexity.
- Common center frequencies are essential to interoperability, and commonality of other signal characteristics is desirable.
- Multiple constellations broadcasting interoperable open signals will result in improved observed geometry, increasing end user accuracy everywhere and improving service availability in environments where satellite visibility is often obscured.
- Geodetic reference frames and system time standards should also be considered.
- Any additional solutions to improve interoperability are encouraged."

The concept of interoperability was first introduced when the design of the Galileo OS signal in E1 and the GPS 2nd generation signal in L1 was under definition. It must be underlined that being compatible does not necessarily imply that two systems are also interoperable from the signal point of view. On the other hand, no interoperability can be achieved as far as the compatibility between the involved systems is not guaranteed.

The terms 'short-code' and 'long-code' have been introduced in [32], in the context of radio-frequency interference assessment, for the purpose of discriminating the following two categories:

- **Long-code signals** – Signals for which the 'continuous spectrum' modelling is valid. In this case the Doppler shift between the different signals has a negligible effect in the overall interference assessment.
- **Short-code signals** – Signals for which the 'real spectrum' modelling, also called 'line spectrum', is required. This more realistic modelling takes into account the real properties of the signals, such as data rate and spreading code characteristics (code lengths and presence of pilot and/or data channels), through time/frequency transformation of the modulated signal. The Doppler shift between the desired signal and the interfering signals is to be accounted for in this case.

There is no mathematical criterion to determine whether a certain spreading code associated to a GNSS signal is 'short' or 'long'. It is only a qualitative characterisation based on the frequency spectrum observation.

Another uncommon terminology used in [32] but also in other sources ([21], [35], [36]) is the definition of 'continuous spectrum' and 'line spectrum'. The distinction is of particular importance for radio-frequency interference assessment:

- **Line Spectrum** – Real spectra of signals with periodic spreading codes are characterized by an envelope and a fine structure. The fine structure is a sequence of spectral lines, which have different levels. When there is data, the fine structure spectral lines are smoothed. The spectral lines depend on the chip rate, the code length, the presence of a pilot code, and on the code structure, as described in Chapter 2. For RFC evaluation, short-code signals shall be represented with the line spectrum model.
- **Continuous spectrum** – This analytical model approximates the spectrum of the received signals as an aggregate spectrum, where the fine structures of individual signal spectra are averaged together into a smooth spectrum. The methodology in [32] adopts this modelling for the representation of long-code signals spectrum.

An in-depth analysis of 'continuous spectrum' and 'line spectrum' representation for Galileo signals is provided in Appendix A.

The main objective of this thesis is to propose a new methodology for assessing the CDMA isolation of a PRN code set with it-self and with another PRN code set. The definitions of 'self-interference' and 'cross-interference' are fundamental:

- **PRN Codes Self-interference** – The interference caused by a PRN code set on it-self is referred to as self-interference (SI); in communications this is also called Multiple Access Interference (MAI) and it represents the opposite concept of CDMA isolation. Self-interference is also referred to as 'spreading codes auto- and cross-correlation characteristics' or 'PRN code family correlation performance' (see [23],[24],[27],[29]). For a mathematical description of self-interference it is referred to Section 3.4.
- **PRN Codes Cross-interference** – The interference cause by a PRN code set (interference source) onto another set (desired source) is called cross-interference, abbreviated with CI. This effect is also referred to as 'inter-system spreading codes cross-correlation characteristics' and it is investigated for the case of Galileo E1 OS and GPS L1C spreading codes in [24]. A mathematical description of cross-interference is provided in Section 3.5.

2. Navigation Signal Structure

Most of the current and new GNSS signals are built as a combination of two components: a data signal and a data-free signal, also called pilot signal. In general both signals result from the product of two elements which are a sinusoidal carrier and a spreading code, with the option of an overlay code. The data signal is further multiplied by the binary data sequence.

Each of these elements has a specific scope. While the carrier puts the signal in the allocated region of the radio-frequency spectrum, the spreading code or Pseudo-Random Noise (PRN) sequence is used to perform time measurements and to provide multiple access. The binary data sequence, also known as navigation message, carries out different important tasks like delivering the information used to compute the satellite's position and clock bias and the time reference to calculate the pseudorange. Regarding the overlay code, also called tiered or secondary code, there are various reasons that have brought to the introduction of it. One of the main purposes is indeed to modulate the primary code with the effect of spreading the power over more spectral lines; as a consequence, the signal results in an increased resistance to narrow-band interference.

All these elements reflect on the navigation signals' waveform giving to each of them a unique spectral content. In most of the assessments on GNSS performance however the representation of signals in the frequency domain is done by an approximation of the actual Power Spectral Density (PSD). A common assumption in fact is to assume that PRN codes and overlay codes show ideal properties, i.e. random, non-periodic, identically distributed, equiprobable, and independent sequences. Under this hypothesis the signal waveform simplifies to its chip waveform and the PSD assumes the characteristic smooth shape that is typically considered.

In reality, the non-ideal spreading codes reflect on the PSD and the correlation function shape with effects that depend on the specific signal design. For some assessments, like the evaluation of radio-frequency compatibility between signals or the susceptibility of a signal to a certain narrow-band interference source, the simplistic assumption just explained could be inadequate.

Scope of this chapter is to provide a flexible representation for current GNSS signal structures which allows expressing the contribution from the different signal

components separately, accounting for various chip shapes, modulations, spreading codes, overlay codes, and presence or absence of data. A deep understanding of the navigation signal structure and models is at the basis of the spreading codes analysis performed later in this thesis.

The chapter is composed of the following parts:

- Section 2.1 provides an overview of the transmit chain for a typical navigation payload and the mathematical model to describe a generic navigation signal at the output of the transmit antenna.
- Section 2.2 provides a high-level description of a typical receiver chain and the mathematical model to describe the received navigation signal at the input of the digital signal processing.

2.1 Transmit Signal

GNSS signals are typically transmitted by navigation payloads on board of MEO or GEO satellites. The transponder architecture may be a regenerative or a transparent one depending on the GNSS space segment design. A generic regenerative payload architecture is represented in Figure 2–1.

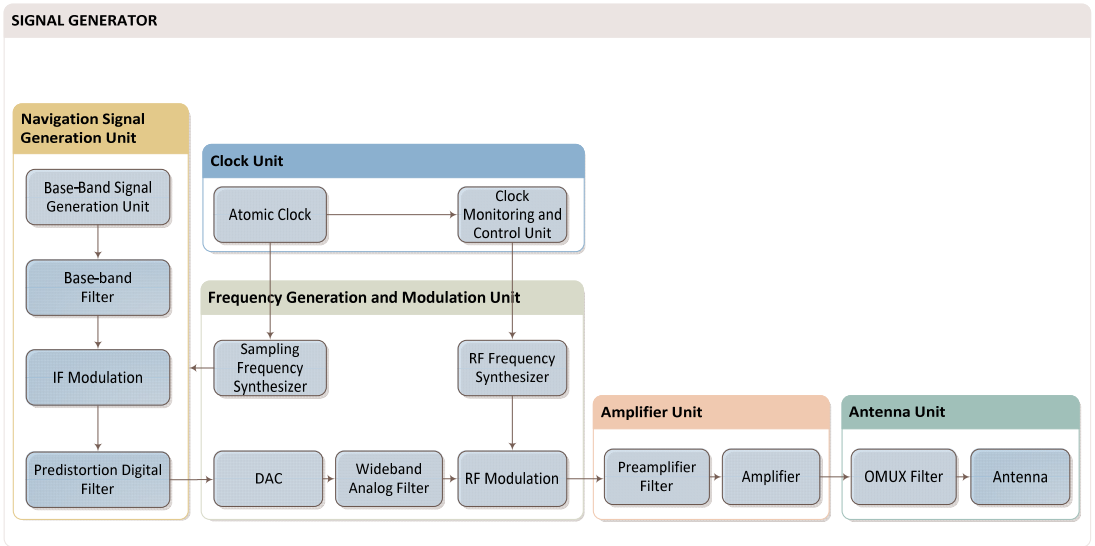

Figure 2–1: Transmit Chain, Functional Block Diagram.

The following five units can be identified in a conventional navigation signal generation chain:

- The Clock Unit, composed of a set of atomic clocks and a Clock Management and Control Unit (CMCU). The CMCU is used to generate the

Master Timing Reference (MTR), typically at 10.23 MHz for navigation signals, that is used by the whole generation block.

- The Navigation Signal Generation Unit (NSGU), which generates the navigation signal, and is composed of a modulator and a pre-distortion digital filter. The modulator generates the base-band digital signals, and usually transposes it digitally towards an IF. The pre-distortion filter is used to limit out-of-band emissions, avoid spectrum mixing, and compensate for DAC shaping or any distortion brought by the following analog processing.
- The Frequency Generation and Modulation Unit (FGMU), which is composed of frequency synthesizers, a Digital-to-Analog Conversion (DAC), and mixers. Usually, a wide-band analog filter is also used in order to limit out-of-band emissions, spectrum distortions due to the DAC, and spectrum re-combinations after up-conversion. At the output of the FGMU, the signals should be within its transmission frequency.
- The Amplifier Unit, composed of Solid State Power Amplifiers (SSPAs) or Travelling Wave Tube Amplifiers (TWTAs). The characteristics of these amplifiers are given by their amplitude and phase response, as well as their bandwidth. In order to limit the distortions brought by the amplifier non-linearities, constant envelope signals have been traditionally used by navigation satellites. However, this might not be the best solution for all cases and this work will investigate the impact of the use of signals with a non-constant envelope.
- The Antenna Unit, composed of an Output MUltipleX (OMUX) filter that permits eliminating the inter-modulation products as well as the secondary lobes caused by the amplification stage, and a transmit antenna.

The names CMCU, NSGU and FGMU are taken from the structure of the Galileo satellites payload (see [41]).

Note that the mathematical models described later are valid under the assumption of no distortions in the payload generation chain. In other words, the transmit chain is simplified to an ideal base-band generation unit, RF up-conversion and transmission thorough the satellite antenna. An in-depth analysis of nominal and non-nominal signal distortions is provided in Appendix A.

2.1.1 Time Domain Representation

Assume that $s_{BB}(t)$ is the navigation base-band signal as it is generated by an ideal base-band signal generation unit. It is possible to write separately the three elements contributing to the signal waveform as $s_P(t)$, $s_S(t)$ and $s_D(t)$, being respectively the primary code, secondary code (or overlay code), and data stream:

$$s_P(t) = \sum_{n=-\infty}^{+\infty} c_P[n] \cdot p_P(t - nT_P) \tag{2.1}$$

$$s_S(t) = \sum_{n=-\infty}^{+\infty} c_S[n] \cdot p_S(t - nT_S) \tag{2.2}$$

$$s_D(t) = \sum_{n=-\infty}^{+\infty} c_D[n] \cdot p_D(t - nT_D) \tag{2.3}$$

with $c_X[n]$ the amplitude of the symbol sequence, T_X the time interval between two consecutive symbols, and $p_X(t)$ the symbol shape defined over $[0, KT_X]$ and normalized to unit power. Note that the word 'symbol' is here used to refer to the generic information unit, not necessarily binary, which can be the chip of a PRN code or the data bit of a navigation message. Also the symbol shape is a generic definition that encompasses any kind of pulse function. The base-band normalized Signal-In-Space (SIS) can be written as the product of the three contributions:

$$s_{BB}(t) = s_P(t) \cdot s_S(t) \cdot s_D(t) \tag{2.4}$$

Starting with the primary and secondary codes, it is well known that in actual GNSS signals these components are generated with periodic sequences so that $c_X[n + N_X] = c_X[n]$, being N_X the number of chips characterizing the generic PRN code. The expressions in Eq. (2.1) and (2.2) can be written as:

$$\bar{s}_X(t) = \sum_{n=0}^{N_X-1} c_X[n] \cdot p_X(t - nT_X) \tag{2.5}$$

Further, the PRN sequence can be expressed as the convolution of the pulse shape $p_X(t)$ with a unit impulse sequence, weighed by the code chips $c_X[n]$ and as long as the code length N_X:

$$\bar{s}_X(t) = p_X(t) * \left[\sum_{n=0}^{N_X-1} c_X[n] \cdot \delta(t - nT_X) \right] \tag{2.6}$$

where $\delta(t)$ is the Dirac delta function or impulse function, and '$*$' stands for linear convolution.

This expression allows writing Eq. (2.1) and (2.2) as the convolution of a basic PRN sequence with a unit impulse sequence whose inter-distance is the PRN code periodicity:

$$\begin{aligned} s_X(t) &= \bar{s}_X(t) * \left[\sum_{m=-\infty}^{+\infty} \delta\left(t - mT_{code,X}\right) \right] \\ &= p_X(t) * \left[\sum_{n=0}^{N_X-1} c_X[n] \cdot \delta(t - nT_X) \right] * \left[\sum_{m=-\infty}^{+\infty} \delta\left(t - mT_{code,X}\right) \right] \end{aligned} \tag{2.7}$$

where $T_{code,X} = N_X \cdot T_X$ is the code repetition period.

The expression in Eq. (2.7) represents the starting point for the derivation of the frequency-domain representation in Section 2.1.2.

Concerning the data component, also Eq. (2.3) can be written as to underline the contribution coming from the pulse shape and the contribution coming from the data stream:

$$s_D(t) = p_D(t) * \left[\sum_{n=-\infty}^{+\infty} c_D[n] \cdot \delta(t - nT_D) \right] \tag{2.8}$$

Most of nowadays GNSS signals based on Code Division Multiple Access (CDMA) technology can be expressed with Eq. (2.4) or as a summation of basic signals described by Eq. (2.4).

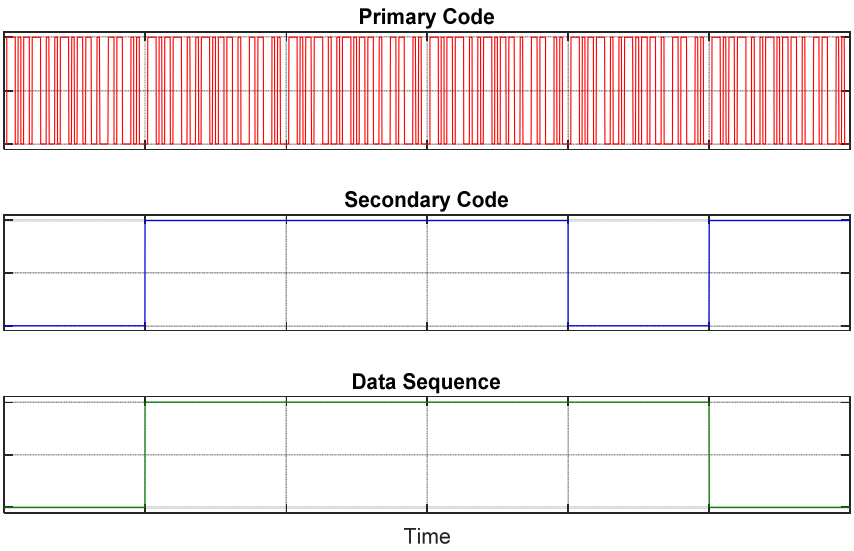

Figure 2–2: Generic navigation SIS in the time domain as defined in Eq. (2.4).

Figure 2–2 provides an illustration of the three navigation signal components described above: the primary code (top, red line) repeats 6 times within the

represented time frame; the secondary code (middle, blue line) is 4-symbols long [+1, +1, +1, -1] and each symbol is as long as a primary code sequence; the data stream (bottom, green line) is the sequence [-1, +1, -1] and its bit duration matches with the secondary code period.

Note that in Figure 2–2 all symbols are rectangular shaped. Most second generation GNSS signals however are transmitted together with one or more sub-carrier components. As widely discussed in [40], these modulations (e.g. BOC, CBOC, AltBOC) can be seen as specific cases of a more generalised signal class based on Multi-level Coded Symbols (MCS). For the simplest case of Binary Offset Carrier (BOC) modulation each primary code symbol $p_P(t)$ is represented with a binary sequence of equal-length segments, also called sub-chips, obtained by extracting the sign of a sine or cosine wave. An illustration of the BOC_{sin} and BOC_{cos} pulse shape is provided in Figure 2–3.

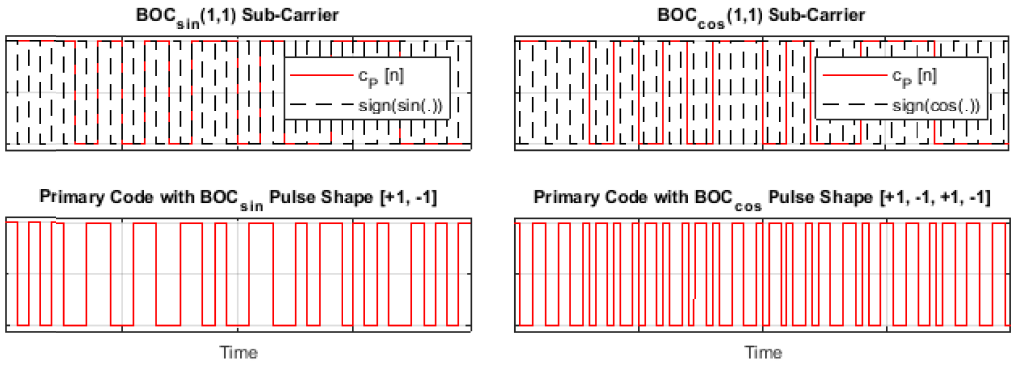

Figure 2–3: BOCsin (left) and BOCcos (right) pulse shapes applied to a primary code sequence.

Other pulse shapes commonly used for telecommunication applications have been investigated for their suitability to satellite navigation domain, such as Square-Root Raised Cosine (SRRC), Gaussian pulse, Prolate Spheroidal Wave Functions (PSWF). However none of these modulations are currently adopted in GNSS.

All existing navigation signals can be described with the generalised notation provided in chapter. The mathematical expression of each adopted modulation in terms of MCS signals (or a sum of them) is derived in [40].

An important operator, widely used in signal processing and in the following chapters, is the linear Auto-Correlation Function (ACF) of the signal $s_{BB}(t)$:

$$R_s(\tau) = \int_{-\infty}^{+\infty} {s_{BB}}^*(t) \cdot s_{BB}(t+\tau)dt = {s_{BB}}^*(-\tau) * s_{BB}(\tau) \tag{2.9}$$

The linear ACF $R_s(\tau)$ relates to the linear convolution operator '*' as expressed in Eq. (2.9) and to the power spectral density as:

$$R_s(\tau) = \int_{-\infty}^{+\infty} {S_{BB}}^*(f) \cdot S_{BB}(f) \cdot e^{j2\pi f\tau}df = \mathcal{F}^{-1}\{|S_{BB}(f)|^2\} \tag{2.10}$$

where $S_{BB}(f)$ is the Fourier transform of $s_{BB}(t)$ and $\mathcal{F}^{-1}\{\cdot\}$ represent the inverse Fourier transform operator.

Up to now the basic components of conventional GNSS signals are described for their deterministic properties. However both data streams and spreading codes are or tend to behave like stationary random processes and their statistical properties, as often described in literature [1]-[5], must also be mentioned.

Each signal defined in Eq. (2.6) and (2.8) can be described as the output of a linear time-invariant (LTI) system defined by its transfer function $p_X(t)$. The mean function $\mu_s(t)$ of a random process $s_X(t)$ is defined by:

$$\begin{aligned}\mu_s(t) = \mathrm{E}\{s_X(t)\} &= \mathrm{E}\left\{\int_{-\infty}^{+\infty}\left[\sum_{n=-\infty}^{+\infty} c_X[n]\cdot\delta(\alpha - nT_X)\right]\cdot p_X(t-\alpha)d\alpha\right\} \\ &= \int_{-\infty}^{+\infty}\mathrm{E}\left\{\sum_{n=-\infty}^{+\infty} c_X[n]\cdot\delta(\alpha - nT_X)\right\}\cdot p_X(t-\alpha)d\alpha \\ &= \int_{-\infty}^{+\infty}\mu_c(\alpha)\cdot p_X(t-\alpha)d\alpha\end{aligned} \tag{2.11}$$

While the statistical autocorrelation function $\tilde{R}_s(t_1, t_2)$ is expressed as:

$$\begin{aligned}\tilde{R}_s(t_1,t_2) &= \mathrm{E}\{s_X(t_1)s_X^*(t_2)\} \\ &= \iint_{-\infty}^{+\infty}\mathrm{E}\left\{\left[\sum_{n=-\infty}^{+\infty} c_X[n]\cdot\delta(\alpha - nT_X)\right]\cdot\left[\sum_{n=-\infty}^{+\infty} c_X[n]\cdot\delta(\beta - nT_X)\right]^*\right\}\cdot \\ &\qquad p_X(t_1-\alpha)\cdot p_X^*(t_2-\beta)d\alpha\, d\beta \\ &= \iint_{-\infty}^{+\infty}\tilde{R}_c(\alpha-\beta)\cdot p_X(t_1-\alpha)\cdot p_X^*(t_2-\beta)d\alpha\, d\beta\end{aligned} \tag{2.12}$$

and by a substitution of variables (see [5]), it can be demonstrated that:

$$\tilde{R}_s(\tau) = \int_{-\infty}^{+\infty} G_c(f)|P(f)|^2 e^{j2\pi f\tau}df = \tilde{R}_c(\tau) * R_p(\tau) \tag{2.13}$$

being $G_c(f)$ the PSD of the symbol sequence $c_X[n]$ and $P(f)$ the FT of the pulse shape $p_X(t)$.

Finally, the covariance $C_s(t_1, t_2)$ of the random process $s_X(t)$ can be expressed as a function of the statistical autocorrelation and the mean:

$$C_s(t_1, t_2) = \mathrm{E}\{[s_X(t_1) - \mu_s(t_1)] \cdot [s_X(t_2) - \mu_s(t_2)]^*\} = \tilde{R}_s(t_1, t_2) - \mu_s(t_1) \cdot \mu_s^*(t_2) \tag{2.14}$$

To conclude on the time domain representation of transmit signals, the RF expression at the output of the satellite antenna is provided below:

$$s_{RF}(t) = A_T \cdot s_{BB}(t) \cdot cos(2\pi f_{RF} t) \tag{2.15}$$

where A_T is the signal amplitude and f_{RF} the carrier frequency. Note that A_T is related to the radiated power by the expression $EIRP = {A_T}^2/2$, being the Equivalent Isotropically Radiated Power (EIRP) defined as:

$$EIRP(\alpha) = \frac{P_T G_T}{L_c} \tag{2.16}$$

with:

P_T transmission power at satellite [W]

G_T transmit antenna gain for a given off-boresight angle α [unitless]

L_c loss of the transmission line [unitless]

2.1.2 Frequency Domain Representation

As known from signal theory, a periodicity in the time domain corresponds to a sampling in the frequency domain and vice-versa. Thus, the repetition of the basic PRN code sequence every $T_{\mathrm{code},X} = N_X \cdot T_X$ implies sampling its Fourier transform with a frequency step Δf_X equal to $1/T_{\mathrm{code},X}$. In formulas:

$$S_X(f) = \bar{S}_X(f) \cdot \sum_{k=-\infty}^{+\infty} \delta(f - k\Delta f_X) = S_X[k] \tag{2.17}$$

being $S_X(f)$ and $\bar{S}_X(f)$ the FT of respectively $s_X(t)$ and $\bar{s}_X(t)$. Note that the second term of the product represents a unit impulse sequence and stands for the sampling operation.

A further step can be done by considering the representation of the repeating basic signal as given in Eq. (2.6). This expression allows writing the Fourier transform of $\bar{s}_X(t)$ as a product of two elements: the FT of the pulse shape, $P_X(f)$, and the FT of a discrete sequence, which is the periodic FT of the PRN code sequence, $C_X(f)$:

$$\bar{S}_X(f) = P_X(f) \cdot \sum_{n=0}^{N_X-1} C_X(f - nf_X) \tag{2.18}$$

Being f_X the chip rate equal to $1/T_X$. Substituting Eq. (2.18) in Eq. (2.17), the following expression is obtained:

$$S_X[k] = P_X[k] \cdot \sum_{n=0}^{N_X-1} C_X[k - nf_X] \tag{2.19}$$

This notation shows a very useful property when it comes to the spectral description of the signal. Note in fact that the periodicity of $S_X(f)$, as observed in [21], allows a fast Discrete Fourier Transform (DFT) computation: it is sufficient to compute $C_X(f)$ for $n = 0$, to replicate it over the desired frequency band, and to weigh it with the pulse shape $P_X(f)$.

Starting from Eq. (2.19), it is straightforward to derive the PSD as:

$$G_{S_X}[k] = G_{P_X}[k] \cdot \sum_{n=0}^{N_X-1} G_{C_X}[k - nf_X] \tag{2.20}$$

being $G_{P_X}[k] = |P_X[k]|^2$ and $G_{C_X}[k] = |C_X[k]|^2$ the discrete PSDs of respectively the pulse shape and the repeating code sequence. Note that, as already mentioned in Section 2.1.1, a typical assumption in GNSS is to consider the PRN codes as ideal, i.e. to be statistically characterized as an infinite random noise sequence and not as a periodic one. Under the hypothesis of ideal PRN codes, the chips of the sequence $c_X[n]$ are i.i.d. random variables that assume values in the discrete sample space $\{-1, +1\}$. The statistical autocorrelation $\tilde{R}_s(t_1, t_2)$ of such a process is a Dirac delta in the origin $\mathrm{E}\{c[k]c^*[n]\} \approx \delta[0]$, thus $G_{C_X}[k]$ tends to be constant in the frequency domain. The statistical representation of the PSD becomes:

$$G_{S_X}[k] \approx |P_X[k]|^2 \tag{2.21}$$

For the data component the Fourier transform $S_D(f)$ is given by:

$$S_D(f) = P_D(f) \cdot \sum_{m=-\infty}^{+\infty} C_D\left(f - m\frac{1}{T_D}\right) \tag{2.22}$$

In this case the data sequence $c_D[n]$ represents a real stationary random process that, for binary transmission, assumes values in the discrete sample space $\{-1, +1\}$. The PSD of the data signal can be written as:

$$G_{S_D}(f) = G_{P_D}(f) \tag{2.23}$$

In other words, under the hypothesis of ideal random data, the PSD contribution of the data component is equal to the PSD of its pulse shape.

Going back to the base-band expression of the overall signal-in-space in Eq. (2.4), it is possible to write its Fourier transform as:

$$S(f) = S_P(f) * S_S(f) * S_D(f) \tag{2.24}$$

The PSD of $s(t)$ is simply calculated as $G_s(f) = |S(f)|^2$. Under the hypothesis of statistical random process described above, the following simplification can be applied to the navigation signal representation:

$$G_s(f) = |S_P(f) * S_S(f) * S_D(f)|^2 \approx |P_P(f)|^2 \tag{2.25}$$

For illustration purposes the spectral contribution of a primary code, secondary code, and data stream taken from the Galileo E1 OS are shown below.

Figure 2–4 displays the normalized PSD of the Galileo E1-B Code as transmitted by SVID 1 with $N_P = 4092$.

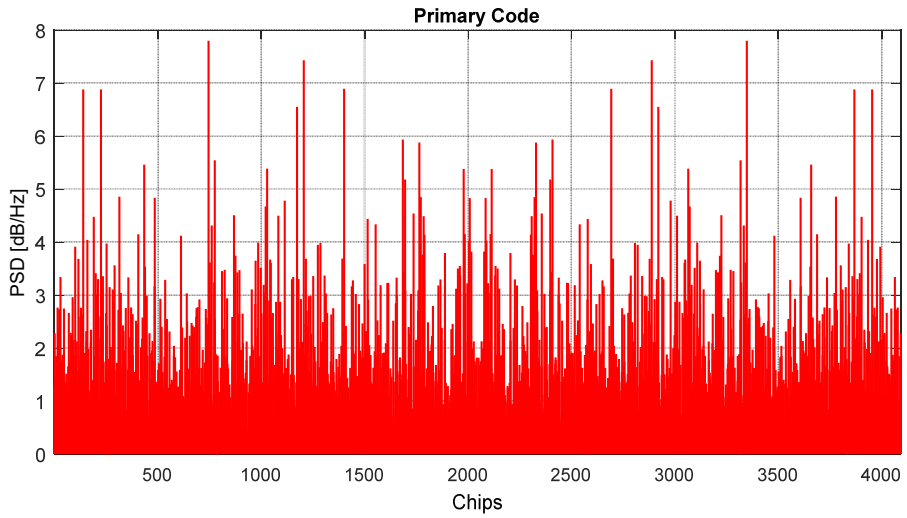

Figure 2–4: Power Spectral Density of Galileo E1-B SVID 1 Primary Code.

Figure 2–5 shows the normalized PSD $G_{S_P}(m\Delta f_P)$ for SVID 1 obtained from Eq. (2.20), where the pulse shape is a Binary Offset Carrier (BOC). In particular the modulation here adopted is the BOCs(1,1), which means that a PRN sequence with

chip rate $f_P = f_0$ is modulated by a sub-carrier that is a squared sine waveform with frequency f_0, being $f_0 = 1.023$ MHz the reference frequency.

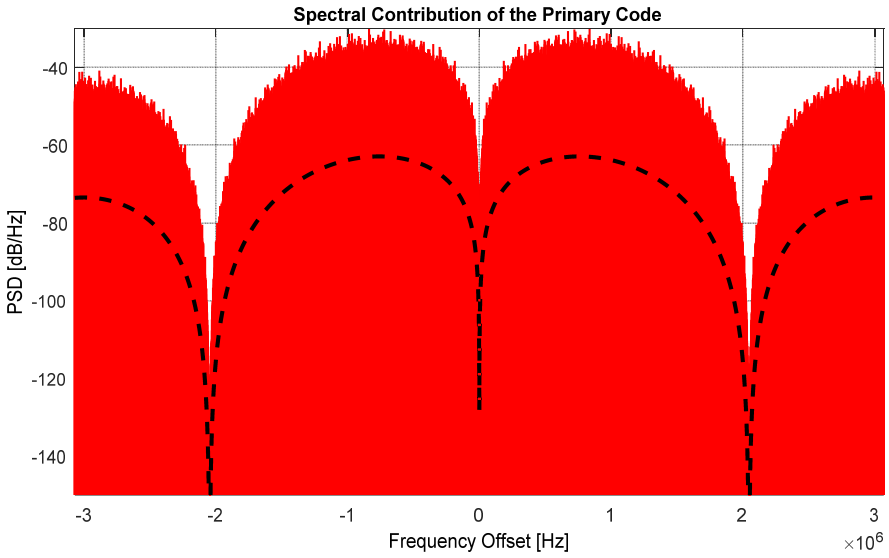

Figure 2–5: Spectral Contribution of Galileo E1-B SVID 1 Primary Code to the tansmitted SIS.

The frequency step Δf_P can be easily computed starting from $T_{\text{code},P} = 4$ ms and is equal to 250 Hz. The red lines in Figure 2–5 represent the normalized PSD sequence in Figure 2–4, periodically repeated every $1/T_P = f_P$ and modulated by the pulse shape, represented with the black dashed line.

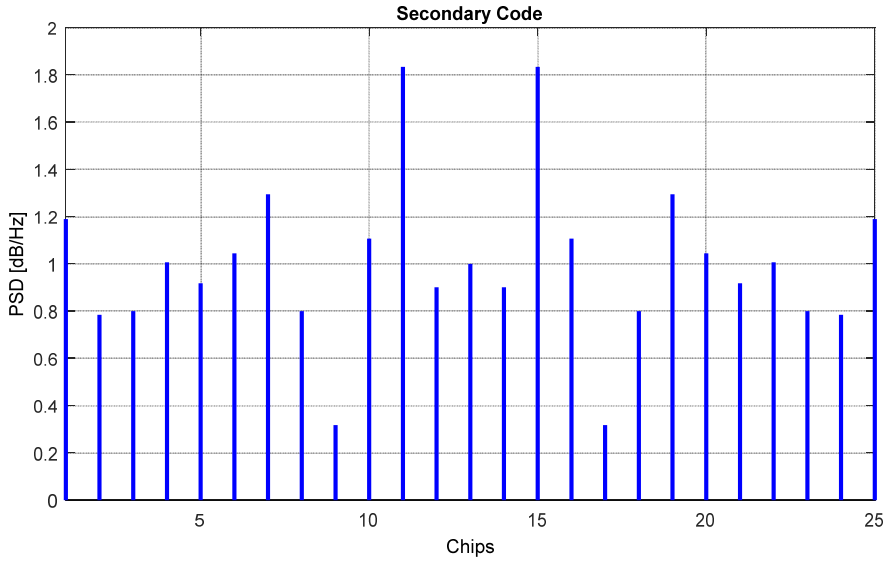

Figure 2–6: Power Spectral Density of Galileo E1-C Secondary Code.

The same plots are proposed in Figure 2–6 and Figure 2–7 for the Galileo secondary code CS25_1 with $N_S = 25$. Note that in this case the pulse shape is a rectangle of

width $T_S = 4$ ms and the frequency step, derived from the code period $T_{\text{code},S} = 100$ ms, is equal to 10 Hz.

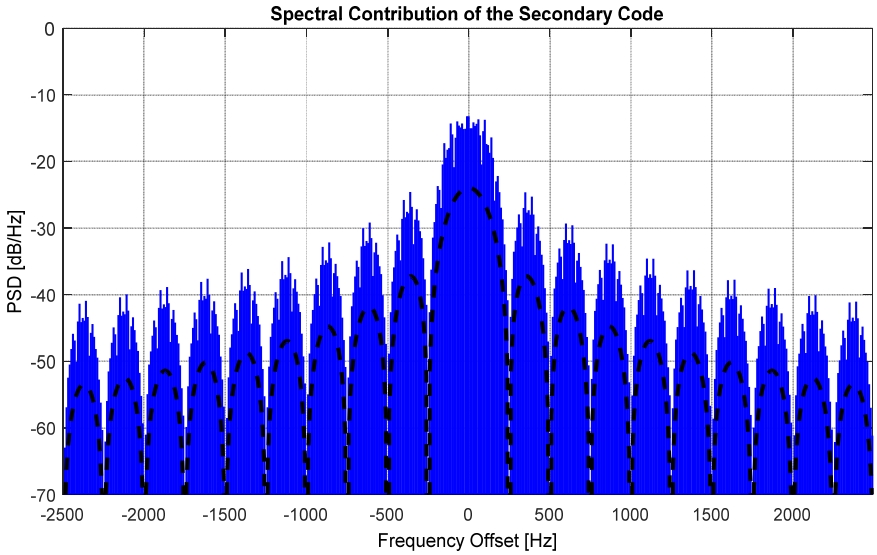

Figure 2–7: Spectral Contribution of Galileo E1-C Secondary Code to the tansmitted SIS.

The spectral contribution of the Galileo E1-B data signal is shown in Figure 2–8. In this case the pulse shape is a rectangle of width $T_D = 4$ ms.

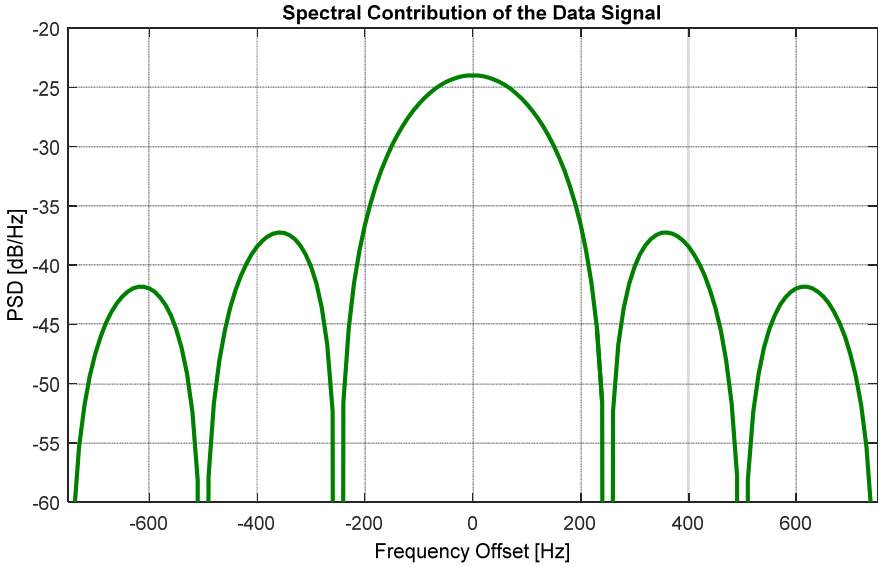

Figure 2–8: Spectral Contribution of Galileo E1-B Data Stream to the tansmitted SIS.

As last example, a frequency portion of the Galileo E1-B and Galileo E1-C signals PSDs for SVID 1 is displayed respectively in Figure 2–9 and Figure 2–10. The spectral contribution of the primary codes and the smooth spectrum are also represented respectively in red line and in dashed black line.

Figure 2–9 shows how the effect of the data sequence is to smooth the spectra lines of the E1-B component; the same is observed in Figure 2–10 where the effect of the

secondary code is to modulate the primary code spreading the power over more spectral lines. Even with the effect of the secondary code, note that the power of E1-C is by nature concentrated on spectral lines while the E1-B spectrum is continuous.

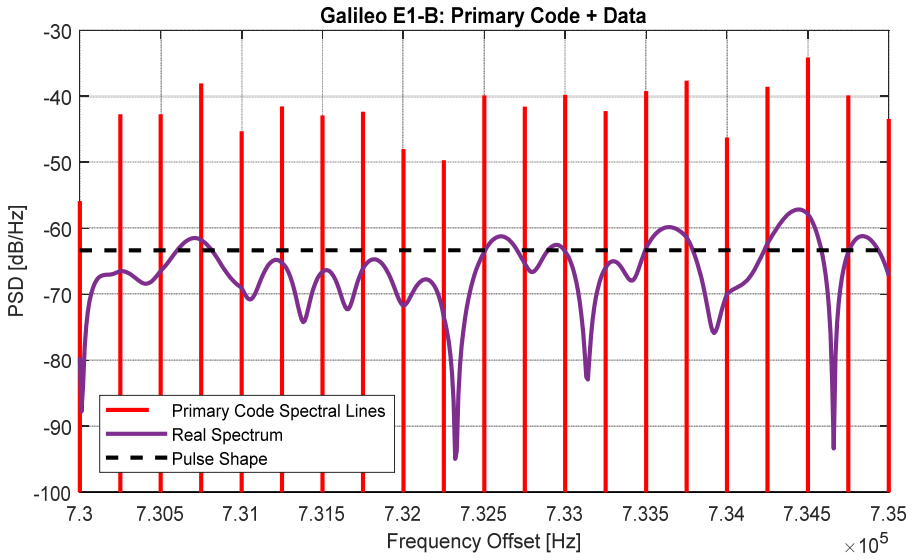

Figure 2–9: PSD of Galileo E1-B SVID 1 transmitted SIS (detail).

Further details on the Galileo E1 OS signal are given in Appendix A, where the computation of the PSD with the spectral line approach is applied to the complete Galileo signals baseline.

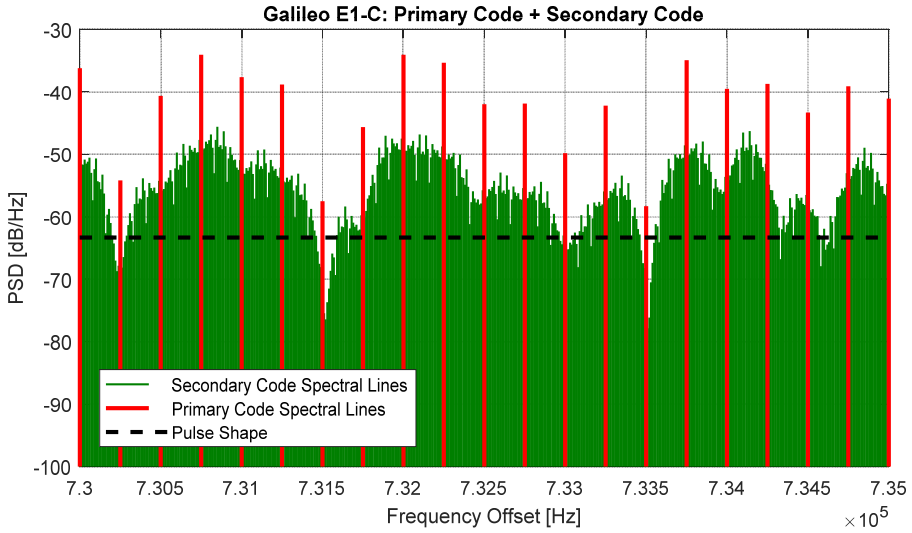

Figure 2–10: PSD of Galileo E1-C SVID 1 transmitted SIS (detail).

2.2 Receive Signal

Figure 2–11 depicts the block diagram of a generic GNSS user receiver from the antenna reception until the PVT computation. The following five functional units can be identified:

- The Antenna Unit, that can be either a passive or active element, represents the first part of the receive chain and it acquires the broadcasted navigation signals. A typical GNSS antenna can be single-frequency (L1 only) or dual-frequency (e.g. L1/L2 or L1/L5) depending on the application. Active antennas often include analog pass-band filtering for out-of-band rejection and a first stage Low-Noise Amplifier (LNA).
- The RF Front-End Unit, that is responsible for conditioning the analog signal so that it is suitable for digital signal processing. The main stages are identified as low-noise amplification, band-pass filtering for Out-Of-Band (OOB) interference rejection, down-conversion and digitalization (sampling and quantization). The down-conversion can be performed either at intermediate frequency or directly to base-band.

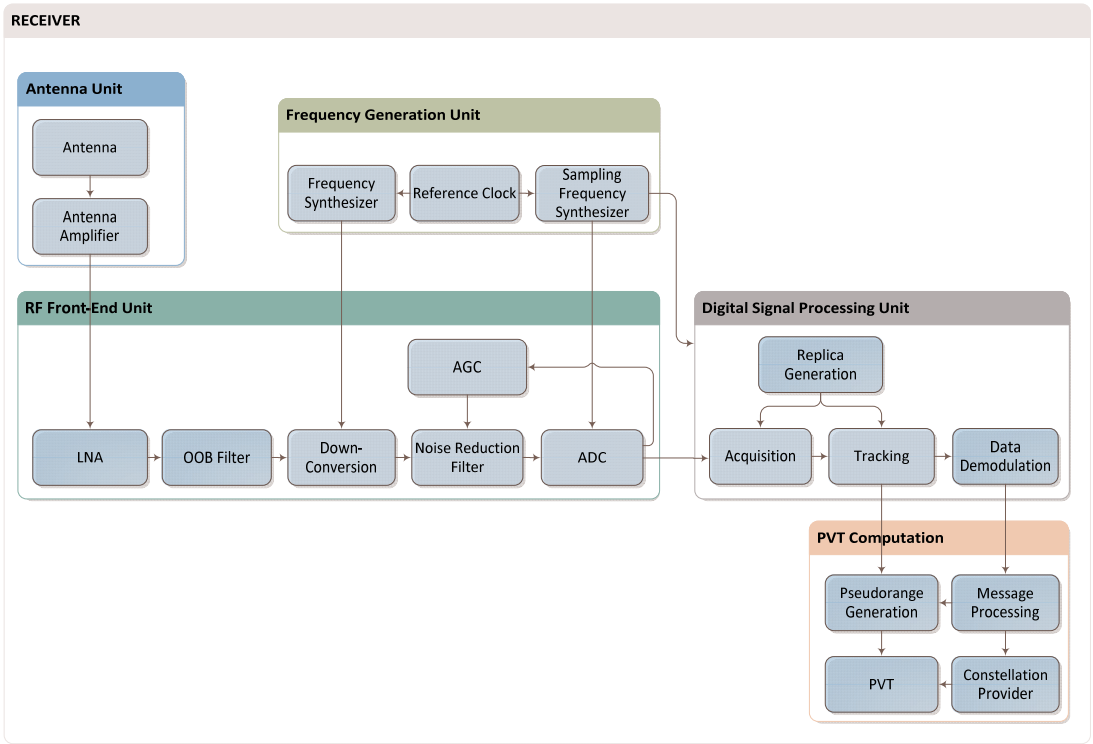

Figure 2–11: Receive Chain, Functional Block Diagram.

- The Frequency Generation Unit, in charge of providing the reference frequency signal for all internal timing and synchronization.

- The Digital Signal Processing Unit, that takes as input the streams of In-phase/Quadrature (I/Q) digitalized samples and implements the following functionalities: acquisition and tracking of the navigation signals, computation of pseudorange and carrier phase measurements, and decoding of navigation data messages.
- The PVT Computation, that starts from the measures provided by the DSP Unit and calculates for all tracked signals the corresponding satellite positions, satellite velocities, and atmospheric corrections. This information is used for resolving the measurements ambiguity and generating pseudoranges that are combined to obtain the Position, Velocity, and Time (PVT) information.

Before entering into the time and frequency domain representation of GNSS signals at receiver side, it is worth dedicating few more lines to the RF Front-End Unit. The key component of the front-end is the down-conversion that converts the RF signal to a lower frequency, while providing gain and filtering. In GNSS receivers, two approaches are commonly used to implement the down-conversion function.

The first and oldest method is the heterodyning chain. In this approach the RF signal is first filtered and then multiplied with a sine wave to convert it to an IF frequency, usually between 50 and 400 MHz. A band-pass filter further rejects OOB signals, after which the IF signal is amplified. Sometimes the process is repeated in a second stage with similar topology. Finally the signal is quantized by the ADC. The sampling frequency of the ADC is directly related to the IF frequency to make sure that the signal is captured without aliasing effects.

More recently the direct conversion architecture gained popularity. In this architecture the RF signal is multiplied with a complex sinusoid, introducing an in-phase and quadrature branch. This is filtered by a low-pass filter and amplified. The amplified signal is quantized by a two-channel ADC running at a frequency higher than the targeted signal bandwidth. The approaches are almost equivalent but the latter is taken as assumption for the following signal description.

Further, typical GNSS user receiver features such as secondary channels for aiding information, integrity algorithms for safety critical applications, and sensor fusion are not depicted in Figure 2–11 as they are out of the scope of this thesis.

The receive signal model introduced in the next section is based on the same assumption taken for the transmit signal that no distortions are introduced in the payload generation chain. Additionally, it is supposed that the propagation channel is not dispersive in time or frequency, thus the useful signal is only attenuated and delayed.

2.2.1 Time Domain Representation

The expression of the receive signal at the input of the receiving antenna is given by:

$$\begin{aligned} r_{RF}(t) &= y_{RF}(t) + v_{RF}(t) + \eta_{RF}(t) \\ &= A_R \cdot s_{BB}(t-\tau) \cdot cos(2\pi(f_{RF}+f_D)t + \varphi) + v_{RF}(t) + \eta_{RF}(t) \end{aligned} \quad (2.26)$$

where:

$y_{RF}(t)$	navigation signal
A_R	amplitude coefficient at reception
τ	delay of the navigation signal
f_D	Doppler frequency of the navigation signal
φ	phase offset of the navigation signal
$v_{RF}(t)$	interference term
$\eta_{RF}(t)$	noise term

The amplitude A_R is related to the received power level by the relation $P_R = {A_R}^2/2$, that can be further expressed as a function of the user location (φ, θ) and time instant t through the link budget:

$$P_R(t,\varphi,\theta) = \frac{EIRP \cdot G_R}{L_{FS} L_{\text{other}}}\Big|_{(t,\varphi,\theta)} \quad (2.27)$$

where:

P_R	user received power [W]
$EIRP$	EIRP as defined in Eq. (2.16) [W]
G_R	user receiver antenna gain [unitless]
L_{FS}	free space path loss [unitless]
L_{other}	other losses [unitless]

The free space loss is the loss in signal strength of an electromagnetic wave that results from a Line-Of-Sight (LOS) path through free space, i.e. a space with no

obstacles nearby to cause reflection or diffraction. This term is defined by the following well-known formula:

$$L_{FS} = \left(\frac{c}{4\pi f_{RF} R}\right) \tag{2.28}$$

being c the speed of light [m/s^2] and R the distance [m] between the user receiver and the satellite vehicle (SV). The inter-distance between user and SV can be further expressed by the following equation:

$$R = \begin{cases} \dfrac{\sin(\pi/2 - \beta - \varepsilon)}{\sin(\varepsilon + \pi/2)}, & \varepsilon \neq \pi/2 \\ R_{SV} - R_{\text{user}}, & \text{otherwise} \end{cases} \tag{2.29}$$

with R_{SV} the SV position and R_{user} the user position in ECEF Cartesian coordinate frame. ε is the elevation angle [rad] of the satellite with respect to the user position and β the off-boresight angle [rad].

For what concerns L_{other}, it groups all the other contributions to the signal attenuation at the input of the receiver antenna. It can be broken down into the product of different terms, usually the atmospheric loss L_{ATM}, the polarization mismatch loss L_{PM} and the depointing loss L_D.

The dominant sources of signal attenuation in the atmosphere are atmospheric gases such as dry air (Oxygen, O_2) and water vapour (or H_2O molecules), rain fall, clouds or fog, tropospheric scintillation, and ionospheric effects. Each of these components has been studied in literature and various theoretical models exist to analyse the signal power attenuation caused by the attenuation sources described above.

Another source contributing to the signal attenuation is the polarization mismatch loss, which occurs when the polarization of the incident wave is different from the polarization of the receiving antenna. This mismatch can be caused by two major reasons: the atmospheric effects or the Faraday rotation. Moreover, the transmitting and receiving antennas do have different polarizations with respect to each other, due to imperfections in manufacture.

Finally an imperfect alignment of the transmitting and receiving antennas due to satellite attitude error, array antenna pointing misalignment, or gain fluctuation by temperature variation, can cause a fallout of the antenna gain with respect to the maximum gain. This is referred to as depointing loss.

With reference to the block diagram in Figure 2–11, assuming an ideal RF Front-End Unit, the following digital signal model is obtained at the output of the ADC module:

$$r_{BB}(nT_s) = A_R \cdot s_{BB}(nT_s - \tau) \cdot cos(2\pi f_D nT_s + \varphi) + \nu_{BB}(nT_s) + \eta_{BB}(nT_s) \quad (2.30)$$

being T_s the sampling period, inverse of the sampling frequency f_s.

In the following, the notation $x[n]$ or x_n is used to indicate discrete-time signals $x[nT_s]$ obtained by sampling continuous-time signals $x(t)$ with a sampling frequency of f_s. The digital received signal is then written as:

$$r_{BB}[n] = A_R \cdot s_{BB}[n - T] \cdot cos[2\pi\theta_D n + \varphi_0] + \nu_{BB}[n] + \eta_{BB}[n] \quad (2.31)$$

where $T = \tau/T_s$ and $\theta_D = f_D/f_s$.

A convenient choice is normally to sample the down-converted BB signal with a sampling frequency $f_s = 2B_{FE}$, where B_{FE} is the front-end frequency. In this case the discrete-time random process $\eta_{BB}[k]$ is a white sequence with zero mean and variance ${\sigma_\eta}^2 = N_0\, f_s/2$.

The term $\nu_{BB}[n]$ represents various sources of interference. The first source of in-band interference is represented by the so-called GNSS intra- and inter-system interference:

$$\nu_{BB}[n] = \sum_{m=1}^{M^X} \sum_{n=1}^{N_m^X} A_R^{m,n} \cdot s_{BB}^{m,n}[n - T^{m,n}] \cdot cos[2\pi\theta_D^{m,n} n + \varphi^{m,n}] \quad (2.32)$$

where M^X is the number of visible satellites in the constellation identified by X (e.g. GPS, Galileo, BeiDou, IRNSS), N_m^X is the number of signals transmitted by the m-th satellite in the constellation identified by X, and all variables are defined as for the desired navigation signal in Eq. (2.31). The relevance of this interference contribution is strongly related to the main objective of this thesis and it is widely discussed in the following chapters.

Regarding the external sources of interference, depending on the GNSS signal bandwidth it may be categorized as being of the narrow-band (NB) type, if the interferer bandwidth $B_i \ll B_{GNSS}$, or wide-band (WB) type, if B_i is comparable or larger than B_{GNSS}. Looking at its characteristics in the time domain, an interfering signal may be either continuous or pulsed. Additionally, an interference source may be either in-band, partially in-band, or out-of-band with respect to the radio-frequency spectrum occupied by the GNSS signal of interest. Figure 2–12 displays

typical external interference sources and ITU allocations versus the RNSS frequency spectrum.

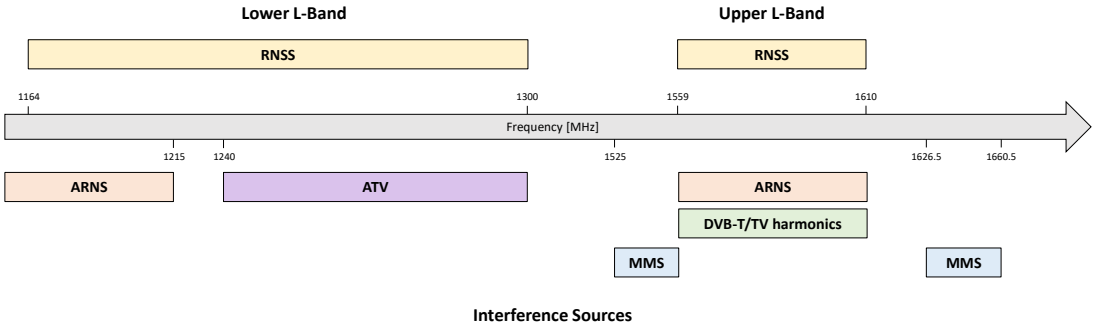

Figure 2–12: Interference sources frequency bands.

A very useful operator at receiver side is represented by the linear Cross-Correlation Function (CCF) between the sampled received signal $r_{BB}[n]$ and the digital local replica. The CCF is at the basis of the acquisition and tracking functions of the DSP Unit shown in Figure 2–11. The expression of the CCF is given by:

$$R_{r,s}[m] = \frac{1}{N_I}\sum_{n=0}^{N_I-1} \bar{s}^*[n]\cdot r_{BB}[n+m] = \bar{s}^*[-m] * r_{BB}[m] \tag{2.33}$$

being $\bar{s}[n]$ the discrete-time version of the $s_{BB}(t)$ periodic sequence described in Eq. (2.6) and N_I the number of samples in the integration window. The CCF $R_{r,s}[m]$ relates to the linear convolution operator '*' as expressed in Eq. (2.33) and to the power spectral density as:

$$R_{r,\bar{s}}[m] = T_s \int_{-1/2T_s}^{+1/2T_s} \bar{S}^*(f) R_{BB}(f) e^{j2\pi f T_s m} df = \mathcal{F}^{-1}\{\bar{S}^*(f) R_{BB}(f)\} \tag{2.34}$$

where $\bar{S}(f)$ and $R_{BB}(f)$ are the Fourier transform of respectively $\bar{s}[n]$ and $r_{BB}[n]$. By considering the random nature of the navigation signals it is possible to express the statistical cross-correlation function $\tilde{R}_{r,\bar{s}}(t_1, t_2)$ as defined by:

$$\begin{aligned}\tilde{R}_{r,\bar{s}}[m_1, m_2] &= \mathrm{E}\{\bar{s}^*[m_1] r_{BB}[m_2]\} \\ &= \int_{-\infty}^{+\infty}\int_{-\infty}^{+\infty} \mathrm{E}\left\{\left[\sum_{n=-\infty}^{+\infty} c[n]\cdot\delta(\alpha - nT_X)\right]\cdot\left[\sum_{n=-\infty}^{+\infty} c[n]\cdot\delta(\beta - nT_X)\right]\right\}\cdot \\ &\qquad p_{\bar{s}}(m_1-\alpha) p_r(m_2-\beta) d\alpha \\ &= \int_{-\infty}^{+\infty}\int_{-\infty}^{+\infty} \tilde{R}_c(\alpha-\beta)\, p_{\bar{s}}(t_1-\alpha) p_r(t_2-\beta) d\alpha\, d\beta\end{aligned} \tag{2.35}$$

and by a substitution of variables (see [5]), it can be demonstrated that:

$$\tilde{R}_{r,\bar{s}}[m] = T_s \int_{-1/2T_s}^{+1/2T_s} G_c(f) P_{\bar{s}}(f) P_r^*(f) e^{j2\pi f T_s m} df = \tilde{R}_c[m] * p_{\bar{s}}[m] * p_r^*[m] \quad (2.36)$$

Note that in general the pulse shape of the transmit signal and the receiver local replica is the same, leading to the following simplification:

$$\tilde{R}_{r,\bar{s}}[m] = \tilde{R}_c[m] * R_p[m] \quad (2.37)$$

An exception is represented by the Galileo E1 OS service that is transmitted with the CBOC modulation and it is processed by aviation receivers as a BOC(1,1) signal.

2.2.2 Frequency Domain Representation

The periodic structure of navigation signals results in a frequency spectral content of discrete nature. As a result, the linear CCF operation described before turns out to be equivalent to a circular CCF. Approximating the linear CCF with the circular one has the advantage that the correlation values can be calculated in the frequency domain with the FFT approach allowing for a fast computation.

The difference between linear and circular CCF is illustrated in Figure 2–13 and Figure 2–14:

- Linear CCF (Figure 2–13): for each relative delay m, the conjugated local replica $\bar{s}[n]$ is multiplied by a portion, of equal duration T_I, of the receive signal $r_{BB}[n+m]$; the product is then integrated over the local replica length. The portion of the receive signal shifts with index m and the samples discarded on one side are substituted with zeros on the other (zero-padding).

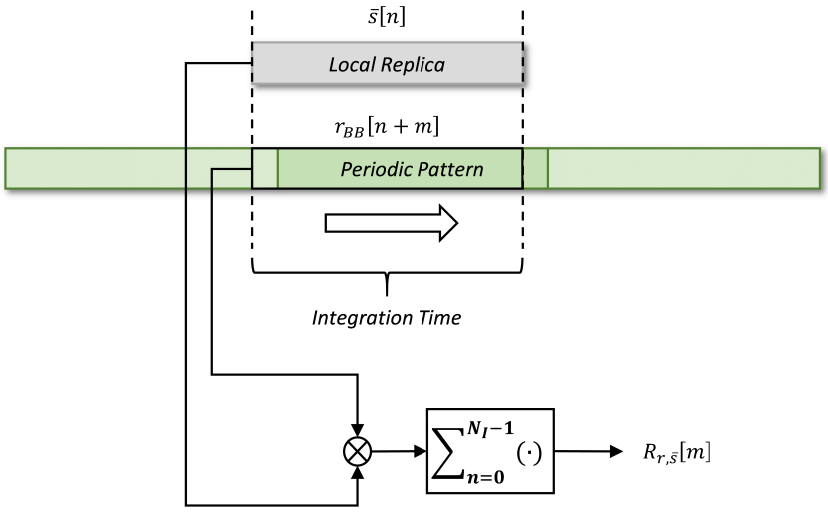

Figure 2–13: Linear Cross-Correlation Function: Illustration.

- Circular CCF (Figure 2–14): for each relative delay m, the conjugated local replica $\bar{s}[n]$ is multiplied by a portion, of equal duration T_I, of the receive signal $r_{BB}[n+m]$; the product is then integrated over the local replica length. The portion of the receive signal shifts with index m and the samples discarded on one side are added on the other in a circular manner.

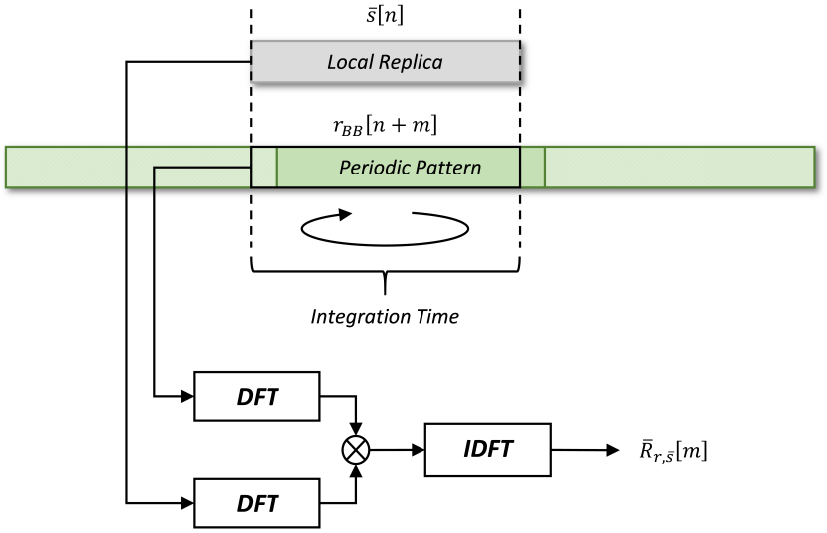

Figure 2–14: Circular Cross-Correlation Function: Illustration.

Note that, in principle, when considering the CCF between the local replica and the entire receive signal, the linear operation equals de facto the circular one as, given the periodic pattern characterizing the signal structure, if the previous and following sequences are not sign-inverted for a bit or secondary code chip transition, a linear shift is equivalent to a circular shift.

3. Pseudo-Random Noise Codes

Most of nowadays GNSS systems are based on Direct Sequence Spread Spectrum (DSSS) signalling. This technique consists of adding a third component, namely spreading code or Pseudo Random Noise (PRN) code, which is typically periodic, known at the receiver, and transmitted at a higher rate than the navigation data. The signal just described is also called spread spectrum because of the wider bandwidth resulting from the spreading operation. The transmission of multiple DSSS signals having different spreading sequences on a common carrier frequency is referred to as Code Division Multiple Access (CDMA). A complete overview of spread spectrum systems can be found in [4].

In every CDMA based navigation system the design of PRN sequences requires the generation but also the evaluation of different code sets in order to select the best possible design. Hence criteria need to be identified in order to measure their performance. Selecting the best code means selecting the code that performs best when measured against a metric considered to represent the 'goodness' of a code. The PRN codes design for satellite navigation systems is driven by the following desired signal properties:

- Each individual signal needs to be distinguishable from a time shifted version of itself.
- Any individual signal must not be mixed up with any other signal originating from the same set.

The first point mentioned above refers to the auto-correlation properties, expressed in Chapter 2 with Eq. (2.9). By definition, only white noise signals present an ideal ACF, i.e. a Dirac delta function in the origin and zero for any other delay. In the discrete domain, good auto-correlation properties are achievable through pseudo-random sequences with a good statistical 'randomness'. The identification of sequences with good performance in terms of auto-correlation is essential not only for GNSS but also for ranging applications (e.g. radar systems), cryptographic systems, and CDMA-based communication systems.

The second property is described by the cross-correlation function, defined in Chapter 2 with Eq. (2.33). Again, only white noise signals present ideal CCF. The

identification of pseudo-random sequences as much as possible uncorrelated is essential for distinguishing one signal source from any other in CDMA systems.
The selection of spreading sequences showing optimal auto- and cross-correlation properties must be performed considering some design constraints related to the following parameters:

- code rate or chip rate,
- code length or period,
- chip shape and/or modulation.

System designers need to select the best code structure and, within it, the best PRN code set from the spreading code family.
Two methods for the generation of spreading codes can be identified when looking at the current open service navigation signals. The first one is based on m-sequences produced by shift registers. Operations like shifting and combining m-sequences enables the creation of more complex pseudo-random codes. This is the case of the Gold codes for the GPS L1 C/A signal. Other examples are the Galileo E5a and E5b and GPS L5 codes which are truncated Gold-codes. A detailed description of the generation of this type of codes can be found in [8], [9], [11]. The second method is based on the design of an optimization algorithm to fulfil simultaneously different selection criteria (see [23]). Such codes are referred as randomly optimized spreading codes and a typical example is represented by the Galileo E1 OS signals. A good overview of spreading code families commonly adopted in GNSS signals design is provided in [28]. The investigation of new PRN code families or a mathematical analysis on the randomness properties of existing ones is out of scope of the thesis.
The objective of this chapter is to provide the means for assessing the CDMA isolation of a PRN code set with it-self (self-interference) and with another PRN code set (cross-interference). A deep understanding of the PRN code properties, design parameters, and performance figures is at the basis of the radio-frequency compatibility analysis performed in Chapter 4.
The chapter is composed of the following parts:

- Section 3.1 provides an overview of all publicly known PRN codes currently (or planned to be) transmitted by GNSS providers.

- Section 3.2 recalls for completeness the measures of randomness for a spreading code set, i.e. the three Golomb's postulates.
- Section 3.3 derives the auto- and cross-correlation formulas at the basis of spreading codes performance figures and describes well recognized figures of merit for PRN codes design.
- Section 3.4 presents a sensitivity study based on the figures of merit introduces in Section 3.3 that explores the CDMA isolation of a PRN code set with respect to some signal design parameters as well as Doppler frequency and receiver integration time.
- Section 3.5 describes the approach of how to extend the figures of merit in Section 3.3 for assessing the CDMA isolation between two different PRN code sets.

Note that GLONASS signals are left out from the spreading codes overview and from the following correlation performance analysis. The Russian satellite navigation system is currently the only one adopting a combination of FDMA and CDMA techniques for implementing multiple access. The allocation of PRN sequences and frequency sub-channels to the SVs is based on the constellation geometry with the purpose of minimising intra-system interference. GLONASS signals require a dedicated analysis as the correlation properties of PRN codes need to be analysed in combination with the frequency allocation.

3.1 Overview on GNSS Legacy PRN Codes

An overview on the current and planned GNSS signal characteristics is provided below. Table 3-1, Table 3-2, Table 3-3, Table 3-4, and Table 3-5 summarize the main parameters related to PRN codes for GPS, Galileo, BeiDou, QZSS, and IRNSS legacy signals. The information is mostly taken from public ICDs and refers to open services.

Table 3-1: GPS Open Services: PRN Codes Parameters [9], [10], [11].

Signal Name		*Primary Codes*			*Secondary Codes*			*Data*	
		Length [chip]	*Period [ms]*	*Chip Rate [Mcps]*	*Length [chip]*	*Period [ms]*	*Chip Rate [cps]*	*Rate [sps]*	*Duration [ms]*
GPS L1	**L1-C/A**	1,023 Code No 1-32	1	1×1.023	-	-	-	50	20
	L1-C data	10,230 Code No 1-63	10	1×1.023	-	-	-	100	10
	L1-C pilot	10,230 Code No 1-63	10	1×1.023	1800 $L1C_{01\text{-}63}$	18000	100	-	-
GPS L5	**L5-I**	10,230 Code No 1-37	1	10×1.023	10 NH10	10	1000	100	10
	L5-Q	10,230 Code No 1-37	1	10×1.023	20 NH20	20	1000	-	-
GPS L2	**L2-CM**	10,230 N/A	20	0.5×1.023	-	-	-	50	20
	L2-CL	767,250 N/A	1500	0.5×1.023	-	-	-	-	-

Table 3-2: Galileo Open Services: PRN Codes Parameters [8].

Signal Name		*Primary Codes*			*Secondary Codes*			*Data*	
		Length [chip]	*Period [ms]*	*Chip Rate [Mcps]*	*Length [chip]*	*Period [ms]*	*Chip Rate [cps]*	*Rate [sps]*	*Duration [ms]*
GAL E1	**E1-B**	4,092 No 1-50	4	1×1.023	-	-	-	250	4
	E1-C	4,092 No 1-50	4	1×1.023	25 $CS25_1$	100	250	-	-

Signal Name		*Primary Codes*			*Secondary Codes*			*Data*	
		Length [chip]	*Period [ms]*	*Chip Rate [Mcps]*	*Length [chip]*	*Period [ms]*	*Chip Rate [cps]*	*Rate [sps]*	*Duration [ms]*
GAL E5	**E5a-I**	10,230 No 1-50	1	10×1.023	20 $CS20_1$	20	1000	50	20
	E5a-Q	10,230 No 1-50	1	10×1.023	100 $CS100_{1-50}$	100	1000	-	-
	E5b-I	10,230 No 1-50	1	10×1.023	4 $CS4_1$	4	1000	250	4
	E5b-Q	10,230 No 1-50	1	10×1.023	100 $CS100_{51-100}$	100	1000	-	-
E6 CS	**E6-B**	5,115 N/A	1	5×1.023	-	-	-	1000	1
	E6-C	5,115 N/A	1	5×1.023	100 $CS100_{1-50}$	100	1000	-	-

Table 3-3: BeiDou Open Services: PRN Codes Parameters [12].

Signal Name		*Primary Codes*			*Secondary Codes*			*Data*	
		Length [chip]	*Period [ms]*	*Chip Rate [Mcps]*	*Length [chip]*	*Period [ms]*	*Chip Rate [cps]*	*Rate [sps]*	*Duration [ms]*
B1	**B1-I**	2,046 Code No 1-37	1	2×1.023	20 NH20	20	1000	50	20
B2	**B2-I**	2,046 Code No 1-37	1	2×1.023	20 NH20	20	1000	50	20

Table 3-4: QZSS Open Services: PRN Codes Parameters [14].

Signal Name		*Primary Codes*			*Secondary Codes*			*Data*	
		Length [chip]	*Period [ms]*	*Chip Rate [Mcps]*	*Length [chip]*	*Period [ms]*	*Chip Rate [cps]*	*Rate [sps]*	*Duration [ms]*
QZS L1	**L1-C/A**	1,023 N/A	1	1×1.023	-	-	-	50	20
	L1-SAIF	1,023 N/A	1	1×1.023	-	-	-	500	2
	L1-C data	10,230 N/A	10	1×1.023	-	-	-	100	10
	L1-C pilot	10,230 N/A	10	1×1.023	1800 $L1C_{01-63}$	18000	100	-	-
QZS L5	**L5-I**	10,230 N/A	1	10×1.023	10 NH10	10	1000	100	10
	L5-Q	10,230 N/A	1	10×1.023	20 NH20	20	1000	-	-
QZS L2	**L2-CM**	10,230 N/A	20	0.5×1.023	-	-	-	50	20
	L2-CL	767,250 N/A	1500	0.5×1.023	-	-	-	-	-
QZS L6	**LEX data**	10,230 Code No 193-197		2.5×1.023	-	-	-	250	
	LEX pilot	1,048,575 Code No 193-197		2.5×1.023	-	-	-	-	-

Table 3-5: IRNSS Open Services: PRN Codes Parameters [13].

Signal Name		*Primary Codes*			*Secondary Codes*			*Data*	
		Length [chip]	*Period [ms]*	*Chip Rate [Mcps]*	*Length [chip]*	*Period [ms]*	*Chip Rate [cps]*	*Rate [sps]*	*Duration [ms]*
SPS	**L5**	1,023 Code No 1-37		1×1.023	-	-	-	50	20

3.2 Randomness Properties

The main target in the design of pseudo-random codes is to approach as much as possible the characteristics of pure random sequences. The measure of randomness for a spreading code set can be computed by evaluating the three Golomb's postulates as described in [25]. For completeness, the postulates are stated below and the figures of merit derived in [25] for evaluating the postulates are also recalled. Note that it is out of scope of this thesis to assess the randomness properties of existing spreading code families. This section however helps understanding the performance figures at the basis of the PRN code set selection.

3.2.1 Definitions

Let $c[n] = c[0], c[1], \ldots, c[N-1]$ be a finite binary sequence of length N. A run of $c[n]$ is defined as a sub-sequence consisting of uninterrupted equal symbols (0's or 1's) preceded and succeeded by the opposite symbol. A run of 0's is called 'gap' and a run of 1's is called 'block'. The sequence $c[n]$ can be considered random if it satisfies the three Golomb's postulates:

1. *Balance*: the number of 1's should differ from the number of 0's by at most one.
2. *Run Property*: at least half of the total number of runs should have length 1, at least one-fourth length 2, one-eight length 3, and so forth until the number of runs left is one. Additionally, for each of these equal-length groups, there should be almost an equal number of blocks and gaps.
3. *Ideal Autocorrelation*: The autocorrelation function ACF should be two-valued, i.e. $R[m] = 1$ for $m = 0$, and $R[m] = -1/N$ for $m \neq 0$.

3.2.2 Randomness Performance Criteria

The performance figures derived in [25] for evaluating the postulates are summarised in the following.

Normalised Balance Factor (NBF):

$$NBF = \begin{cases} \frac{1}{K}\sum_{k=1}^{K}\frac{|N_k^0 - N_k^1|}{N} & \text{for } N \text{ even} \\ \frac{1}{K}\sum_{k=1}^{K}\frac{|N_k^0 - N_k^1| - 1}{N} & \text{for } N \text{ odd} \end{cases} \tag{3.1}$$

where K is the cardinality of the PRN code set, N_k^0 is the number of 0's and N_k^1 is the number of 1's for the spreading code $c_k[n]$.

Run Factor (RF) and Average RF:

Let C_k^ℓ be the number of runs of length $\ell, \ell \in [1, L_{\max}]$ for the spreading code $c_k[n]$, and let C_k be the total number of runs.

$$RF_k = \frac{1}{L_{\max,k}}\sum_{\ell=1}^{L_{\max,k}}\left(\frac{C_k^\ell}{C_k}\right)^2\left(1 - 2^\ell\frac{C_k^\ell}{C_k}\right)^2 \tag{3.2}$$

$$ARF = \frac{1}{K}\sum_{k=1}^{K} RF_k \tag{3.3}$$

Gaps to Blocks Factor (GBF) and Average GBF:

Let $C_k^{G,\ell}$ be the number of gaps and $C_k^{B,\ell}$ the number of blocks of length $\ell, \ell \in [1, L_{\max}]$ for the spreading code $c_k[n]$.

$$GBF_k = \frac{1}{L_{\max,k}}\sum_{\ell=1}^{L_{\max,k}}\left(\frac{C_k^\ell}{C_k}\right)^2\left(1 - \frac{C_k^{G,\ell}}{C_k^{B,\ell}}\right)^2 \tag{3.4}$$

$$AGBF = \frac{1}{K}\sum_{k=1}^{K} GBF_k \tag{3.5}$$

Auto-Correlation Deviation Factor (ACDF) and Average ACDF:

$$ACDF_k = \frac{1}{N-1}\sum_{n=2}^{N}\left(1 - \frac{ACF_k[n]}{-1/N}\right)^2 \tag{3.6}$$

$$AACDF = \frac{1}{K}\sum_{k=1}^{K} ACDF_k \tag{3.7}$$

The randomness properties are strictly linked to the auto- and cross-correlation properties discussed in Section 3.3.

3.3 Auto- and Cross-Correlation Properties

As already mentioned above, two commonly used metrics to weight the goodness of spreading codes are the auto-correlation and the cross-correlation.

The derivation of the correlation function between spreading codes is well known from literature ([3] and others), therefore it is out of the scope of this thesis to repeat

it. The correlation expressions valid for any PRN code family are only recalled, as they constitute the basis for the following analysis. Below the assumptions underlying the correlation expressions are listed:

- With reference to the notation adopted in Chapter 2, no distinction is done whether the spreading code family is for primary or secondary use, thus the subscripts P, S, or X are omitted.
- As this chapter focusses on the PRN codes properties, only the discrete code sequence $c[n]$ is considered instead of the complete navigation signal $s(t)$ described in Eq. (2.4). The discrete code sequence is sampled at chip rate.
- It is assumed that the generic couple of codes $c_\ell[n]$ and $c_j[n]$ belong to the same code family with length N. The removal of this assumption is discussed in Section 3.5.
- In a first place the integration window length N_I, as defined in Eq. (2.33), is assumed to be equal to the code length N. Section 3.4.1 explains the impact of the integration window on the correlation properties in relation to other parameters.
- Symbols overlying the spreading codes (navigation data bits or secondary code chips) have an impact on the correlation properties. A stream of binary symbols modulated with BPSK technique is assumed as it is the most commonly adopted for navigation signals.

3.3.1 Definitions

The discrete-time linear correlation function between codes $c_\ell[n]$ and $c_j[n]$ is defined as:

$$R_{j,\ell}[m] = \frac{1}{N_I}\sum_{n=0}^{N_I-1} c_j^*[n]\cdot c_\ell\,[n-m]\,, \text{for } m \in [0, 2N_I-1] \tag{3.8}$$

where '*' as superscript denotes the complex conjugation. The expression above gives an indication about the interaction between the two codes. In order to distinguish one signal from the other, the function $R_{j,\ell}[m]$ shall be:

- as small as possible for $j \neq \ell$ and for any value of m,
- as small as possible for $j = \ell$ and for any value of $m \neq 0$,
- as big as possible for $j = \ell$ and for $m = 0$.

The first bullet point refers to the CCF while the second and the third points refer to the ACF out-of-phase and in-phase values. Here it is assumed that the same mathematical expression is valid for both CCF and ACF by simply considering $j \neq \ell$ for the former and $j = \ell$ for the latter.

In order to take into account for the impact of the modulated symbols onto the function $R_{j,\ell}[m]$, it is reminded that a phase shift of $\pm\pi$, as it is the case for BPSK, can be expressed also as an Amplitude Modulation (AM). In other words, the BPSK overlay sequence assumes values in the discrete sample space $\{-1, +1\}$. As a matter of fact, the sign of the PRN code sequence is inverted if the signal is modulated by BPSK symbols.

The presence of two consecutive symbols with opposite sign leads to the inversion of the spreading code sequence in the received signal. When no sign flip occurs, the correlation function is represented by Eq. (3.8) and it is referred to as 'even' CF. In the case of a sign flip, the corresponding CF is called 'odd' and it is defined as:

$$R_{j,\ell}[m] = \frac{1}{N_I} \sum_{n=0}^{N_I-1} (-1)^b \cdot c_j^*[n] \cdot c_\ell\ [n-m]\,, \text{for } m \in [0, 2N_I - 1] \tag{3.9}$$

$$\text{with } b = \begin{cases} 1 & \text{if } n \leq m \\ 0 & \text{else} \end{cases}$$

The difference between even and odd correlation is illustrated in Figure 3–1 and Figure 3–2.

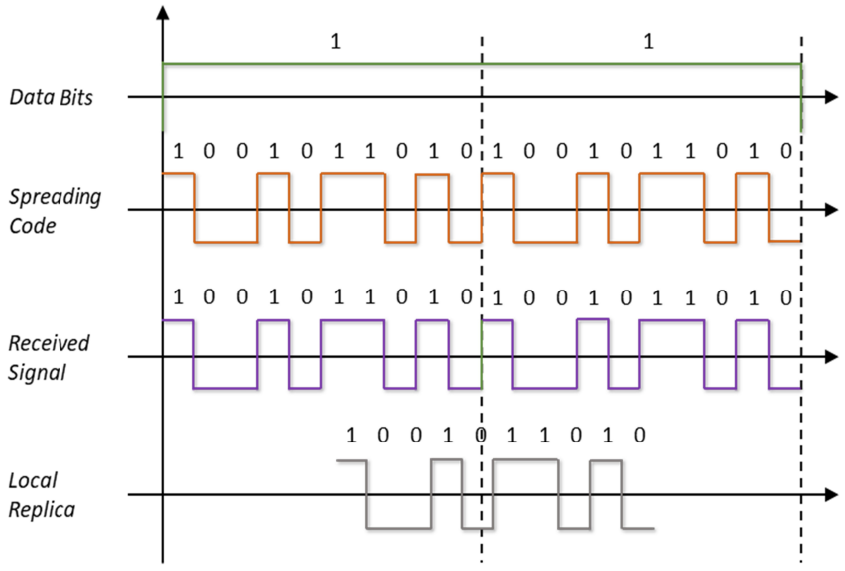

Figure 3–1: Even Correlation.

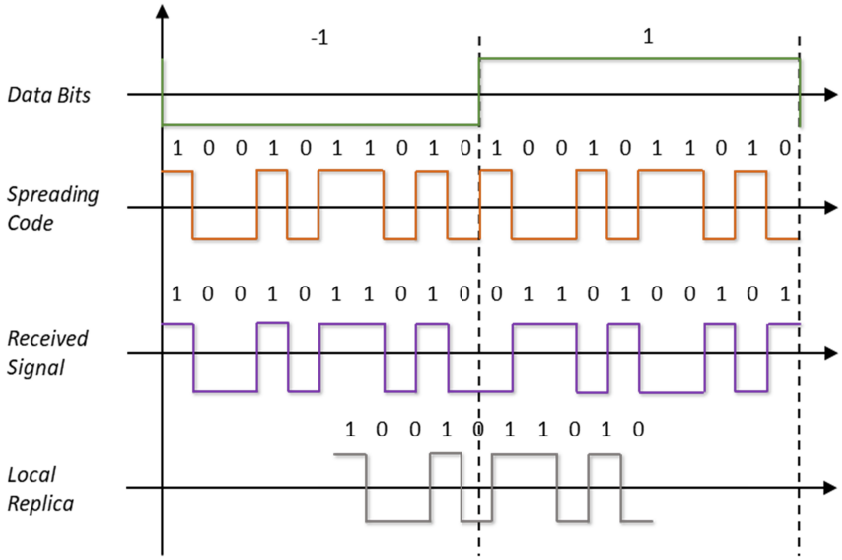

Figure 3–2: Odd Correlation.

The definition of the correlation function in Eq. (3.8) and (3.9) does not account for the impact of the relative motion between satellite and user. When looking at correlation properties in a dynamic system, it becomes necessary not only to consider offsets in the time domain but also a potential offset in the frequency domain caused by the Doppler frequency f_D, which can be as high as ±6 kHz for a static user on Earth observing a passing MEO satellite in L-band.

The correlation function accounting for the Doppler frequency offset between two PRN codes can be defined as:

$$R_{j,\ell}[m] = \frac{1}{N_I}\sum_{n=0}^{N_I-1}(-1)^b \cdot c_j^*[n] \cdot c_\ell\ [n-m] \cdot e^{i(2\pi\Delta\theta_D n+\varphi)}\ \text{, for } m\ \epsilon\ [0, 2N_I-1] \tag{3.10}$$

with $b = 1$ for the even case and $b = \begin{cases} 1 & \text{if } n \le m \\ 0 & \text{else} \end{cases}$ for the odd case

where $\Delta\theta_D = \Delta f_D / f_s$ is the normalized Doppler frequency offset between PRN code j and ℓ, f_s represents the sampling frequency, and φ the Doppler phase rotation.

An important remark must be done regarding the actual software implementation of Eq. (3.10). As explained in Section 2.2.2 there is a difference between linear and circular correlation. The Discrete Fourier Transform is the preferred approach because of its computational efficiency and also because it is at the basis of acquisition techniques typically used in commercial receivers. Additionally, for taking into account the effects of sign flips, the correlation function is computed by extending the integration time to twice the length of the spreading code sequence

and by zero-padding the local replica. The software implementation of the correlation function becomes:

$$R_{j,\ell}[m] = \frac{1}{2N_I} \sum_{k=0}^{2N_I-1} \bar{C}_j^*[k] \cdot C_\ell^D[k] \cdot e^{i2\pi \frac{k}{2N_I} m} = \text{IDFT}\{\bar{C}_j^*[k] \cdot C_\ell^D[k]\} \tag{3.11}$$

where $\bar{C}_j[k]$ is the DFT of the local replica zero-padded over $2N_I$ and $C_\ell^D[k]$ is the Fourier Transform of the received signal including the Doppler frequency offset defined over $2N_I$. Figure 3–3 provides a visual representation of Eq. (3.11).

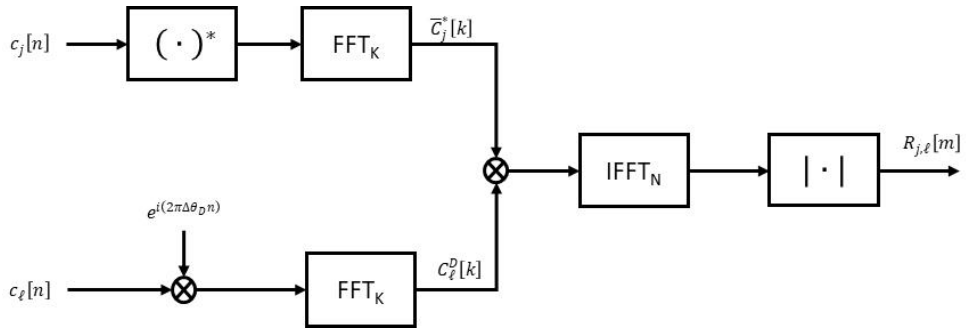

Figure 3–3: Correlation Values Implementaiton.

The result of this operation is displayed in Figure 3–4 where the even and odd ACF are computed for Galileo E1-C SVID 1.

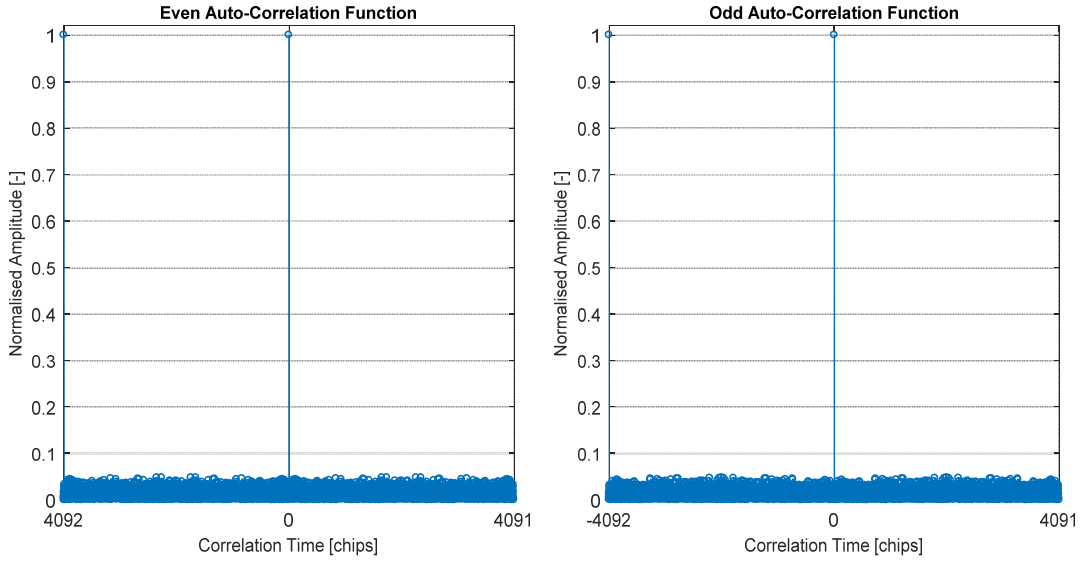

Figure 3–4: Auto-Correlation Function for Galileo E1-C PRN Code 1.

Note that correlation values are doubled due to the circular nature of the DFT computed over a support twice the length of the PRN code ($2N_I = 8184$). In the same way, spreading codes correlation characteristics do not change by integrating over multiple replicas. The effect obtained by applying the correlation operation

over multiple PRN codes is that the signal power, i.e. the correlation magnitudes, grows linearly with the number of replicas. However, when looking at the normalized ACF and CCF magnitudes the amplitude of the correlation peaks is unchanged.

Eq. (3.11) is the selected approach adopted in the next sections for computing the statistics at the basis of spreading codes performance criteria. The integration over multiple replicas is further discussed in Section 3.4.3.

Finally, note that the statistical correlation formulas provided in Chapter 2 are also recalled later and shall be considered as asymptotic behaviour for the linear and circular correlation functions of pseudo-random codes.

3.3.2 Correlation Performance Criteria

Designing codes optimized for all potential GNSS applications and various types of receiver implementations is practically impossible. Therefore, given that the design space of PRN codes is already highly complex and multi-dimensional, the application of a code-centric approach seems the one followed by both Galileo and GPS when designing PRN code sets in the last years.

Calculating all correlation levels for any PRN code set, accounting not only for their relative delay but also including the impact of Doppler frequency offset and data modulation, results in an extremely huge amount of data, which needs to be condensed in some way in order to result in a small number of significant figures being able to characterize the goodness of the set itself. Here are some very well-known approaches taken from [28].

A benchmark for PRN code correlation properties is represented by the so-called Welch Lower Bound, which defines the theoretical minimum of the maximum achievable out-of-phase auto- and cross-correlation magnitudes. [27] provides a mathematical definition of the Welch Bound for any set of PRN sequences. The expression is reported in Eq. (3.12), where K is the cardinality of the PRN code set and N is the length of the sequence. R_W is normalized to the ACF peak.

$$\max_{j,\ell,m}\{R_{j,\ell}[m]\} \geq R_W = \sqrt{\frac{K-1}{KN-1}} \tag{3.12}$$

Taking GPS L1-C/A as an example, the 32 Gold codes with length $N = 1023$ chip result in a maximum side-lobe higher or equal to $20log_{10}\left(\sqrt{\frac{32-1}{32\cdot1023-1}}\right) \cong -30.2$ dB.

One criterion to measure the performance of PRN code sequences is to compare the maximum correlation magnitude with the Welch Lower Bound. The comparison tells, for a given cardinality K and code length N, how good the PRN code family is and if there is margin for improvement. This approach however does not take into account for the statistical distribution of the correlation values, which in some cases can be very low except few outliers.

A way to overcome the limitations represented by this criterion is to look at the so-called Correlation Percentiles (CP). The correlation percentile criterion is a highly valuable figure of merit as it identifies not only potential outliers but also the maximum correlation magnitude and some information about the statistical distribution.

For a given family of PRN codes, the percentiles are computed on the cumulative distribution function of the auto- and cross-correlation magnitudes. In probability theory, given a set of PRN codes $\{c_j[n]\}_{j=1}^{K}$, the following countable sample spaces can be defined:

- $\Omega^{ACF} \subset \mathbb{Q}_o^+$, is the sample space represented by all possible correlation values $R_{j,\ell}^{ACF}[m]$, computed according to Eq. (3.8) and (3.9) respectively for the even and odd case, with $m \in \{1, \dots, N\}, j \in \{1, \dots, K\}, \ell = j$.
- $\Omega^{CCF} \subset \mathbb{Q}_o^+$, is the sample space represented by all possible correlation values $R_{j,\ell}^{CCF}[m]$, computed as in Eq. (3.10), with $m \in \{1, \dots, N\}$, $(j, \ell) \in \{1, \dots, K\}$, $\ell \neq j$ and for a given θ_D.

$R_{j,\ell}^{ACF}[m]$ and $R_{j,\ell}^{CCF}[m]$ are considered as magnitudes (absolute value) and normalized to $R_{j,\ell}^{ACF}[0]$.

Defining the Probability Density Function (PDF) $f_R(r)\colon \Omega \to [0,1]$ for R as $f_R(r) = P(R = r)$, the correlation percentile CP is expressed by the equality:

$$P(R \leq CP) = \int_{-\infty}^{CP} f_R(\rho) d\rho = \hat{P} \tag{3.13}$$

where $\hat{P}$ is a given probability. In words, the $\hat{P}$-th percentile is the value CP below which $\hat{P}$ percent of the correlation magnitudes fall, in the group of all possible correlation values.

Figure 3–5 shows the histogram of occurrences for the discrete set of auto-correlation magnitudes Ω^{ACF} of Galileo E1-C primary PRN codes. Note that formally an histogram of occurrences is not a probability density function, however in this case it is treated as an approximation of $f_R(r)$. The PDF is intentionally not normalized to 1 so that the number of occurrences can be read. The number of events is represented by 50 PRN codes times a code length of 4092 chip (204,600 events). Note that the distribution is mostly concentrated around zero as it is expected for pseudo random noise codes: Figure 3–6 (left) and Figure 3–6 (right) represent narrow slices of the PDF in Figure 3–5, respectively for ACF values respectively close to 0 and 1. A small peak shows the occurrence of $R_{j,\ell}^{ACF}[0] = 1$ that is equal to 50 for a PRN code family of 50 codes.

Going back to the correlation percentiles computation, the smaller the probability $\hat{P}$, the smaller the CP. On the other hand, for $\hat{P} = 100\%$ the correlation percentile CP corresponds to the maximum normalized correlation magnitude, which is always equal to 1 (or 0 dB) for the case of even and odd auto-correlation analysis.

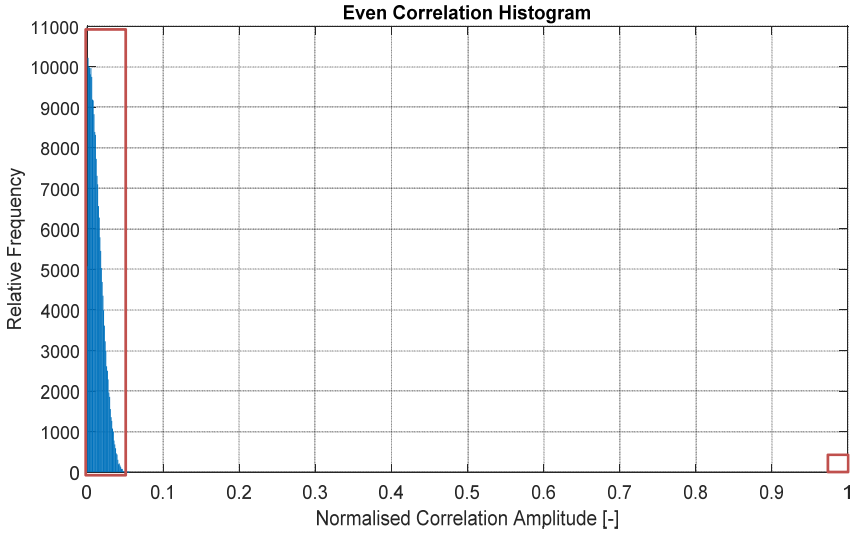

Figure 3–5: Even Auto-Correlation Histogram for Galileo E1-C Primary PRN Codes.

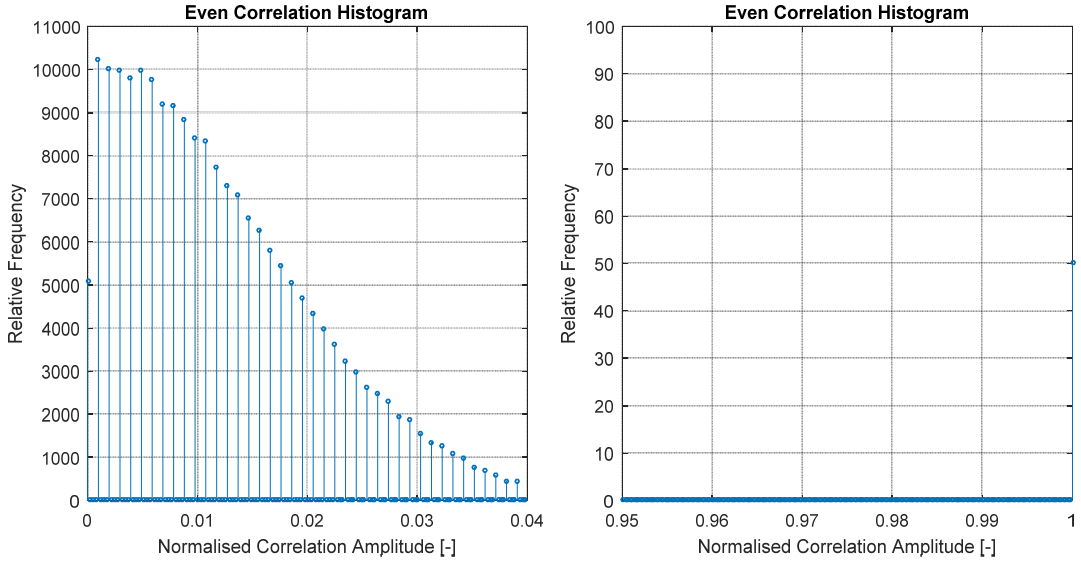

Figure 3–6: Even Auto-Correlation Histogram for Galileo E1-C Primary PRN Codes (details).

Correlation percentiles for Galileo E1-C PRN codes family are provided in Table 3-6.

Table 3-6: Correlation Percentiles for Galileo E1-C PRN Codes.

		Percentiles					
		68%	***95%***	***99.7%***	***99.99%***	***99.999%***	***100%***
ACF [dB]	***Even***	-36.1	-30.4	-27.5	0	0	0
	Odd	-36.1	-30.5	-27.4	0	0	0
CCF [dB]	***Even***	-36.0	-30.3	-27.1	-25.5	-24.9	-24.5
	Odd	-36.0	-30.3	-27.1	-25.6	-25.0	-24.4

Note that, while the limits for the normalised correlation magnitudes are set by definition, the resolution or bin width used for the generation of the histogram plays an important role. A typical choice in this thesis is to assume the resolution equal to $1/N$, however smaller bins can be used especially when comparing correlation performance of PRN code sets with different length. The percentiles computed from the histogram of occurrences may slightly differ depending on the histogram scale.

The last figure of merit here considered is the correlation histogram that consists in a two-dimensional plot representing the relative occurrence of correlation magnitudes in dB. The frequency of occurrence is normalized by the amount of correlation operations which are computed over the set of spreading codes. Figure 3–7 and Figure 3–8 show respectively the auto- and cross-correlation histograms for Galileo E1-C PRN code set.

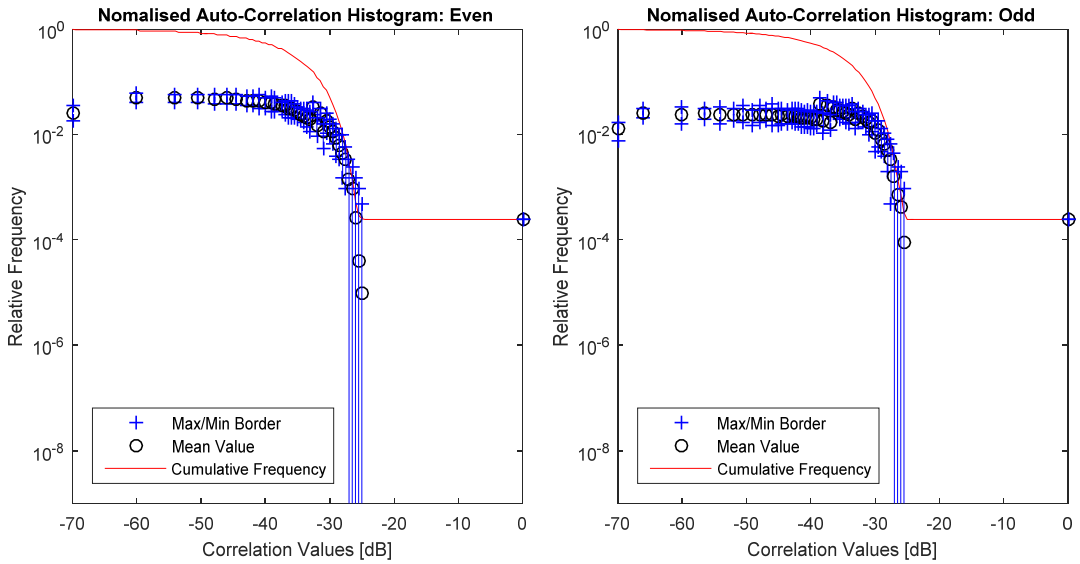

Figure 3–7: Auto-Correlation Histograms for Galileo E1-C PRN Codes.

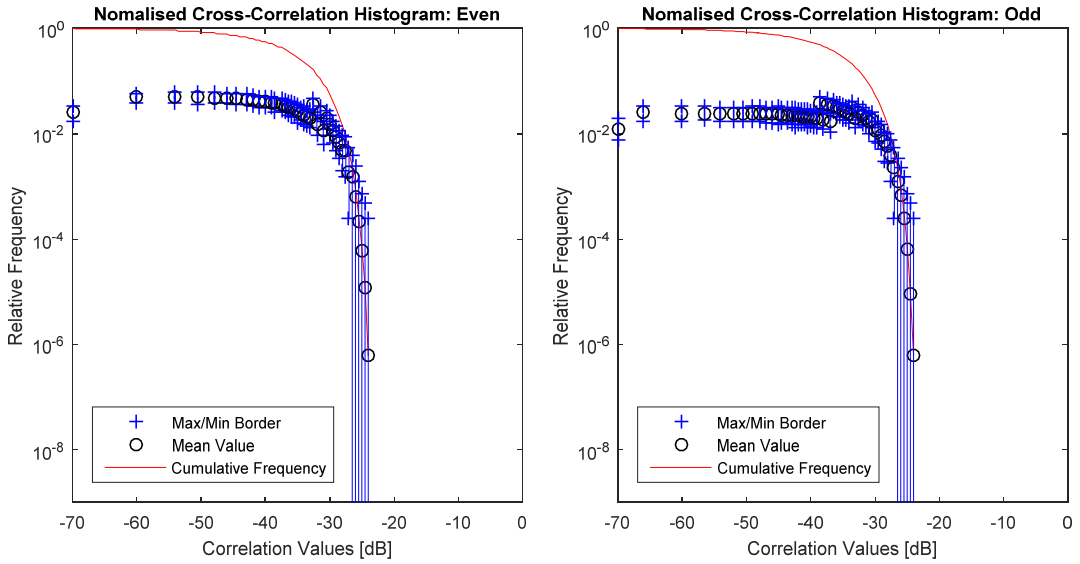

Figure 3–8: Cross-Correlation Histograms for Galileo E1-C PRN Codes.

Three series are depicted for each correlation histogram:

- The minimum/maximum relative frequency of occurrence of each correlation magnitude over all given couples (c_j, c_ℓ) are represented with blue '+' connected by a continuous line. When at least one couple does not show a correlation magnitude, the minimum relative frequency is zero and the blue line disappears beyond the axis representation.
- The mean frequency of occurrence of each correlation magnitude over the whole set of correlation operations are represented with black 'o'.

- The cumulative frequency of occurrence of correlation amplitudes is depicted with a red line. This curve must not be confused the cumulative density function $P(R \leq r)$ used to compute the correlation percentiles. In this case the cumulative frequency corresponds to $P(R \geq r)$.

Finally, the following rule-of-thumb for the average PRN codes properties is recalled from [3]:

- From a statistical analysis, it is demonstrated that the standard deviation for auto-correlation side-lobes tends to $20log_{10}(1/\sqrt{N})$. As an example, the side-lobes for a $N = 1023$ code are approximately 30 dB below the main peak.
- The standard deviation for cross-correlation side-lobes is the same as for auto-correlation side-lobes.

Note that the Welch Bound approaches the above rule-of-thumb for long spreading codes:

$$R_W \approx \frac{1}{\sqrt{N}}, \text{for } N \to \infty \tag{3.14}$$

3.4 PRN Code Set Self-Interference

In this thesis the interference caused by a PRN code set on it-self is referred to as self-interference (SI); in communications this is also called Multiple Access Interference (MAI) and it represents the opposite concept of CDMA isolation.
In the previous section the properties and performance criteria of spreading codes are described only by looking at the pure binary PRN sequences. This section provides a sensitivity analysis on the influence of signal design parameters such as overlay codes, chip shape, and sub-carrier onto the PRN code set self-interference. The effects of Doppler frequency offset and integration time are also analysed with computational examples taken from legacy GNSS signals.

3.4.1 Tiered Codes

It is well known that a method of generating longer ranging codes is to use a slower and smaller length code, the secondary code, in combination with a faster and medium length primary code to form the so-called tiered code. Tiered codes are a common feature of new GNSS signals; however understanding the pros and cons of

this code structure is not so straight forward. According to literature, the use of secondary codes brings the following advantages:

- **Narrow-band interference resistance.** Secondary codes modulate the primary codes with the effect of spreading the power over more spectral lines; as a consequence, the signal results in an increased resistance to continuous waves and narrow-band interference. This is most likely the main reason for the extensive use of overlay codes in GNSS L5 band which lies within the ARNS band (see Figure 2–12).
- **Bit synchronization.** For data components, when the bit duration is equal to multiple primary code periods (e.g. GPS L1-C/A), a bit synchronization algorithm based on the histogram of sign changes is generally adopted. The introduction of a secondary code allows for easy and fast bit synchronization through the sequence alignment. This is for instance the design choice for the Galileo E5a-I and E5b-I data components.
- **Time ambiguity resolution.** Spreading codes longer than the travel time allow the receiver to determine unambiguously the time of transmission without the need to demodulate the navigation message. In other words, if the a-priori course time is known to within the length of the overlay code, the precise time of transmission can be determined through code alignment. An example is represented by the Galileo E1-C secondary code which 100 ms periodicity covers the Galileo satellites maximum ranging distance, in numbers: $(29600\ \text{km} - 6.371\ \text{km}) \cdot 10^3/(3 \cdot 10^8\ \text{m/s}) = 98.6\ \text{ms}$.
- **CDMA isolation.** The modulation of primary code sequences with a secondary code also enables the receiver to perform longer coherent integrations in weak signal conditions. It is common understanding that longer ranging codes result in reduced multiple access interference.

Focusing on the last point, in the author's knowledge there is currently no reference in the literature that showing the actual advantage introduced by tired codes on the correlation properties.

In the following, an assessment of the CDMA isolation properties characterizing tiered codes is presented. The starting point for investigating CDMA isolation properties of tiered sequences is represented by the current and planned GNSS signal

characteristics summarized in Section 3.1. By looking at the PRN codes parameters from Table 3-1 to Table 3-5, the following general observations can be done.

- All primary codes are characterized by a length integer multiple of 1023 chips, as well as a chip rate multiple (or fraction) of the fundamental frequency 1.023 Mcps. This results in a primary code periodicity always multiple (or fraction) of 1 ms.
- L1 Band: The primary code length varies from 1023 to 10,230 chip. The secondary code in some cases is not present (GPS L1-C/A, Galileo E1-B), while in some other cases it is either only one sequence (Galileo E1-C, BeiDou B1) transmitted by all SVs or a full set of overlay sequences (GPS L1-C pilot).
- L5 Band: Galileo E5 and GPS L5 signals are all characterized by a primary code length of 10,230 chips and the presence of secondary codes.
    - Galileo E5a-I, E5b-I and GPS L5-I, L5-Q present the same secondary code for all SVs. Three different lengths of secondary codes are used (4 chip, 10 chip, 20 chip), in accordance with the three different data rates (250 bps, 100 bps, 50 bps).
    - Galileo E5a-Q and E5b-Q on the other hand present a whole PRN secondary code family, which means that each SV transmits a different couple of primary and secondary codes.

In [25] the effect of secondary codes on the Galileo E5a-I spreading sequences are briefly discussed and it is concluded that tiered codes benefit from the additional CDMA isolation provided by the secondary codes as long as the relative delay between the two spreading sequences is not a multiple of the secondary code period. However simulations of the Galileo constellation over one day with 1 s step show that the difference between the minimum and maximum pseudoranges observed by any user on the Earth can be up to about 20 ms. When comparing this relative delay with the periods of secondary codes in Galileo signals baseline, it is clear that the case described in [25] never occurs for the pilot components E1-C, E5a-Q and E5b-Q; on the other hand, data components E5a-I, E5b-I, and E1-B are subject to self-interference when integrating over the secondary codes duration.

It is of interest to compute the correlation performance of tiered codes in case each SV transmits the same overlay code and in case each SV transmit a different couple of primary and secondary codes, and to compare the obtained results with the CDMA isolation properties of the primary codes alone.

Starting from the navigation signal description provided in Section 2.2.1, the periodic pattern combining primary codes $s_P(t)$ and secondary codes $s_S(t)$ is constructed by multiplying in Eq. (2.6) the generic secondary code pulse shape $p_S(t)$ with the periodic sequence of the primary code $\bar{s}_P(t)$:

$$\begin{cases} \bar{s}_{P,S}(t) = \left(\bar{s}_P(t) \cdot p_S(t)\right) * \left[\sum_{n_S=0}^{N_S-1} c_S[n_S] \cdot \delta(t - n_S T_S)\right] \\ \bar{s}_P(t) = p_P(t) * \left[\sum_{n_P=0}^{N_P-1} c_P[n_P] \cdot \delta(t - n_P T_P)\right] \end{cases} \tag{3.15}$$

Further, it is assumed that the pulse shapes $p_P(t)$ and $p_S(t)$ are rectangular functions normalised to unit area:

$$\bar{s}_{P,S}(t) = \left[\sum_{n_P=0}^{N_P-1} c_P[n_P] \cdot rect(t - n_P T_P)\right] * \left[\sum_{n_S=0}^{N_S-1} c_S[n_S] \cdot \delta(t - n_S T_S)\right] \tag{3.16}$$

being $T_S = N_P \cdot T_P$, and by sampling at sampling frequency $f_P = 1/T_P$, it results:

$$\bar{s}_{P,S}[n] = \sum_{n_S=0}^{N_S-1} c_S[n_S] \cdot \sum_{n_P=0}^{N_P-1} c_P[n - n_P - N_P \cdot n_S] \tag{3.17}$$

The statistical auto-correlation function of the signal described in Eq. (3.17) can be expressed as (see [5]):

$$\tilde{R}_{\bar{s}}[m] = \tilde{R}_{c_S}[m] * \tilde{R}_{c_P}[m] \tag{3.18}$$

Additionally, the statistical cross-correlation function between two period patterns $\bar{s}_{P,S}[n]$ transmitted respectively by SVIDs j and ℓ is provided below:

$$\tilde{R}_{\bar{s},j,\ell}[m] = \tilde{R}_{c_S,j,\ell}[m] * \tilde{R}_{c_P,j,\ell}[m] \tag{3.19}$$

Note that, in case the same secondary code is transmitted on all signals, $\tilde{R}_{c_S,j,\ell}[m]$ assumes always the same value $\tilde{R}_{c_S}[m]$.

In the following the even/odd correlation histograms and percentiles are computed for the Galileo E5a legacy signal which represents the best candidate for this analysis as its spreading codes design on components E5a-I and E5a-Q offers both types of tiered codes under investigation.

The percentiles of interest for this analysis are the 68%, 95% and 99.7% corresponding respectively to 1-σ, 2-σ and 3-σ of a Gaussian distribution. The 100% percentile corresponds to the maximum normalized correlation magnitude, which is always equal to 1 (or 0 dB) for the case of even and odd auto-correlation analysis.
The Doppler frequency offset is not considered in this section and θ_D is set to 0 in Eq. (3.9) and (3.10).

Galileo E5a-I

Galileo E5a-I data component transmits a 10,230 chip primary code at 10.230 Mcps. The spreading code periodicity is thus 1 ms as for GPS L1-C/A. However, being the sequence 10 times longer that the L1-C/A Gold codes, the CDMA isolation is also on average 10 dB better. This statement is confirmed by computing the Welch Bound in Eq. (3.12) for the following two cases:

- GPS L1-C/A: $N = 1023$ chip and $K = 32$, $R_W \cong -30.2$ dB
- Galileo E5a-I: $N = 10{,}230$ chip and $K = 50$, $R_W \cong -40.2$ dB

As already shown in Eq. (3.14), the cardinality of the PRN code set tends to be negligible for long codes. The auto- and cross-correlation histograms for Galileo E5a-I primary codes are shown in Figure 3–9 and Figure 3–10.

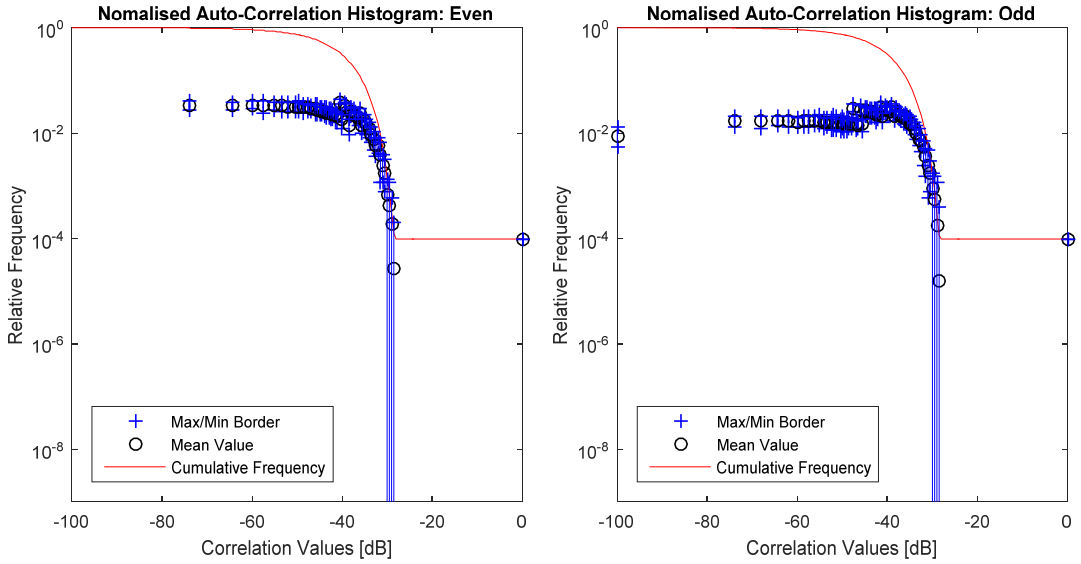

Figure 3–9: Galileo E5a-I Primary PRN Codes, Auto-Correlation Histograms.

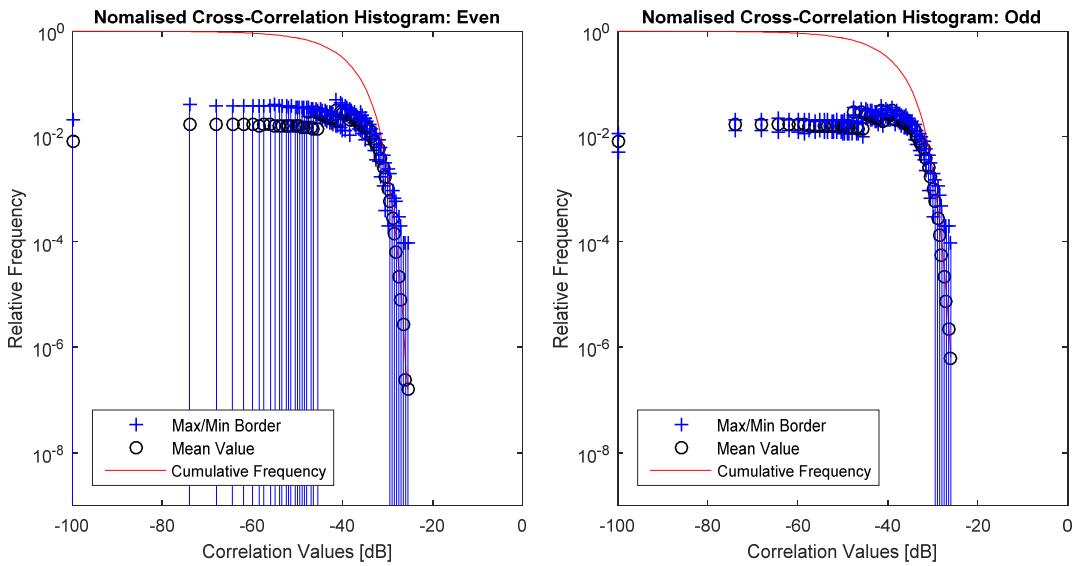

Figure 3–10: Galileo E5a-I Primary PRN Codes, Cross-Correlation Histograms.

Note that the maximum normalized magnitude for auto-correlation side-lobes is about -28.5 dB, and for cross-correlation side-lobes about -25.5 dB. These values are quite far from the Welch Bound.

Combining E5a-I primary codes with the 20 chip secondary code transmitted at 1 kcps, a tiered sequence 204,600 chip long and with 20 ms periodicity is obtained. The secondary code sequence period matches with the data bit duration, resulting in a data rate of 50 bps. The analogy with GPS L1-C/A is again strong as both signals transmit the navigation message at 50 bps. However, while L1-C/A transmits 20 consecutive primary codes without modulation, E5a-I secondary sequence modulates the 20 primary codes by adding on average a sign flip at each primary code change.

The auto- and cross-correlation histograms for Galileo E5a-I tiered codes are shown in Figure 3–11. While the cross-correlation properties show a good behaviour and even an improvement w.r.t. the E5a-I primary PRN codes, the auto-correlation function presents high side-lobes at -14 dB and -20 dB. These undesired correlation peaks are no surprise as they originate from the auto-correlation of the secondary code.

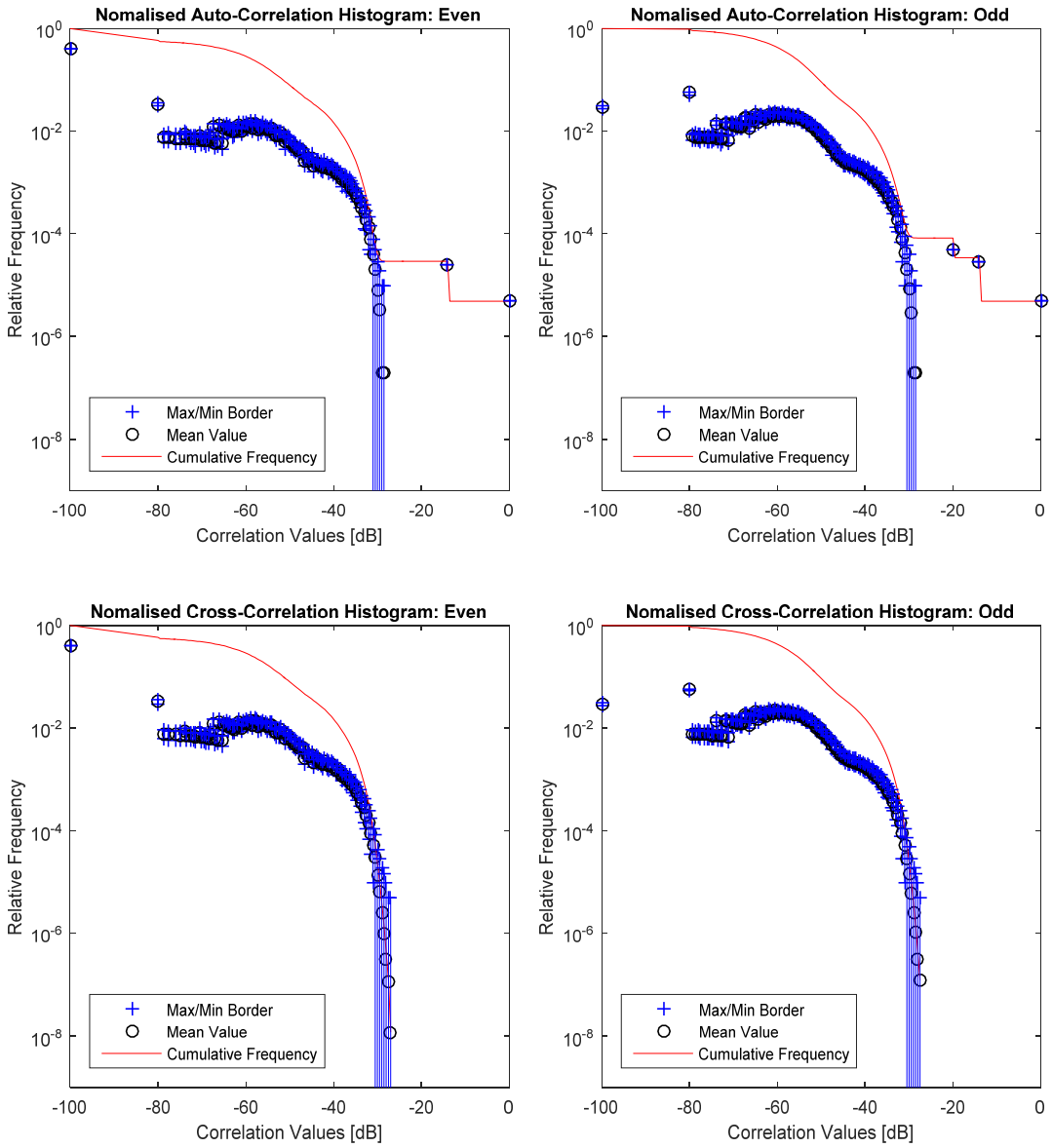

Figure 3–11: Galileo E5a-I Tiered PRN Codes, Correlation Histograms.

Figure 3–12 shows that the normalized correlation magnitudes of Galileo E5a-I secondary code assume values in the discrete set {0.2, 0.1, 0}, which in dB corresponds to {-14dB, -20dB, -Inf}. Even case is marked with blue 'o' and odd case with red '*'.

Table 3-7 provides a summary of E5a-I correlation properties in terms of percentiles. Even if the maximum correlation magnitude is not close to the Welch Bound, the 68th correlation percentile for E5a-I primary codes follows the average performance for standard deviation as expressed by Eq. (3.14). The same cannot be stated for the tiered codes: PRN codes 204,600 chip long would result in a standard deviation of

about -53.1 dB, while the tiered codes show a 1-σ value of -61.5dB and -57.5dB for respectively the even and odd case.

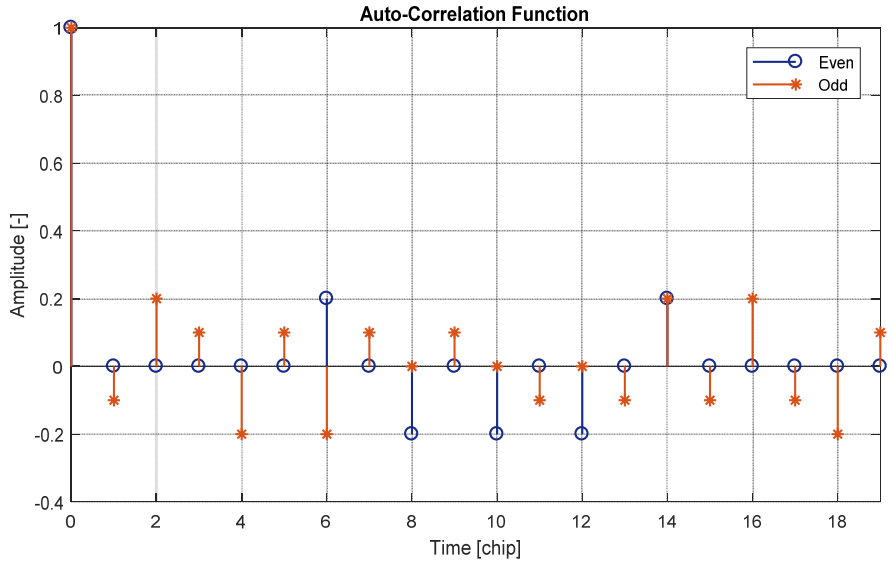

Figure 3–12: Galileo E5a-I Secondary PRN Code, Auto-Correlation Amplitudes.

With reference to the CDMA isolation property, it can be stated that the tiered codes show some improvement in cross-correlation performance with respect to the simple primary code sequence mainly for low correlation values. On the other hand, the auto-correlation analysis reveals inconveniently high side-lobes that could lead to false lock during acquisition. The integration over the full E5-I tired code period does not seem to be an advantage from the point of view of the correlation properties.

Table 3-7: Galileo E5a-I, Correlation Percentiles.

			Percentiles					
			68%	***95%***	***99.7%***	***99.99%***	***99.999%***	***100%***
E5a-I Primary	***ACF [dB]***	***Even***	-40.4	-34.1	-30.7	-28.6	0	0
		Odd	-40.4	-34.2	-30.7	-28.6	0	0
	CCF [dB]	***Even***	-40.4	-34.1	-30.5	-28.3	-27.2	-25.7
		Odd	-40.4	-34.1	-30.5	-28.3	-27.2	-25.9
E5a-I Tiered	***ACF [dB]***	***Even***	-61.5	-47.4	-35.5	-31.2	-14.0	0
		Odd	-57.6	-47.1	-35.4	-30.4	-14.0	0
	CCF [dB]	***Even***	-61.5	-47.3	-35.4	-31.2	-29.7	-27.2
		Odd	-57.5	-47.0	-35.4	-31.2	-29.7	-27.3

Galileo E5a-Q

Like Galileo E5a-I, Galileo E5a-Q pilot component transmits a 10,230 chip primary code at 10.230 Mcps, resulting in a spreading code periodicity of 1 ms. The auto-

and cross-correlation histograms for Galileo E5a-Q primary codes are shown in Figure 3–13.

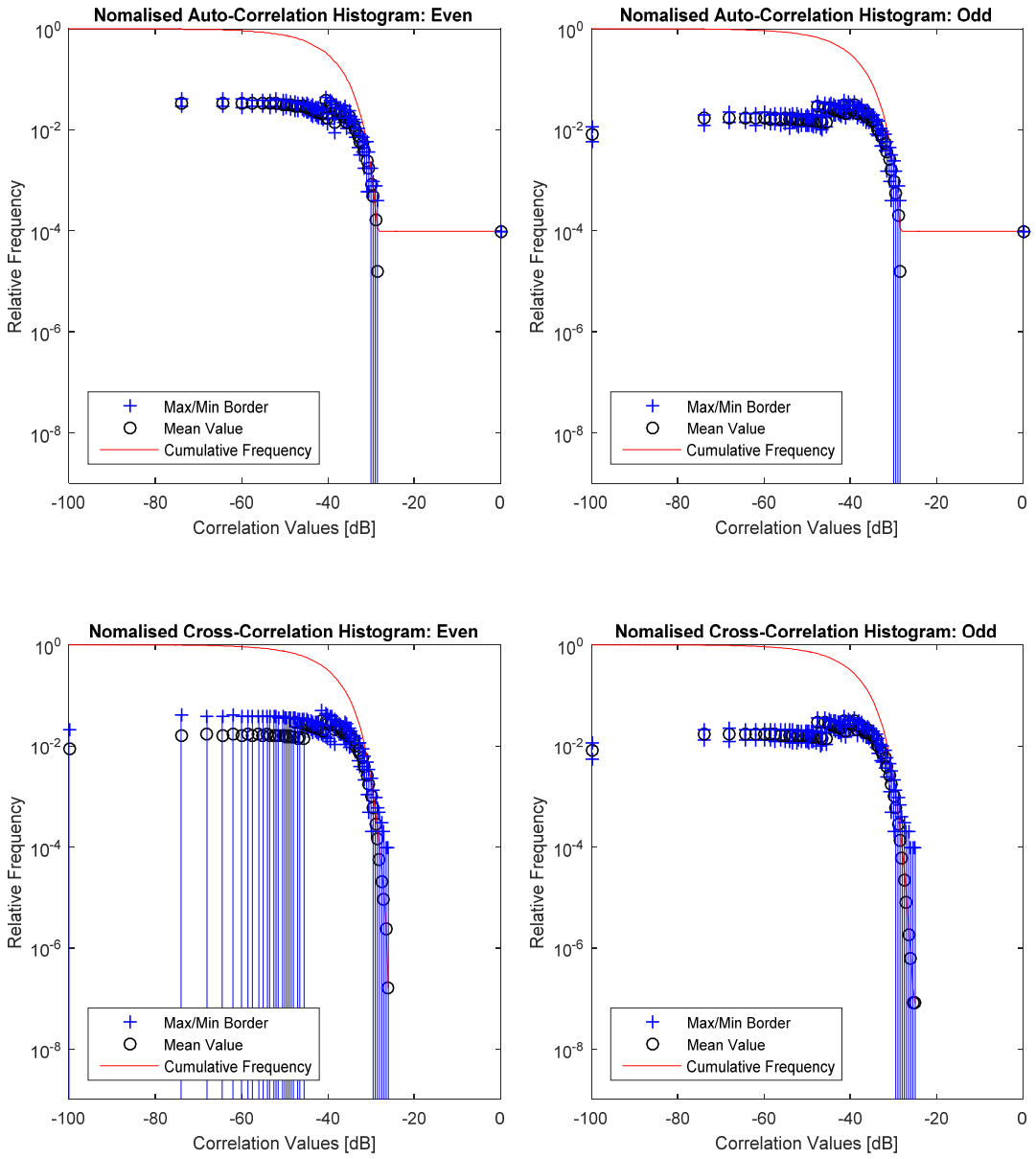

Figure 3–13: Galileo E5a-Q Primary PRN Codes, Correlation Histograms.

The correlation properties of E5a-Q primary codes are the same as those of E5a-I primary sequences as it can be seen by comparing the correlation percentiles in Table 3-7 with the values provided in Table 3-8.

Table 3-8: Galileo E5a-Q, Correlation Percentiles.

			Percentiles					
			68%	***95%***	***99.7%***	***99.99%***	***99.999%***	***100%***
E5a-Q Primary	***ACF [dB]***	***Even***	-40.4	-34.3	-30.7	-28.6	0	0
		Odd	-40.4	-34.1	-30.6	-28.6	0	0
	CCF [dB]	***Even***	-40.4	-34.1	-30.5	-28.3	-27.2	-26.2
		Odd	-40.4	-34.1	-30.5	-28.3	-27.2	-25.2
E5a-Q Tiered	***ACF [dB]***	***Even***	-70.0	-60.5	-40.3	-31.9	-21.9	0
		Odd	N/A	N/A	N/A	N/A	N/A	N/A
	CCF [dB]	***Even***	-62.6	-53.5	-47.1	-42.9	-40.9	-35.4
		Odd	N/A	N/A	N/A	N/A	N/A	N/A
E5a-Q Secondary	***ACF [dB]***	***Even***	-28.0	-21.9	0	0	0	0
		Odd	N/A	N/A	N/A	N/A	N/A	N/A
	CCF [dB]	***Even***	-20.0	-14.0	-10.5	-8.4	-7.5	-7.5
		Odd	N/A	N/A	N/A	N/A	N/A	N/A

Combining E5a-Q primary codes with 100 chip overlay codes, a tiered sequence 1,023,000 chip long and with 100 ms periodicity is obtained. Figure 3–14 provides the auto- and cross-correlation histograms for the E5a-Q tired codes. Only the even case is displayed as no navigation message is transmitted on the pilot component.

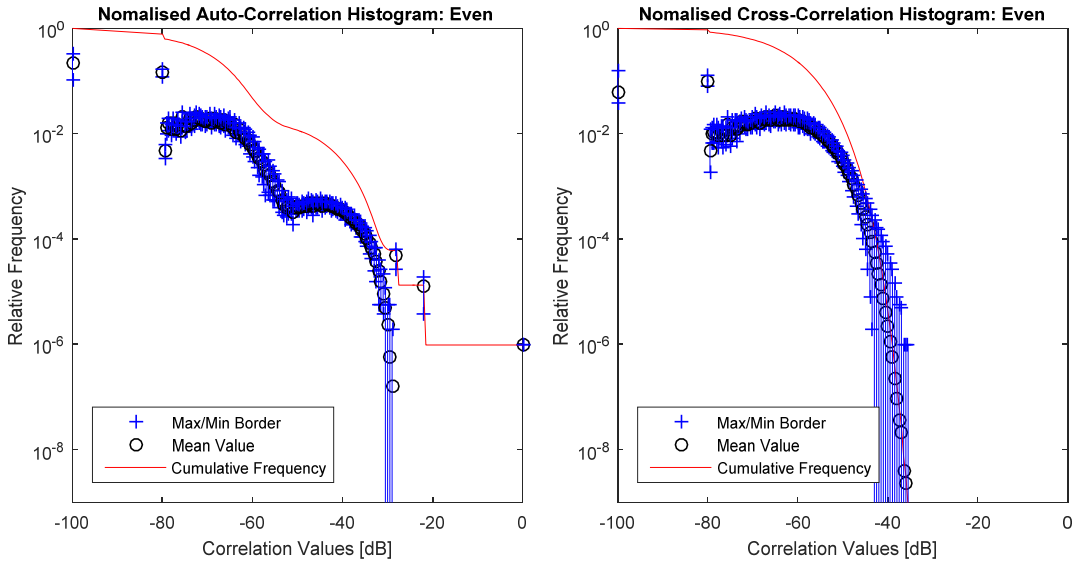

Figure 3–14: Correlation Histograms for Galileo E5a-Q Tiered PRN Codes.

Note that:

- the cross-correlation properties are improved w.r.t. the E5a-Q primary PRN codes;
- the auto-correlation function presents some side-lobes starting from -22 dB and -28 dB. These values can be observed also in the auto-correlation histogram of the E5a-Q secondary codes family (Figure 3–15).

With reference to the CDMA isolation property, it can be stated that the E5a-Q tiered codes show a significant improvement in cross-correlation performance with respect to the simple E5a-Q primary codes. The auto-correlation analysis on the other hand shows high side-lobes. The integration over the full E5-Q tired code period is feasible from the point of view of the correlation properties.

The results in Table 3-8 also reveal that the 68th correlation percentile for E5a-Q tiered codes reaches the -60.2 dB average performance for standard deviation as expressed by Eq. (3.14).

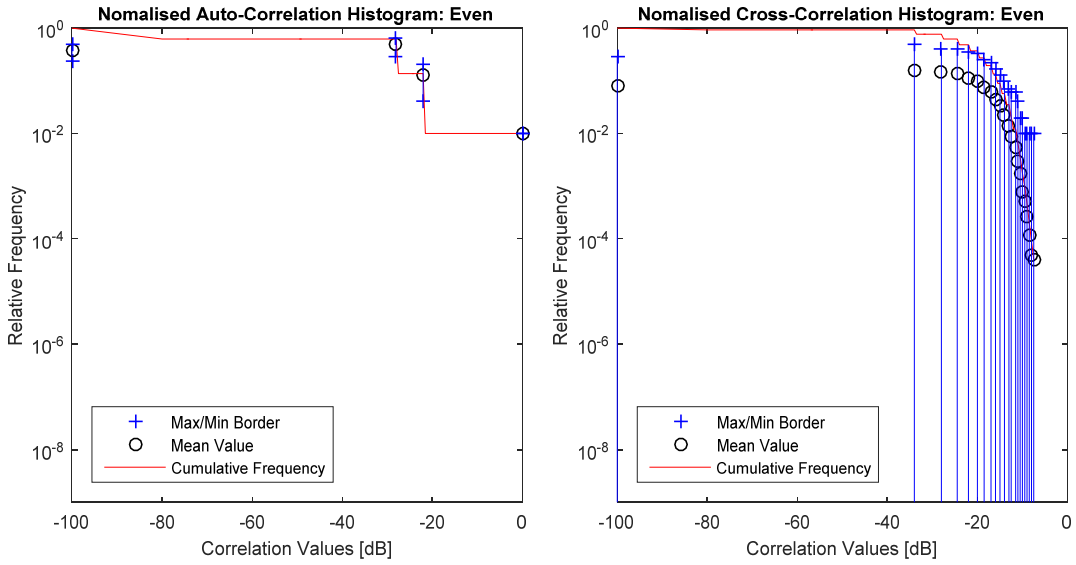

Figure 3–15: Galileo E5a-Q Secondary PRN Codes, Correlation Histograms.

To summarise on the findings of this section, the following conclusions on the CDMA isolation of tired codes can be drawn:

- The use of 'short' secondary codes, whether they are the same for all SVs or different ones, results in degraded auto-correlation properties. This represents a disadvantage on the receiver side for signal acquisition operations.
- When the transmitted secondary code is the same on all SVs, the cross-correlation properties do not show a significant improvement compared to the cross-correlation properties of the primary code set.
- The use of different secondary codes on the SVs improves significantly the cross-correlation properties compared to the cross-correlation properties of the primary code set.

3.4.2 Sub-Carrier and Chip Shape

Second generation GNSS signals are mostly characterized by a BOC-type modulation, where the chip sequence is multiplied by a rectangular sub-carrier of frequency equal or higher to the chip rate. Following this sub-carrier multiplication, the spectrum of the signal is split into two parts, therefore BOC modulation is also known as a split-spectrum modulation (see [19]).

The multiplication with one or more square sub-carriers results in a multi-modal autocorrelation function that makes acquisition and tracking operations more difficult. In some cases, like for the CBOC modulation adopted for the transmission of Galileo E1 OS described in [18], the multiplication with square sub-carriers also results in a multi-level chip shape as the one depicted in Figure 3–16 representing the anti-phase E1 pilot component.

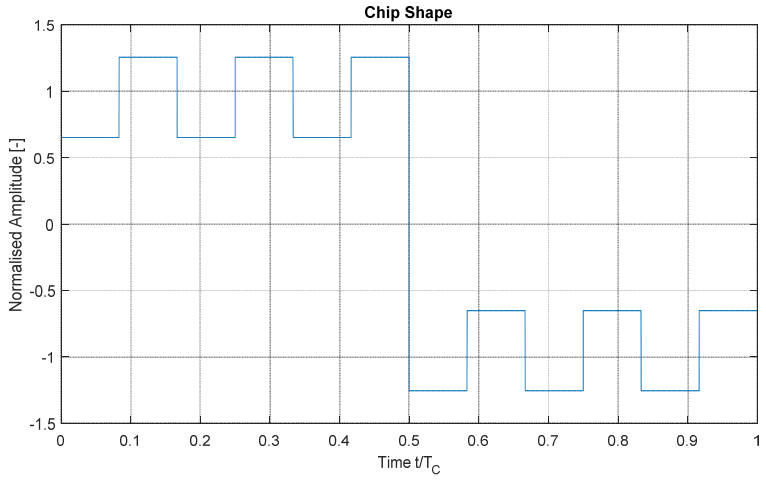

Figure 3–16: Castle Chip Shape for Galileo E1-C.

The effect of a multi-level chip shape can be observed through the performance criteria described in Section 3.3.2. The expression of the auto- and cross-correlation function can be easily derived taking into account the statistical properties of the spreading codes. By recalling Eq. (2.13), the statistical auto-correlation function can be expressed in the discrete domain as:

$$\tilde{R}_s[m] = \tilde{R}_c[m] * R_p[m] \tag{3.20}$$

were the sampling frequency is higher than the chip rate and shall be chosen to satisfy the Shannon theorem for the pulse shape, the sign '~' stands for 'statistical', and $R_p[m]$ is the deterministic auto-correlation of the pulse or chip shape. The same hold for the statistical cross-correlation:

$$\tilde{R}_c[m] = \tilde{R}_{c,j,\ell}[m] * \tilde{R}_p[m] \tag{3.21}$$

Following the example of Galileo E1-C, it is of interest to compute the correlation percentiles and the correlation histogram for the E1-C PRN code family by introducing the effect of the chip shape in the following two cases: BOC(1,1) modulation, and CBOC(6,1,1/11) modulation.

The auto- and cross-correlation histograms for Galileo E1-C signal in the two abovementioned cases are shown respectively in Figure 3–17 and Figure 3–18.

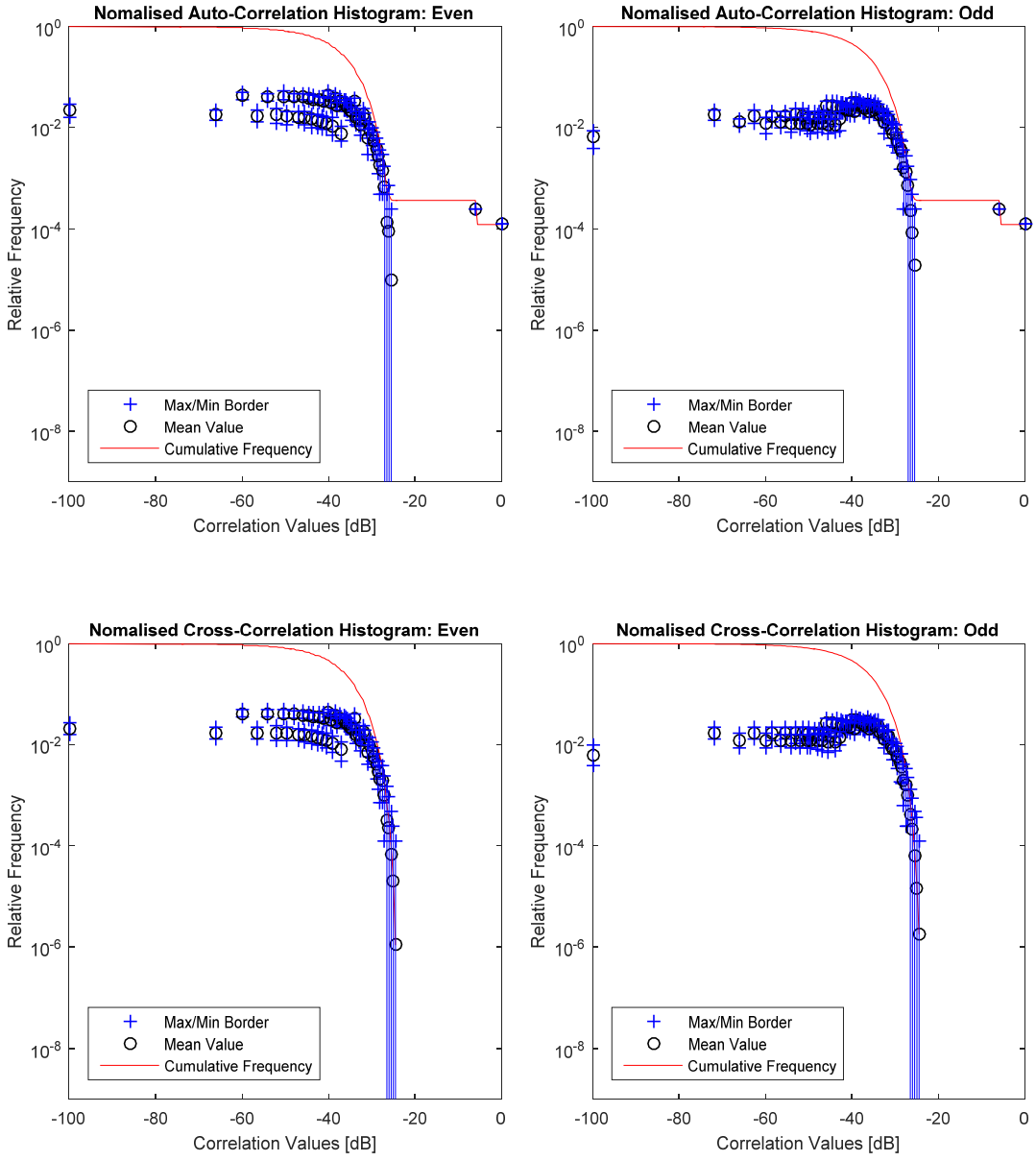

Figure 3–17: Galileo E1-C, Correlation Histograms, BOC(1,1) Chip Shape.

The PRN code auto-correlation histograms for BOC(1,1) chip shape clearly show the presence of the secondary lobes with magnitude -6 dB and occurrence twice the occurrence of the main ACF peak. The cross-correlation histograms do not present any sensitive improvement or deterioration with respect to the case of the pure E1-C PRN codes analysed in Section 3.3.2.

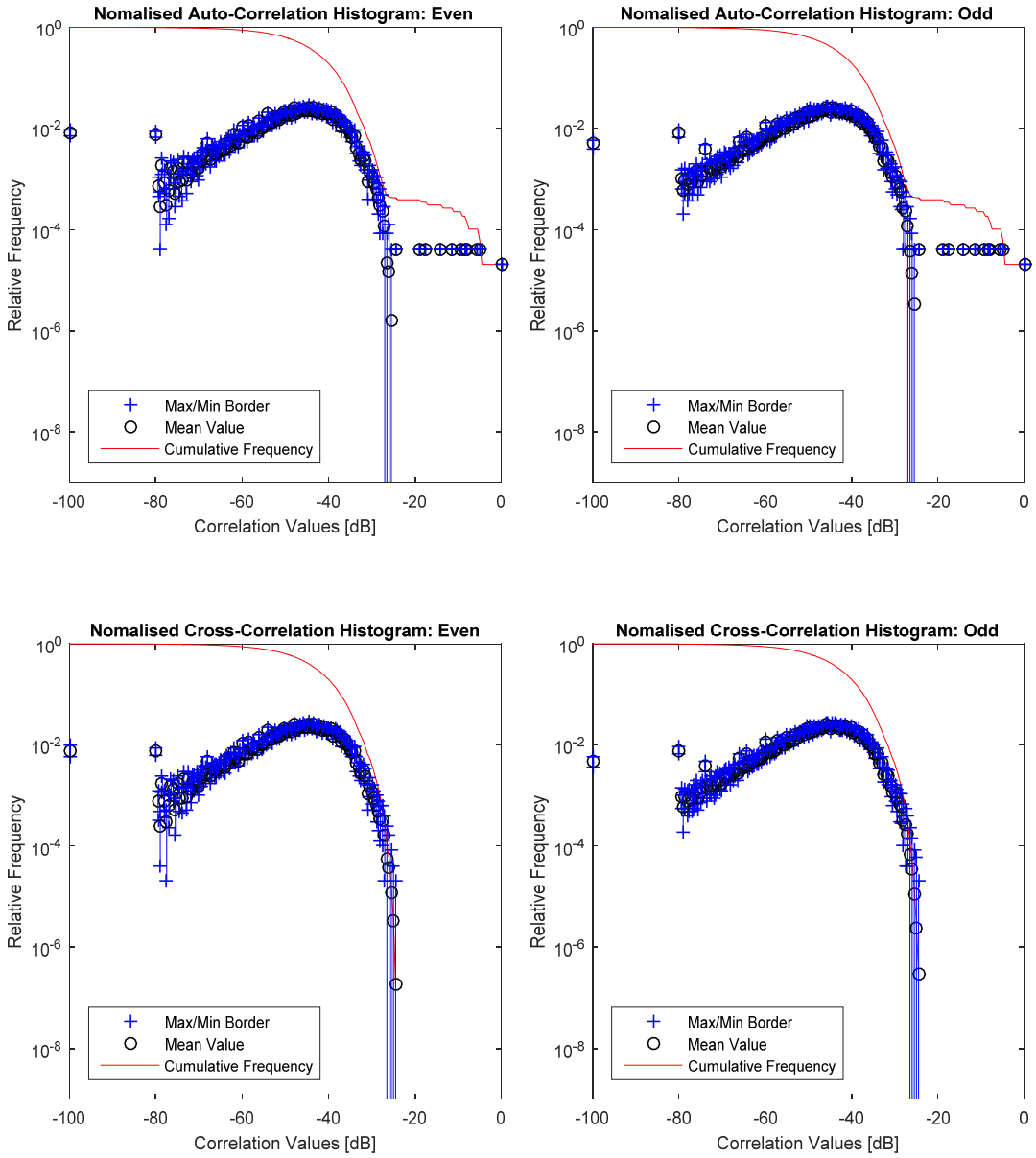

Figure 3–18: Galileo E1-C, Correlation Histograms, CBOC(6,1,1/11) Chip Shape.

For the CBOC(6,1,1/11) modulation, the PRN code ACF properties are strongly impacted by the multi-level chip shape which results in very high correlation values such as -5 dB, -5.5 dB, -8 dB, -8.5 dB etc. The CCF magnitudes on the other hand are more spread towards lower values revealing some improvement with respect to

the pure E1-C PRN codes. This can be observed by comparing the CPs in Table 3-9. It has to be noted however that the maximum values of the CCF are those that represent the worst self-interference case and these remain unchanged in all three modulation cases.

Table 3-9: Galileo E1-C, Correlation Percentiles.

			Percentiles					
			68%	***95%***	***99.7%***	***99.99%***	***99.999%***	***100%***
No Chip Shape	***ACF [dB]***	***Even***	-36.1	-30.4	-27.5	0	0	0
		Odd	-36.1	-30.5	-27.4	0	0	0
	CCF [dB]	***Even***	-36.0	-30.3	-27.1	-25.5	-24.9	-24.5
		Odd	-36.0	-30.3	-27.1	-25.6	-25.0	-24.4
BOC Chip	***ACF [dB]***	***Even***	-37.9	-31.6	-27.9	0	0	0
		Odd	-37.8	-31.6	-27.8	0	0	0
	CCF [dB]	***Even***	-37.6	-31.4	-27.7	-25.9	-25.1	-24.5
		Odd	-37.6	-31.4	-27.7	-25.8	-25.2	-24.4
CBOC Chip	***ACF [dB]***	***Even***	-43.3	-35.6	-29.6	-5.5	0	0
		Odd	-43.2	-35.6	-29.7	-5.5	0	0
	CCF [dB]	***Even***	-43.1	-35.5	-29.8	-26.6	-25.7	-24.5
		Odd	-43.1	-35.5	-29.7	-26.6	-25.6	-24.4

Table 3-9 also reveals the limitations of the CP criterion with respect to other methods like the correlation histogram: ACF side-lobe values are not entirely captured by the selected CPs but these are all visible on the correlation histogram.

Note that the correlation points highlighted by the correlation histogram are ‘proper’ side-lobes only for the case of the BOC(1.1) modulation, where ‘proper’ means that these are stationary points (or local maxima/minima) of the correlation function. The specific shape of the CBOC(6,1,1/11) results in an ACF with saddle points, still difficult to handle in tracking. This is the main reason for limiting the choice of early-late spacing values in Galileo E1 OS tracking.

From the results of this section, the following observations can be made:

- Multi-level coded symbols, such as BOC(1,1) CBOC(6,1,1/11) modulations, do not lead to a significant improvement of the spreading codes CDMA isolation in terms of cross-correlation properties;
- On the other hand, the analysed chip shapes introduce undesired high peaks in the auto-correlation function that can lead to false acquisition or tracking. Being the position of secondary lobes deterministic w.r.t. the main peak, several techniques have been proposed in literature for ensuring the correct code phase lock.

3.4.3 Integration Time and Doppler Frequency

In Eq. (3.10) the expression of the CCF is provided as a function of the Doppler frequency offset. This parameter, up to now neglected, also plays an important role in the CDMA isolation, especially in relation to the integration window.

As widely discussed in Chapter 2, the fine structure of GNSS signals is represented by spectral lines which magnitude and location depend on the specific spreading code. By looking at the cross-correlation operation in the frequency domain, the Doppler frequency offset between two signal spectra translates into a relative displacement on the frequency axis. It is straightforward that the CCF amplitude is higher when the spectral lines overlap and it is lower in all other cases. In other words the self-interference is maximized for Doppler frequency offsets integer multiple of the lines spacing ([35]).

On the other hand, the 'line spectrum' as described in Chapter 2 is represented by an analytical expression that matches the measured PSD only for an infinite observation time. The receiver however works with finite integration windows which duration depends on many factors, both related to the navigation signal structure and to the receiver technological constraints. The presence of data symbols or overlay code chips intrinsically limit the coherent integration to the chip or symbol duration.

The best example to clarify this concept is represented by the GPS L1-C/A signal, which is designed to transmit 20 spreading codes in a symbol period. It is a typical approach for commercial receivers to acquire and track this signal by integrating over multiple PRN code sequences. However, as shown in [38], the average bit alignment loss increases as the coherent interval increases. The coherent interval for the C/A code continues to be useful up to 13 ms. It is of interest in the following to analyse the effect of multiple integrations in terms of auto- and cross-correlation performance. To this scope, the even and odd normalised auto-correlation function computed according to the methodology in Section 3.3.1 is represented in Figure 3–19 for an integration time of 1 ms.

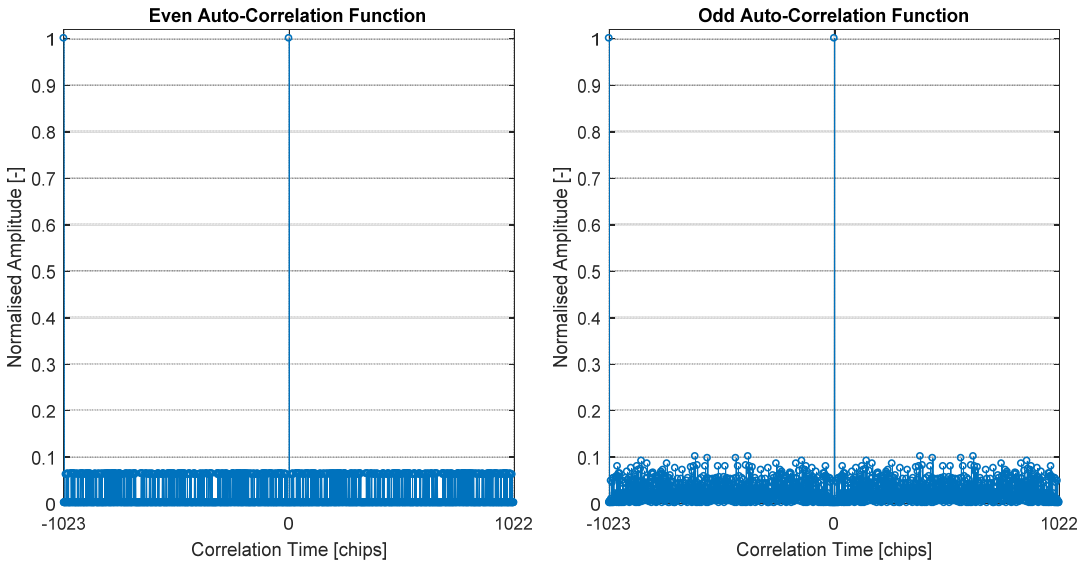

Figure 3–19: GPS L1-C/A PRN Code 1, Auto-Correlation Function, $T_I = 1$ ms.

Further, the same functions are provided in Figure 3–20 and Figure 3–21 for an integration time of respectively 3 ms and 7 ms.

Note that by increasing the integration time the statistics is unchanged for the even CF values, while new peaks and magnitude values appear in the odd case. The explanation is straightforward as the sign flip causes the elimination of opposite contributions accumulated by coherent integration.

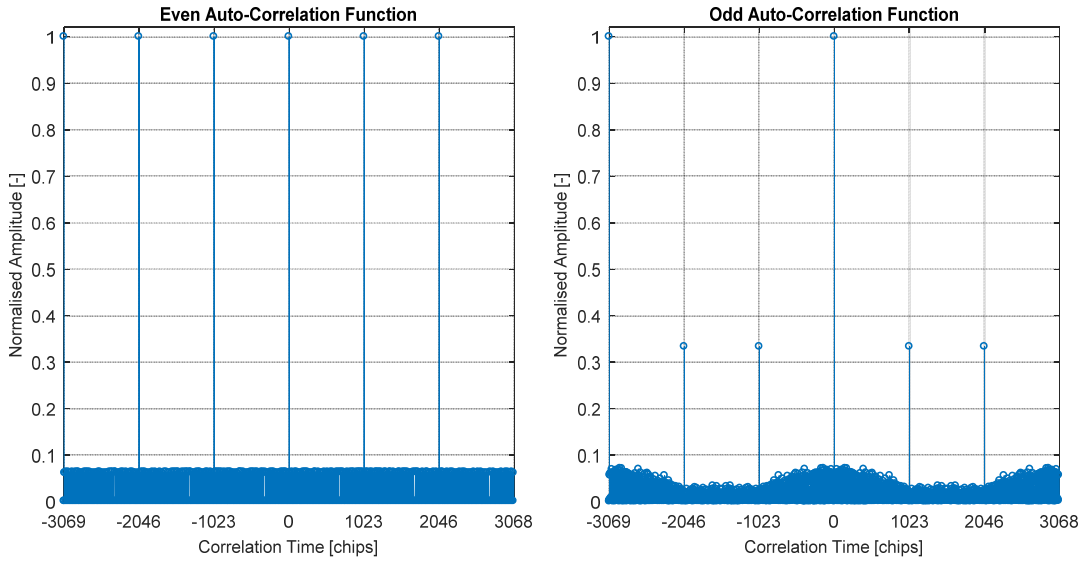

Figure 3–20: GPS L1-C/A PRN Code 1, Auto-Correlation Function, $T_I = 3$ ms.

In particular, for the case of 3 ms integration time the normalised odd ACF presents four peaks with value 0.33, that corresponds to -9.6dB. While for the case of 7 ms,

the normalized odd correlation presents high peaks in the set {0.71, 0.43, 0.14}, which in dB corresponds to {-3dB, -7.3dB, -17.1dB}.

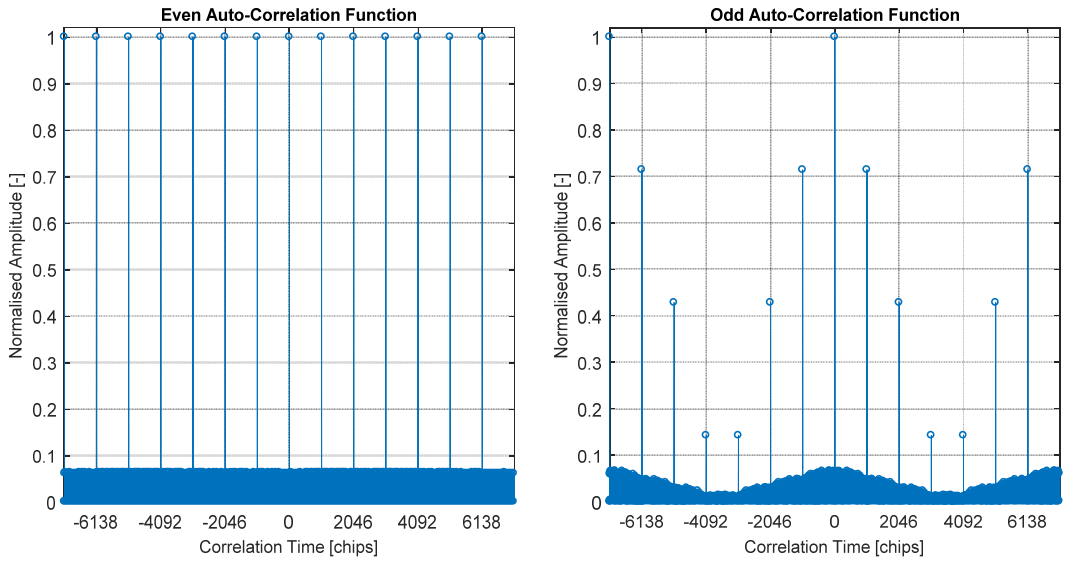

Figure 3–21: GPS L1-C/A PRN Code 1, Auto-Correlation Function, $T_I = 7$ ms.

The GPS L1-C/A correlation percentiles are provided in Table 3-8 for three different values of coherent integration and 0 Hz Doppler offset.

Table 3-10: GPS L1-C/A CPs versus Integration Time, 0 Hz Doppler Offset.

			Percentiles					
			68%	***95%***	***99.7%***	***99.99%***	***99.999%***	***100%***
T_I = 1 ms	***ACF [dB]***	***Even***	-60.2	-23.9	-23.9	0	0	0
		Odd	-30.4	-23.9	-20.3	0	0	0
	CCF [dB]	***Even***	-60.2	-23.9	-23.9	-23.9	-23.9	-23.9
		Odd	-30.4	-23.9	-20.6	-18.4	-17.7	-16.5
T_I = 3 ms	***ACF [dB]***	***Even***	-60.2	-23.9	-23.9	0	0	0
		Odd	-38.4	-25.7	-23.3	0	0	0
	CCF [dB]	***Even***	-60.2	-23.9	-23.9	-23.9	-23.9	-23.9
		Odd	-38.4	-25.7	-23.3	-22.1	-21.5	-20.8
T_I = 7 ms	***ACF [dB]***	***Even***	-60.2	-23.9	-23.9	0	0	0
		Odd	-44.4	-26.0	-23.8	0	0	0
	CCF [dB]	***Even***	-60.2	-23.9	-23.9	-23.9	-23.9	-23.9
		Odd	-44.8	-26.1	-23.9	-23.3	-23.0	-22.6

The previous observation is confirmed by looking at the even percentiles of the ACF: these values are unchanged w.r.t. the integration time. The odd percentiles, on the other hand, fluctuate but not significantly. As pointed out in Section 3.4.2, the limitations of the CP criterion with respect to the correlation histogram are evident: ACF peak values are not entirely captured by the selected CPs but these are all visible on the correlation histogram (see Figure 3–21).

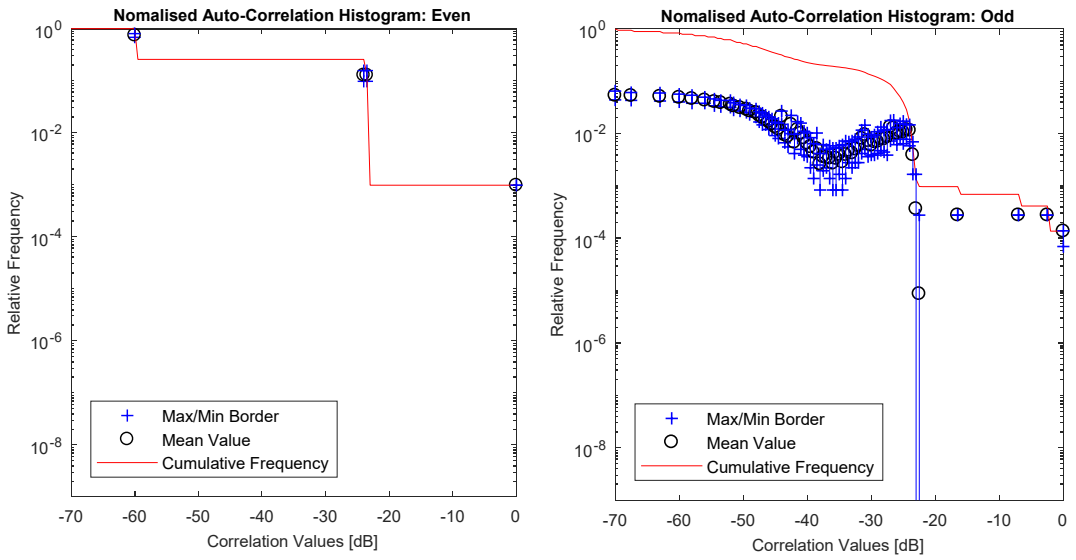

Figure 3–22: GPS L1-C/A PRN Code 1, Auto-Correlation Histograms, $T_I = 7$ ms.

The relationship between the correlation values and the integration window can be further extended to the Doppler frequency offset for the cross-correlation case. In the following, a set of CCF percentiles {60%, 90%, 98%, 99.9%} is displayed as a function of the Doppler frequency offset for different durations of the integration window. The percentiles have been selected in order to allow a comparison with those provided in [1] Table 4.8 and 4.9. For visualisation purposes, and give the periodic behaviour of the curves, in the following figures the frequency axis is limited to the interval 0 Hz – 5,000 Hz; the Doppler offset however can reach values up to about 8,000 Hz for the GPS constellation as shown in Chapter 4, Figure 4–22.

Figure 3–23 displays the behaviour of the correlation percentiles for an integration window of 1 ms. Note that for this value of integration the correlation percentiles are almost constant with respect to the Doppler frequency offset variation. The result seems in contradiction with the statement above, i.e. that the self-interference is maximized for Doppler frequency offsets integer multiple of the lines spacing which for GPS L1-C/A is equal to 1 kHz.

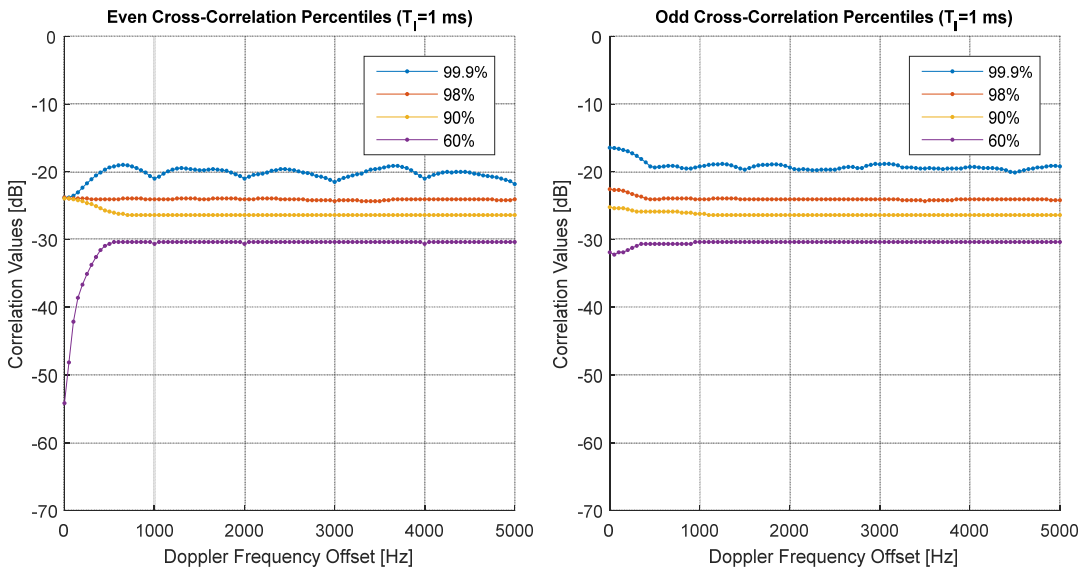

Figure 3–23: GPS L1-C/A CPs versus Doppler Offset, $T_I = 1$ ms.

By looking at the correlation percentiles in Figure 3–24, the forecasted behaviour is already visible with an integration time of 3 ms: the correlation percentile values repeat, after the first interval 0 – 500 Hz, with 1 kHz periodicity and the maximum values correspond to frequency values integer multiples of 1 kHz.

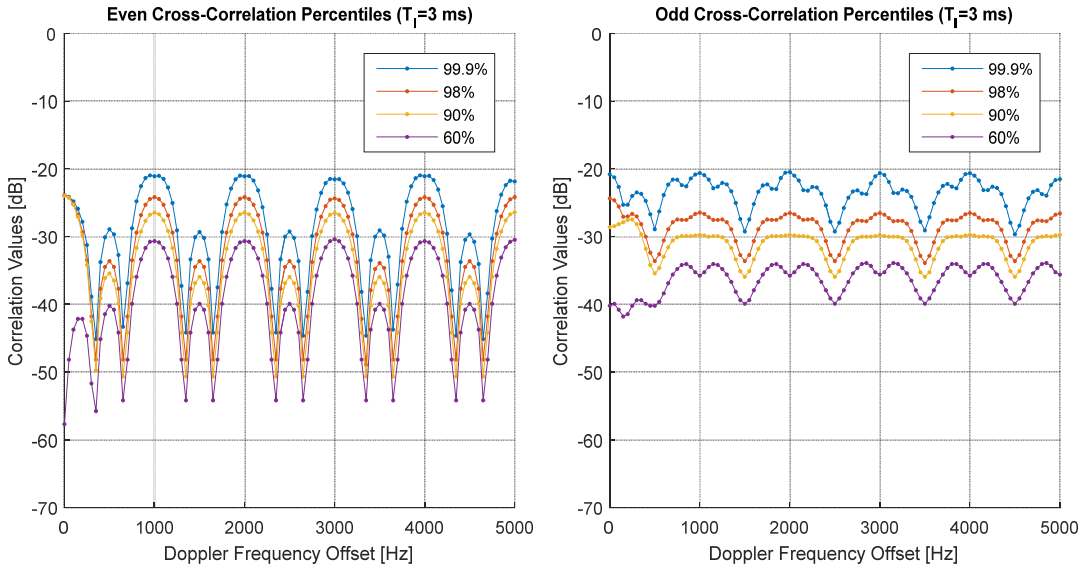

Figure 3–24: GPS L1-C/A CPs versus Doppler Offset, $T_I = 3$ ms.

Further, Figure 3–25 shows the correlation percentiles for an integration time of 7 ms. Note that the percentiles at integer multiples of 1 kHz are unvaried disregarding

the integration time. The correlation percentiles in between fluctuate following the side lobe of a sinc function.

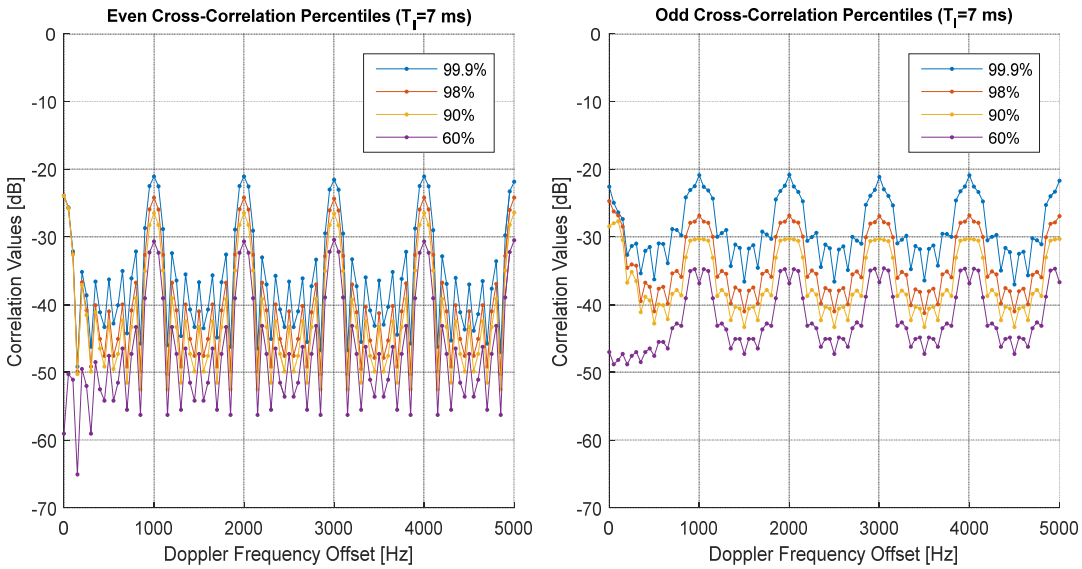

Figure 3–25: GPS L1-C/A CPs versus Doppler Offset, $T_I = 7$ ms.

Figure 3–26 and Figure 3–27 show the behaviour of the 99.9% correlation percentile as a function of the Doppler frequency offset for different integration windows (1, 3, 7, 13 and 20 ms).

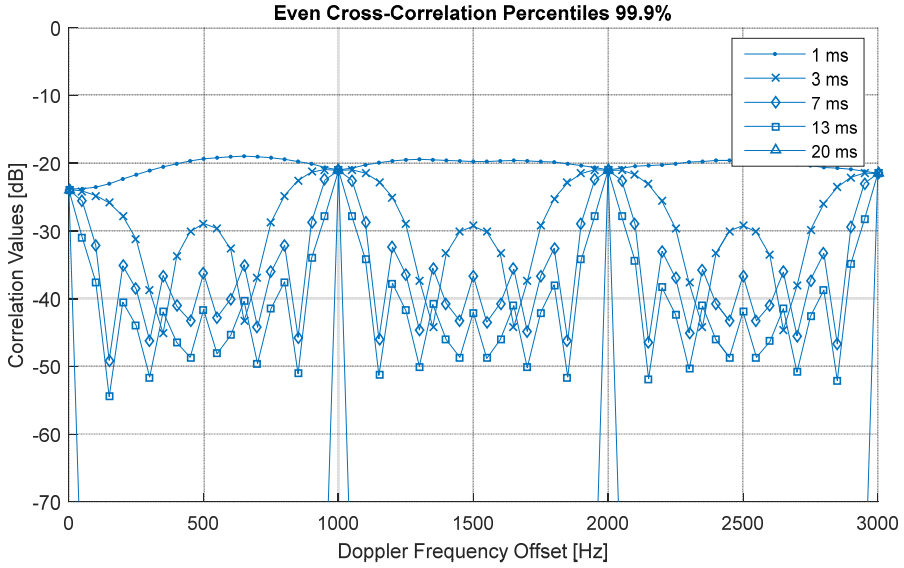

Figure 3–26: GPS L1-C/A 99.9% Even CP versus Doppler Offset.

From this analysis it can be concluded that the curves corresponding to 1 ms integration window represent an envelope or the worst-case correlation interference

w.r.t. integration time. The results are further confirmed in [26] where the maximum of the CAF is represented as a function of the integration time and Doppler frequency for the GPS L1-C/A and Galileo E1 OS signals.

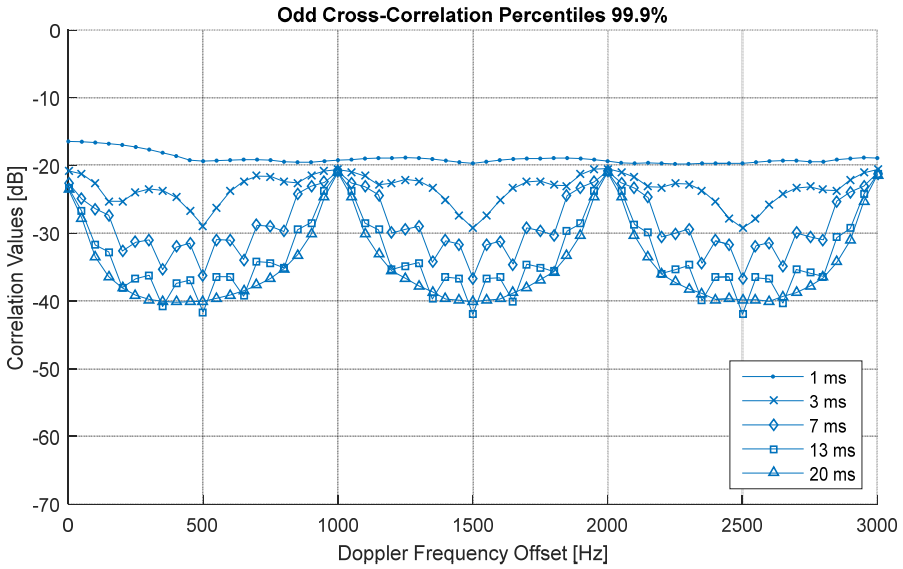

Figure 3–27: GPS L1-C/A 99.9% Odd CP versus Doppler Offset.

Another intersting result is obtained by computing the correlation statistics over the entire Doppler freuquency offset axis. In this case, a reference interval of 0 – 8,000 Hz is taken and the occurrence of PRN code couples w.r.t. Doppler offset values is assumed uniform. The outcome is provided in terms of correlation percetiles in Table 3-11. As expected, the worst-case is represented by 1 ms integration, and for increasing integration time the correlation percentiles decrease. With respect to Table 3-10, a difference of almost -6 dB can be observed on the highest value of the even cross-correlation function.

Table 3-11: GPS L1-C/A CPs versus Integration Time, Uniform Doppler Offset Weighting.

			Percentiles					
			68%	***95%***	***99.7%***	***99.99%***	***99.999%***	***100%***
T_I = 1 ms	CCF [dB]	*Even*	-29.6	-24.9	-22.4	-20.5	-19.8	-19.0
		Odd	-29.3	-25.2	-22.2	-20.1	-19.1	-16.4
T_I = 3 ms	CCF [dB]	*Even*	-36.3	-28.1	-23.9	-21.4	-21.1	-20.9
		Odd	-34.9	-29.2	-25.4	-22.9	-21.6	-20.5
T_I = 7 ms	CCF [dB]	*Even*	-44.6	-30.8	-24.3	-21.9	-21.1	-21.1
		Odd	-40.6	-31.8	-26.7	-23.7	-22.3	-20.8

Signals with a 'continuous spectrum', smoothed by the presence of data bits or secondary code chips transmitted with relatively high rate, do not behave like GPS C/A codes, i.e. they do not present sensitivity to particular values of the Doppler frequency offset. An example is represented by Galileo E1-C spreading codes whose correlation percentiles as a function of the Doppler frequency offset are represented in Figure 3–28. In this case the coherent integration window is set to 4 ms as the only possible value. Note the flat behaviour of correlation percentiles w.r.t. the Doppler frequency offset.

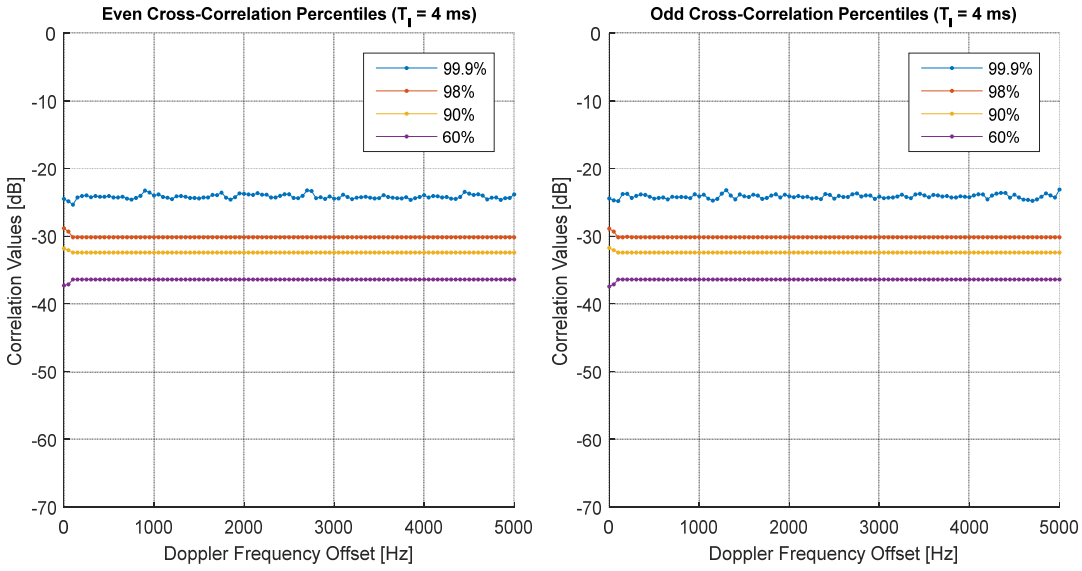

Figure 3–28: Galileo E1-C CPs versus Doppler Offset, $T_I = 4$ ms..

It is also interesting to observe the case of Galileo E5a-I primary codes with overly code. One of the main reasons for introducing the secondary codes on Galileo E5 signals was in fact smoothing the spectral lines, with consequent improvement of narrow-band interference resistance and CDMA isolation. Figure 3–29 shows the correlation percentiles for Galileo E5a-I when an integration time of 20 ms is chosen. The behaviour w.r.t. the Doppler frequency in this case is not as flat as for Galileo E1-C but varies of several dBs. Despite the presence of the overlay code, the periodicity of the correlation percentile values at integer multiples of the spectral line spacing is still visible.

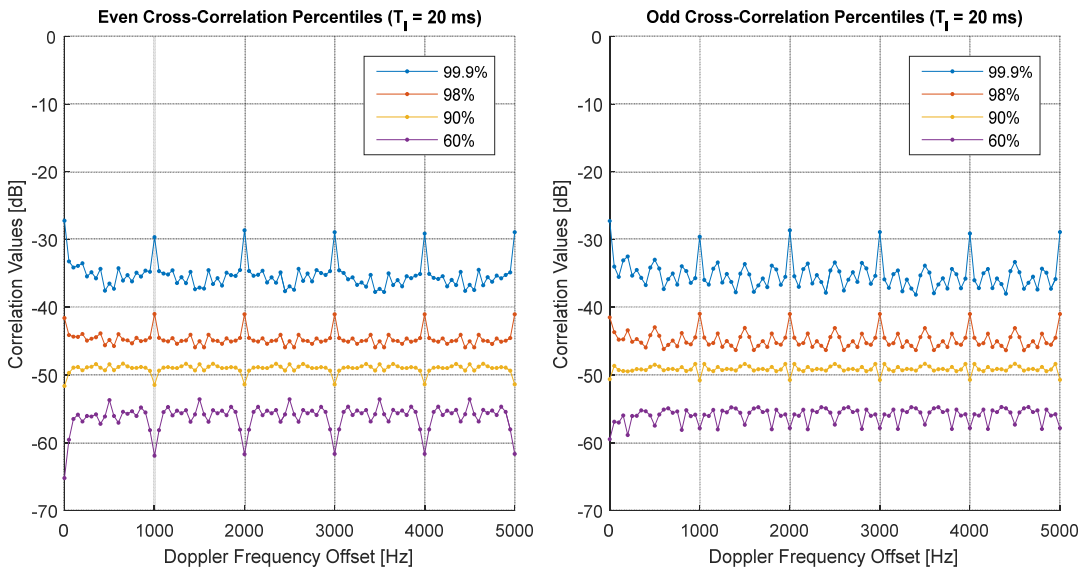

Figure 3–29: Galileo E5a-I CPs versus Doppler Offset, $T_I = 10$ ms.

To conclude on the analysis presented in this section, the following can be stated:

- The effect of multiple integrations onto auto- and cross-correlation performance is investigated taking as reference case the GPS L1-C/A signal. As expected, the even ACF and CCF are left unvaried by multiple integrations. On the other hand, odd auto-correlation over multiple sequences shows high peaks in correspondence of the PRN codes periodicity. This result was expected and it does not represent any impairment for acquisition/tracking operations, as the receiver can lock on the code phase of any PRN sequence within the integration time. It is up to the bit synchronization algorithm to detect sign changes corresponding to data symbols' transitions.
- The analysis between correlation values and integration window is further extended to the Doppler frequency offset. For short codes it is shown that the worst cross-correlation interference results from the shortest integration time. The curve of correlation percentiles versus Doppler frequency offset obtained with the smallest integration window represents an envelope for the other cases.
- Long-code signals with a 'continuous spectrum', smoothed by the presence of data bits or secondary code chips transmitted with relatively high rate, do not present sensitivity to particular values of the Doppler frequency offset.

3.5 PRN Code Sets Cross-Interference

With the increasing number of GNSS signals sharing the same navigation bands and – in some cases – even the same modulation, the impact of spreading codes transmitted by other system providers cannot be neglected. In the previous sections some of the most common figures of merit to measure the CDMA isolation are described and the effect of other signal and receiver design parameters onto the cross-correlation characteristics is assessed. It is of interest to extend the spreading codes' figures of merit for assessing the CDMA isolation between two different PRN code sets that can be transmitted either by the same GNSS provider or by two different ones.

For the purpose of this analysis, the spreading codes subject to interference are identified with the desired PRN code set $\left\{c_\ell^{\mathrm{DES}}[n]\right\}_{\ell=1}^{N^{DES}}$, while the spreading codes representing the source of interference are referred to as the interfering PRN code set $\left\{c_j^{\mathrm{INT}}[n]\right\}_{j=1}^{N^{INT}}$. Additionally, the interference cause by a PRN code set onto another set is called cross-interference, abbreviated with CI.

Before calculating the cross-interference, the problem of working with different code lengths has to be solved. In general it is assumed that the code length of the desired PRN code set N^{DES} is different from the one of the interfering code set N^{INT}. It is also assumed that the chip rate used to transmit the two PRN code sets can be different. For this reason the code periods T^{DES} and T^{INT} are taken as a reference instead of the code lengths. In this case the two PRN code sets under analysis need to be sampled at the same sampling frequency $f = \max(f^{DES}, f^{INT})$. With respect to the code periods, three possibilities can occur:

- $T^{\mathrm{INT}} > T^{\mathrm{DES}}$: This case is handled by applying a zero-padding to the desired spreading sequences so to reach the code length of the interfering code set. Because the interfering sequence is longer than the desired one, there can be only one sign flip in the interfering signal due to the presence of two consecutive symbols with opposite sign. A number of zeros to cover the time difference $T^{\mathrm{INT}} - T^{\mathrm{DES}}$ is added to the desired code set for calculating the even and odd cross-correlation (Figure 3–30).

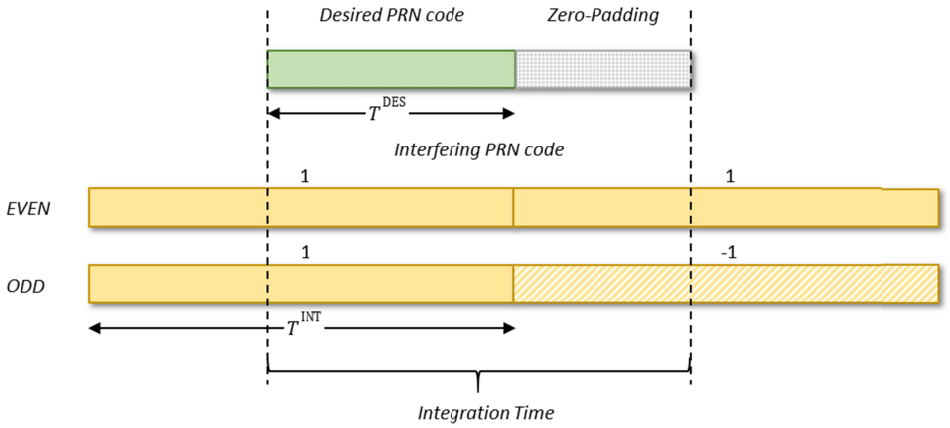

Figure 3–30: Correlation patterns illustration for $T^{INT} > T^{DES}$.

- $T^{INT} < T^{DES}$: In this case, being the interfering PRN code set shorter than the desired one, there can be more sign flips due to the transmission of secondary codes or navigation symbols. All possible correlation patterns together with their probability of appearance have to be considered for the computation of the cross-correlation properties (Figure 3–31). In particular, keeping the naming convention introduced before, there will be one even CCF but more odd CCFs, depending on the number of correlation patterns. The probability of occurrence of each CCF case can be computed assuming that the overlay sequence of symbols or chips is represented by an i.i.d. random variable.

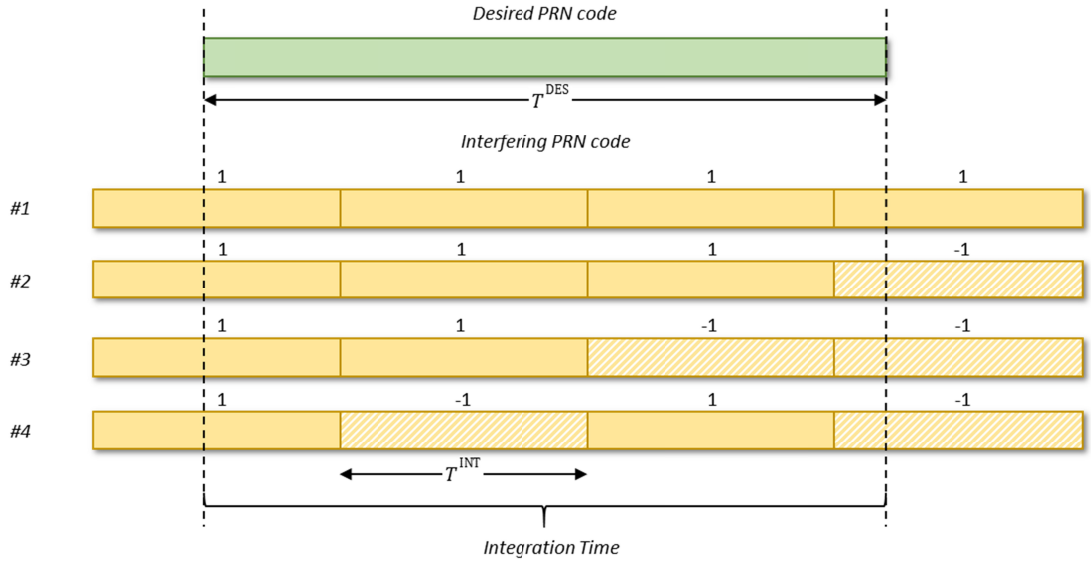

Figure 3–31: Correlation patterns illustration for $T^{INT} < T^{DES}$.

- $T^{INT} = T^{DES}$: When the code period is the same for the interfering and the desired code sets there is no need for zero-padding. Only one even CCF and one odd CCF need to be computed.

In formulas, the cross-interference between different PRN code sets can be expressed as:

$$R_{j,\ell}^{b}[m] = \frac{1}{N_I}\sum_{n=0}^{N_I-1}\left(\hat{c}_j^{DES}[n]\right)^{*}\cdot \hat{c}_\ell^{INT}[n-m]\cdot e^{i(2\pi\Delta\theta_D n+\varphi)} \text{ , for } m\,\epsilon\,[0, 2N_I-1] \quad (3.22)$$

where the integration time depends on the relationship between T^{INT} and T^{DES} as explained before, $\hat{c}_j^{DES}[n]$ is an extended version of c_j^{DES} when $N^{\mathrm{INT}} > N^{\mathrm{DES}}$, and $\hat{c}_\ell^{INT}$ is an extended and version of c_ℓ^{INT} that takes into account the sign flip pattern b.

The most discussed case of cross-interference is represented by the Galileo E1-OS and GPS L1-C interoperable signals. These two signals are both transmitted in L-band at the central frequency of 1575.42 MHz. As described in [18] and [19], the Galileo E1-OS modulation called CBOC slightly differs from the TMBOC modulation adopted for GPS L1-C but the two signal waveforms result in the same MBOC(6,1,1/11) power spectral density. This design choice, while ensures a high level of interoperability between the two systems, also raised concerns about the PRN codes cross-correlation interference level.

The analysis proposed in [24] computes the PRN codes performance figures described in Section 3.3.2 between the Galileo E1-OS and GPS L1-C PRN code sets in order to assess whether GPS could lead to high level of interference for Galileo signals or vice versa. For this purpose the two following cases are analysed:

- Galileo E1-OS interference onto GPS L1-C,
- GPS L1-C interference onto Galileo E1-OS.

The analysis proposed in [24] is repeated below for verification purposes and later other cases are investigated.

3.5.1 Galileo E1-OS and GPS L1-C

The CDMA isolation between Galileo E1-OS and GPS L1-C spreading codes is assessed below by using the Correlation Percentiles (CP) as performance figure. The parameters describing the two PRN code sets under analysis are summarised in Table 3-12.

Table 3-12: Galileo E1-OS and GPS L1-C Code Sets parameters.

	Galileo E1-OS	***GPS L1-C***
Primary Code Length [chip]	4,092	10,230
Primary Chip Rate [Mcps]	1.023	1.023
Secondary Code Length [chip]	25	1800
Secondary Chip Rate [cps]	250	100
Symbol Rate [sps]	250	100
PRN Code Set Size [-]	50 x 2 = 100	63 x 2 = 126
Integration Time [ms]	4	10

GPS L1-C → Galileo E1-OS

This combination falls into the case $T^{\mathrm{INT}} > T^{\mathrm{DES}}$ described above. Table 3-13 provides the correlation percentiles for the even and odd CCF between the two PRN code sets. Additionally, the cross-correlation percentiles for the Galileo E1-OS PRN code set are provided for comparison. According to the results in Table 3-13 the interference caused by GPS L1-C signals is higher than the self-interference of Galileo E1-OS, up to 3 dB on the highest peak.

Table 3-13: GPS L1-C → Galileo E1-OS CPs, T_I = 4 ms, 0 Hz Doppler Offset.

			Percentiles					
			99.0%	***99.9%***	***99.99%***	***99.999%***	***99.9999%***	***100%***
L1-C → E1-OS	***Even CCF [dB]***	***50%***	-27.9	-25.7	-24.3	-23.2	-22.4	-21.1
	Odd CCF [dB]	***50%***	-27.9	-25.7	-24.3	-23.2	-22.3	-21.2
E1-OS	***Even CCF [dB]***	***50%***	-28.2	-26.5	-25.5	-24.9	-24.6	-24.5
	Odd CCF [dB]	***50%***	-28.2	-26.5	-25.6	-24.9	-24.5	-24.4

Galileo E1-OS → GPS L1-C

This case is characterised by $T^{\mathrm{INT}} < T^{\mathrm{DES}}$, thus multiple combinations need to be taken into account for the cross-correlation between the two PRN code sets. In particular, the following four correlation patterns are identified:

P_1 = 12.5%	+1	+1	+1	+1
P_2 = 50%	+1	+1	+1	–1
P_3 = 25%	+1	+1	–1	–1
P_4 = 12.5%	+1	–1	+1	–1

Table 3-14 shows the computed correlation percentiles for the even and odd CCF between the two PRN code sets. Additionally, the cross-correlation percentiles for the GPS L1-C PRN code set are provided for comparison. Also in this case, the self-

interference of the desired code set is lower than the cross-interference produced by the interfering code set.

Table 3-14: Galileo E1-OS → GPS L1-C CPs, T_I = 10 ms, 0 Hz Doppler Offset.

			Percentiles					
			99.0%	***99.9%***	***99.99%***	***99.999%***	***99.9999%***	***100%***
E1-OS → L-1C	***Even CCF [dB]***	***12.5%***	-31.9	-29.7	-28.3	-27.2	-26.4	-25.2
	Odd CCF [dB]	***50%***	-31.9	-29.7	-28.3	-27.2	-26.3	-25.1
	Odd CCF [dB]	***25%***	-31.9	-29.7	-28.3	-27.2	-26.3	-25.2
	Odd CCF [dB]	***12%***	-31.9	-29.7	-28.3	-27.2	-26.4	-25.3
L-1C	***Even CCF [dB]***	***50%***	-32.5	-30.6	-29.1	-28.1	-27.5	-27.2
	Odd CCF [dB]	***50%***	-32.1	-29.9	-28.5	-27.4	-26.6	-26.2

3.5.2 GPS L1-C/A and SBAS L1

The cross-interference between GPS L1-C/A and SBAS L1 represents an interesting case as both services transmit short codes. Additionally, the two PRN code sets are broadcasted at the same centre frequency with the same modulation. This case is expected to show high cross-correlation peaks.

The parameters describing the two PRN code sets under analysis are summarised in Table 3-15.

Table 3-15: GPS L1-C/A and SBAS L1 Code Sets parameters.

	GPS L1-C/A	***SBAS L1***
Primary Code Length [chip]	1,023	1,023
Primary Chip Rate [Mcps]	1.023	1.023
Secondary Code Length [chip]	-	-
Secondary Chip Rate [cps]	-	-
Symbol Rate [sps]	50	500
PRN Code Set Size [-]	32	39
Integration Time [ms]	1, 20	1, 2

SBAS L1 → GPS L1-C/A

This combination falls into the case $T^{\mathrm{INT}} = T^{\mathrm{DES}}$. Table 3-16 provides the correlation percentiles for the following cases:

- Even and odd CCF for the GPS L1-C/A PRN code set;
- Even and odd CCF for the SBAS L1 PRN code set;

- Even and odd CCF between the two PRN code sets.

Table 3-16: SBAS L1 → GPS L1-C/A CPs, T_I = 1 ms, 0 Hz Doppler Offset.

			Percentiles					
			99.0%	***99.9%***	***99.99%***	***99.999%***	***99.9999%***	***100%***
SBAS L1 → L1-C/A	***Even CCF [dB]***	***50%***	-23.8	-23.8	-23.8	-23.8	-23.8	-23.8
	Odd CCF [dB]	***50%***	-21.8	-19.8	-18.4	-17.8	-16.5	-16.4
L1-C/A	***Even CCF [dB]***	***50%***	-23.8	-23.8	-23.8	-23.8	-23.8	-23.8
	Odd CCF [dB]	***50%***	-21.8	-19.8	-18.4	-17.7	-16.4	-16.4
SBAS L1	***Even CCF [dB]***	***50%***	-23.8	-23.8	-23.8	-23.8	-23.8	-23.8
	Odd CCF [dB]	***50%***	-21.8	-19.8	-18.4	-17.6	-17.0	-17.0

According to the results, the interference caused by SBAS L1 signals onto GPS L1-C/A is exactly the same as the self-interference of GPS L1-C/A.

Further, given the spectral line nature of these PRN code sets, the analysis is extended to include the Doppler frequency offset values by computing the correlation statistics in the following cases:

- Even and odd CCF for the GPS L1-C/A PRN code set over 0 – 8,000 Hz;
- Even and odd CCF for the SBAS L1 PRN code set over 0 – 200 Hz;
- Even and odd CCF between the two PRN code sets over 0 – 4,500 Hz.

Table 3-17: SBAS L1 → GPS L1-C/A CPs, T_I = 1 ms, Uniform Doppler Offset Weighting.

			Percentiles					
			99.0%	***99.9%***	***99.99%***	***99.999%***	***99.9999%***	***100%***
SBAS L1 → L1-C/A	***Even CCF [dB]***	***50%***	-23.4	-21.5	-20.4	-19.5	-18.8	-17.0
	Odd CCF [dB]	***50%***	-23.3	-21.4	-20.0	-19.0	-18.1	-16.5
GPS L1-C/A	***Even CCF [dB]***	***50%***	-23.4	-21.6	-20.5	-19.8	-19.4	-19.0
	Odd CCF [dB]	***50%***	-23.3	-21.5	-20.1	-19.1	-18.0	-16.4
SBAS L1	***Even CCF [dB]***	***50%***	-23.8	-23.5	-23.2	-22.8	-22.5	-22.4
	Odd CCF [dB]	***50%***	-21.9	-19.9	-18.5	-17.8	-17.1	-17.0

For the even CCF, the interference caused by SBAS L1 signals onto GPS L1-C/A is slightly higher than the self-interference of GPS L1-C/A.

3.5.3 Galileo E5b-I and BeiDou B2-I

Another case for investigation is represented by the Galileo E5b-I and BeiDou B2-I signals which are transmitted at the same centre frequency of 1207.140 MHz. The two signals are characterised by different modulations, respectively a BPSK(10) for Galileo E5b-I ([8]) and a BPSK(2) for BeiDou B2-I ([12]). While filtering the Chinese signal decreases the spectrum overlap and thus reduces the interference, the same cannot be done for the European signal which occupied bandwidth fully includes the BPSK(2). The CDMA isolation between the Galileo E5b-I and BeiDou B2-I is analysed below by looking at the correlation percentiles. The parameters describing the two PRN code sets under analysis are summarised in Table 3-18.

Table 3-18: Galileo E5b-I and BeiDou B2-I Code Sets parameters.

	Galileo E5b-I	***BeiDou B2-I***
Primary Code Length [chip]	10,230	2,046
Primary Chip Rate [Mcps]	10.230	2.046
Secondary Code Length [chip]	4	20
Secondary Chip Rate [cps]	1000	1000
Symbol Rate [sps]	250	50
PRN Code Set Size [-]	50	37
Integration Time [ms]	1, 4	1, 20

<u>BeiDou B2-I → Galileo E5b-I</u>

As shown in Table 3-18, both signals are composed of primary codes, secondary codes, and navigations symbols. The integration time values considered in this analysis are the primary code period and the secondary code period. The following cases are taken into account:

- $T_I = 1$ ms for Galileo E5b-I and $T_I = 1$ ms for BeiDou B2-I
- $T_I = 4$ ms for Galileo E5b-I and $T_I = 1$ ms for BeiDou B2-I
- $T_I = 4$ ms for Galileo E5b-I and $T_I = 20$ ms for BeiDou B2-I

The case of $T_I = 1$ ms for Galileo E5b-I and $T_I = 20$ ms for BeiDou B2-I is discarded as an integration time window of 1 ms does not allow to see the tired codes of BeiDou B2-I and this case falls back into the first one listed above.

Table 3-19 provides the correlation percentiles for the even and odd CI between the two PRN code sets when only the primary codes are taken into account.

Additionally, the cross-correlation percentiles for the Galileo E5b-I primary code set are provided for comparison.

Table 3-19: BeiDou B2-I → Galileo E5b-I CPs, T_I = 1 ms, 0 Hz Doppler Offset.

			Percentiles					
			99.0%	***99.9%***	***99.99%***	***99.999%***	***99.9999%***	***100%***
B2-I → E5b-I	***Even CCF [dB]***	***50%***	-31.8	-29.7	-28.3	-27.2	-26.3	-25.1
	Odd CCF [dB]	***50%***	-31.8	-29.7	-28.3	-27.2	-26.1	-25.4
E5b-I	***Even CCF [dB]***	***50%***	-31.7	-29.7	-28.3	-27.2	-25.9	-25.2
	Odd CCF [dB]	***50%***	-31.7	-29.7	-28.3	-27.2	-26.3	-25

Note that the correlation percentiles for B2-I → E5b-I are almost equal to the values for the E5b-I self-interference.

Assuming now an integration time of 4 ms for the Galileo E5b-I tired codes, the interfering PRN codes of BeiDou B2-I fall in the case $T^{\mathrm{INT}} < T^{\mathrm{DES}}$, being the primary code period 1 ms long. Thus multiple combinations need to be taken into account for the cross-correlation between the two PRN code sets. In particular, the following four correlation patterns with probabilities of occurrence are identified:

P_1 = 6.25%	+1	+1	+1	+1	+1
P_2 = 31.25%	+1	+1	+1	+1	–1
P_3 = 31.25%	+1	+1	+1	–1	–1
P_4 = 31.25%	+1	+1	–1	+1	–1

Table 3-20 provides the computed CCF correlation percentiles in all above correlation patterns (B2-I → T-E5b-I).

Finally, the case for BeiDou B2-I tired codes interfering to Galileo E5b-I tired codes is analysed. This time $T^{\mathrm{INT}} > T^{\mathrm{DES}}$ and only the even and odd CCF percentiles are computed (T-B2-I → T-E5b-I, Table 3-20). The cross-correlation percentiles for the Galileo E5b-I tired PRN code set are provided for comparison.

Looking at the results in Table 3-19 and Table 3-20 it turns out that the case B2-I → T-E5b-I presents a highest correlation peak around -25 dB 62.5% of the times, similarly to B2-I → E5b-I; the other correlation values however are lower. The case T-B2-I → T-E5b-I on the other hand can be seen as an ‘average’ of the correlation percentiles for the four correlation patterns in B2-I → T-E5b-I.

The analysis shows the benefit of increasing the integration time to the secondary code duration.

Table 3-20: BeiDou B2-I → Galileo E5b-I CPs, T_I = 4 ms, 0 Hz Doppler Offset.

			Percentiles					
			99.0%	***99.9%***	***99.99%***	***99.999%***	***99.9999%***	***100%***
B2-I → T-E5b-I	***Even CCF [dB]***	***6.25%***	-37.8	-35.7	-34.3	-33.2	-32.3	-31.1
	Odd CCF [dB]	***31.25%***	-35.0	-32.0	-30.1	-28.7	-27.6	-25.2
	Odd CCF [dB]	***31.25%***	-35.0	-32.0	-30.1	-28.7	-27.6	-25.3
	Odd CCF [dB]	***31.25%***	-39.1	-36.7	-35.0	-33.8	-32.8	-31.3
T-B2-I → T-E5b-I	***Even CCF [dB]***	***50%***	-37.4	-34.9	-33.1	-31.8	-30.7	-28.7
	Odd CCF [dB]	***50%***	-37.5	-34.9	-33.1	-31.8	-30.7	-28.7
T-E5b-I	***Even CCF [dB]***	***50%***	-34.6	-31.8	-30.1	-29.0	-28.2	-27.2
	Odd CCF [dB]	***50%***	-34.2	-31.5	-29.9	-28.8	-27.8	-26.5

4. Radio Frequency Compatibility Analysis

With the growth in number and power of GNSS and SBAS signals transmitted in the RNSS frequency bands, aggregate interference levels need to be carefully assessed and regulated for ensuring that legacy and new-generation GNSS receivers will work properly within defined coverage areas and can achieve desired performance.

With the European Union decision in the 1990s to set up Galileo as own CDMA based navigation system, the need to assure compatibility with GPS grew in importance as it was planned to use the same centre frequencies of GPS for Galileo signals. One of EU main objectives was in fact to set up a system not only compatible with GPS but also interoperable.

After lengthy negotiations between EU and US, the agreement on the common use of the L1/E1 frequency band was signed on June 9th, 2004. In the context of this agreement a methodology for the computation of the Radio Frequency Compatibility (RFC) between GPS and Galileo was established [31]. The method is based on the computation of the Carrier-to-Noise Density Ratio (C/N_0) of the desired signal transmitted by the reference system in the presence of in-band interference generated by an interfering system. More in details, the following interference sources are identified and taken into account:

- signals other than the desired one and transmitted by the same reference system (intra-system interference);
- signals transmitted by the interfering system (inter-system interference);
- interference originating from signals transmitted by all other RNSS systems other than the reference and the interfering system (inter-system interference);
- External interference originating from other sources than RNSS.

The methodology quantifies the degree of radio frequency compatibility among RNSS signals through two criteria:

- The Effective C/N_0 observed by a reference receiver processing the desired signal when different sources of interference are accounted for, i.e. intra-system interference, inter-system interference and external interference.

- The C/N_0 Degradation caused by the presence of a new interfering system onto the effective C/N_0 observed by a reference receiver processing the desired signal.

The two identified criteria act complementarily: on the one hand the user performance needs to be ensured following the effective C/N_0 criterion; on the other hand, for a fair regulation of all systems sharing the same radio frequency band, the impact of each transmitted service needs to be limited by the C/N_0 degradation criterion. A combination of both criteria together with criteria limits can provide a full picture of the RNSS compatibility analysis of a desired signal for a given interference scenario.

Further, the methodology described in [31] presents two alternative approaches or models at the basis of the RFC assessment that differentiate for the underlying assumptions and thus the approximation of the computed results. Looking at the major differences, in the analytical approach the fine spectral structures of the received navigation signals coming from the same RNSS are averaged together into a smooth spectrum. As a result, the Doppler shift between the desired and interfering signals is negligible and it is not taken into account in the analytical model. The 'combined' interfering signals are characterized in terms of maximum received power and worst-case aggregate gain factor over the constellation repetition cycle, and the computation of each interference contribution is done for each location on the Earth. Conversely, the simulation approach propagates each RNSS constellation for the constellation period and computes the dynamic link budget for every location on the Earth at each time. The worst-case assumption is in this case replaced by punctual power levels and aggregate gain. Additionally, the model allow representing the signals considered in the assessment either with line spectra or continuous spectra, depending on which assumption fits best with the specific PRN codes length.

In the evolving GNSS scenario, compatibility assessments on a multilateral base are gaining more and more importance. In particular there is the need for assessing the effects of the growing number of GNSS and SBAS signals that will be sharing the L-band portion of the radio frequency spectrum in the next years. In order to regulate this complex scenario a specific ITU recommendation called Rec. ITU-R

M.1831 was issued in 2007 [32]. In this document a coordination methodology for RNSS inter-system interference estimation was established, mostly following the approach described in [31].

In this context, other RFC assessment criteria have been proposed to complement and possibly improve Rec. ITU-R M.1831. Among these, a special mention should be given to the proposal from the European Commission in the framework of the ICG activities ([33], [34]): the suggested approach is to assess the noise floor increase caused by the current/planned transmitted GNSS signals in order to agree on a maximum interference level and to limit the contributions from each GNSS provider.

Another important aspect is represented by the assumption on the frequency representation of the signals. The analytical approach described later in this chapter approximates the spectrum of the received signals as a continuous spectrum, where the fine structures of individual signal spectra are averaged together into a smooth spectrum. This near-continuous noise-like spectral density modelling is valid for long-code signals and assumes that the Doppler shift between the different signals has a negligible effect onto the overall interference assessment.

However, as widely described in Chapter 2, real spectra of signals with periodic spreading codes are characterized by a fine structure of spectral lines, whose frequency position and magnitude depends on the specific spreading code sequence, chip rate, presence of secondary codes and/or navigation data. For short-code signals the continuous spectrum modelling is not appropriate as the signal power is significantly concentrated in the spectral lines. Since most modernized GNSS signals belong to the category of long-code signals, the analytical approach of Rec. ITU-R M.1831 is the most employed in ITU coordination activities for RNSS inter-system interference estimation. Nevertheless it is believed in the navigation community that this approach has shortfalls when it comes to the GPS L1 C/A self-interference and in general to GNSS signals that belong to the category of the so-called short-code signals (see [35], [36]).

Models have been developed to reflect the qualitative characteristics of L1 C/A self-interference and to assess its effects on receiver performance (e.g. in [37]), but no currently available model is recognised as standard reference and adopted for compatibility assessments.

The RFC methodologies mentioned above are mainly based on the assessment of aggregate interfering power levels. However, another important compatibility aspect is the degradation of spreading codes isolation of the desired signal caused by the presence of other RNSS systems also based on CDMA. As widely discussed in Chapter 3, every navigation system provider needs to ensure for each service not only a good isolation of the selected PRN code set with it-self (self-interference, SI) but also with all other PRN code sets transmitted in the same radio frequency band (cross-interference, CI). Until recently, GPS signals along with a few low-powered SBAS signals were the only signals occupying L-band and investigation on PRN code correlation properties for the evaluation of self- and cross-interference was primarily of academic interest for the following reasons:

- the power of individual navigation signals is far less than the noise power in a receiver front-end;
- the aggregate power of interfering navigation signals is comparable to the receiver noise floor and the aggregate smooth spectrum is used for interference computation as described in the abovementioned methodologies [31], [32];
- the assumption of aggregate smooth spectrum is justified for most GNSS signals.

Nevertheless, while the effects of SI and intra-system CI are under control of the navigation system provider and are duly taken into account in the signal design, the same cannot be ensured for the inter-system CI. The signal design and the choice of the spreading codes should be based on criteria that minimise the inter-system interference with legacy GNSS signals, but the navigation services are constantly increasing and new signals are upcoming. GPS L1 C/A currently represents the most relevant case of short-code signal for global systems but other system providers already plan new services for fast acquisition also based on short codes. If this will happen, the ITU methodology should be ready to assess not only the compatibility between transmitted power levels but also between PRN code sets.

In the following a new methodology complementary to Rec. ITU-R M.1831 is proposed based on the computation of spreading codes cross-correlation interference. The new method combines the PRN codes performance figures

described in Chapter 3 with the RFC approaches in [31] and [32] to provide an overall PRN codes CI performance figure.
This chapter is composed of the following parts:

- Section 4.1 provides a complete description of Rec. ITU-R M. 1831. The overall assumptions, computation steps, and performance criteria are explained as well as the two methodology approaches (analytical and simulation). A deep understanding of [31] is fundamental for the introduction of the proposed method.
- Section4.2 describes the new proposed RFC analysis based on PRN codes and the assessment criteria for the evaluation of self-interference and cross-interference within and between PRN code sets.
- Section 4.3 lists all the reference assumptions required for carrying out the PRN codes based RFC assessments. The systems under analysis are GPS, Galileo, EGNOS and BeiDou.
- Section 4.4 provides several simulation results that prove the effectiveness of the proposed methodology and highlight relevant aspects related to the PRN codes compatibility among signals.

4.1 Recommendation ITU-R M.1831

4.1.1 Methodology

This methodology is intended to provide a technique for assessing RNSS inter-system interference. The methodology applies to RNSS systems that use CDMA and FDMA to allow sharing of RNSS bands, and recognizes that a simple summation of transmission power density is inadequate to determine what effect an RNSS system has on others. Two are the criteria defined in [32] for assessing compatibility between RNSS systems:

- Effective C/N_0,
- C/N_0 Degradation.

As already explained, the effective C/N_0 measures the absolute C/N_0 level that a reference receiver would observe. This value should be higher than a given operational threshold, typically defined in system ICDs, in order to ensure that the performance of the service is satisfactorily provided. On the other hand, the

degradation of the C/N_0 measures the decrease of the C/N_0 when additional interference is introduced. In other words, the degradation criterion gives a relative measure while the effective criterion provides an entire picture of the interference environment.

The methodology adopted in order to estimate the Effective C/N_0 and C/N_0 Degradation can be summarized in five high-level steps:

1. Link budgets are computed from each satellite to each user location. This computation is done in order to get the desired signal power, the aggregate power level, and the Doppler shifts for each satellite.
2. Spectral separation coefficients are computed based on the power spectral densities and the Doppler shifts.
3. The effective power of the desired signal and each interference source are computed.
4. These results, combined with the thermal noise and external interference, yield to the Effective C/N_0: $[C/N_0]_{\text{eff}}$.
5. Combining this result with a reference allows assessing the C/N_0 Degradation: $\Delta[C/N_0]$.

In order to apply the methodology just described, it is fundamental to identify and compute some key parameters required for the Effective C/N_0 estimation. The main elements needed for computing the RFC assessment criteria are:

- respective orbit and constellation parameters;
- respective satellite parameters (antenna gain pattern);
- desired and interfering signals' characteristics (modulation, data rate and spreading codes characteristics) and minimum/maximum received power levels (link budget assumptions for propagation);
- external interference from other RNSS and/or non-RNSS sources;
- reference receiver parameters (implementation losses, user antenna gain);
- reference receiver locations.

4.1.2 Assessment Criteria

The Effective C/N_0 of the desired signal transmitted by a given navigation system interfered by RF signals coming from other RNSS systems is defined as follows:

$$[C/N_0]_{\text{eff}} = \frac{C}{\nu N_0 + I_{REF} + I_{INT} + I_{EXT}} \tag{4.1}$$

with

$$I_{INT} = I_{ALT} + I_{REM} \tag{4.2}$$

where:

C User received power of the desired signal [W]

N_0 Receiver thermal noise floor density [W/Hz]

ν Effective thermal noise factor [dimensionless], defined as:

$$\nu = \int_{-B_T/2}^{B_T/2} G_S(f)df \leq 1$$

with B_T the bilateral bandwidth of the transmit filter.

I_{REF} Equivalent noise power density introduced into the system and originating from signals transmitted by the same navigation satellite system than the desired signal [W/Hz]

I_{INT} Equivalent noise power density introduced into the system and originating from signals transmitted by all other RNSS satellites than the desired constellation [W/Hz]

I_{ALT} Equivalent noise power density introduced into the system and originating from signals transmitted by a specific alternate RNSS satellite system [W/Hz]

I_{REM} Equivalent noise power density introduced into the system and originating from signals transmitted by all remaining RNSS systems [W/Hz]

I_{EXT} External interference originating from other sources than RNSS [W/Hz]

The above expression comes out from the total interference power density formulation which, in the most general case, is the sum of the four interference components:

$$I_{TOT} = I_{REF} + I_{ALT} + I_{REM} + I_{EXT} \tag{4.3}$$

Observe that I_{INT} gives the total contribution to the interference coming from RNSS satellite systems other than the reference one.

The C/N_0 Degradation concept can be transferred into mathematical equations in different ways. The different C/N_0 Degradation formulas here considered according to [32] are listed below.

$$\Delta[C/N_0]^1 = 1 + \frac{I_{ALT}}{\nu N_0 + I_{REF}} \tag{4.4}$$

$$\Delta[C/N_0]^2 = 1 + \frac{I_{ALT}}{\nu N_0 + I_{REF} + I_{REM} + I_{EXT}} \tag{4.5}$$

In the next sections all the elements to be computed for the estimation of $[C/N_0]_{\text{eff}}$ and $\Delta[C/N_0]$ are explained.

4.1.3 Link Budget

In the framework of RFC assessment the link budget computation is fundamental for the determination of the user received power levels to be considered for both the desired and interfering signals.

In order to compute the minimum and maximum user received power, some assumptions have to be made about the constellation and satellite models, as well as for the propagation environment and the user receiver.

Starting from the transmit chain and the receive chain, simplified models are considered in [32] with respect to the functional block diagrams in Figure 2–1 and Figure 2–11. The transmitter model is characterized by the signal generation block, the transmit filter and the transmit antenna (Figure 4–1).

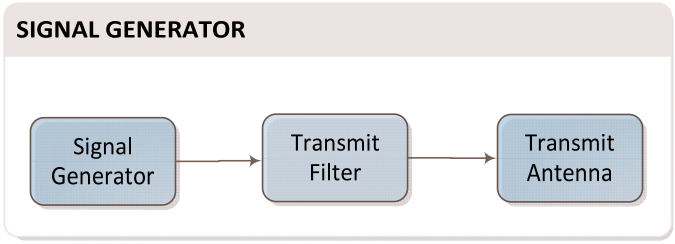

Figure 4–1: Transmit Chain Model for RFC Assessment, Functional Block Diagram.

Regarding the user receiver model, the first stage is the receiver antenna, the output of which is input to the receiver front-end filter. Then the AGC loop is used to keep the voltage input to the ADC within its dynamic range. Finally, correlation is performed using the received signal and a locally generated replica matched to the transmitted signal. The considered losses, namely filtering, ADC and the correlator mismatch losses, are grouped into a single loss factor (Figure 4–2).

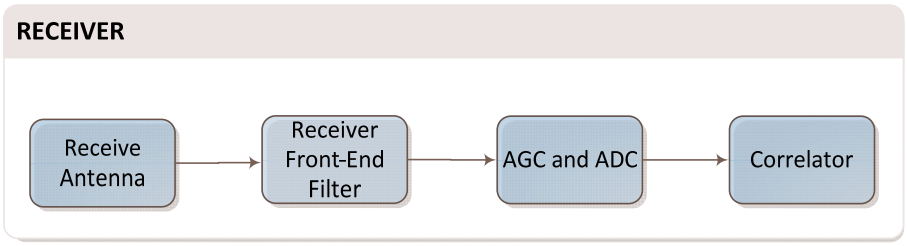

Figure 4–2: Receive Chain Model for RFC Assessment, Functional Block Diagram.

For each individual signal the received power level is computed according to the user location and time instant as described by Eq. (2.27). Three possible ways of computing the signal power levels on ground are considered, depending on the information made available to perform the RFC assessment:

a) If the power transmitted by the navigation payload is known, the computation of the link budget is done 'forward' from the SV to the reference receiver. The assumptions on the antenna gain patterns, propagation environment, and additional losses allow identifying the minimum and maximum power levels on ground. In other words, the two received power levels are the results of a best-case and worst-case link budget computation. The transmit power however in an information typically not shared by RNSS system providers.

b) If only the minimum received power is known, the link budget is first computed 'backward' from the reference receiver to the satellite payload under worst-case assumptions. Once the transmit power is derived, the best-case link budget is computed 'forward' from the SV to the reference receiver to obtain the maximum received power.

c) Finally if the minimum and maximum power levels on ground are both known, the worst-case and best-case link budget computations are performed 'backward'. This operation may result in a minimum and maximum transmit power levels that differ. The offset could reflect transmit antenna gain fluctuations, typically in in the order of 1 dB, or flexible power capabilities.

An example of best-case and worst-case link budget computation based on case c) is provided below in Figure 4–3 and in Table 4-1 for an isotropic user antenna.

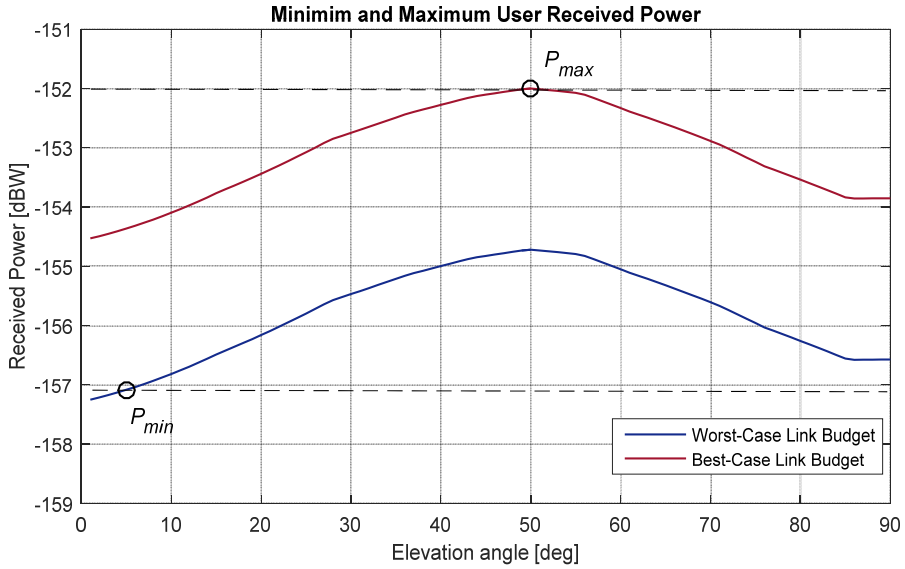

Figure 4–3: Link Budget Values over Elevation: Example for Galileo E1 OS.

As explained later in Section 4.1.5, the analytical approach makes use of the minimum received power on ground for the desired signal (marked in Figure 4–3 as P_{min}), and the maximum received power curve for pre-computing the aggregate gain of the interfering signals. On the other hand, the simulation approach computes dynamically the received power for each location and time instant: the worst-case link budget applies for the desired signal and the best-case link budget applies for the interfering signal.

Table 4-1: Link Budget Computation: Example for Galileo E1 OS.

	$P_{min}^{RX} \rightarrow P_{min}^{TX}$	$P_{max}^{RX} \rightarrow P_{max}^{TX}$
Min/Max Received Power [dBW]	-157.25	-152
@ [deg]	5	50
FSL [dB]	185.45	184.15
Other Losses [dB]	1.5	0
EIRP [dBW]	29.86	32.15
Transmit Antenna Gain [dB]	15.12	16.19
Min/Max Transmit Power [dBW]	14.74	15.96

4.1.4 Spectral Separation Coefficients

The Spectral Separation Coefficient (SSC) is a powerful indicator of the level of interference that a signal suffers due to another interfering signal sharing the same frequency band. The concept at the basis of SSC is measuring the power of the desired signal and its reduction due to the interfering signal at the correlator output.

In Rec. ITU-R M.1831 it is assumed that the RNSS interfering signal is band limited at the satellite transmitter. The transmit filter is modelled as an ideal rectangular band-pass transfer function with linear phase, centred at the signal's carrier frequency, with bandwidth B_T. Thus, the spectrum of the signal, normalized to unit power, is given by:

$$\bar{G}_S(f) = \begin{cases} \dfrac{G_S(f)}{\int_{-B_T/2}^{B_T/2} G_S(f)df} & \text{for } |f| \le B_T/2 \\ 0 & \text{for } |f| > B_T/2 \end{cases} \tag{4.6}$$

where $G_S(f)$ is the two-sided power spectral density [1/Hz], at frequency f, of the unfiltered signal, normalized to unity over an infinite bandwidth.

The spectral separation coefficient between the desired signal and an interfering signal is defined as:

$$SSC^{m,n}(\Delta f^m) = \int_{-B_R/2}^{B_R/2} |H_R|^2 \bar{G}_S(f) \bar{G}_I{}^{m,n}(f - \Delta f^m) df \tag{4.7}$$

where:

H_R Normalized transfer function of the receiver front-end filter [unitless]

$\bar{G}_S(f)$ Two-sided normalized power spectral density of the desired signal, computed according to Eq. (4.6) [1/Hz]

$\bar{G}_I{}^{m,n}(f)$ Two-sided normalized power spectral density of the interfering signal, computed according to Eq. (4.6), where m identifies the transmit satellite and n the signal number transmitted by the m-th satellite [1/Hz]

Δf^m Doppler difference at user position between the desired satellite and the interfering m-th satellite [Hz]

B_R Receiver bandwidth [Hz]

Note that, when $H_R(f) = 1$, the SSC is equal to the cross-correlation between the desired and the interfering normalized PSDs:

$$SSC^{m,n}(\Delta f^m) = \bar{G}_S(f) * \bar{G}_I{}^{m,n}(f)\big|_{f=\Delta f^m} \tag{4.8}$$

Regarding the power spectral densities $\bar{G}_S(f)$ and $\bar{G}_I{}^{m,n}(f)$ representation, it is common assumption to approximate them by a continuous spectrum, where the fine structures of individual signal spectra are averaged together into a smooth shape. Under this hypothesis, the dependency of SSC from the Doppler difference is negligible. This leads to the most commonly used formulation:

$$SSC^{m,n}(0) = \bar{G}_S(f) * \bar{G}_I{}^{m,n}(f)\big|_{f=0} \tag{4.9}$$

Effects of spreading code lines need to be considered in case of short-code signals for which the assumption of continuous spectrum is not accurate. The analytical approach as described in [31] and [32] does not allow simulating the effects of line spectra. In this case, the use of the simulation model is required. The computation of SSCs for short-code signals is out of scope of this thesis. For further details see [40].

4.1.5 Interference Computation

The equivalent noise power densities I_{REF}, I_{ALT} and I_{REM} are calculated according to the following generic formula:

$$I_X = \sum_{m=1}^{M^X} \sum_{n=1}^{N_m^X} \frac{SSC_X^{m,n}(\Delta f^m) P_{R,X}^{m,n}}{L_{R,X}^{m,n}} \tag{4.10}$$

where:

I_X Equivalent noise power density [W/Hz] for GNSS $X \in \{REF, ALT, REM\}$

M^X Number of visible satellites in the constellation identified by X

N_m^X Number of signals transmitted by the m-th satellite in the constellation identified by X

$P_{R,X}^{m,n}$ User received power of the n-th interfering signal transmitted by the m-th satellite in the constellation identified by X [W]

$SSC_X^{m,n}(\Delta f^m)$ Spectral separation coefficient between the desired signal and the n-th interfering signal transmitted by the m-th satellite in the constellation identified by X [1/Hz], expressed as a function of the Doppler difference between the two satellites of interest

$L_{R,X}^{m,n}$ Additional implementation losses of the n-th interfering signal transmitted by the m-th satellite in the constellation identified by X [unitless]

As already stated previously, in [31] and [32] two different methods for assessing the RNSS inter-system interference are described, based on a different way to compute the interference contribution in Eq. (4.10).

The simulation approach provides highly accurate results at the cost of requiring a significantly complex simulation of the environment. For generating the RFC

metrics according to the simulation model a full orbit propagator needs to run over time. In this case the interference scenario is processed at every user location on Earth at each time instant. Clearly the computational load required to perform the RFC assessment according to the simulation model is significant in most occasions.
To the contrary, for the analytical approach the complexity required to carry out the interference analysis is significantly lower. Indeed, the impact of the satellites' orbits as well as the influence of the user and satellite antenna gain is accounted for in a simplified way by means of the Aggregate Gain factor. This figure is one of the main input of the analytical model. In spite of this simplification, the analytical model is still capable of reproducing accurate results comparable with the more complex simulation tools.
Sections 4.1.5.1 and 4.1.5.1 describe the interference computation respectively for the simulation and the analytical approach.

4.1.5.1 Simulation Model

The fundamental characteristic of the simulation model is that, in order to calculate the user received signal power, the link budget has to be performed for each user position and at each time instant. The user received power from each satellite is therefore evaluated as a function of the instantaneous satellite elevation, off-boresight angle, and distance between user position and satellite vehicle.
With this approach, the equivalent noise power density expressed by Eq. (4.10) is further expanded for each user position at each time instant:

$$I_X(t,\varphi,\theta) = \sum_{m=1}^{M^X(t,\varphi,\theta)} \frac{G_T(t,\varphi,\theta)G_R(t,\varphi,\theta)}{L_{FS,X}^m(t,\varphi,\theta)L_{\text{other},X}^m} \sum_{n=1}^{N_m^X} \frac{SSC_X^{m,n}(\Delta f^m)P_{T,X}^{m,n}}{L_{R,X}^{m,n}} \tag{4.11}$$

where:

$I_X(t,\varphi,\theta)$ Equivalent noise power density [W/Hz] for RNSS $X \in \{REF, ALT, REM\}$

$I^X(t,\varphi,\theta)$ Number of visible satellites in the constellation identified by X

J_m^X Number of signals transmitted by the m-th satellite in the constellation identified by X

$G_T(t,\varphi,\theta)$ Transmitting antenna gain at place identified by position coordinates (φ,θ) and at time t for the m-th satellite of the constellation

identified by X [unitless]

$G_R(t, \varphi, \theta)$ User receiver antenna gain at place identified by position coordinates (φ, θ) and at time t for the m-th satellite of the constellation identified by X [unitless]

$L_{FS,X}^{m}(t, \varphi, \theta)$ Free space path loss from the m-th satellite of the constellation identified by X to the place identified by position coordinates (φ, θ) and at time t [unitless]

$L_{\text{other},X}^{m}$ Other losses (atmospheric loss, polarization mismatch loss, depointing loss) [unitless]

$P_{T,X}^{m,n}$ Transmit power of the n-th interfering signal transmitted by the m-th satellite in the constellation identified by X [W]

$SSC_X^{m,n}(\Delta f^m)$ Spectral separation coefficient between the desired signal and the n-th interfering signal transmitted by the constellation identified by X [1/Hz]

$L_{R,X}^{m,n}$ Additional implementation losses of the n-th interfering signal transmitted by the m-th satellite in the constellation identified by X [unitless]

Note that, differently from the analytical approach, the simulation model allows taking into account for the Doppler frequency offset between the desired signal and the interfering signal. However, as explained in Section 4.1.4, for long-code signals the dependency of SSCs from the Doppler difference is negligible.

The defined equivalent noise power density $I_X(t, \varphi, \theta)$ is used to evaluate the different interference metrics. As a result, also the Effective C/N_0 and C/N_0 Degradation depend on (t, φ, θ), and therefore a strategy to represent the metrics is needed. A common approach is to take the mean over time, reducing the dependency only to geographical coordinates (φ, θ), and then to represent the results in a plot over the Earth. Representative values can be also extracted by taking the variance or the minimum/maximum values over time.

4.1.5.2 Analytical Model

In case the analytical model is selected, the equivalent noise power densities coming from the interfering systems are computed according to the following formula, which is a simplified expression for equation (4.10):

$$I_X = \sum_{n=1}^{N_m^X} G_{\text{agg},X}^n \frac{SSC_X^n(0)\max\left\{P_{R,X}^n\right\}}{L_{R,X}^j} \tag{4.12}$$

where

I_X Equivalent noise power density [W/Hz] for RNSS $X \in \{REF, ALT, REM\}$

N_m^X Number of signals transmitted by the m-th satellite in the constellation identified by X

$G_{\text{agg},X}^n$ Aggregate gain factor [unitless]

$\max\{P_{R,X}^n\}$ Maximum user received power of the n-th interfering signal transmitted by the constellation identified by X [W]

$SSC_X^n(0)$ Spectral separation coefficient between the desired signal and the n-th interfering signal transmitted by the constellation identified by X [1/Hz], the Doppler difference is assumed to be 0

$L_{R,X}^n$ Additional implementation losses of the n-th interfering signal transmitted by the constellation identified by X [unitless]

Note that, as explained in Section 4.1.4, the assumption of Doppler frequency offset equal to 0 is justified only for long PRN codes. In case of short codes, the analytical model cannot be adopted and the simulation approach needs to be used instead.

The Aggregate Gain G_{agg} factor is a fundamental element of the analytical interference methodology. As described in [32], the G_{agg} factor depends on a specific simulation scenario, i.e. satellite constellation, satellite antenna gain pattern, user antenna gain pattern and carrier frequency of the signal. The overall G_{agg} computation is based on the link budget which provides the user receiver power level.

Given a user position defined by longitude φ and latitude θ, and a time instant t, the aggregate user received power $P_{R\,\text{agg},X}(t, \varphi, \theta)$ from all satellites of a given RNSS constellation is given by:

$$P_{R\,\mathrm{agg},X}(t,\varphi,\theta) = \sum_{m=1}^{M^X(t,\varphi,\theta)} P_{R,X}^{m}(t,\varphi,\theta) \tag{4.13}$$

where:

$I^X(t,\varphi,\theta)$ Number of visible satellites within the constellation identified by X at time instant t and user position (φ,θ)

$P_{R,X}^{m}(t,\varphi,\theta)$ User received power transmitted by the m-th satellite in the constellation identified by X at time instant t and user position (φ,θ)

The aggregate user received power is dependent on both time and user location on Earth. For simulation purposes, the aggregate user received power is calculated over an Earth and time grid, which resolution and granularity strongly influence the time of computation.

In order to obtain the G_{agg} factor, the aggregate user received power $P_{R\,\mathrm{agg},X}(t,\varphi,\theta)$ is normalized by the maximum received user power for an isotropic user antenna. The maximum G_{agg} value is expressed by

$$G_{\mathrm{agg},X}(\varphi,\theta) = \frac{\max\limits_{t}\left\{P_{R\,\mathrm{agg},X}(t,\varphi,\theta)\right\}}{\max\left\{P_{R\,\mathrm{iso},X}\right\}} \tag{4.14}$$

The maximum G_{agg} factor is the maximum $G_{\mathrm{agg},X}(\varphi,\theta)$ over all longitudes and latitudes:

$$G_{\mathrm{agg},X} = \max_{\varphi,\theta}\left\{G_{\mathrm{agg},X}(\varphi,\theta)\right\} \tag{4.15}$$

In addition to the methodology expressed by equation (4.15) adopted in [32], it is also possible to assess the aggregate impact of a GNSS constellation by keeping the spatial information of the G_{agg}. Therefore a variant of the methodology described in [32] takes into account the $G_{\mathrm{agg}}(\varphi,\theta)$ matrix over the Earth. In this way, the geographical distribution of RNSS interference is taken into account and the resulting interference analysis is more realistic, especially when considering regional RNSS systems.

4.2 New RFC Analysis based on PRN Codes

This new methodology is intended to complement Rec. ITU-R M.1831 by providing the means for estimating the spreading codes cross-interference within and between RNSS systems. The methodology strictly applies to navigation systems based on the CDMA technology that share the same radio-frequency band. The validity of the PRN codes based RFC analysis explained in this chapter is general, however its relevance is mostly significant for short-code signals.

The main idea behind the proposed method is an adaptation of Rec. ITU-R M.1831 that, starting from the consolidated models and assumptions described in Section 4.1, computes the spreading codes correlation performance criteria presented in Chapter 3. When looking at the transmission of spreading codes from a real RNSS constellation, the following two important aspects shall be introduced in the auto- and cross-correlation metrics.

Signal power levels: It is always assumed that signals are normalised to unit power and the cross-correlation interference evaluation takes into account only for the spreading code properties. In reality, as detailed in Section 4.1.3, each navigation signal of a RNSS service is received with different power levels depending on the satellite orbit, payload characteristics, propagation environment, and reference receiver parameters. The minimum and maximum receive power can be derived from the link budget computation provided realistic assumptions on the previously mentioned elements. With respect to Rec. ITU-R M.1831, the analytical approach assumes the worst-case power levels: for each user location on Earth, the desired signal is received with minimum power while the interfering signals are received with maximum power. On the other hand, the assessment based on the simulation model computes the actual power levels by calculating the link budget for each user location and at each time instant. The signal power levels need to be introduced in the cross-correlation interference evaluation as the signal power has a direct impact on the correlation magnitudes.

Doppler offset values: in Chapter 3 the effect of the Doppler frequency offset onto the CDMA isolation is analysed by computing the correlation percentiles in a typical frequency offset range (0 kHz – 5 kHz). The analysis however evaluates the cross-correlation for every PRN codes couple and for each Doppler offset value by assuming that all PRN code combinations are possible and with equal probability. In

reality, even by considering all user locations and time instants, there are combinations that never appear. The distribution of Doppler offset values for each PRN code couple needs to be taken into account for a more accurate assessment, especially for short-code signals which spreading code properties are strongly impacted by spectral lines.

In order to remove the two above-mentioned simplifications, the actual RNSS constellation geometry must be considered and in particular the association between SVs and PRN codes. The Doppler shift between the desired signal and the interfering signals needs to be accounted for as well as the link budget.

4.2.1 Methodology

The methodology here described is meant for assessing the following cases:

- Self-Interference of a PRN code set with it-self;
- Cross-Interference between two PRN code sets, one called ‘desired’ and the other ‘interfering’.

The method can be extended to the case of more than two RNSS services sharing the same navigation frequency band by computing the ‘aggregate’ cross-interference. The multi-RNSS scenario however is not investigated in this thesis.

With respect to the in-band interference classification presented in Rec. ITU-R M.1831, the mapping between naming conventions is described below.

- Interference caused by a PRN code set on it-self is referred to as PRN code set self-interference (e.g. GPS L1-C/A transmitted by different SVs). The PRN code set self-interference contributes to the term I_{REF}.
- Interference cause by a PRN code set onto another set is referred to as PRN code sets cross-interference and can refer to one of the following two cases:
    - Intra-system interference between signals transmitted by the same GNSS system and sharing the same frequency band (e.g. GPS L1-C/A and L1-C); this contribution is also part of I_{REF}.
    - Inter-system Interference between signals with the same band allocation but belonging to different navigation systems (e.g. GPS L1-C and Galileo E1-OS signals); the Inter-system interference belongs to the term I_{INT}.

The following methodology focusses on the spreading codes correlation interference between CDMA based systems, thus external sources I_{EXT} are not taken into account.

Two are the assessment criteria identified for the PRN codes based RFC analysis:

- Self-interference histogram of the desired PRN code set correlation values,
- Cross-interference histogram of correlation values between the desired and the interfering PRN code sets.

Recalling the definition provided in Section 3.3, the self-interference histogram is the histogram of occurrences for the discrete set of cross-correlation magnitudes Ω^{CCF} of a given PRN code set. Similarly, the cross-interference histogram is the histogram of occurrences for the discrete set of cross-correlation magnitudes Ω^{CCF} obtained by computing the cross-correlation between the desired and the interfering PRN code sets.

The methodology proposed for the assessment of a PRN code set self-interference can be summarized with the following steps:

1. Satellite orbits of the reference system are computed over the simulation time in order to generate satellites' position and velocity.
2. Link budgets and Doppler shifts are computed from each satellite to each reference receiver location.
3. Based on the power levels and the Doppler frequency offsets, the SI histograms are computed.

A representation of the algorithm steps is depicted in Figure 4–4. The block diagram provides a high-level view of the input parameters, output values and key functions.

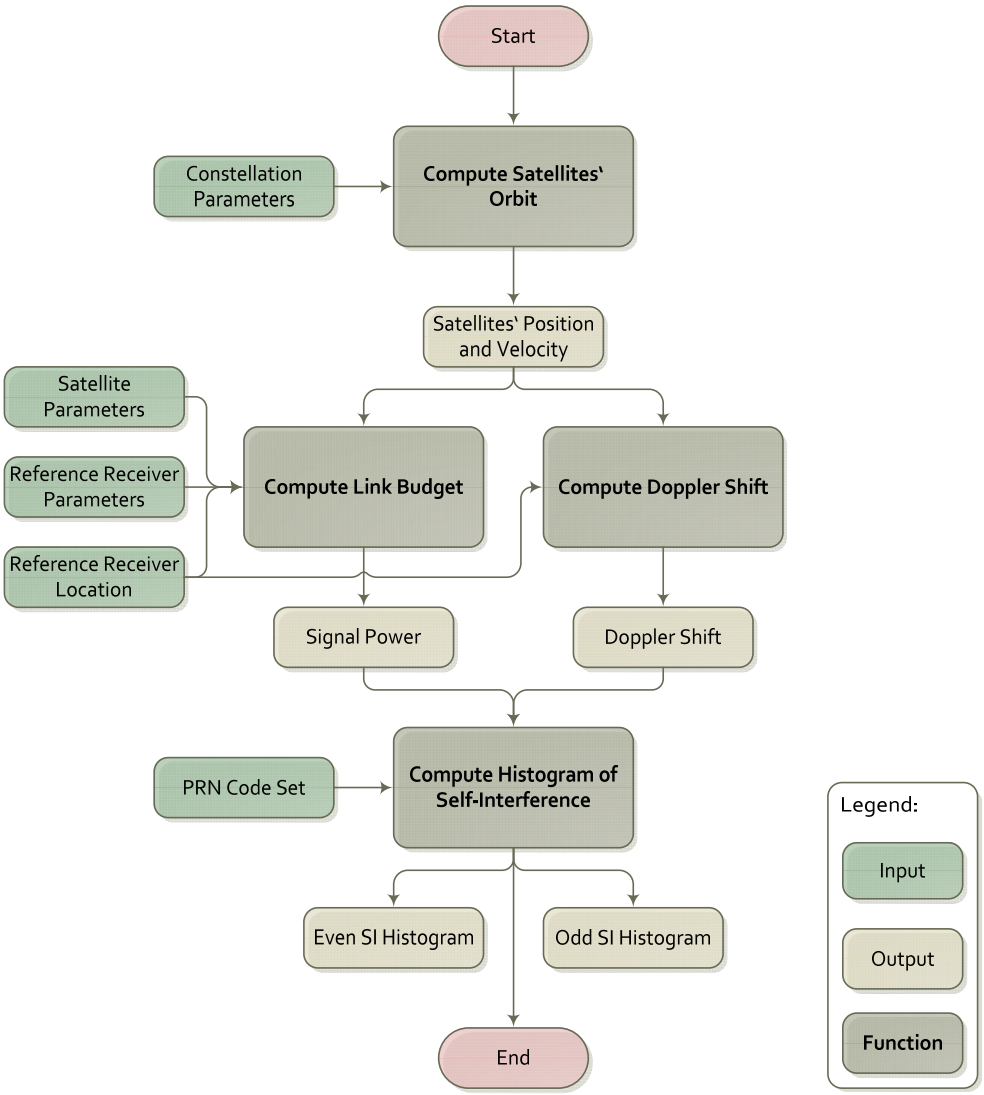

Figure 4–4: Methodology Synthesis for Self-Interference Assessment.

Similarly, the methodology proposed for the assessment of the cross-interference between desired and interfering PRN code sets can be summarized with the following steps:

1. Satellite orbits are computed over the simulation time for the reference system and the interfering system in order to generate satellites' position and velocity.
2. Link budgets and Doppler shifts are computed from each satellite to each reference receiver location for the desired signals and the interfering signals.
3. Based on the power levels and the Doppler frequency offsets, the CI histograms are computed.

Figure 4–5 shows the block diagram of the above described methodology.

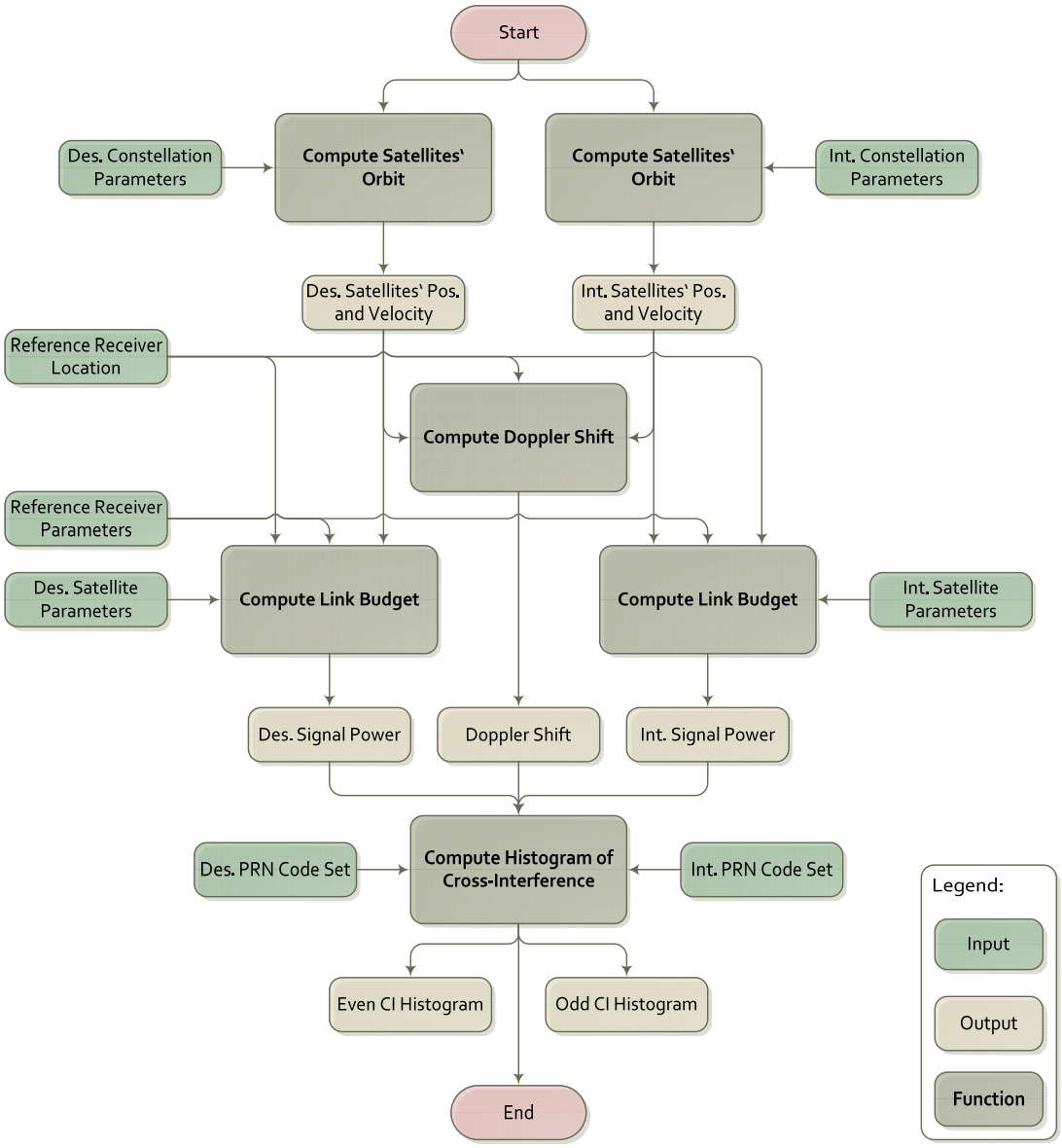

Figure 4–5: Methodology Synthesis for Cross-Interference Assessment.

Note that in both cases of self- and cross-interference assessment the Doppler frequency shift takes into account only for the relative motion of the SV w.r.t. the receiver location. As in Rec. ITU-R M.1831 user dynamics are neglected. This assumption is justified by considering the general scope of the methodology that aims at providing system performance on a service volume.

In order to apply the methodology just described, it is fundamental to identify some key parameters required for computing the PRN codes based RFC assessment criteria:

- respective orbit and constellation parameters;
- respective satellite parameters (antenna gain pattern);

- desired and interfering signals' characteristics (modulation, data rate and spreading codes characteristics) and minimum/maximum received power levels (link budget assumptions for propagation);
- reference receiver parameters (implementation losses, user antenna gain);
- reference receiver locations.

Section 4.3 provides the complete set of assumptions and key parameters at the basis of the simulation results presented in Section 4.4.

In the following the PRN codes based RFC assessment criteria are explained in details. Note that a description of constellation models and satellites' orbit propagation is out of scope of this thesis. For a general understanding of orbital equations it is reminded to the literature [1],[2],[3]. The transmit payload model, receive model, and link budget computation are already described in Section 4.1.3 therefore they are not repeated here.

4.2.2 Assessment Criteria

Similarly to Rec. ITU-R M.1831, two different approaches are proposed in order to assess the PRN code set self-interference and cross-interference. Before providing the expression of the SI and CI some variables need to be defined.

The total number of reference receiver locations $[\varphi, \theta]$ defined for the RFC assessment is called $N_{[\varphi,\theta]}$. Each analysis is performed over a selected simulation time T_{sim} broken down into discrete time instants t uniformly spaced at ΔT; both T_{sim} and ΔT shall be chosen carefully, taking into account the repetition cycle of the RNSS system constellation and the relative motion performed by its SVs with respect to ground in the time interval ΔT. The total number of simulated time instants is referred to as N_t.

4.2.2.1 Simulation Model

The simulation approach implies that the received power levels as well as Doppler shifts due to satellite motion are computed dynamically through link budgets based on the orbital parameters of the different systems, satellite and user antenna gain patterns, as well as user receiver location.

Starting from the computation of self-interference, for any reference receiver location $[\varphi, \theta]$, $M^X[t, \varphi, \theta]$ represents the number of visible satellites at time t for

the RNSS system identified by X. Assuming that each satellite transmits a different PRN code, j and ℓ are the indices of two PRN codes belonging to the set $\{c_\ell[n]\}_{\ell=1}^{N}$ and visible at time t from the location $[\varphi,\theta]$. Additionally, $\Delta\theta_{Dj,\ell}[t,\varphi,\theta] = \Delta f_{Dj,\ell}[t,\varphi,\theta]/f_s$ is the normalized Doppler frequency offset between PRN codes j and ℓ, and $P_j(t,\varphi,\theta)$ is the power received from satellite j computed according to Eq. (2.27) at time t from location $[\varphi,\theta]$. According to Section 4.1.3, the worst-case link budget applies for the desired signal and the best-case link budget applies for the interfering signal.

The expression of the correlation function in Eq. (3.10) is recalled with the addition of the power levels contribution:

$$R_{j,\ell}^{EVEN}[m,t,\varphi,\theta] = \frac{1}{N_I}\sum_{n=0}^{N_I-1}\left(P_j^{max}[t,\varphi,\theta]\cdot c_j[n]\right)^*\cdot\left(P_\ell^{min}[t,\varphi,\theta]\cdot c_\ell[n-m]\right) \cdot \exp\{i(2\pi\Delta\theta_{Dj,\ell}[t,\varphi,\theta]n+\varphi)\}, \text{ for } m\,\epsilon\,[0,2N_I-1] \tag{4.16}$$

$$R_{j,\ell}^{ODD}[m,t,\varphi,\theta] = \frac{1}{N_I}\sum_{n=0}^{N_I-1}(-1)^b\cdot\left(P_j^{max}[t,\varphi,\theta]\cdot c_j[n]\right)^*\cdot\left(P_\ell^{min}[t,\varphi,\theta]\cdot c_\ell[n-m]\right) \cdot \exp\{i(2\pi\Delta\theta_{Dj,\ell}[t,\varphi,\theta]n+\varphi)\}, \text{ for } m\,\epsilon\,[0,2N_I-1] \tag{4.17}$$

$$b = \begin{cases} 1 & \text{if } n \le m \\ 0 & \text{else} \end{cases}$$

For a given PRN code set $\{c_\ell[n]\}_{\ell=1}^{N}$ transmitted by RNSS X, the even/odd SI histogram of correlation values is computed for each receiver location over time as:

$$H^{SI}[m,\varphi,\theta] = \sum_{n=1}^{N_t}\sum_{j=1}^{M^X[t,\varphi,\theta]}\sum_{\substack{\ell=1\\ \ell\neq j}}^{M^X[t,\varphi,\theta]} R_{j,\ell}[m,t,\varphi,\theta] \tag{4.18}$$

where $R_{j,\ell}[m,t,\varphi,\theta]$ is computed according to Eq. (4.16) for the even case and to Eq. (4.17) for the odd case.

The histogram of correlation values for the self-interference analysis is nothing else than the probability density function $f_R(r)$ of the cross-correlation magnitudes $R_{j,\ell}^{CCF}[m]$ described in Section 3.3.2, extended to account for the actual power levels and Doppler over receiver locations and simulation time instants.

Regarding the integration time N_I, a conservative assumption is to take the smallest possible value, i.e. the length of one PRN code sequence. It is demonstrated in Section 3.4.3 that this corresponds to the worst-case scenario.

In the same way, the cross-interference between a desired PRN code set $\{c_\ell^{\mathrm{DES}}[n]\}_{\ell=1}^{N^{DES}}$ transmitted by RNSS X and an interfering PRN code set

$\{c_j^{\mathrm{INT}}[n]\}_{j=1}^{N^{INT}}$ transmitted by RNSS Y is computed as the histogram of correlation values for each receiver location over time:

$$H^{CI}[m,\varphi,\theta] = \sum_{n=1}^{T_t} \sum_{j=1}^{M^Y[t,\varphi,\theta]} \sum_{\ell=1}^{M^X[t,\varphi,\theta]} R_{j,\ell}[m,t,\varphi,\theta] \tag{4.19}$$

$R_{j,\ell}[m,t,\varphi,\theta]$ is defined as in Eq. (3.22) with the addition of the power levels:

$$R_{j,\ell}[m,t,\varphi,\theta] = \frac{1}{N_I} \sum_{n=0}^{N_I-1} \left(P_j^{max}[t,\varphi,\theta] \cdot \hat{c}_j^{INT}[n]\right)^* \cdot \left(P_\ell^{min}[t,\varphi,\theta] \cdot \hat{c}_\ell^{DES}[n-m]\right) \cdot \exp\{i(2\pi\Delta\theta_{Dj,\ell}[t,\varphi,\theta]n + \varphi)\} \text{ , for } m \in [0, 2N_I - 1] \tag{4.20}$$

where the integration time N_I depends on the relationship between T^{INT} and T^{DES} as explained in Section 3.5, $\hat{c}_\ell^{DES}[n]$ is an extended version of c_ℓ^{DES} when $N^{\mathrm{INT}} > N^{\mathrm{DES}}$, and $\hat{c}_j^{INT}$ is an extended and version of c_j^{INT} that takes into account the sign flip pattern b. In this case there are as many CI histograms $H^{CI}[m,\varphi,\theta]$ as the identified correlation patterns.

The SI and CI histograms computed with the simulation approach depend on $[m,\varphi,\theta]$ and therefore a strategy to represent the metrics is needed. In Section 4.4 a selected set of correlation percentiles are displayed over the geographical coordinates $[\varphi,\theta]$.

4.2.2.2 Analytical Model

Given the extremely high computational load required to perform the PRN codes based RFC assessment according to the simulation model just described, the analytical approach is introduced as a simplified computation that can be adopted by taking some elements into consideration.

Similarly to Rec. ITU-R M.1831, the dynamic link budget calculation over receiver locations and simulation time instants is substituted by taking instead the pre-computed minimum and maximum power levels for respectively the desired PRN codes and the interfering ones. However, in the RFC analytical approach explained in Section 4.1.5.2 the maximum interfering power for an isotropic user antenna is scaled by the aggregate gain that is representative for the maximum number of visible satellites and the user receiver antenna gain. For the PRN codes based RFC assessment the aggregate gain cannot be used as the correlation interference is computed signals' couple wise. The absolute power levels are in this case not relevant and what counts is only the offset between power levels. It can be

demonstrated by simulation that the average offset tends to the difference between the best-case and worst-case link budget curves that is constant over the elevation (see results in Section 4.4). In other words, in the analytical approach the received power offset ΔP is pre-computed and it is assumed constant for each PRN code couple. This simplification clearly represents a worst-case assumption when compared to the simulation model.

In the same way, the Doppler frequency offset statistics can be pre-computed for each PRN code couple over the receiver locations and simulation time instants $[t, \varphi, \theta]$. The occurrences of Doppler offset values between code pairs can be used to weight the summation of cross-correlation values $R_{j,\ell}[m]$ that generate the SI and CI histograms.

Let $k_{Dj,\ell}(d)$ be the histogram of occurrences for the Doppler frequency offset values $\Delta\theta_{Dj,\ell}[t, \varphi, \theta]$ between spreading codes $c_j[n]$ and $c_\ell[n]$ over the entire set of receiver locations $N_{[\varphi,\theta]}$ and time instants N_t:

$$k_{Dj,\ell}(d) = \frac{\text{n° of occurrences for} \Delta\theta_{Dj,l}[t, \varphi, \theta] \in [(d-1)\cdot\Delta\Theta, d\cdot\Delta\Theta)}{N_{[\varphi,\theta]} \cdot N_t}, d = \{1, \dots, N_d\} \quad (4.21)$$

where d is the counter of Doppler offset bins, $\Delta\Theta$ is the bin width, and N_d is the total number of frequency bins. The product $N_{[\varphi,\theta]} \cdot N_t$ represents the total number of observations. An illustration of $k_{Dj,\ell}(d)$ histograms for different PRN code couples is provided in Figure 4–6.

The integral of $k_{Dj,\ell}(d)$ over Doppler offset bins gives the probability of occurrence for the PRN code couple (j, ℓ) w.r.t. the total number of observations. The following cases are identified:

$$K_{Dj,\ell} = \sum_{d=1}^{N_d} k_{Dj,\ell}(d) \begin{cases} = 0, & \text{couple } (j,\ell) \text{ never occurs} \\ = 1, & \text{couple } (j,\ell) \text{ is always visible} \\ < 1, & \text{for MEO constellations} \end{cases} \quad (4.22)$$

The case of PRN code couple (j, ℓ) always visible happens for instance for GEO satellites when the reference receiver locations are all in the service area. The correlation performance assessment is Section 3.4.3 with uniformly distributed Doppler offset values corresponds to the case of $k_{Dj,\ell}(d) = 1/N_d\,, \forall d$ and $K_{Dj,\ell} = 1$.

By further normalising the histogram $k_{Dj,\ell}(d)$ with the probability of occurrence $K_{Dj,\ell}$, the numerical probability density function of each PRN code couple Doppler offset $f_{Dj,\ell}(d)$ is obtained.

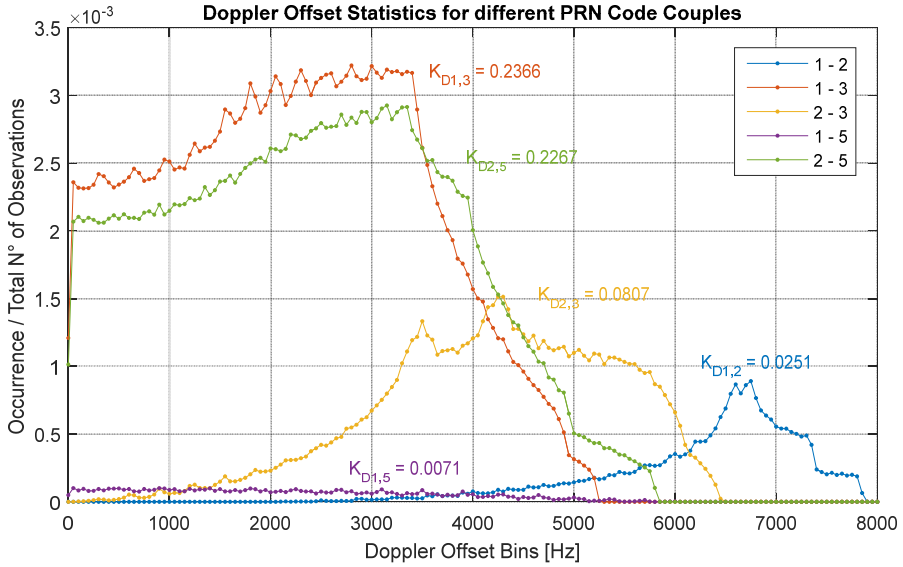

Figure 4–6: Doppler Offset Statistics for different PRN code couples: Example for GPS.

Let K be the sum of all probabilities of occurrence $K_{Dj,\ell}$:

$$K = \sum_{j=1}^{M^X} \sum_{\substack{\ell=1 \\ \ell \neq j}}^{M^X} K_{Dj,\ell} \begin{cases} = N_{couples}, & \text{all couples always visible} \\ < N_{couples}, & \text{for MEO constellations} \end{cases} \tag{4.23}$$

For a given PRN code set $\{c_\ell[n]\}_{\ell=1}^{N}$ transmitted by RNSS X, the even/odd SI histogram of correlation values is computed as:

$$H^{SI}[m] = \sum_{j=1}^{M^X} \sum_{\substack{\ell=1 \\ \ell \neq j}}^{M^X} \frac{K_{Dj,\ell}}{K} \sum_{d=1}^{N_d} f_{Dj,\ell}(d) \cdot H_{j,\ell}[m,d] \tag{4.24}$$

Where the histogram $H_{j,\ell}[m,d]$ is derived for each PRN code couple (j,ℓ) from the correlation functions $R_{j,\ell}[m,d]$ defined as:

$$R_{j,\ell}^{EVEN}[m,d] = \frac{1}{N_I} \sum_{n=0}^{N_I-1} \Delta P \cdot c_j[n]^* \cdot c_\ell[n-m] \cdot \exp\{i(2\pi d \cdot \Delta\Theta \cdot n + \varphi)\}, \text{for } m \in [0, 2N_I - 1] \tag{4.25}$$

For the even case, and for the odd case:

$$R_{j,\ell}^{ODD}[m,d] = \frac{1}{N_I} \sum_{n=0}^{N_I-1} (-1)^b \cdot \Delta P \cdot c_j[n]^* \cdot c_\ell[n-m] \cdot \exp\{i(2\pi d \cdot \Delta\Theta \cdot n + \varphi)\}, \text{for } m \in [0, 2N_I - 1] \tag{4.26}$$

$$b = \begin{cases} 1 & \text{if } n \leq m \\ 0 & \text{else} \end{cases}$$

The cross-interference between a desired PRN code set $\left\{c_{\ell}^{\mathrm{DES}}[n]\right\}_{\ell=1}^{N^{DES}}$ transmitted by RNSS X and an interfering PRN code set $\left\{c_{j}^{\mathrm{INT}}[n]\right\}_{j=1}^{N^{INT}}$ transmitted by RNSS Y is computed as the histogram of correlation values for each receiver location over time:

$$H^{CI}[m] = \sum_{j=1}^{M^{Y}} \sum_{\ell=1}^{M^{X}} \frac{K_{Dj,\ell}}{K} \sum_{d=1}^{N_d} f_{Dj,\ell}(d) \cdot H_{j,\ell}[m,d] \tag{4.27}$$

$R_{j,\ell}[m,d]$ is defined as:

$$R_{j,\ell}[m,d] = \frac{1}{N_I} \sum_{n=0}^{N_I-1} \Delta P \cdot \hat{c}_{j}^{INT}[n]^{*} \cdot \hat{c}_{\ell}^{DES}[n-m] \cdot \exp\{i(2\pi 2\pi d \cdot \Delta d \cdot n + \varphi)\} \text{ , for } m \in [0, 2N_I - 1] \tag{4.28}$$

The representation of $H^{SI}[m]$ and $H^{CI}[m]$ can be done as in Chapter 3 since the analytical approach reduces the assessment metrics to a histogram of one-dimension.

4.3 Reference Assumptions and Scenarios

The assumptions and scenarios described in this section are used for producing the simulation results in Section 4.4.

4.3.1 Orbit and Constellation Parameters

Nominal parameters for the RNSS constellations under analysis are provided in this section. The tables below are mainly indicative as the precise satellite orbit parameters used in the simulations are the Two-Line Element (TLE) files downloaded from [39]. TLE is a data format for encoding a list of orbital elements describing the motion of any Earth-orbiting object for a given point in time or epoch. Further details on the data format and the orbit parameters description can be found in [39].

Note that the association between orbital slot, SV number, and PRN code for each RNSS system is done according to the constellations status on January 2nd, 2017. When the SV number is not indicated in the table it means that the orbital slot is currently empty or the satellite does not transmit in nominal mode. As the scope of simulation results in Section 4.4 is to validate the proposed methodology by providing some computational examples of PRN codes based RFC assessment, constellation variations following the reference date are not taken into account.

4.3.1.1 GPS

Nominal parameters for the GPS satellite orbits are provided in Table 4-2. The constellation is composed of 36 satellites in 6 orbital planes. The so called 'repeat cycle' for the GPS satellite orbits is 1 day. The situation on the reference date is that 5 orbital slots are not active and, with respect to the GPS L1-C/A family of 32 PRN codes, PRN code n° 4 is not transmitted.

Table 4-2: GPS Nominal Orbital Parameters.

Plane/Slot	*SV*	*Semi-major axis*	*Ecc.*	*Inclination*	*RAAN*	*Argument of Perigee*	*Mean Anomaly*
	-	*[km]*	*-*	*[deg]*	*[deg]*	*[deg]*	*[deg]*
A01	24	26559.8	0	55	296.23	0	272.394
A02	31	26559.8	0	55	296.23	0	296.124
A03	30	26559.8	0	55	296.23	0	59.124
A04	07	26559.8	0	55	296.23	0	168.874
A05	-	26559.8	0	55	296.23	0	32.594
A06	-	26559.8	0	55	296.23	0	160.000
B01	16	26559.8	0	55	356.23	0	332.174

B02	25	26559.8	0	55	356.23	0	76.774
B03	28	26559.8	0	55	356.23	0	110.624
B04	12	26559.8	0	55	356.23	0	213.674
B05	26	26559.8	0	55	356.23	0	191.294
B06	20	26559.8	0	55	356.23	0	170.000
C01	29	26559.8	0	55	56.23	0	359.224
C02	27	26559.8	0	55	56.23	0	126.774
C03	19	26559.8	0	55	56.23	0	238.424
C04	17	26559.8	0	55	56.23	0	262.674
C05	08	26559.8	0	55	56.23	0	22.974
C06	-	26559.8	0	55	56.23	0	210.000
D01	02	26559.8	0	55	116.23	0	35.874
D02	01	26559.8	0	55	116.23	0	62.124
D03	21	26559.8	0	55	116.23	0	151.174
D04	06	26559.8	0	55	116.23	0	175.124
D05	11	26559.8	0	55	116.23	0	287.574
D06	-	26559.8	0	55	116.23	0	195.000
E01	03	26559.8	0	55	176.23	0	82.174
E02	22	26559.8	0	55	176.23	0	201.174
E03	05	26559.8	0	55	176.23	0	222.554
E04	18	26559.8	0	55	176.23	0	304.724
E05	-	26559.8	0	55	176.23	0	337.574
E06	10	26559.8	0	55	116.23	0	195.000
F01	14	26559.8	0	55	236.23	0	123.224
F02	15	26559.8	0	55	236.23	0	146.954
F03	09	26559.8	0	55	236.23	0	246.474
F04	23	26559.8	0	55	236.23	0	355.224
F05	32	26559.8	0	55	236.23	0	20.654
F06	13	26559.8	0	55	236.23	0	170.000

Figure 4–7 represents the ground track of GPS satellites for 1 day orbits propagation starting from the reference date.

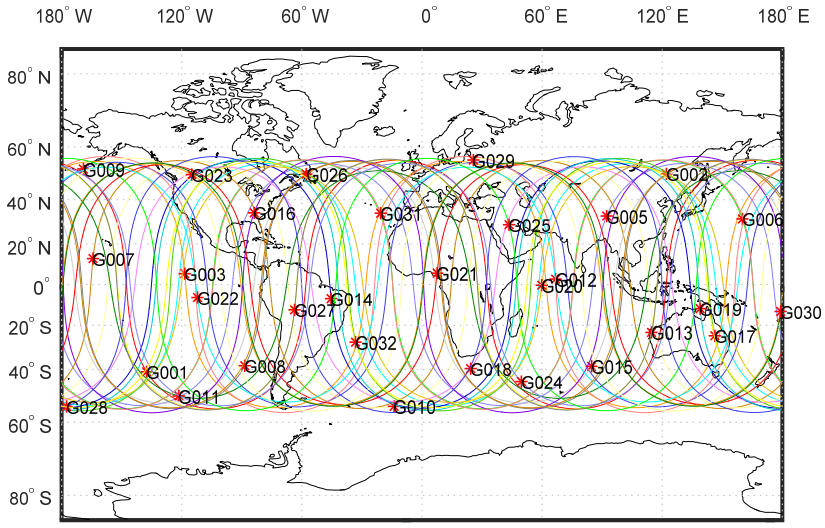

Figure 4–7: GPS Constellation Groud Track.

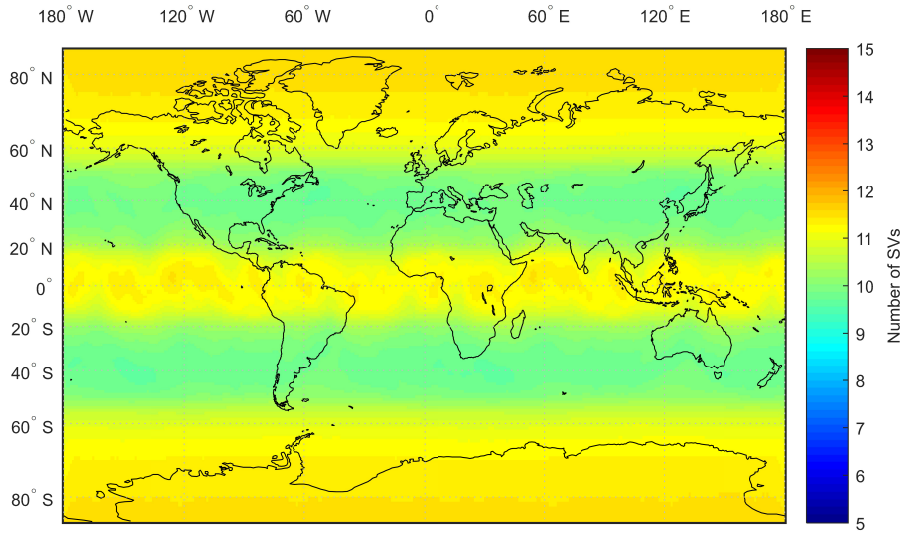

Figure 4–8: GPS Constellation, Average Number of Visible Satellites.

A world chart with the average number of GPS visible satellites is shown in Figure 4–8. The masking angle used to produce the figure is 5° elevation.

4.3.1.2 Galileo

Nominal parameters for the Galileo satellite orbits are provided in Table 4-3. The constellation is composed of 24 operational satellites in 3 orbital planes (Walker 24/3/1) plus up to 6 active spares. The repeat cycle for Galileo satellite orbits is 10 days, nevertheless simulations over 1 day are considered enough representative of the constellation behaviour. The situation on the reference date is that 8 orbital slots are not yet filled. With respect to the Galileo PRN code families of 50 codes, the PRN codes n° 06, 10, 13, 15, 16, 17, 21, 23, 25, 27, 28, 29, 31-50 are not transmitted while PRN codes n° 14 and 18 are assigned to satellites on wrong orbits (GSAT0201 and GSAT0202).

Table 4-3: Galileo Nominal Orbital Parameters.

Plane/Slot	*SV* -	*Semi-Major Axis* [km]	*Ecc.* -	*Inclination* [deg]	*RAAN* [deg]	*Argument of Perigee* [deg]	*True Anomaly* [deg]
A01	-	29599.8	0	56.0	25.0	0.0	-21.67
A02	01	29599.8	0	56.0	25.0	0.0	23.33
A03	-	29599.8	0	56.0	25.0	0.0	68.33
A04	-	29599.8	0	56.0	25.0	0.0	113.33
A05	30	29599.8	0	56.0	25.0	0.0	158.33
A06	02	29599.8	0	56.0	25.0	0.0	-156.67
A07	-	29599.8	0	56.0	25.0	0.0	-111.67
A08	24	29599.8	0	56.0	25.0	0.0	-66.67
B01	-	29599.8	0	56.0	145.0	0.0	-6.67
B02	-	29599.8	0	56.0	145.0	0.0	38.33

B03	22	29599.8	0	56.0	145.0	0.0	83.33
B04	-	29599.8	0	56.0	145.0	0.0	128.33
B05	11	29599.8	0	56.0	145.0	0.0	173.33
B06	12	29599.8	0	56.0	145.0	0.0	-141.67
B07	-	29599.8	0	56.0	145.0	0.0	-96.67
B08	26	29599.8	0	56.0	145.0	0.0	-51.67
C01	05	29599.8	0	56.0	265.0	0.0	8.33
C02	09	29599.8	0	56.0	265.0	0.0	53.33
C03	04	29599.8	0	56.0	265.0	0.0	98.33
C04	19	29599.8	0	56.0	265.0	0.0	143.33
C05	20	29599.8	0	56.0	265.0	0.0	-171.67
C06	07	29599.8	0	56.0	265.0	0.0	-126.67
C07	08	29599.8	0	56.0	265.0	0.0	-81.67
C08	03	29599.8	0	56.0	265.0	0.0	-36.67

For illustration purposes the ground track of Galileo satellites for 1 day orbits propagation is provided in Figure 4–9 starting from the reference date.

A world chart with the average number of Galileo visible satellites is shown in Figure 4–10. As for GPS, the masking angle used to produce the figure is 5° elevation.

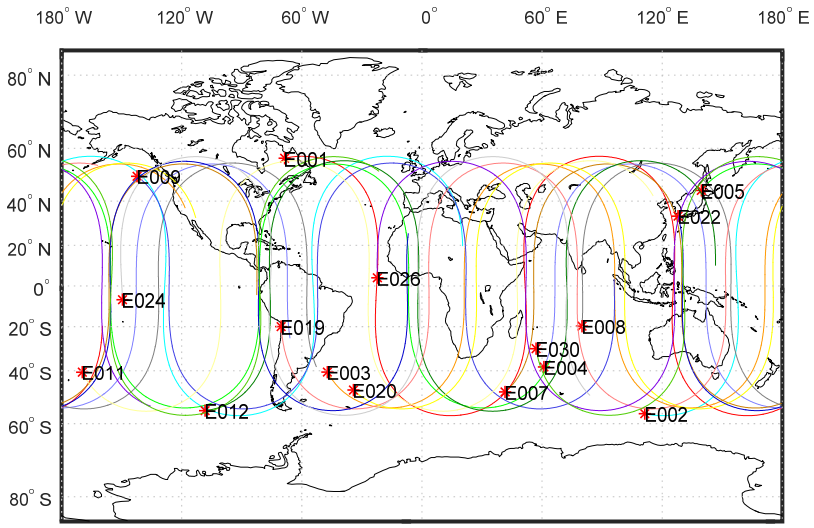

Figure 4–9: Galileo Constellation Ground Track.

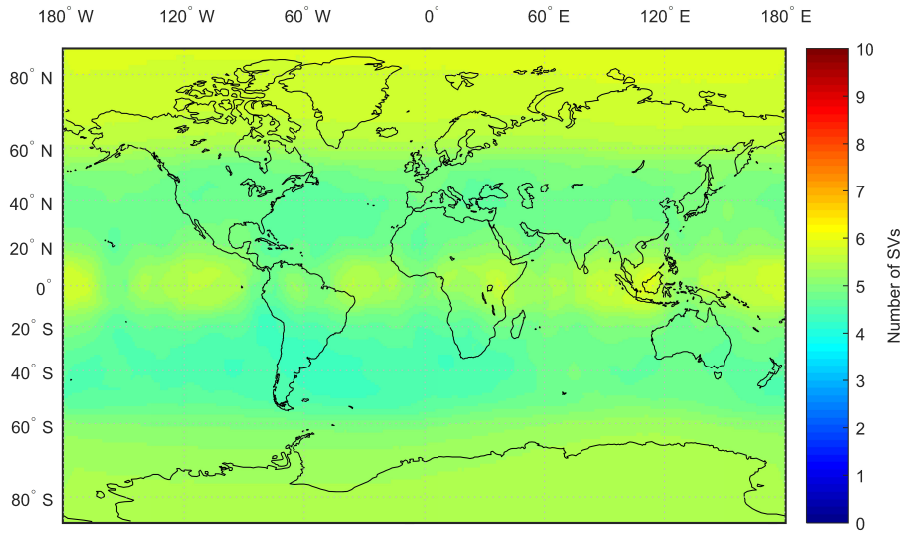

Figure 4–10: Galileo Constellation, Average Number of Visible Satellites.

4.3.1.3 EGNOS

Nominal parameters for the EGNOS satellite orbits are provided in Table 4-4. The constellation is composed of 3 satellites placed on the GEO orbit with 2 operational SVs plus 1 in-orbit spare for testing and qualification activities. The situation at the observation time (03.01.2017) is the one represented below, with PRN codes n° 120 and 123 actively transmitting the EGNOS service, while 126 and 136 are used for testing purposes. The actual orbital placement of EGNOS hosting satellites is subject to change over time due to commercial or operational requirements.

Table 4-4: EGNOS Nominal Orbital Parameters.

SV Name	*Slot [deg]*	*PRN -*	*Semi-Major Axis [km]*	*Ecc. -*	*Inclination [deg]*	*Status*
AOR-E	15.5 W	120	42164.2	0	0	active
ARTEMIS	21.5 E	124	42164.2	0	0	retired
IOR-W	25.0 E	126	42164.2	0	0	testing
SES-5	5.0 E	136	42164.2	0	0	testing
Astra 5B	31.5 E	123	42164.2	0	0	active

Figure 4–11 shows the ground track of EGNOS satellites for one day propagation from the reference date. As expected, the satellites are stationary w.r.t. reference location on Earth.

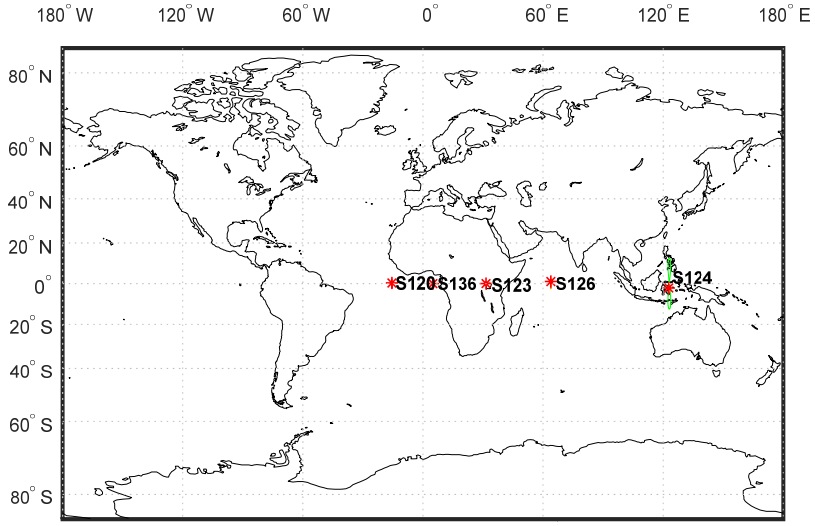

Figure 4–11: EGNOS Constellation Ground Track.

For the simulations in Section 4.4 both active and testing satellites are taken into account since testing satellites produce PRN codes cross-interference even if they are not transmitting a valid EGNOS signal. A world chart with the average number of EGNOS satellites is shown in Figure 4–12. The masking angle used to produce the figure is 5° elevation.

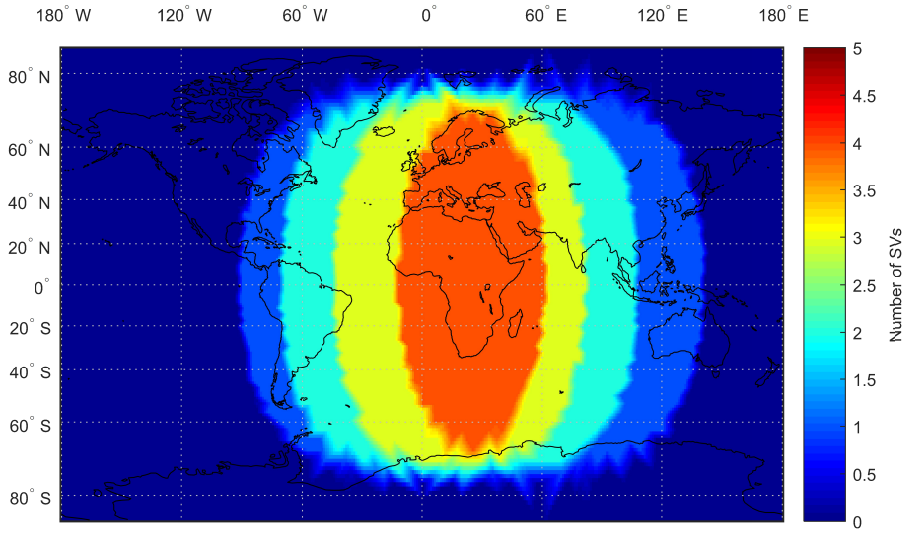

Figure 4–12: EGNOS Constellation, Average Number of Visible Satellites.

4.3.1.4 BeiDou

The BeiDou satellites constellation is currently under deployment and it is planned according to the following phases:

- Phase II or BD-2 (actual): the operational constellation is composed of 5 GSO, 5 IGSO, and 4 MEO.

- Phase III or BD-3 (future): the operational constellation is composed of 3 GSO, 3 IGSO, and 24 MEO satellites deployed in 3 orbital planes (Walker 24/3/1) plus 3 spares.

Nominal parameters for the BeiDou GSO SVs are provided in Table 4-5. The first column indicates for each satellite its deployment phase. With respect to the 5 GSOs planned for Phase II, G7 has been added for reliability redundancy improving.

Table 4-5: BeiDou GSO Nominal Orbital Parameters.

SV Name	*Slot* *[deg]*	*PRN* *-*	*Semi-Major Axis* *[km]*	*Ecc.* *-*	*Inclination* *[deg]*	*Status*
BD-2/3 G 1	140 E	1	42164.2	0	0	active
BD-2/3 G 3	110.5 E	3	42164.2	0	0	active
BD-2 G 4	160 E	4	42164.2	0	0	active
BD-2 G 5	58.75 E	5	42164.2	0	0	active
BD-2/3 G 6	80 E	2	42164.2	0	0	active
BD-2/3 G 7	144 E	17	42164.2	0	0	active

Table 4-6 summarises the nominal parameters for the BeiDou IGSO/MEO satellites. The first 6 IGSOs and the following 4 MEOs belong to Phase II. The PRN codes assignment is indicated according to the current status.

Table 4-6: BeiDou IGSO/MEO Nominal Orbital Parameters.

Plane/Slot	*SV* *-*	*Semi-major axis* *[km]*	*Ecc.* *-*	*Inclination* *[deg]*	*RAAN* *[deg]*	*Argument of Perigee* *[deg]*	*Mean Anomaly* *[deg]*
IGSO 1	6	42164.2	0	55	248.82	0	0
IGSO 2	7	42164.2	0	55	128.82	0	120
IGSO 3	8	42164.2	0	55	8.8247	0	240
IGSO 4	9	42164.2	0	55	175.73	0	60
IGSO 5	10	42164.2	0	55	55.732	0	180
IGSO 6	13	42164.2	0	55	N/A	0	N/A
M 3	11	27878	0	55	120	0	105
M 4	12	27878	0	55	120	0	150
M 5	-	27878	0	55	240	0	300
M 6	14	27878	0	55	240	0	345
BD-3 I1	31	42164.2	0	55	0	0	187.6
BD-3 I2	32	42164.2	0	55	120	0	67.6
BD-3 I3	-	42164.2	0	55	240	0	307.6
BD-3 M1	33	27878	0	55	0	0	0
BD-3 M2	34	27878	0	55	0	0	45
BD-3 M3	35	27878	0	55	0	0	90
BD-3 M4	-	27878	0	55	0	0	135
BD-3 M5	-	27878	0	55	0	0	180
BD-3 M6	-	27878	0	55	0	0	225
BD-3 M7	-	27878	0	55	0	0	270
BD-3 M8	-	27878	0	55	0	0	315
BD-3 M9	-	27878	0	55	120	0	15

Plane/Slot	*SV*	*Semi-major axis*	*Ecc.*	*Inclination*	*RAAN*	*Argument of Perigee*	*Mean Anomaly*
	-	*[km]*	*-*	*[deg]*	*[deg]*	*[deg]*	*[deg]*
BD-3 M10	-	27878	0	55	120	0	60
BD-3 M11	-	27878	0	55	120	0	105
BD-3 M12	-	27878	0	55	120	0	150
BD-3 M13	-	27878	0	55	120	0	195
BD-3 M14	-	27878	0	55	120	0	240
BD-3 M15	-	27878	0	55	120	0	285
BD-3 M16	-	27878	0	55	120	0	330
BD-3 M17	-	27878	0	55	240	0	30
BD-3 M18	-	27878	0	55	240	0	75
BD-3 M19	-	27878	0	55	240	0	120
BD-3 M20	-	27878	0	55	240	0	165
BD-3 M21	-	27878	0	55	240	0	210
BD-3 M22	-	27878	0	55	240	0	255
BD-3 M23	-	27878	0	55	240	0	300
BD-3 M24	-	27878	0	55	240	0	345
BD-3 M25	-	27878	0	55	0	0	10
BD-3 M26	-	27878	0	55	120	0	55
BD-3 M27	-	27878	0	55	240	0	105

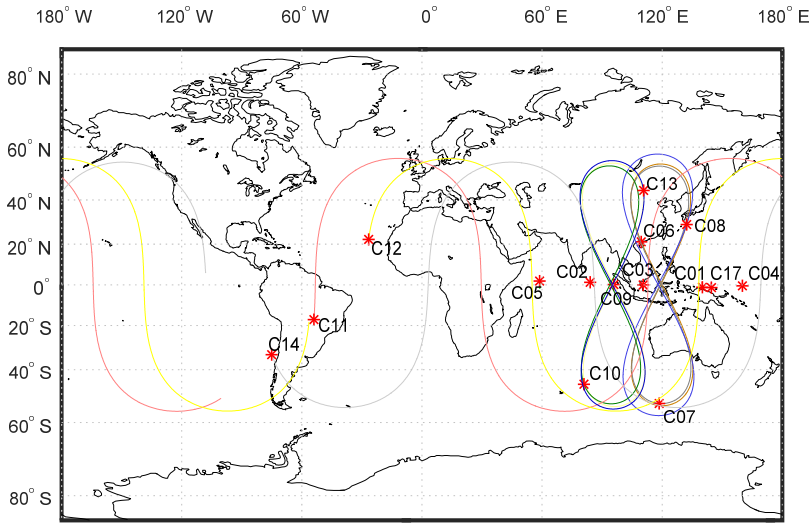

Figure 4–13: BeiDou Phase II Constellation Groud Track.

For the simulations in Section 4.4 only BeiDou Phase II constellation is taken into account. In Figure 4–13 the ground track of BD-2 satellites is represented over 24 hours. A world chart with the average number of BeiDou satellites is shown in . The masking angle used to produce the figure is 5° elevation.

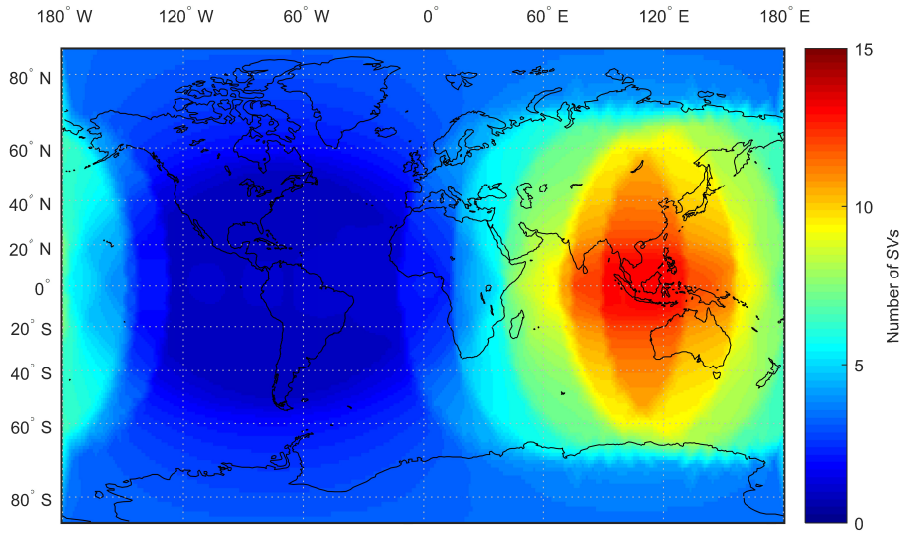

Figure 4–14: BeiDou Phase II Constellation, Average Number of Visible Satellites.

4.3.2 Satellite Antenna Characteristics

Representative satellite antenna gain patterns are provided below for GPS, Galileo, EGNOS, and BeiDou systems for the navigation frequency bands of interest. The values reported are nominal mean values over azimuth. It is understood that this assumption is a simplification and it does not take into account the variation of antenna patterns among satellites of the same constellation. This simplified approach is still considered to be a good approximation for the purpose of this study.

4.3.2.1 GPS

Table 4-7 provides reference antenna gain patterns for GPS L1 and L5 bands.

Table 4-7: GPS Nominal Satellite Antenna Gain.

Off-Boresight Angle [deg]	*L1 Band Gain @1575.42 MHz [dBic]*	*L5 Band Gain @1176.45 MHz [dBic]*
0	13.6	13.6
2	13.4	13.5
4	13.2	13.1
6	13.4	12.6
8	14.3	12.5
10	15.0	12.8
12	15.1	13.3
14	14.4	13.5
16	12.7	13.2

4.3.2.2 Galileo

Table 4-8 provides reference antenna gain patterns for Galileo E1 and E5 bands.

Table 4-8: Galileo Nominal Satellite Antenna Gain.

Off-Boresight Angle [deg]	*E1 Band Gain @1575.42 MHz [dBic]*	*E5 Band Gain @1191.795 MHz [dBic]*
0	13.9	13.7
1	13.9	13.7
2	14.2	13.8
3	14.5	14.0
4	14.9	14.4
5	15.25	14.8
6	15.6	15.1
7	16	15.4
8	16.2	15.6
9	16.2	15.7
10	16.1	15.7
11	15.9	15.6
12	15.4	15.3
13	14.7	14.9
14	13.7	14.2
15	12.9	13.5

4.3.2.3 EGNOS

Table 4-9 provides reference antenna gain patterns for EGNOS L1 and L5 bands.

Table 4-9: EGNOS Nominal Satellite Antenna Gain.

Off-Boresight Angle [deg]	*L1 Band Gain @1575.42 MHz [dBic]*	*L5 Band Gain @1176.45 MHz [dBic]*
0	18.8	18.8
1	18.8	18.8
2	18.6	18.6
3	18.4	18.4
4	18.1	18.1
5	17.8	17.8
6	17.3	17.3
7	16.8	16.8
8	16.2	16.2
9	15.6	15.6

4.3.2.4 BeiDou

Table 4-13 provides reference antenna gain patterns for BeiDou Phase II satellites transmitting in B1 and B2 bands.

Table 4-10: BeiDou Nominal Satellite Antenna Gain.

	GSO/IGSO		MEO	
Off-Boresight Angle [deg]	***B1 Band Gain @1561.098 MHz [dBic]***	***B2 Band Gain @1207.140 MHz [dBic]***	***B1 Band Gain @1561.098 MHz [dBic]***	***B2 Band Gain @1207.140 MHz [dBic]***
0	14.2	13.4	12.5	12.4
1	14.2	13.4	12.5	12.4
2	14.2	13.5	12.6	12.5
3	14.3	13.6	12.8	12.7
4	14.4	13.7	13	12.9
5	14.4	13.9	13.3	13.1
6	14.5	14.1	13.6	13.4
7	14.5	14.2	13.9	13.7
8	14.5	14.4	14.1	13.9
9	14.4	14.5	14.3	14.2
10	14.3	14.5	14.2	14.3
11	14.0	14.6	14	14.4
12	13.6	14.5	13.6	14.4
13	13.1	14.4	13	14.3
14	12.5	14.2	12.3	14.1
15	11.8	14	12.3	14.1

4.3.3 Signal Characteristics

The navigation signal characteristics of interest are provided below for GPS, Galileo and EGNOS systems. The information reported in the tables is mainly taken from the navigation systems' respective SIS ICDs.

Note that the 'PRN Code Set Size' indicates the cardinality of the full spreading codes set reported on the SIS ICD, however the PRN codes used in the simulations are only those actually transmitted according to the constellations status described in Section 4.3.1.

Note also that the values reported under 'Integration Time' are to be meant as values of interest for the simulations and not necessarily all possible values. The primary code period is always indicated as the minimum integration time. When the signal is modulated by navigation symbols, the symbol period is also indicated as the maximum integration time. If secondary codes are present, the secondary code chip length and secondary code period are possible integration time values.

4.3.3.1 GPS

Table 4-11: GPS Signals Characteristics.

	L1-C/A	***L1-C data***	***L1-C pilot***	***L5-I***	***L5-Q***
Carrier Frequency [MHz]	1575.42	1575.42	1575.42	1176.45	1207.14
Modulation	BPSK(1)	BOC(1,1)	TMBOC	BPSK(10)	BPSK(10)
Tx Bandwidth [MHz]	30.69	30.69	30.69	24.0	24.0
Primary Code Length [chip]	1,023	10,230	10,230	10,230	10,230
Primary Chip Rate [Mcps]	1.023	1.023	1.023	10.230	10.230
Secondary Code Length [chip]	-	-	1800	10	20
Secondary Chip Rate [cps]	-	-	100	1000	1000
Symbol Rate [sps]	50	100	-	100	-
PRN Code Set Size [-]	32	63	63	37	37
Integration Time [ms]	1, 20	10	10	1, 10	1, 20
Fraction of Power (%)	100	25	75	50	50
Min Power [dBW]	-158.5	-157		-154.9	
Max Power [dBW]	-153.0	-152		-148.0	

In Table 4-11 the minimum received power is measured at the output of a 3 dBi linearly polarised terrestrial user receiving antenna (located near ground) at worst normal orientation, when the SV is at or above 5 degree elevation angle, accounting for free space path loss, 0.5 dB excess atmospheric loss, and worst-case polarization ellipticity (4 dB) of the transmitted signal. The maximum received power is measured at the output of a 0 dBi circularly polarised user receiving antenna (located near ground), for any elevation angle, accounting for free space path loss, no excess atmospheric loss, and no polarization loss.

4.3.3.2 Galileo

Table 4-12: Galileo Signals Characteristics.

	E1-B	***E1-C***	***E5a-I***	***E5a-Q***	***E5b-I***	***E5b-Q***
Carrier Frequency [MHz]	1575.42	1575.42	1176.45	1176.45	1207.14	1207.14
Modulation	CBOC+	CBOC-	BPSK(10)	BPSK(10)	BPSK(10)	BPSK(10)
Tx Bandwidth [MHz]	32.84	32.84	55.59	55.59	55.59	55.59
Primary Code Length [chip]	4,092	4,092	10,230	10,230	10,230	10,230
Primary Chip Rate [Mcps]	1.023	1.023	10.230	10.230	10.230	10.230
Sec. Code Length [chip]	-	25	20	100	4	100
Sec. Chip Rate [cps]	-	250	1000	1000	1000	1000
Symbol Rate [sps]	250	-	50	-	250	-
PRN Code Set Size [-]	50	50	50	50	50	50
Integration Time [ms]	4	4, 100	1, 20	1, 100	1, 4	1, 100
Fraction of Power (%)	50	50	50	50	50	50
Min Power [dBW]	-157.25		-155.25		-155.25	

Max Power [dBW]	-152	-150	-150

In Table 4-12 the minimum and maximum received power levels are measured at the antenna port of a RHCP 0 dBi terrestrial user receiving antenna on-ground when the SV is at any elevation angle above a 5 degree. For the minimum link budget, 0.5 dB excess atmospheric loss and 1 dB polarisation mismatch loss are considered.

4.3.3.3 EGNOS

Table 4-13: EGNOS Signals Characteristics.

	L1	***L5-I***	***L5-Q***
Carrier Frequency [MHz]	1575.42	1176.45	1207.14
Modulation	BPSK(1)	BPSK(10)	BPSK(10)
Tx Bandwidth [MHz]	24.0	24.0	24.0
Primary Code Length [chip]	1,023	10,230	10,230
Primary Chip Rate [Mcps]	1.023	10.230	10.230
Secondary Code Length [chip]	-	-	-
Secondary Chip Rate [cps]	-	-	-
Symbol Rate [sps]	500	500	TBD
PRN Code Set Size [-]	39	39	39
Integration Time [ms]	1, 2	1, 2	1, TBD
Fraction of Power (%)	100	50	50
Min Power [dBW]	-158.5	-161.0	
Max Power [dBW]	-152.5	-153.0	

In Table 4-13 the minimum and maximum received power levels assumption is the same as for Table 4-12.

4.3.3.4 BeiDou

Table 4-14: BeiDou Signals Characteristics.

	B1-I	***B2-I***
Carrier Frequency [MHz]	1561.098	1207.140
Modulation	BPSK(2)	BPSK(2)
Tx Bandwidth [MHz]	20.46	20.46
Primary Code Length [chip]	2,046	2,046
Primary Chip Rate [Mcps]	2,046	2,046
Secondary Code Length [chip]	-	-
Secondary Chip Rate [cps]	-	-
Symbol Rate [sps]	500	500
PRN Code Set Size [-]	37	37
Integration Time [ms]	1, 2	1, 2
Fraction of Power (%)	100	100

Min Power [dBW]	-158.2 (GSO/IGSO) -156.4 (MEO)	-157.7 (GSO/IGSO) -156.0 (MEO)
Max Power [dBW]	-153.0 (GSO/IGSO) -151.3 (MEO)	-152.9 (GSO/IGSO) -151.0 (MEO)

4.3.4 Reference Receiver Parameters

The front-end filter of the reference receiver is designed according to the desired navigation signal and it results from a trade-off between the target performance and the receiver complexity, cost and size. For the RFC assessment only the receive bandwidth is relevant as it determines the filtering loss and thus impacts the link budget computation. In accordance with Rec. ITU-R M.1831, the steps to compute the filtering loss for each signal under analysis are the following:

1. Calculate the signal power spectral density from the analytical expression of the signal modulation (continuous spectrum);
2. Normalise the PSD to unit power in the defined transmit bandwidth, as expressed by Eq. (4.6);
3. Compute the received power by integrating the resulting PSD over the reference receiver bandwidth, assuming an ideal rectangular filter.

For the simulations in Section 4.4 three are the reference receivers or use cases taken into account, each related to a different application: Mass-Market, Aviation, and RIMS Station. Table 4-15 provides the receive bandwidth assumptions for the three use cases and for each frequency band of interest.

Table 4-15: Reference Receiver Bandwidth.

	Mass Market User	***Aviation User***	***RIMS Station***
L1/E1/B1 Rx Bandwidth [MHz]	4	12	24
L5/E5/B2 Rx Bandwidth [MHz]	N/A	12	24

Table 4-16 provides the antenna gain patterns for each of the three use cases' reference receivers.

Table 4-16: Reference Receiver Antenna Gain.

	Mass Market User	***Aviation User***	***RIMS Station***	
Elevation [deg]	***All Bands [dBic]***	***All Bands [dBic]***	***L1 [dBic]***	***L5 [dBic]***
0	0	-7.0	-5	-5.5
5	0	-5.5	-3	-3.5

10	0	-1.4	-2.5	-2.5
15	0	0.0	-1	-1.5
20	0	0.8	0	-0.5
25	0	1.1	0.5	0.5
30	0	1.2	1	1.5
35	0	1.2	2	2.25
40	0	1.2	3	3
45	0	1.3	3.5	3.75
50	0	1.3	4	4.5
55	0	1.5	4.25	5
60	0	1.6	4.5	5.5
65	0	1.8	4.75	6
70	0	1.9	5	6.5
75	0	2.1	5	6.75
80	0	2.2	5	7
85	0	2.3	5	7
90	0	2.3	5	7

4.3.5 Reference Receiver Locations

Three different sets of reference receiver locations are taken into account in the following simulations.

The first one is composed of 4586 points uniformly distributed over an Earth grid with about 3 degrees resolution. This scenario is adopted for global RFC assessments of the mass-market and aviation users (Figure 4–15).

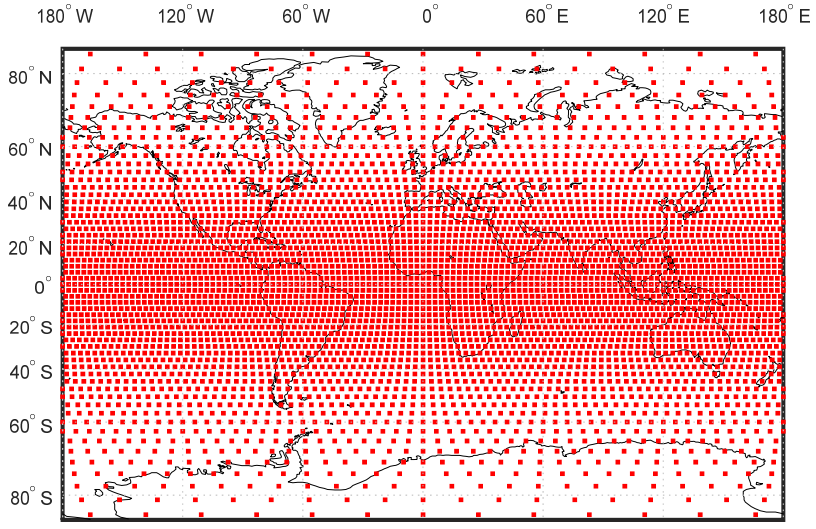

Figure 4–15: Reference Receiver Locations: Earth Grid.

The second set, illustrated in Figure 4–16, is composed of 587 points that correspond to the Earth population sites with more than 500,000 inhabitants. These reference receiver locations are used only in combination with the mass-market use case.

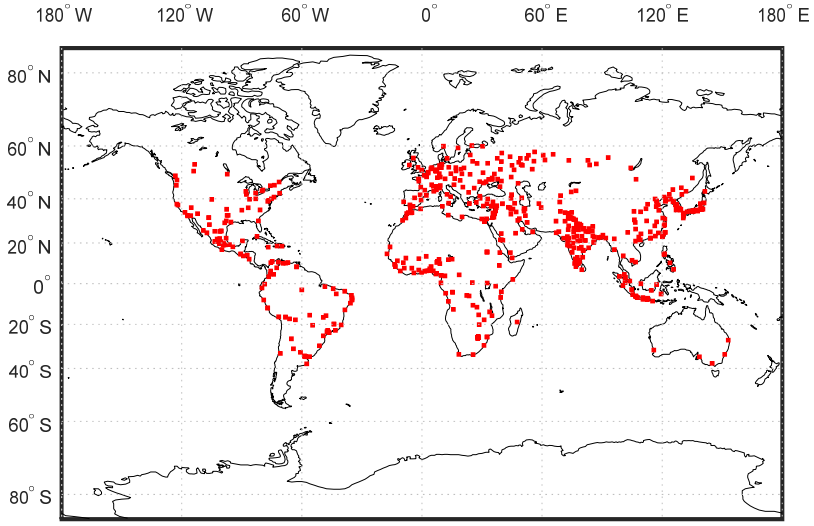

Figure 4–16: Reference Receiver Locations: Cities.

The last set of interest is represented by the EGNOS RIMS Network. The EGNOS ground segment is continuously evolving and new sites have been added recently to the original network. For the purpose of the following RFC assessment only the 39 stations depicted in Figure 4–17 are considered.

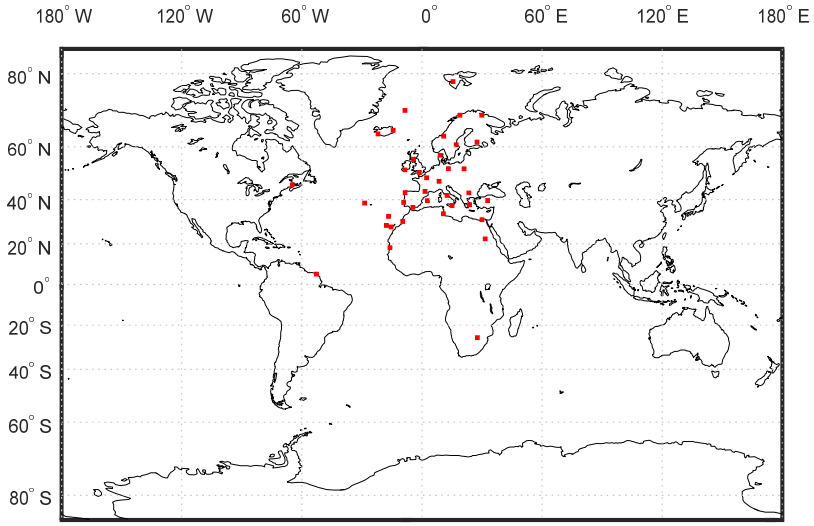

Figure 4–17: Reference Receiver Locations: RIMS Network.

The RIMS sites locations are also provided in Table 4-17. Following the North East Down (NED) coordinate system, positive latitudes indicate North and positive longitudes East. Clearly this scenario is used only for the RIMS station use case.

Table 4-17: RIMS Sites Coordinates.

Station ID	Latitude [°]	Longitude [°]
ALB	57.10	9.09
ACR	38.51	-28.62
BRN	52.32	13.25
CNR	27.95	-15.38
CTN	37.47	15.07
CRK	51.85	-8.50
WRS	52.22	21.07
DJA	33.87	10.77
EGI	65.28	-14.40
GLG	55.70	-4.10
HBK	-25.88	27.70
GOL	39.63	32.80
KOU	5.17	-52.68
LSB	38.78	-9.13
SWA	50.88	-1.28
MAD	32.75	-16.70
MLG	36.68	-4.52
KIR	69.68	29.92
PDM	39.57	2.73
PAR	48.83	2.33

Station ID	Latitude [°]	Longitude [°]
MON	46.07	-64.78
RKK	64.13	-21.93
ROM	41.80	12.58
LAP	61.53	27.55
SDC	42.92	-8.42
SOF	42.80	23.42
GVL	60.67	17.13
TLS	43.42	1.50
TRD	63.45	10.90
TRO	69.67	18.95
ZUR	47.45	8.57
LYR	78.24	15.52
JME	70.99	-8.48
NOU	18.10	-15.95
LPI	28.61	-17.76
ATH	37.85	23.78
ALY	31.18	29.96
AGA	30.40	-9.60
ABS	22.35	31.61

4.4 Simulation Results

Scope of this section is to provide computational examples of the PRN codes based RFC methodology proposed in this thesis and to compare the results obtained by applying the simulation model with respect to the analytical model.

4.4.1 GPS L1-C/A Self-Interference

Three Scenarios are selected for the GPS L1-C/A self-interference assessment as reported in Table 4-18.

Table 4-18: GPS L1-C/A Self-Interference Scenarios.

	Open Sky	***Urban***	***RIMS Sites***
RNSS System	GPS		
Constellation	Table 4-2		
Satellite Antenna Pattern	L1 Band from Table 4-7		
Signal	L1-C/A from Table 4-11		
Reference Receiver	Aviation User	Mass Market User	RIMS Station
Rx Bandwidth [MHz]	Table 4-15 for L1 band		
Integration Time [ms]	1		
Simulation Start	GPS week: 906 Seconds into week: 86400 (02.01.2017)		
Duration	1 day		
Time Interval	60 s		
Reference Receiver Location	Earth Grid	Cities	RIMS Network
Masking Angle	10°	30°	5°

The first scenario named ‘Open Sky’ aims at assessing the global GPS L1-C/A self-interference for a reference aviation user. Starting from the simulation approach, the Even and Odd SI histograms $H^{SI}[m, \varphi, \theta]$ are computed as described in Section 4.2.2.1.

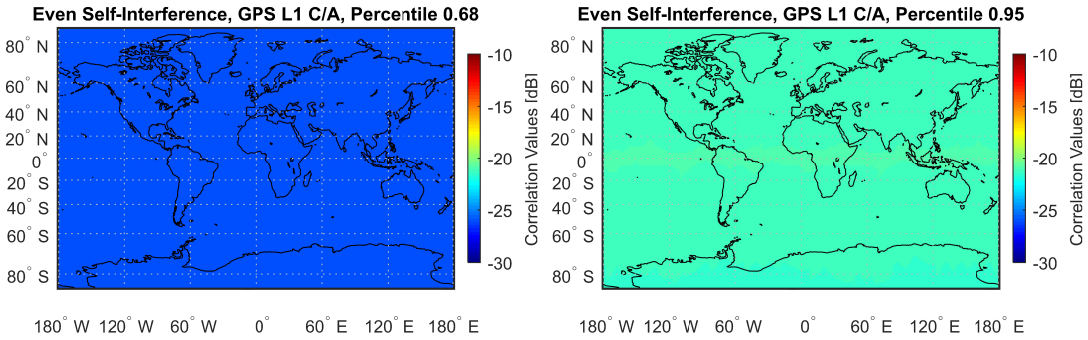

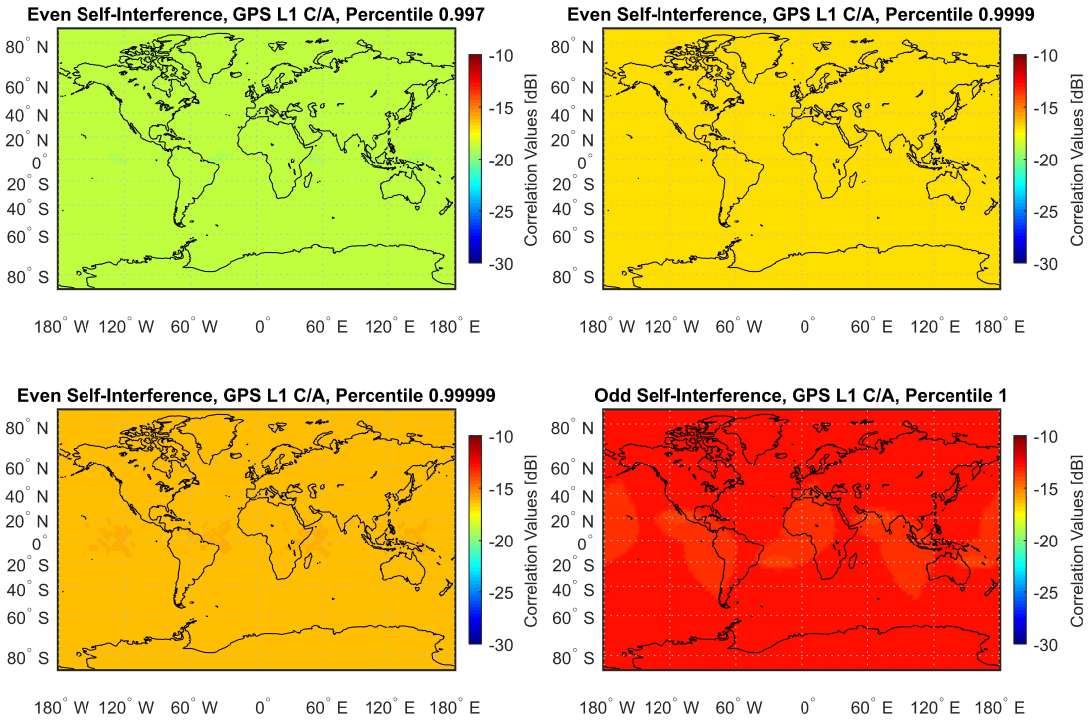

Figure 4–18: GPS L1-C/A Even SI, Open Sky, All Percentiles.

The correlation percentiles for each reference receiver location over simulation time are shown in Figure 4–18 and Figure 4–19. The correlation values, displayed in colour scale, are represented in the same interval [-30, -10] dB for all world charts in order to ease the comparison.

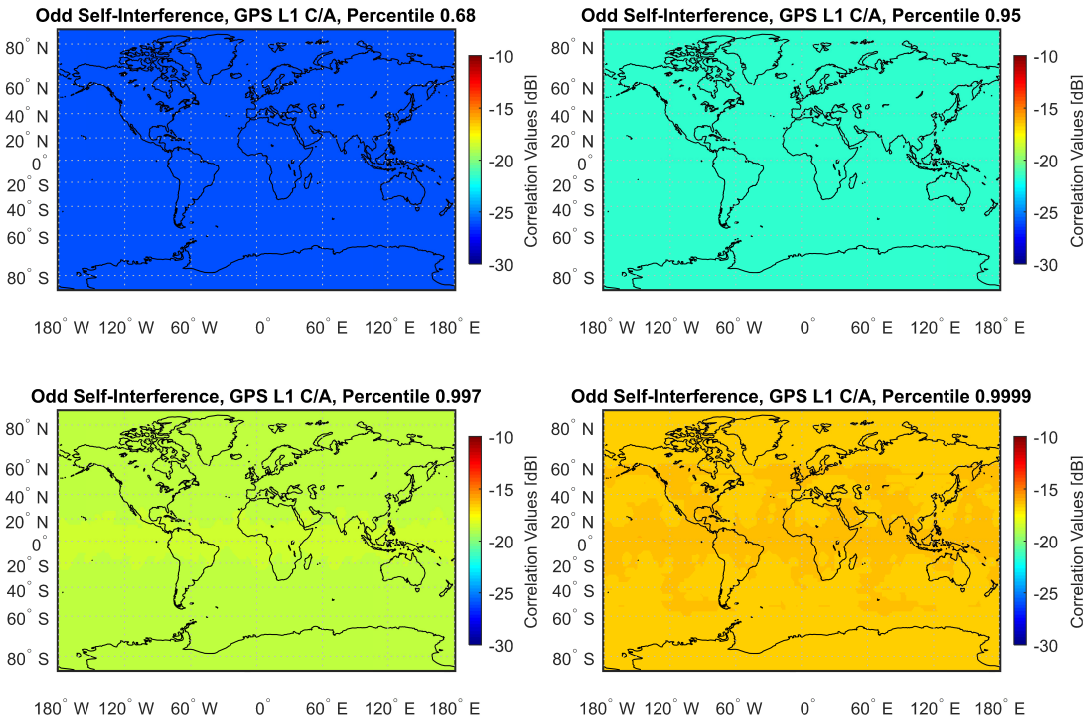

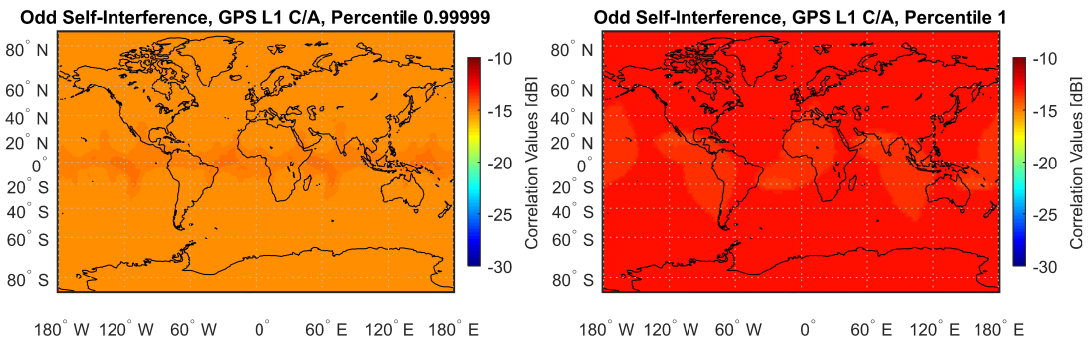

Figure 4–19: GPS L1-C/A Odd SI, Open Sky, All Percentiles.

By looking at the percentile values over the Earth Grid these are clearly constant. The uniform spread of self-interference on the Earth Grid was expected considering the global coverage of GPS constellation – Figure 4–8 shows that the average number of visible satellites fluctuates between 10 and 11 SVs – and the almost flat distribution of correlation percentiles over Doppler offset values for 1 ms integration time (Figure 3–23).

Table 4-19 reports the worst-case correlation percentiles over the reference receiver locations for the three scenarios under analysis. Note that the CPs do not change significantly for the different scenarios. The results confirm that in general power variations due to non-uniform antenna gain, masking angle, and receiver bandwidth do not have a significant impact onto the correlation metrics.

Table 4-19: GPS L1-C/A Worst-Case CPs, Simulation Model, T_I = 1 ms, All Scenarios.

		Percentiles					
		68%	***95%***	***99.7%***	***99.99%***	***99.999%***	***100%***
Open Sky	***CCF Even [dB]***	-26.2	-21.5	-19.1	-17.0	-16.3	-15.8
	CCF Odd [dB]	-26.0	-21.7	-18.8	-16.6	-15.5	-13.1
Urban	***CCF Even [dB]***	-26.2	-21.3	-19.0	-17.0	-16.3	-15.8
	CCF Odd [dB]	-26.0	-21.7	-18.7	-16.5	-15.3	-13.1
RIMS Sites	***CCF Even [dB]***	-26.2	-21.4	-19.1	-17.0	-16.3	-15.8
	CCF Odd [dB]	-26.0	-21.7	-18.8	-16.6	-15.4	-13.1

The minimum and maximum power curves versus elevation are displayed in Figure 4–20 for the three scenarios under analysis. Even if the power levels are different for each scenario, the received power offset is always 3.4 dB as it depends only on the

link budget assumptions that are the same for three cases. The power offset is the most relevant element that sums up linearly to the correlation values (in logarithmic scale).

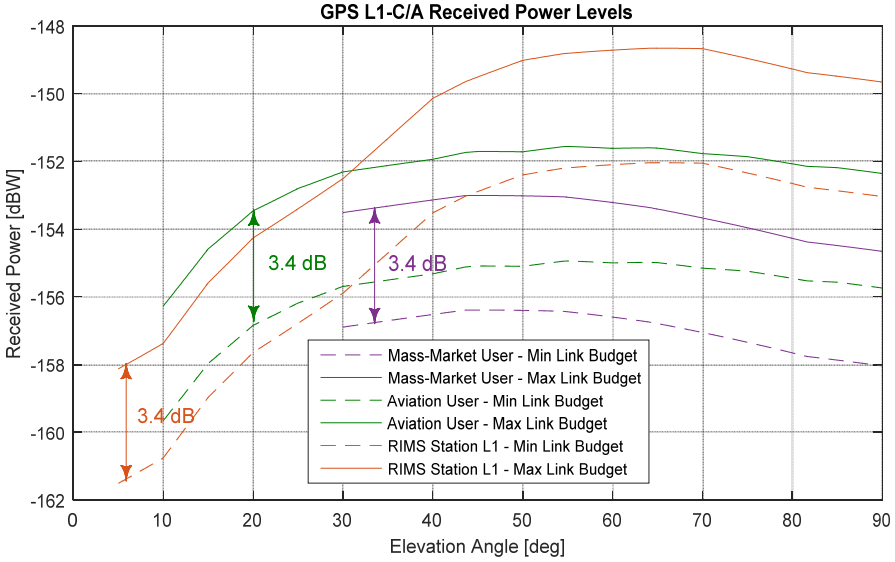

Figure 4–20: GPS L1-C/A Received Power Levels, All Scenarios.

The received power statistics are represented in Figure 4–21 for the Open Sky scenario. The plot on the left shows the numerical probability density function of the received power for each of the 31 transmitted PRN codes. Two distributions are displayed: one represents the worst-case link budget applied to the desired signal (dashed line), and the other one the best-case link budget used for the interfering signals (continuous line).

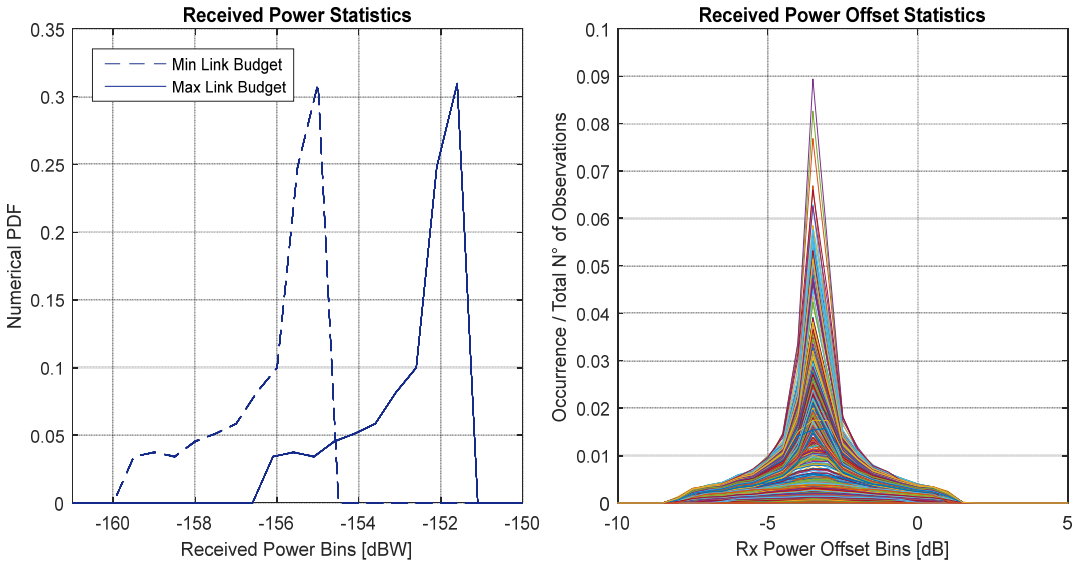

Figure 4–21: GPS L1-C/A Power Offset Statistics, Open Sky.

The horizontal shift between the two curves matches with the 3.4 dB received power offset displayed in Figure 4–20. In Figure 4–21 (right), the receiver power offset statistics is obtained by counting the number of occurrences over the total number of observations. Note that, as anticipated in Section 4.2.2.2, the average receiver power offset tends to 3.4 dB.

The Doppler frequency statistics computed over simulation time are represented in Figure 4–22. On the left, the numerical probability density function for the Doppler frequency values is build up for the transmitted PRN codes. Each curve takes into account for all reference receiver locations over the simulation time. The Doppler frequency resolution of the histogram is set to 50 Hz. Figure 4–22 (right) represents the Doppler offset statistics computed for each PRN code couple over reference receiver locations and simulation time instants. The histogram of occurrences is generated according to Eq. (4.21).

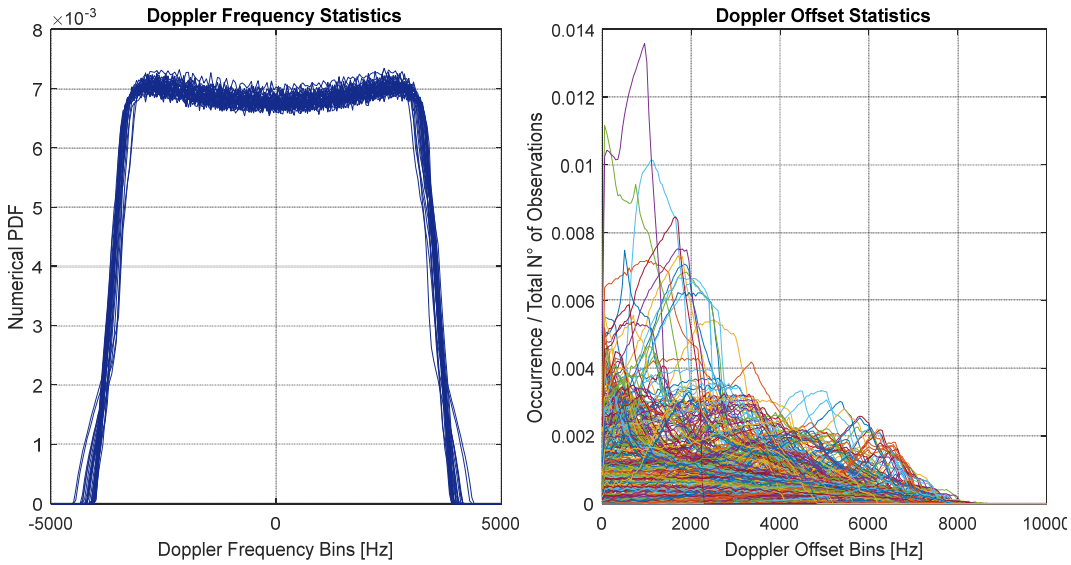

Figure 4–22: GPS L1-C/A Doppler Frequency Statistics, Open Sky.

The analytical approach described in Section 4.2.2.2 makes use of the curves in Figure 4–22 (right), called $k_{Dj,\ell}(d)$, to compute the even and odd SI histograms $H^{SI}[m]$. In Table 4-20 the correlation percentiles computed with the analytical model are summarised for the three scenarios under analysis.

Table 4-20: GPS L1-C/A CPs, Analytical Model, T_I = 1 ms, All Scenarios.

		Percentiles					
		68%	***95%***	***99.7%***	***99.99%***	***99.999%***	***100%***
Open Sky	***CCF Even [dB]***	-26.0	-21.4	-19.0	-17.1	-16.3	-15.6
	CCF Odd [dB]	-26.0	-21.7	-18.8	-16.6	-15.5	-13.1
Urban	***CCF Even [dB]***	-26.0	-21.4	-19.0	-17.0	-16.3	-15.6
	CCF Odd [dB]	-26.0	-21.7	-18.8	-16.6	-15.4	-13.1
RIMS Sites	***CCF Even [dB]***	-26.0	-21.5	-19.0	-17.1	-16.4	-15.6
	CCF Odd [dB]	-26.0	-21.7	-18.8	-16.6	-15.5	-13.1

Again, the correlation percentiles are almost identical for the three use cases analysed. By a comparison between Table 4-19 and Table 4-20 it is observed that the results of the analytical model match with those of the simulation model.

The GPS L1-C/A self-interference assessment with analytical model is repeated for the three scenarios by varying the value of the integration time. Results are reported in Table 4-21 only for Open Sky. Urban and RIMS Sites are omitted as the obtained CPs are almost identical.

Table 4-21: GPS L1-C/A CPs versus Integration Time, Analytical Model, Open Sky.

		Percentiles					
		68%	***95%***	***99.7%***	***99.99%***	***99.999%***	***100%***
$T_I = 3$ ms	***CCF Even [dB]***	-33.3	-24.6	-20.5	-18.0	-17.7	-17.6
	CCF Odd [dB]	-31.6	-25.7	-22.0	-19.5	-18.1	-17.2
$T_I = 7$ ms	***CCF Even [dB]***	-41.7	-27.6	-21.1	-18.7	-17.7	-17.7
	CCF Odd [dB]	-37.4	-28.3	-23.3	-20.4	-18.9	-17.5
$T_I = 13$ ms	***CCF Even [dB]***	-46.9	-31.3	-21.4	-18.7	-17.7	-17.7
	CCF Odd [dB]	-42.6	-30.7	-23.8	-20.6	-18.9	-17.6

As expected, the distribution of correlation magnitudes shifs significantly to lower values for increasing integration time. On the other hand, maximum correlation peaks are almost the same except for $T_I = 1$ ms which represensts the worst-case. The behaviour of maximum correlation percentiles over Doppler offset bins is shown in Figure 4–23. Here an even/odd SI histogram of correlation values is constructed for each Doppler offset bin $\bar{d}$ as:

$$H^{SI}[m,\bar{d}] = \sum_{j=1}^{M^X} \sum_{\substack{\ell=1 \\ \ell \neq j}}^{M^X} \frac{K_{Dj,\ell}}{K} f_{Dj,\ell}(\bar{d}) \cdot H_{j,\ell}[m,\bar{d}] \tag{4.29}$$

Note that the histogram of each correlation couple (j,ℓ) is weighted by the occurrence of the couple it-self over the number of observations.

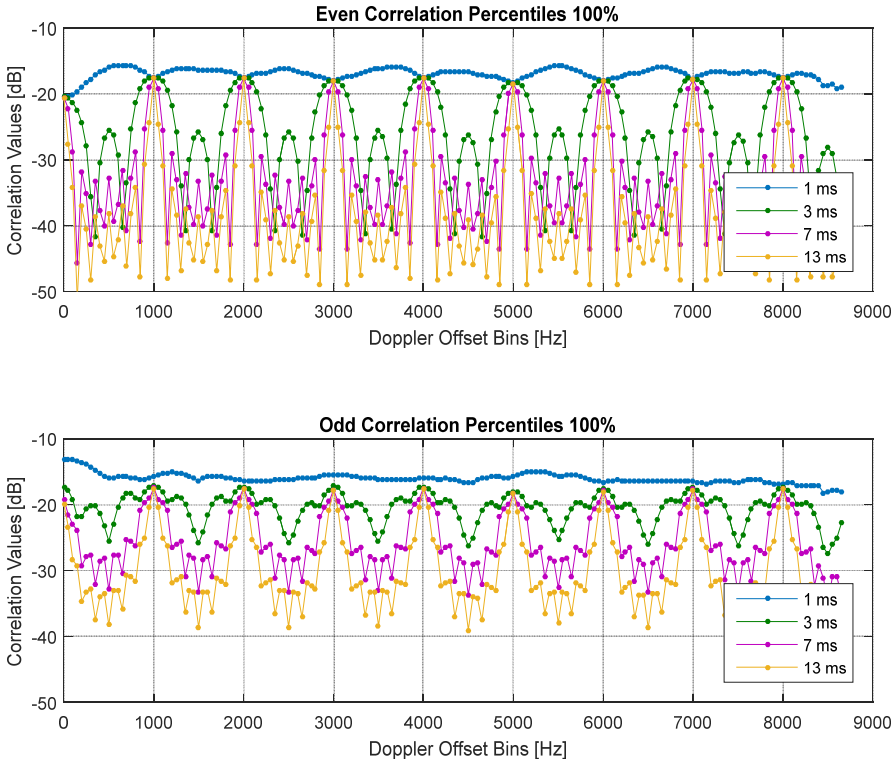

Figure 4–23: GPS L1-C/A 100% CP versus Doppler Offset, Open Sky.

4.4.2 EGNOS L1→GPS L1-C/A Cross-Interference

It is of interest to assess the cross-interference caused by EGNOS L1 singals onto the GPS L1-C/A spreading codes. The assumptions undelying this RFC assessment are summarised in Table 4-22.

Table 4-22: EGNOS L1→GPS L1-C/A Cross-Interference Scenario.

	Open Sky	***RIMS Sites***
Des. RNSS System	GPS	
Des. Constellation	Table 4-2	
Des. Satellite Antenna Pattern	L1 from Table 4-7	
Des. Signal	L1-C/A from Table 4-11	
Int. RNSS System	EGNOS	
Int. Constellation	Table 4-4	
Int. Satellite Antenna Pattern	L1 from Table 4-9	
Int. Signal	L1 from Table 4-13	
Reference Receiver	Aviation User	RIMS Station
Rx Bandwidth [MHz]	Table 4-15 for L1 band	

	Open Sky	***RIMS Sites***
Integration Time [ms]	1	
Simulation Start	GPS week: 906 Seconds into week: 86400 (02.01.2017)	
Duration	1 day	
Time Interval	60 s	
Reference Receiver Location	Earth Grid	RIMS Network
Masking Angle	10°	5°

This scenario is characterised by $T^{\mathrm{INT}} = T^{\mathrm{DES}}$, thus only two bit flip patterns – Even and Odd – are to be taken into account for the CI histogram computation.

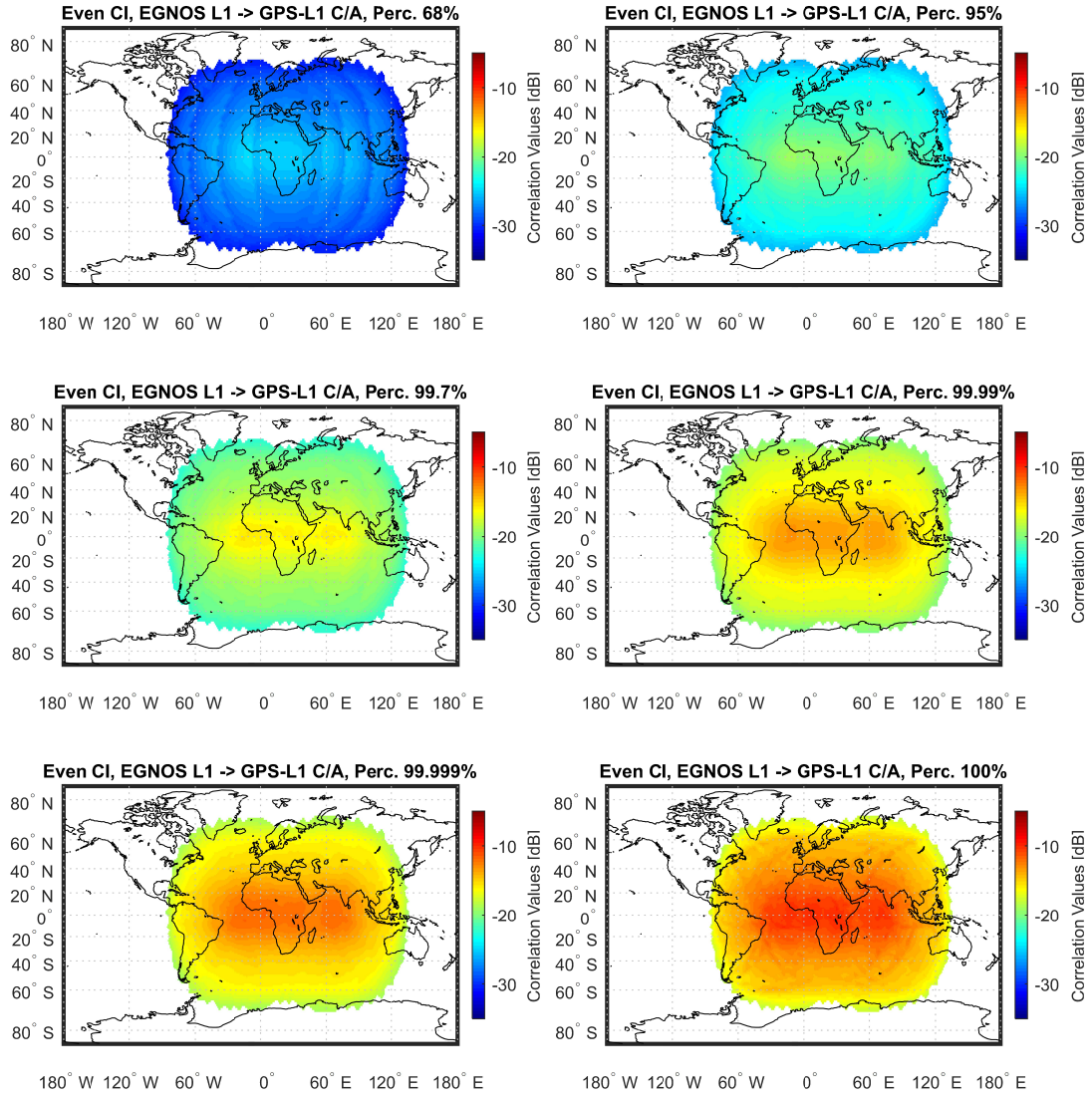

Figure 4–24: EGNOS L1→GPS L1-C/A Even CI, Open Sky.

Starting with the simulation approach, the correlation percentiles obtained for each reference receiver location over the simulation time are displayed in Figure 4–24 and Figure 4–25.

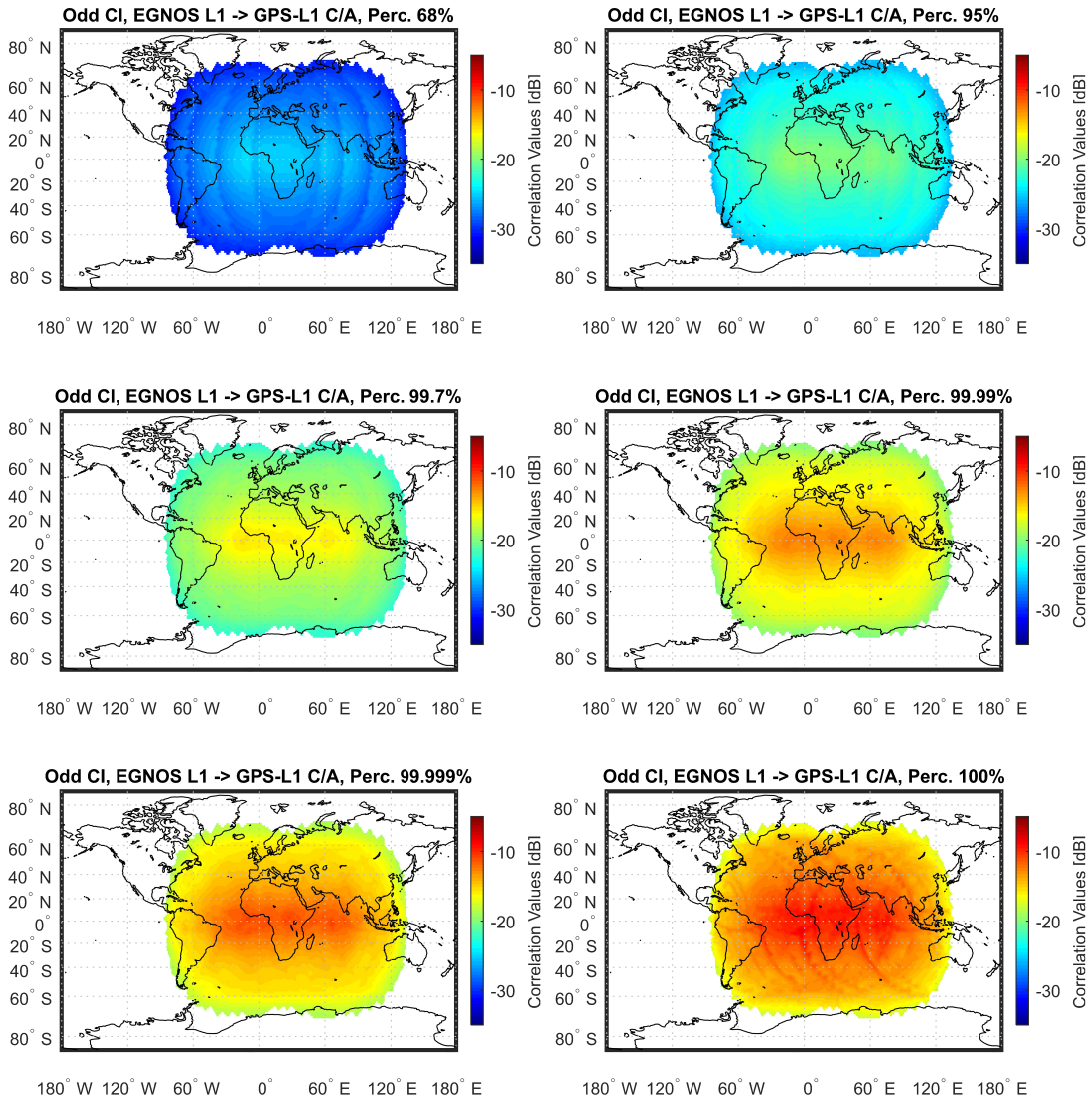

Figure 4–25: EGNOS L1→GPS L1-C/A Odd CI, Open Sky.

The levels or cross-interference displayed are extremely high: the maximum correlation value over the coverage is measured on the equatorial region below Europe and is about -10.0 dB.

EGNOS L1 cross-interference onto GPS L1-C/A is further investigated by taking as reference receiver locations the RIMS Sites scenario. The correlation percentiles obtained are reported in Table 4-23.

Table 4-23: EGNOS L1→GPS L1-C/A CPs, Simulation Model, RIMS Sites.

		Percentiles					
		68%	***95%***	***99.7%***	***99.99%***	***99.999%***	***100%***
ALB	***CCF Even [dB]***	-29.3	-22.8	-18.6	-15.8	-14.8	-13.4
	CCF Odd [dB]	-29.3	-22.8	-18.5	-15.7	-14.4	-11.7
ACR	***CCF Even [dB]***	-27.3	-20.4	-15.1	-12.2	-10.9	-8.8
	CCF Odd [dB]	-27.3	-20.4	-15.2	-11.9	-10.5	-8.6
BRN	***CCF Even [dB]***	-28.6	-22.2	-17.7	-15.2	-14.0	-12.6
	CCF Odd [dB]	-28.6	-22.2	-17.9	-14.8	-13.4	-10.5
CNR	***CCF Even [dB]***	-24.5	-17.7	-12.8	-10.0	-8.9	-7.5
	CCF Odd [dB]	-24.6	-17.7	-12.9	-9.9	-8.5	-6.3
CTN	***CCF Even [dB]***	-25.9	-19.4	-14.6	-11.8	-10.5	-9.0
	CCF Odd [dB]	-26.0	-19.4	-14.7	-11.6	-10	-7.6
CRK	***CCF Even [dB]***	-28.2	-21.8	-17.5	-14.8	-13.7	-11.7
	CCF Odd [dB]	-28.2	-21.8	-17.5	-14.6	-13.2	-11.2
WRS	***CCF Even [dB]***	-28.6	-22.1	-17.8	-15.2	-13.9	-12.4
	CCF Odd [dB]	-28.6	-22.2	-17.9	-14.9	-13.4	-11.2
DJA	***CCF Even [dB]***	-25.4	-18.7	-14.0	-11.1	-9.9	-8.2
	CCF Odd [dB]	-25.4	-18.8	-14.0	-11.0	-9.6	-8.1
EGI	***CCF Even [dB]***	-30.7	-24.6	-20.5	-17.7	-16.6	-15.1
	CCF Odd [dB]	-30.7	-24.6	-20.5	-17.7	-16.3	-14.4
GLG	***CCF Even [dB]***	-28.8	-22.4	-18.2	-15.5	-14.4	-12.6
	CCF Odd [dB]	-28.8	-22.5	-18.1	-15.3	-13.9	-11.8
HBK	***CCF Even [dB]***	-24.5	-18.0	-13.2	-10.1	-8.8	-7.3
	CCF Odd [dB]	-24.6	-18.0	-13.2	-10.0	-8.6	-6.7
GOL	***CCF Even [dB]***	-26.6	-20.0	-15.3	-12.3	-10.9	-9.3
	CCF Odd [dB]	-26.6	-20.0	-15.3	-12.2	-10.6	-8.3
KOU	***CCF Even [dB]***	-26.2	-18.9	-14.1	-11.6	-10.3	-8.9
	CCF Odd [dB]	-26.0	-19.1	-14.2	-11.0	-9.6	-8.1
LSB	***CCF Even [dB]***	-26.4	-19.4	-14.6	-11.8	-10.7	-8.5
	CCF Odd [dB]	-26.4	-19.5	-14.6	-11.6	-10.3	-7.6
SWA	***CCF Even [dB]***	-28.6	-22	-17.5	-14.8	-13.6	-12.1
	CCF Odd [dB]	-28.6	-22.1	-17.5	-14.6	-13.1	-10.9
MAD	***CCF Even [dB]***	-25.2	-18.4	-13.6	-10.8	-9.5	-8.3
	CCF Odd [dB]	-25.2	-18.5	-13.6	-10.6	-9.2	-7.1
MLG	***CCF Even [dB]***	-26.6	-19.4	-14.4	-11.6	-10.3	-8.5
	CCF Odd [dB]	-26.6	-19.4	-14.5	-11.4	-9.9	-7.6
KIR	***CCF Even [dB]***	-31.9	-26	-22.0	-19.2	-18.2	-16.4
	CCF Odd [dB]	-31.9	-26	-22.0	-19.2	-17.9	-16.4
PDM	***CCF Even [dB]***	-26.6	-19.9	-15.0	-12.1	-10.9	-9.5
	CCF Odd [dB]	-26.6	-19.9	-15.1	-12	-10.6	-8.9
PAR	***CCF Even [dB]***	-28.4	-21.7	-17.0	-14.4	-13.2	-11.5
	CCF Odd [dB]	-28.4	-21.8	-17.1	-14.1	-12.7	-10.3
MON	***CCF Even [dB]***	-31.3	-24.8	-20.0	-17.1	-15.9	-14.2
	CCF Odd [dB]	-31.6	-24.8	-20	-17.0	-15.5	-14.2
RKK	***CCF Even [dB]***	-30.7	-24.6	-20.4	-17.5	-16.3	-14.8

		Percentiles					
		68%	***95%***	***99.7%***	***99.99%***	***99.999%***	***100%***
	CCF Odd [dB]	-30.7	-24.6	-20.4	-17.5	-16.1	-14.2
ROM	***CCF Even [dB]***	-26.8	-20.1	-15.4	-12.7	-11.3	-9.7
	CCF Odd [dB]	-26.8	-20.2	-15.5	-12.4	-10.9	-8.5
LAP	***CCF Even [dB]***	-30.1	-23.8	-19.7	-16.9	-15.7	-14.0
	CCF Odd [dB]	-30.1	-23.8	-19.7	-16.8	-15.5	-13.4
SDC	***CCF Even [dB]***	-26.9	-20.2	-15.4	-12.6	-11.4	-9.7
	CCF Odd [dB]	-26.9	-20.2	-15.5	-12.5	-11.1	-8.9
SOF	***CCF Even [dB]***	-26.9	-20.5	-15.7	-12.9	-11.5	-9.9
	CCF Odd [dB]	-26.9	-20.5	-15.8	-12.7	-11.1	-8.6
GVL	***CCF Even [dB]***	-29.8	-23.5	-19.4	-16.5	-15.4	-14.0
	CCF Odd [dB]	-29.8	-23.5	-19.4	-16.5	-15.2	-13.9
TLS	***CCF Even [dB]***	-27.3	-20.6	-15.7	-12.9	-11.7	-9.9
	CCF Odd [dB]	-27.5	-20.6	-15.8	-12.6	-11.3	-8.9
TRD	***CCF Even [dB]***	-30.1	-24.2	-20.0	-17.3	-16.2	-14.6
	CCF Odd [dB]	-30.4	-24.2	-20	-17.3	-16	-14.4
TRO	***CCF Even [dB]***	-31.9	-26.0	-21.9	-19.2	-18.3	-16.6
	CCF Odd [dB]	-31.9	-26.0	-21.9	-19.1	-17.8	-16.5
ZUR	***CCF Even [dB]***	-27.9	-21.4	-16.8	-14.1	-12.9	-11.1
	CCF Odd [dB]	-27.9	-21.5	-16.9	-13.8	-12.3	-10.0
LYR	***CCF Even [dB]***	NaN	NaN	NaN	NaN	NaN	NaN
	CCF Odd [dB]	NaN	NaN	NaN	NaN	NaN	NaN
JME	***CCF Even [dB]***	-31.9	-26.2	-22.2	-19.4	-18.3	-16.9
	CCF Odd [dB]	-31.9	-26.2	-22.1	-19.3	-18	-16.1
NOU	***CCF Even [dB]***	-23.4	-16.7	-11.8	-8.9	-7.7	-6.3
	CCF Odd [dB]	-23.5	-16.7	-11.8	-8.8	-7.4	-5.9
LPI	***CCF Even [dB]***	-24.8	-17.9	-13.1	-10.2	-9.1	-7.7
	CCF Odd [dB]	-24.8	-17.9	-13.1	-10.0	-8.7	-6.8
ATH	***CCF Even [dB]***	-26.2	-19.5	-14.8	-11.9	-10.6	-9.0
	CCF Odd [dB]	-26.2	-19.6	-14.9	-11.7	-10.3	-8.4
ALY	***CCF Even [dB]***	-25.2	-18.5	-13.8	-10.9	-9.6	-8.0
	CCF Odd [dB]	-25.2	-18.5	-13.8	-10.7	-9.4	-7.6
AGA	***CCF Even [dB]***	-29.3	-22.8	-18.6	-15.8	-14.8	-13.4
	CCF Odd [dB]	-25.4	-18.4	-13.4	-10.5	-9.0	-7.3
ABS	***CCF Even [dB]***	-27.3	-20.4	-15.1	-12.2	-10.9	-8.8
	CCF Odd [dB]	-24.1	-17.4	-12.6	-9.5	-8.2	-6.0

The significant difference in correlation percentiles among RIMS sites can be explained by remembering that the EGNOS satellites are on geostationaly orbits and therefore do not move significantly over time when observed from the Earth. Therefore the EGNOS L1 signal power received from a specific location is almost constant during the GPS constellation repeat cycle and it can be always high in some sites and always low in some others.

In Figure 4–26 the minimum and maximum power levels versus elevation are provided for the two scenarios under analysis. The received power offset ΔP between the GPS minimum link budget and the EGNOS maximum link budget is independent from the scenario however, differently from Figure 4–20, ΔP is not constant anymore w.r.t. elevation due to the different transmit antenna patterns for GPS and EGNOS. The offset ranges from 1.4 dB to 5.5 dB for highest elevations.

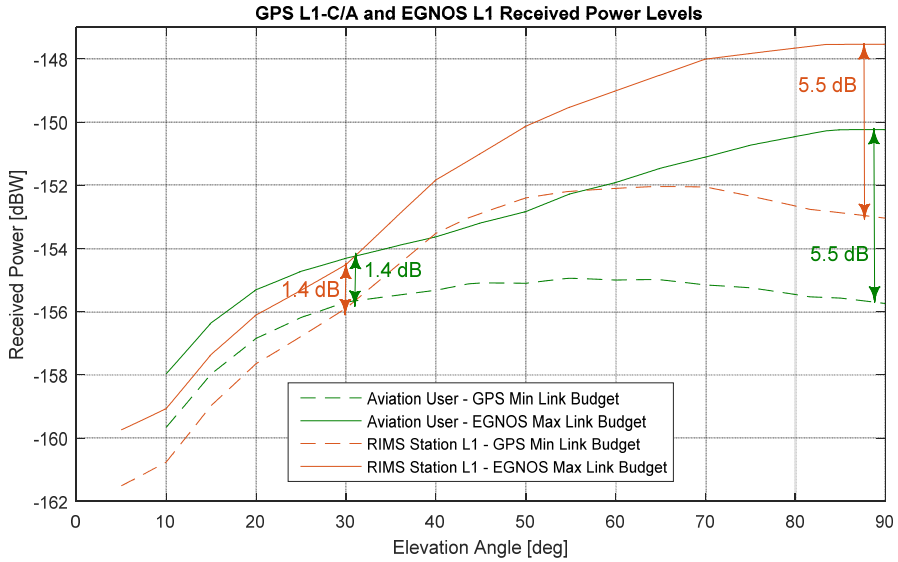

Figure 4–26: EGNOS L1 and GPS L1-C/A Received Power Levels, All Scenarios.

Further, the received power statistics are represented in Figure 4–27 for the Open Sky scenario.

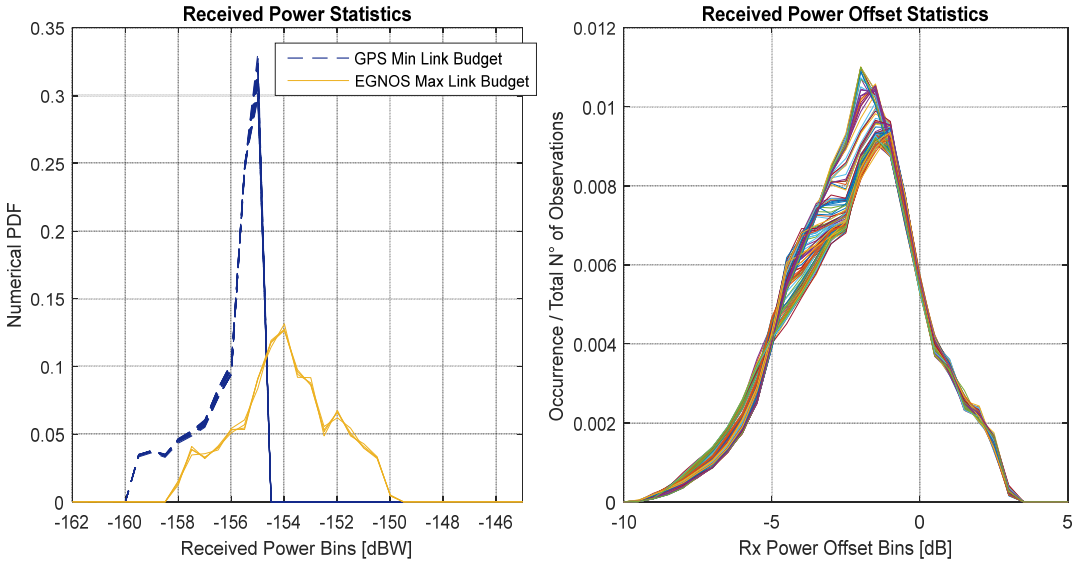

Figure 4–27: EGNOS L1 and GPS L1-C/A Power Offset Statistics, Open Sky.

The plot on the left shows the numerical probability density function of the received power for each of the 31 GPS satellites (blue dashed lines) and the 4 EGNOS satellites (yellow lines).

In Figure 4–27 (right), the receiver power offset statistics is obtained by counting the number of occurrences over the total number of observations. The offset ranges from -9.5 dB to +3 dB with a peak at -2 dB.

Differently from the case of GPS L1-C/A self-interference where the power offset values are highly concentrated around -3.4 dB (Figure 4–21), in this case the distribution is triangularly shaped with highest occurrence for the value -2 dB.

In Figure 4–28 (left) the Doppler frequency statistics of the EGNOS L1 signals are represented for the Open Sky scenario. As expected, Doppler frequency values are very limited around 0 Hz, being the signals transmitted from GEO satellites. The statistics for GPS L1 C/A is omitted as already provided in Figure 4–22 (left). Figure 4–28 (right) shows the Doppler frequency offset computed for each PRN code couple over the simulation duration.

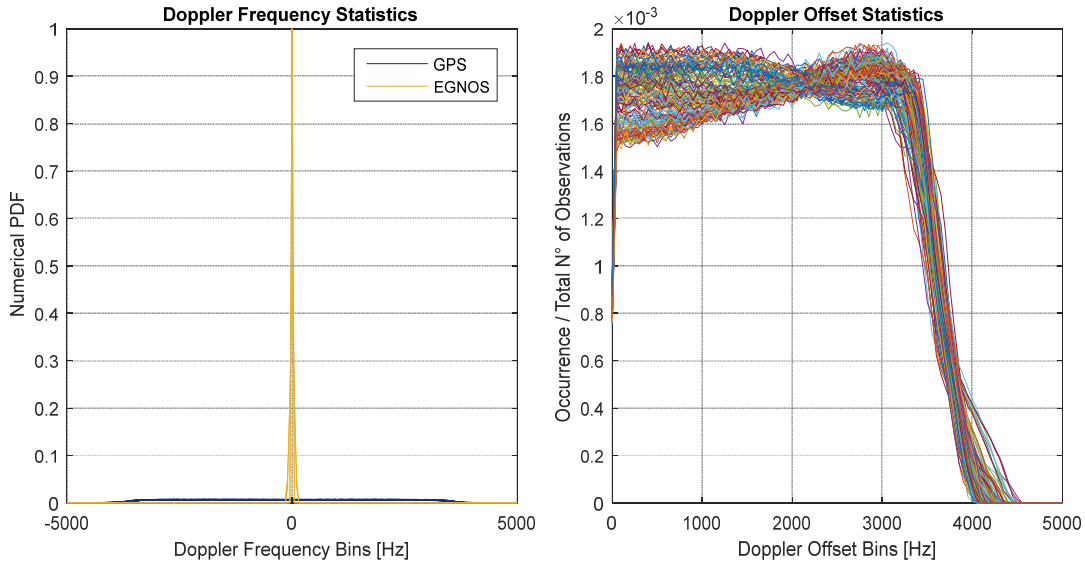

Figure 4–28: EGNOS L1 and GPS L1-C/A Doppler Frequency Statistics, Open Sky.

By comparing the EGNOS L1→GPS L1-C/A cross-interference results with the GPS L1-C/A self-interference correlation percentiles in Section 4.4.1, a significant difference can be noticed when looking at the highest correlation peaks (see Table 4-24).

The explanation however cannot be found in the correlation properties between the GPS and the SBAS spreading code families: Table 3-16 shows that for 0 Hz Doppler offset the interference caused by SBAS L1 signals onto GPS L1-C/A is exactly the same as the self-interference of GPS L1-C/A; Table 3-17 demonstrates that by uniformly weighting the CPs over Doppler offset values the even cross-interference is only slightly higher than the self-interference. The reason for this significant difference in correlation percentiles has to be found mainly in the statistics of received power offset values.

Table 4-24: EGNOS L1→GPS L1-C/A Worst-Case CPs, Simulation Model, Open Sky.

		Percentiles					
		68%	***95%***	***99.7%***	***99.99%***	***99.999%***	***100%***
EGNOSL1 → L1-C/A	***CCF Even [dB]***	-25.5	-20.0	-16.3	-13.6	-12.3	-9.9
	CCF Odd [dB]	-25.5	-20.3	-16.3	-13.0	-11.4	-9.9
GPS L1-C/A	***CCF Even [dB]***	-26.2	-21.5	-19.1	-17.0	-16.3	-15.8
	CCF Odd [dB]	-26.0	-21.7	-18.8	-16.6	-15.5	-13.1

The cross-interference analysis for the Open Sky scenario is repeated with the analytical model. Clearly, the choice of the power offset parameter plays a key role for the analytical results to match with the simulation results.

Table 4-25: EGNOS L1→GPS L1-C/A CPs, Analytical Model, Open Sky.

		Percentiles					
		68%	***95%***	***99.7%***	***99.99%***	***99.999%***	***100%***
Open Sky	***CCF Even [dB]***	-27.5	-22.8	-20.3	-18.3	-17.4	-15.7
	CCF Odd [dB]	-27.5	-23.0	-20.2	-18.0	-16.8	-15.3
RIMS Sites	***CCF Even [dB]***	-27.5	-22.9	-20.4	-18.3	-17.5	-15.7
	CCF Odd [dB]	-27.5	-23.0	-20.2	-18.0	-17.0	-15.3

For a power offset of -2 dB the results obtained with the analytical model do not match with the simulation model and the difference between the two increases for high percentiles. This outcome was expected as the correlation percentiles capture not only the 1-σ, 2-σ and 3-σ statistics (68%, 95% and 99.7% percentiles) but also

the values at the edge of the distribution (99.99%, 99.999%, 100%). The assumption of taking the average power offset can be representative of the average CPs but cannot capture the peaks.

4.4.3 Galileo E1 OS Self-Interference

The same three Scenarios analysed for GPS L1-C/A self-interference are proposed for the Galileo E1 OS signal (Table 4-26). Given the strong similarities between E1-B and E1-C PRN code sets in terms of cross-correlation properties, the following SI histograms are computed only for Galileo E1-C component.

Table 4-26: Galileo E1 OS Self-Interference Scenarios.

	Open Sky	***Urban***	***RIMS Sites***
GNSS System	Galileo		
Constellation	Table 4-3		
Satellite Antenna Pattern	E1 Band from Table 4-8		
Signal	E1-C from Table 4-12		
Reference Receiver	Aviation User	Mass Market User	RIMS Station
Rx Bandwidth [MHz]	Table 4-15 for L1 band		
Integration Time [ms]	4		
Simulation Start	GPS week: 906 Seconds into week: 86400 (02.01.2017)		
Duration	1 day		
Time Interval	60 s		
Reference Receiver Location	Earth Grid	Cities	RIMS Network
Masking Angle	10°	30°	5°

Starting from the simulation approach, Figure 4–29 and Figure 4–30 show the Galileo E1-C self-interference for the Open Sky scenario.

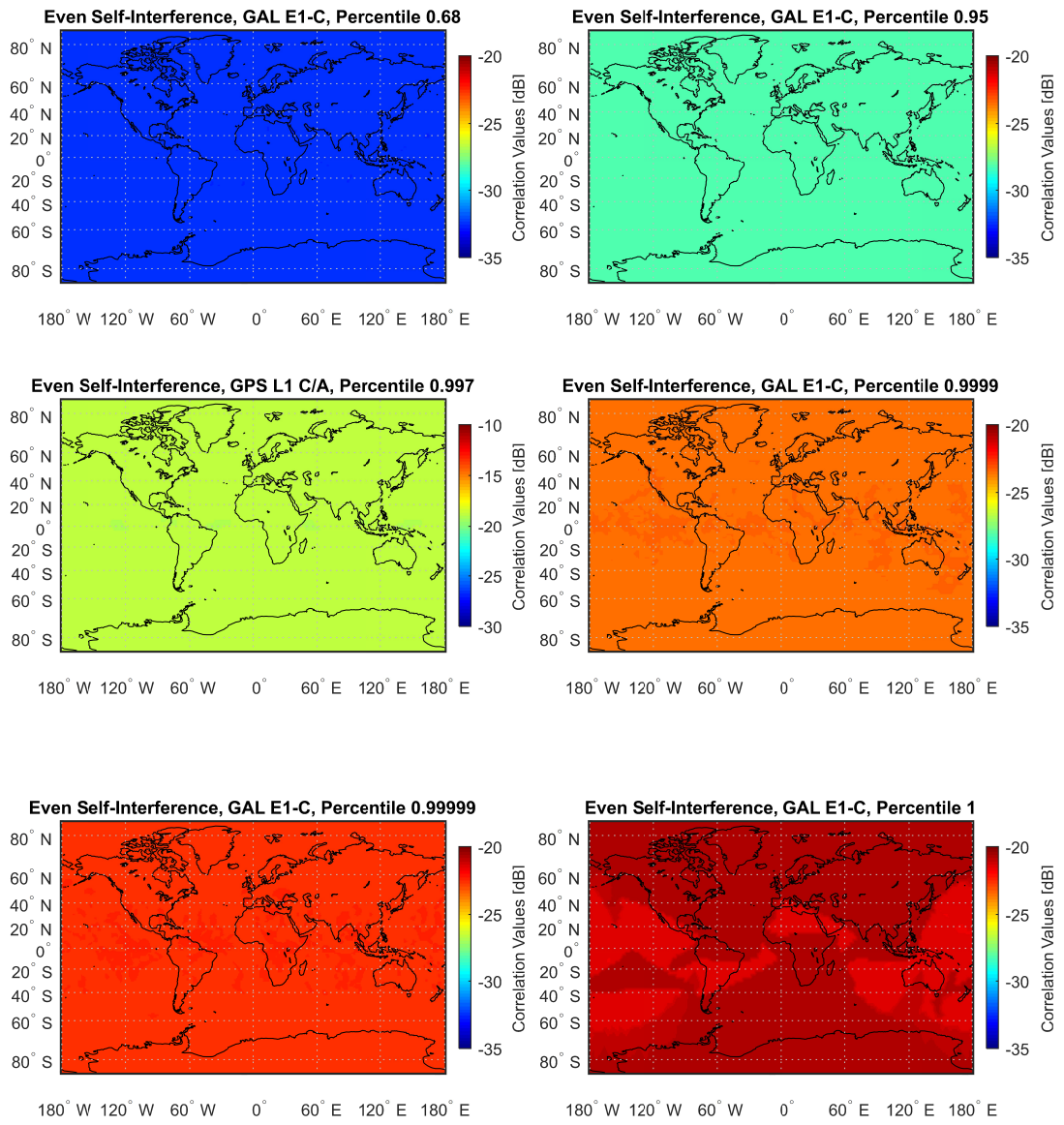

Figure 4–29: Galileo E1-C Even SI, Open Sky, All Percentiles.

As already observed for the GPS L1-C/A, given the global coverage of the Galileo constellation the SI correlation percentiles over the worl chart are flat.

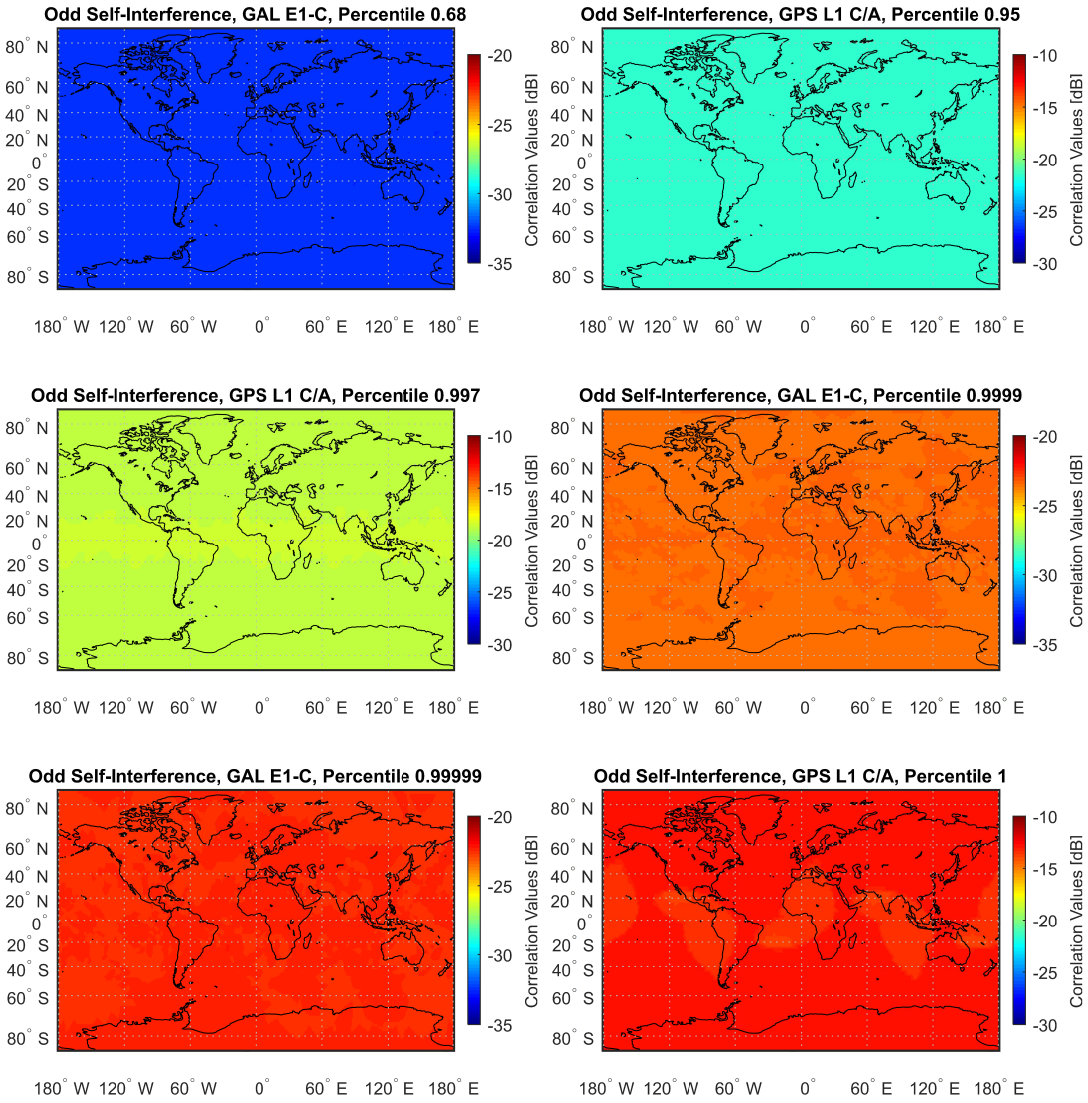

Figure 4–30: Galileo E1-C Odd SI, Open Sky, All Percentiles.

The simulation is repeated for the Urban and the RIMS Sites scenarios. The worst-case results are provided in Table 4-27.

Table 4-27: Galileo E1-C Worst-Case CPs, Simulation Model, All Scenarios.

		Percentiles					
		68%	***95%***	***99.7%***	***99.99%***	***99.999%***	***100%***
Open Sky	***CCF Even [dB]***	-32.6	-28.4	-25.5	-23.5	-22.6	-20.7
	CCF Odd [dB]	-32.6	-28.4	-25.5	-23.5	-22.5	-20.8
Urban	***CCF Even [dB]***	-32.6	-28.4	-25.5	-23.5	-22.6	-20.7
	CCF Odd [dB]	-32.6	-28.4	-25.5	-23.5	-22.4	-20.8
RIMS	***CCF Even***	-32.6	-28.4	-25.5	-23.5	-22.6	-20.7

		Percentiles					
		68%	***95%***	***99.7%***	***99.99%***	***99.999%***	***100%***
Sites	***[dB]***						
	CCF Odd [dB]	-32.6	-28.4	-25.5	-23.5	-22.5	-20.8

By comparing Table 4-27 with Table 3-6 (CCF) a difference between 2 dB and 4 dB can be observed on the correlation percentile values. This offset cannot be solely explained with the power levels introduced by the RFC methodology that scale the cross-correlation values. It is in fact a combination of the Doppler frequency offset and power distribution.

The minimum and maximum power curves versus elevation are displayed in Figure 4–31 for the three scenarios under analysis. Even if the power levels are different for each scenario, the received power offset is always equal to 2.9 dB.

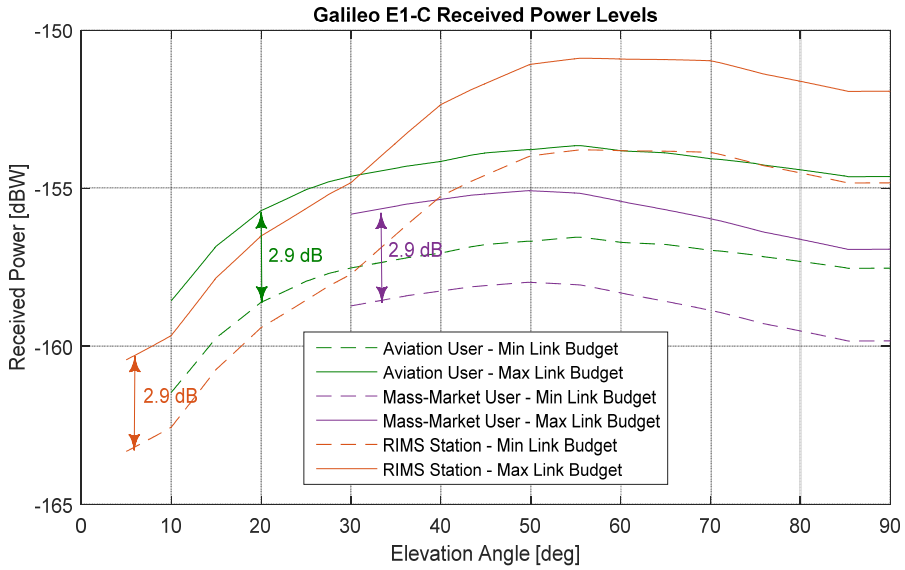

Figure 4–31: Galileo E1-C Received Power Levels, All Scenarios.

Further, the received power statistics are represented in Figure 4–32 for the Open Sky scenario. On the left, the curves represent the numerical probability density function of the received power for each of the 16 transmitted PRN codes. It is possible to identify two main distributions: one for the worst-case link budget applied to the desired signal, and one for the best-case link budget used for the interfering signals. The horizontal shift between the two curves matches with the 2.9 dB received power offset displayed in Figure 4–31.

In Figure 4–32 (right), the receiver power offset statistics is computed by summing up the number of occurrences for each power bin over the total number of observations. As expected, the average receiver power offset tends to 2.9 dB.

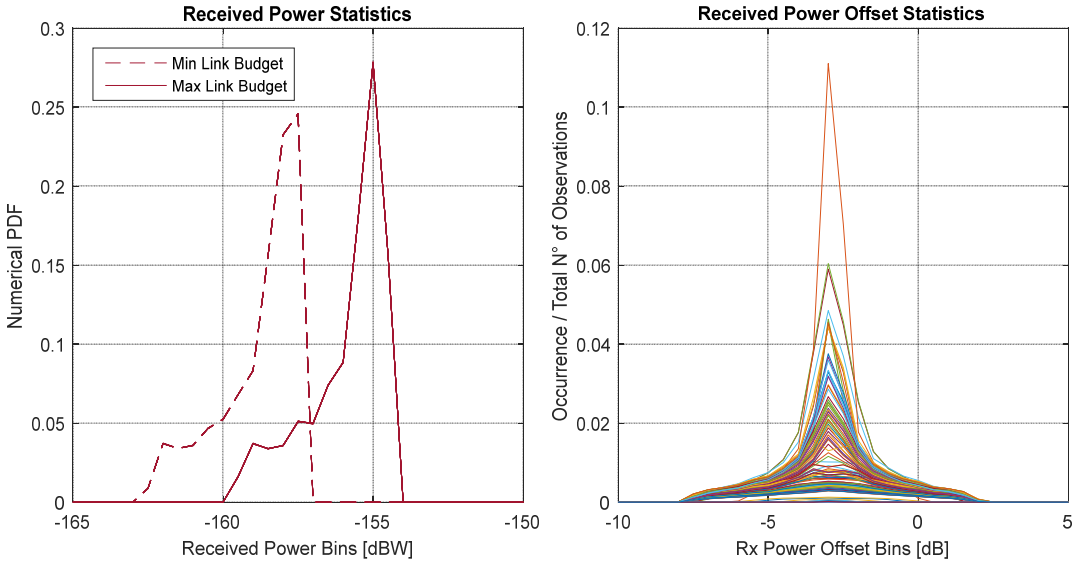

Figure 4–32: Galileo E1-C Power Offset Statistics, Open Sky.

Finally, the Doppler frequency statics for the Galileo satellites are provided in Figure 4–33.

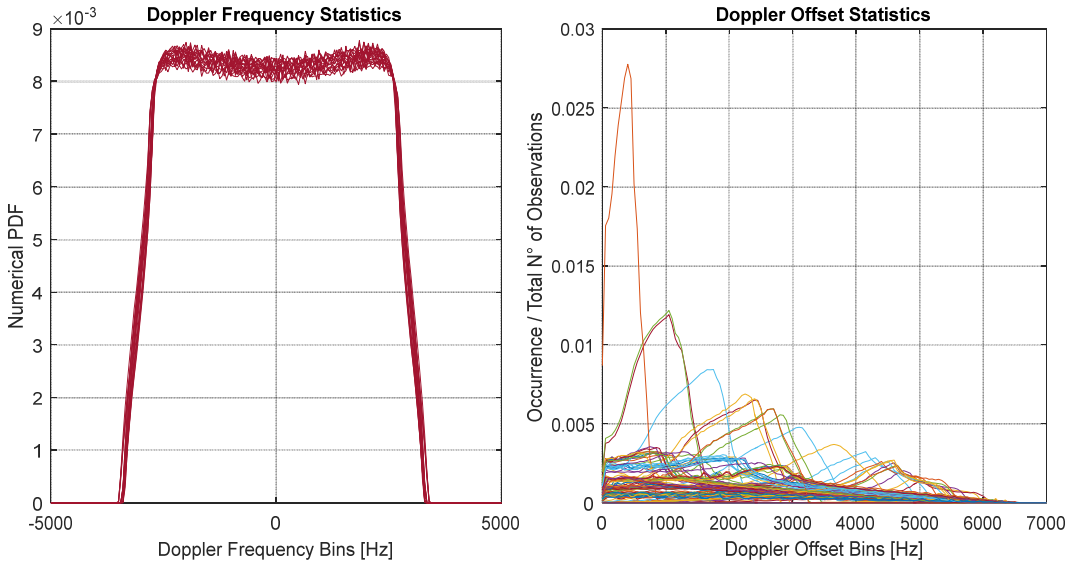

Figure 4–33: Galileo E1-C Doppler Frequency Statistics, Open Sky.

On the left, the numerical probability density function for the Doppler frequency values is build up for the transmitted PRN codes. Each curve takes into account for all reference receiver locations over the simulation time. The Doppler frequency

resolution of the histogram is set to 50 Hz. Figure 4–33 (right) represents the Doppler offset statistics computed for each PRN code couple over reference receiver locations and simulation time instants. The histogram of occurrences is generated according to Eq. (4.21).

Table 4-28 provides the self-interference RFC assessment results obtained with the analytical model for the three scenarios under analysis.

Table 4-28: Galileo E1-C CPs, Analytical Model, All Scenarios.

		Percentiles					
		68%	***95%***	***99.7%***	***99.99%***	***99.999%***	***100%***
Open Sky	***CCF Even [dB]***	-32.6	-28.4	-25.5	-23.5	-22.6	-20.5
	CCF Odd [dB]	-32.6	-28.4	-25.5	-23.6	-22.6	-21.0
Urban	***CCF Even [dB]***	-32.6	-28.4	-25.5	-23.5	-22.6	-20.5
	CCF Odd [dB]	-32.6	-28.4	-25.5	-23.6	-22.7	-21.3
RIMS Sites	***CCF Even [dB]***	-32.6	-28.4	-25.5	-23.5	-22.6	-20.5
	CCF Odd [dB]	-32.6	-28.4	-25.5	-23.6	-22.6	-21.0

Again, by a comparison between Table 4-27 and Table 4-28 it is observed that the results of the analytical model match perfectly with those of the simulation model.

4.4.4 GPS L1-C→Galileo E1-OS Cross-Interference

It is of interest to assess the cross-interference caused by GPS L1-C singals onto the Galileo E1-OS spreading codes. The assumptions undelying this RFC assessment are summarised in Table 4-29.

Table 4-29: GPS L1-C→Galileo E1-OS Cross-Interference Scenario.

	Open Sky	***RIMS Sites***
Des. RNSS System	Galileo	
Des. Constellation	Table 4-3	
Des. Satellite Antenna Pattern	E1 from Table 4-8	
Des. Signal	E1-C from Table 4-12	
Int. RNSS System	GPS	
Int. Constellation	Table 4-2	
Int. Satellite Antenna Pattern	L1 from Table 4-7	
Int. Signal	L1-C pilot from Table 4-11	
Reference Receiver	Aviation User	RIMS Station
Rx Bandwidth [MHz]	Table 4-15 for L1 band	
Integration Time [ms]	4	

	Open Sky	***RIMS Sites***
Simulation Start	GPS week: 906 Seconds into week: 86400 (02.01.2017)	
Duration	1 day	
Time Interval	60 s	
Reference Receiver Location	Earth Grid	RIMS Network
Masking Angle	10°	5°

This scenario is characterised by $T^{\mathrm{INT}} > T^{\mathrm{DES}}$, thus only two bit flip patterns – Even and Odd – are to be taken into account for the CI histogram computation. Given the computational load required to perform the RFC assessment with the simulation model, only the results for the RIMS Sites scenario are computed and reported in Table 4-30.

Table 4-30: GPS L1-C→Galileo E1-C CPs, Simulation Model, RIMS Sites.

		Percentiles					
		68%	***95%***	***99.7%***	***99.99%***	***99.999%***	***100%***
ALB	***CCF Even [dB]***	-30.1	-22.8	-17.6	-14.4	-13.0	-10.3
	CCF Odd [dB]	-30.1	-22.8	-17.6	-14.4	-13.0	-10.5
ACR	***CCF Even [dB]***	-30.0	-22.8	-17.6	-14.4	-13.0	-9.6
	CCF Odd [dB]	-30.0	-22.8	-17.6	-14.4	-13.0	-9.6
BRN	***CCF Even [dB]***	-30.1	-22.7	-17.4	-14.3	-12.9	-8.4
	CCF Odd [dB]	-30.1	-22.7	-17.4	-14.3	-12.9	-8.4
CNR	***CCF Even [dB]***	-29.8	-22.6	-17.5	-14.4	-13.0	-9.0
	CCF Odd [dB]	-29.8	-22.6	-17.5	-14.4	-13.0	-8.7
CTN	***CCF Even [dB]***	-30.2	-23.0	-17.7	-14.5	-13.1	-8.7
	CCF Odd [dB]	-30.2	-23.0	-17.7	-14.5	-13.1	-8.7
CRK	***CCF Even [dB]***	-29.9	-22.7	-17.5	-14.3	-12.9	-9.2
	CCF Odd [dB]	-29.9	-22.7	-17.5	-14.3	-12.9	-9.2
WRS	***CCF Even [dB]***	-30.1	-22.7	-17.4	-14.3	-12.8	-9.1
	CCF Odd [dB]	-30.1	-22.7	-17.4	-14.3	-12.8	-9.1
DJA	***CCF Even [dB]***	-30.0	-22.8	-17.6	-14.4	-13.0	-8.6
	CCF Odd [dB]	-30.0	-22.8	-17.6	-14.5	-13.0	-8.6
EGI	***CCF Even [dB]***	-30.2	-23.3	-18.0	-14.7	-13.3	-8.6
	CCF Odd [dB]	-30.2	-23.3	-18.0	-14.7	-13.3	-8.7
GLG	***CCF Even [dB]***	-30.0	-22.7	-17.5	-14.4	-13.0	-9.6
	CCF Odd [dB]	-30.0	-22.7	-17.5	-14.4	-13.0	-9.9
HBK	***CCF Even [dB]***	-30.0	-22.7	-17.5	-14.4	-13.0	-9.6
	CCF Odd [dB]	-30.2	-22.9	-17.6	-14.4	-13.0	-9.5
GOL	***CCF Even [dB]***	-30.4	-23.1	-17.6	-14.4	-13.0	-9.5
	CCF Odd [dB]	-30.4	-23.1	-17.6	-14.4	-13.0	-9.7
KOU	***CCF Even [dB]***	-30.7	-23.7	-18.3	-14.8	-13.3	-9.6
	CCF Odd [dB]	-30.7	-23.7	-18.3	-14.8	-13.3	-9.6
LSB	***CCF Even [dB]***	-29.8	-22.7	-17.5	-14.4	-13.0	-8.7

		Percentiles					
		68%	***95%***	***99.7%***	***99.99%***	***99.999%***	***100%***
	CCF Odd [dB]	-29.8	-22.7	-17.5	-14.4	-13.0	-9.1
SWA	***CCF Even [dB]***	-30.0	-22.8	-17.5	-14.4	-13.0	-9.2
	CCF Odd [dB]	-30.0	-22.8	-17.5	-14.4	-13.0	-9.2
MAD	***CCF Even [dB]***	-29.8	-22.6	-17.6	-14.4	-13.0	-9.1
	CCF Odd [dB]	-29.8	-22.6	-17.6	-14.4	-13.0	-8.8
MLG	***CCF Even [dB]***	-29.8	-22.6	-17.4	-14.3	-12.9	-8.7
	CCF Odd [dB]	-29.8	-22.6	-17.4	-14.3	-12.9	-8.8
KIR	***CCF Even [dB]***	-30.3	-23.4	-18.2	-14.8	-13.3	-10.1
	CCF Odd [dB]	-30.3	-23.4	-18.2	-14.8	-13.3	-10.1
PDM	***CCF Even [dB]***	-29.9	-22.6	-17.5	-14.4	-13.1	-9.6
	CCF Odd [dB]	-29.9	-22.6	-17.5	-14.4	-13.1	-9.6
PAR	***CCF Even [dB]***	-30.2	-23	-17.8	-14.6	-13.1	-8.7
	CCF Odd [dB]	-30.2	-23	-17.8	-14.6	-13.2	-8.7
MON	***CCF Even [dB]***	-30.0	-22.7	-17.5	-14.4	-13.0	-10.1
	CCF Odd [dB]	-30.0	-22.7	-17.5	-14.4	-13.0	-10.3
RKK	***CCF Even [dB]***	-30.2	-23.2	-18.0	-14.7	-13.3	-9.7
	CCF Odd [dB]	-30.2	-23.2	-18.0	-14.7	-13.3	-9.6
ROM	***CCF Even [dB]***	-30.1	-22.8	-17.6	-14.4	-13.0	-8.9
	CCF Odd [dB]	-30.1	-22.8	-17.6	-14.4	-13.0	-8.9
LAP	***CCF Even [dB]***	-30.2	-23.0	-17.8	-14.6	-13.1	-9.9
	CCF Odd [dB]	-30.2	-23.0	-17.8	-14.6	-13.1	-9.7
SDC	***CCF Even [dB]***	-29.9	-22.8	-17.6	-14.4	-13.0	-8.9
	CCF Odd [dB]	-29.9	-22.8	-17.6	-14.4	-13.0	-8.9
SOF	***CCF Even [dB]***	-30.4	-23.1	-17.7	-14.4	-13.0	-9.5
	CCF Odd [dB]	-30.4	-23.1	-17.7	-14.5	-13.0	-9.5
GVL	***CCF Even [dB]***	-30.2	-23.0	-17.8	-14.5	-13.1	-9.3
	CCF Odd [dB]	-30.2	-23.0	-17.8	-14.6	-13.1	-9.3
TLS	***CCF Even [dB]***	-30.0	-22.8	-17.7	-14.5	-13.1	-9.4
	CCF Odd [dB]	-30.0	-22.8	-17.7	-14.5	-13.1	-9.4
TRD	***CCF Even [dB]***	-30.2	-23.1	-17.9	-14.7	-13.2	-9.8
	CCF Odd [dB]	-30.2	-23.1	-17.9	-14.7	-13.2	-10.1
TRO	***CCF Even [dB]***	-30.3	-23.4	-18.2	-14.8	-13.4	-9.8
	CCF Odd [dB]	-30.3	-23.4	-18.2	-14.8	-13.4	-9.7
ZUR	***CCF Even [dB]***	-30.2	-23.0	-17.8	-14.6	-13.1	-8.9
	CCF Odd [dB]	-30.2	-23.0	-17.8	-14.6	-13.1	-8.9
LYR	***CCF Even [dB]***	-30.4	-23.7	-18.5	-15.1	-13.6	-10
	CCF Odd [dB]	-30.4	-23.7	-18.5	-15.1	-13.6	-10.1
JME	***CCF Even [dB]***	-30.4	-23.5	-18.3	-14.9	-13.4	-9.8
	CCF Odd [dB]	-30.4	-23.5	-18.3	-14.9	-13.4	-9.7
NOU	***CCF Even [dB]***	-29.6	-22.5	-17.5	-14.3	-12.9	-8.4
	CCF Odd [dB]	-29.6	-22.5	-17.5	-14.3	-12.9	-8.4
LPI	***CCF Even [dB]***	-29.9	-22.7	-17.6	-14.4	-13.0	-9.5
	CCF Odd [dB]	-29.9	-22.7	-17.6	-14.4	-13.0	-9.9
ATH	***CCF Even [dB]***	-30.4	-23.2	-17.8	-14.5	-13.1	-8.9
	CCF Odd [dB]	-30.4	-23.2	-17.8	-14.5	-13.1	-8.9

		Percentiles					
		68%	***95%***	***99.7%***	***99.99%***	***99.999%***	***100%***
ALY	***CCF Even [dB]***	-30.4	-23.3	-17.9	-14.6	-13.1	-10
	CCF Odd [dB]	-30.4	-23.3	-17.9	-14.6	-13.1	-10
AGA	***CCF Even [dB]***	-29.7	-22.5	-17.4	-14.3	-12.9	-8.7
	CCF Odd [dB]	-29.7	-22.5	-17.4	-14.3	-12.8	-9.0
ABS	***CCF Even [dB]***	-30.4	-23.1	-17.9	-14.6	-13.2	-9.5
	CCF Odd [dB]	-30.4	-23.1	-17.9	-14.6	-13.2	-9.5

In Figure 4–34 the minimum and maximum power levels versus elevation are provided for the two scenarios under analysis. The received power offset ΔP between the Galileo minimum link budget and the GPS maximum link budget is independent from the scenario and it is almost constant along the elevation.

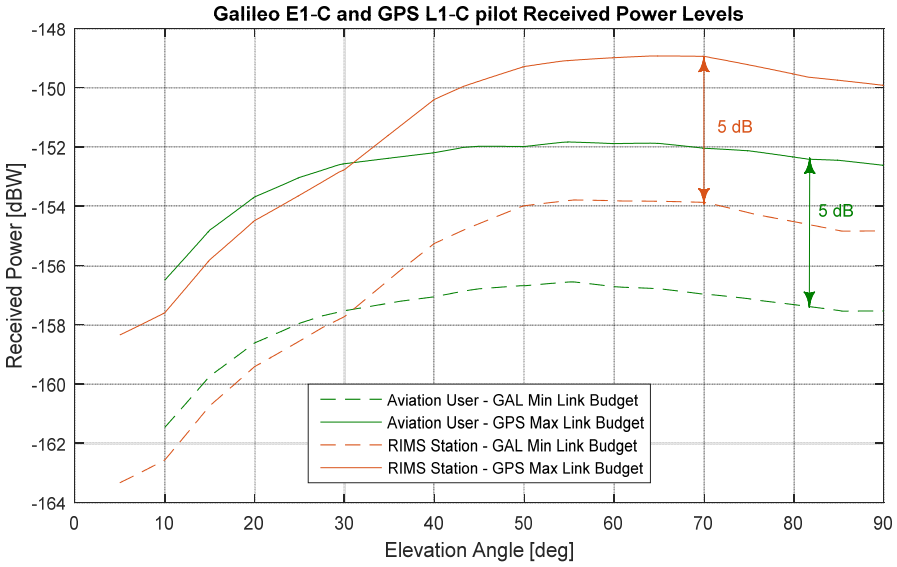

Figure 4–34: GPS L1-C and Galileo E1-C Received Power Levels, All Scenarios.

Further, the received power statistics are represented in Figure 4–35 for the Open Sky scenario. The plot on the left shows the numerical probability density function of the received power for each of the 16 Galileo satellites and the 31 GPS satellites. In Figure 4–35 (right), the receiver power offset statistics is obtained by counting the number of occurrences over the total number of observations. The power offset values are highly concentrated around -5 dB.

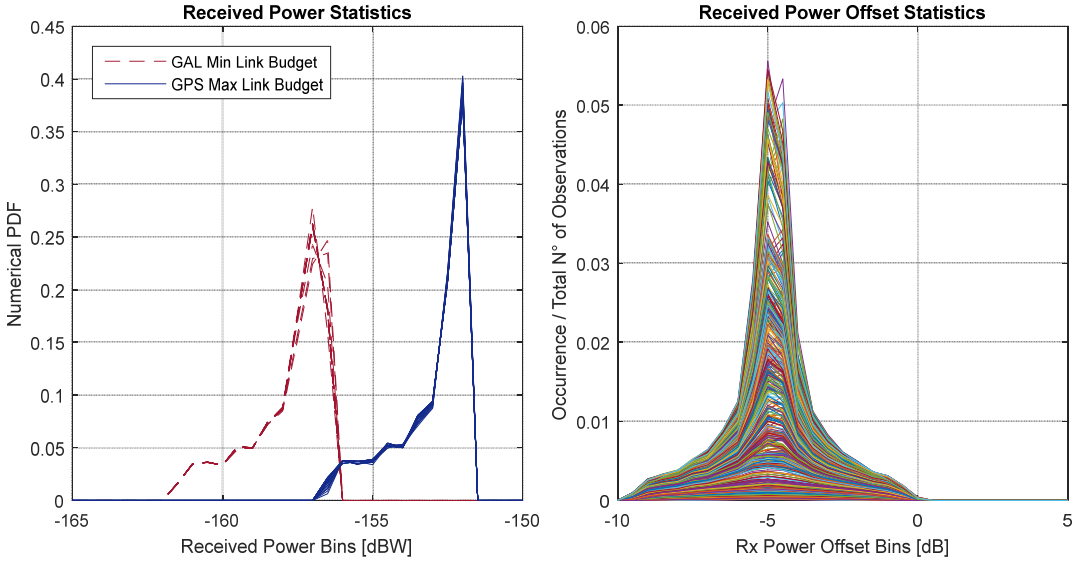

Figure 4–35: GPS L1-C and Galileo E1-C Power Offset Statistics, Open Sky.

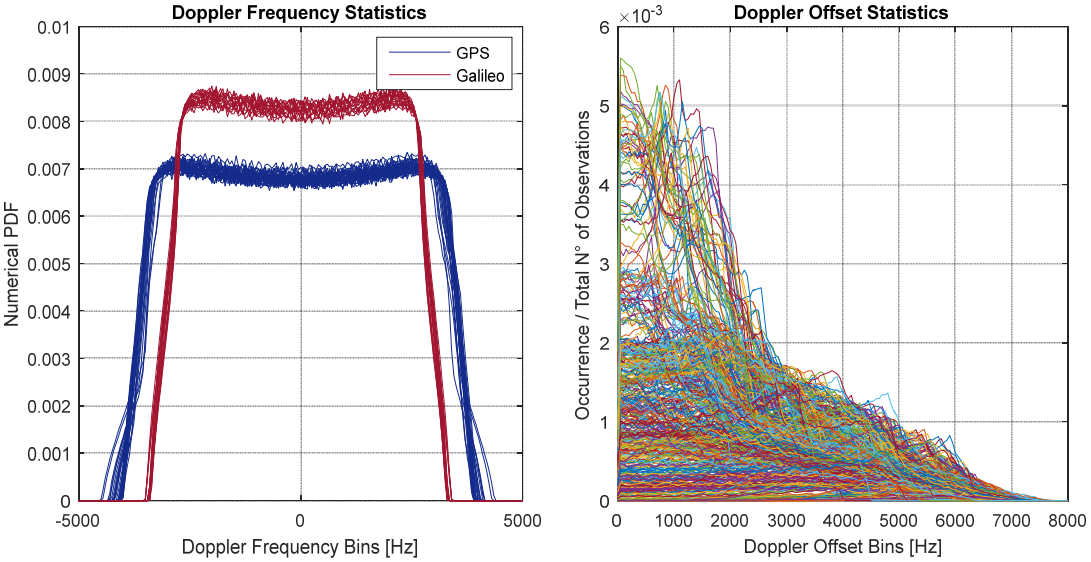

Figure 4–36: GPS L1-C and Galileo E1-C Doppler Frequency Statistics, Open Sky.

In Figure 4–36 (left) the Doppler frequency statistics of the Galileo and GPS signals are represented for the Open Sky scenario. Figure 4–36 (right) shows the Doppler frequency offset computed for each PRN code couple over the simulation duration. Table 4-31 reports the correlation percentiles of the cross-interference caused by GPS L1-C pilot onto Galileo E1-C component computed with the analytical model. As expected, the CPs do not change significantly by comparing Open Sky to RIMS Sites results.

Table 4-31: GPS L1-C → Galileo E1-OS CPs, All Scenarios.

		Percentiles					
		99.0%	***99.9%***	***99.99%***	***99.999%***	***99.9999%***	***100%***
Open Sky	***Even CCF [dB]***	-33.5	-29.3	-26.4	-24.3	-23.1	-20.0
	Odd CCF [dB]	-33.5	-29.3	-26.4	-24.3	-23.2	-19.3
RIMS Sites	***Even CCF [dB]***	-33.5	-29.3	-26.4	-24.3	-23.2	-20.0
	Odd CCF [dB]	-33.5	-29.3	-26.4	-24.3	-23.2	-19.3

The difference between analytical model and simulation model for the RIMS sites scenario is significant. As already observed in Section 4.4.2, the assumption to take the average power offset is only representative of the average performance. In particular, the highly directive antenna of the RIMS sites is responsible for the big variation in received power levels that, as displayed in Figure 4–34, ranges from approximately -149 dB to -163 dB (14 dB offset). This justifies why percentile 100% computed with the analytical model is about 10 dB lower than the one computed with the simulation model with the assumption of 5 dB power offset.

4.4.5 BeiDou B2-I→Galileo E5b-I

In this section the cross-interference caused by BeiDou B2-I singals onto the Galileo E5b-I spreading codes is evaluated. The assumptions undelying this RFC assessment are summarised in Table 4-32.

Table 4-32: BeiDou B2-I→Galileo E5b-I Cross-Interference Scenario.

	Open Sky
Des. RNSS System	Galileo
Des. Constellation	Table 4-3
Des. Satellite Antenna Pattern	E5 from Table 4-8
Des. Signal	E5b-I from Table 4-12
Int. RNSS System	BeiDou Phase II
Int. Constellation	Table 4-5, Table 4-6
Int. Satellite Antenna Pattern	B2 from Table 4-10
Int. Signal	B2-I from Table 4-14
Reference Receiver	Mass Market User
Rx Bandwidth [MHz]	Table 4-15 for L1 band
Integration Time [ms]	1
Simulation Start	GPS week: 906 Seconds into week: 86400 (02.01.2017)
Duration	1 day

	Open Sky
Time Interval	60 s
Reference Receiver Location	Earth Grid
Masking Angle	10°

This scenario is characterised by $T^{\mathrm{INT}} = T^{\mathrm{DES}}$, thus only two bit flip patterns – Even and Odd – are to be taken into account for the CI histogram computation. Given the computational load required to perform the RFC assessment with the simulation model, only the analytical approach is used in this case.

Table 4-33 reports the correlation percentiles of the cross-interference caused by BeiDou B2-I onto Galileo E5b-I component for the two scenarios under analysis. By comparing the results with Table 3-19 an offset of about 5 dB is observed on the correlation percentiles.

Table 4-33: BeiDou B2-I → Galileo E5b-I CPs, Open Sky.

		Percentiles					
		99.0%	***99.9%***	***99.99%***	***99.999%***	***99.9999%***	***100%***
Open Sky	***Even CCF [dB]***	-35.2	-30.7	-27.3	-24.7	-23.4	-20.3
	Odd CCF [dB]	-35.2	-30.7	-27.3	-24.7	-23.4	-20.2

In Figure 4–37 the minimum and maximum power levels versus elevation are provided for the Open Sky scenario.

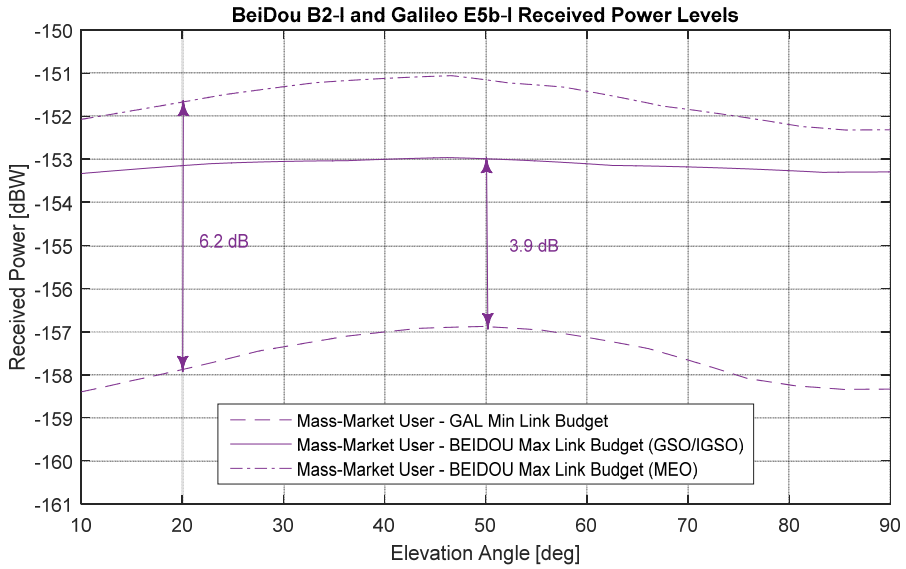

Figure 4–37: BeiDou B2-I and Galileo E5b-I Received Power Levels, All Scenarios.

In this case, the received power offset ΔP between the Galileo minimum link budget and the BeiDou maximum link budget depends on the SV orbit and payload

characteristics. Two values are considered in the analytical simulation, respectively 6 dB for MEO and 4 dB for GSO/IGSO.

Further, the received power statistics are represented in Figure 4–38. The plot on the left shows the numerical probability density function of the received power for each of the 16 Galileo satellites (red) and the 15 BeiDou satellites. The difference between the MEO and GSO/IGSO link budget is clearly visible. In Figure 4–38 (right), the receiver power offset statistics is obtained by counting the number of occurrences over the total number of observations. The power offset values are highly concentrated around -6 dB and -4 dB.

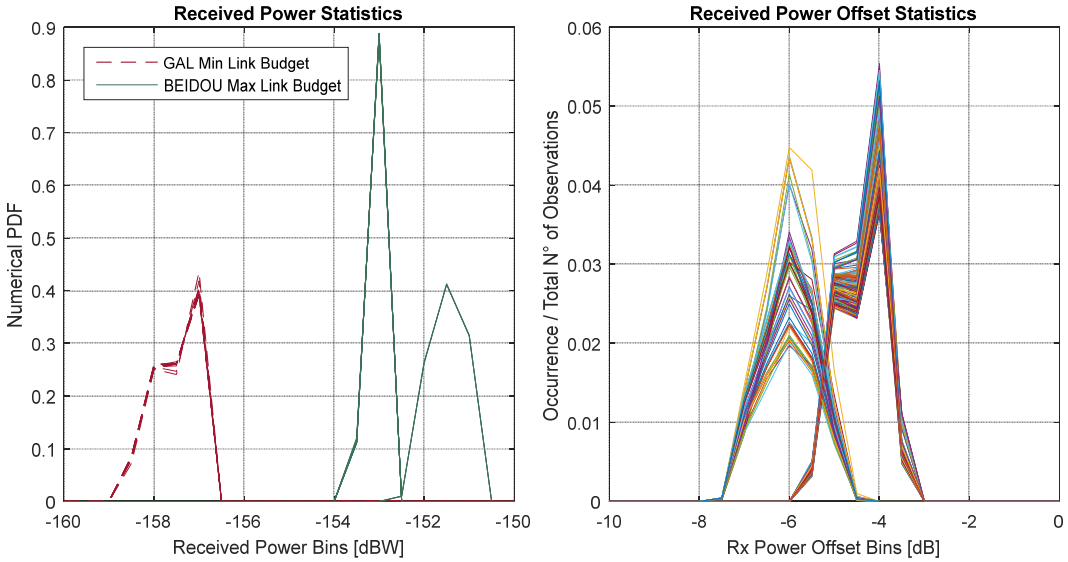

Figure 4–38: BeiDou B2-I and Galileo E5b-I Power Offset Statistics, Open Sky.

In Figure 4–39 (left) the Doppler frequency statistics of the Galileo and BeiDou signals are represented for the Open Sky scenario. Again, the difference between GSO, IGSO, and MEO satellites is visible from distribution of Doppler frequencies. The y-axis is cut to 0.05 in order to display all distributions however the numerical PDF for GSOs goes up to 1. Figure 4–39 (right) shows the Doppler frequency offset computed for each PRN code couple over the simulation duration.

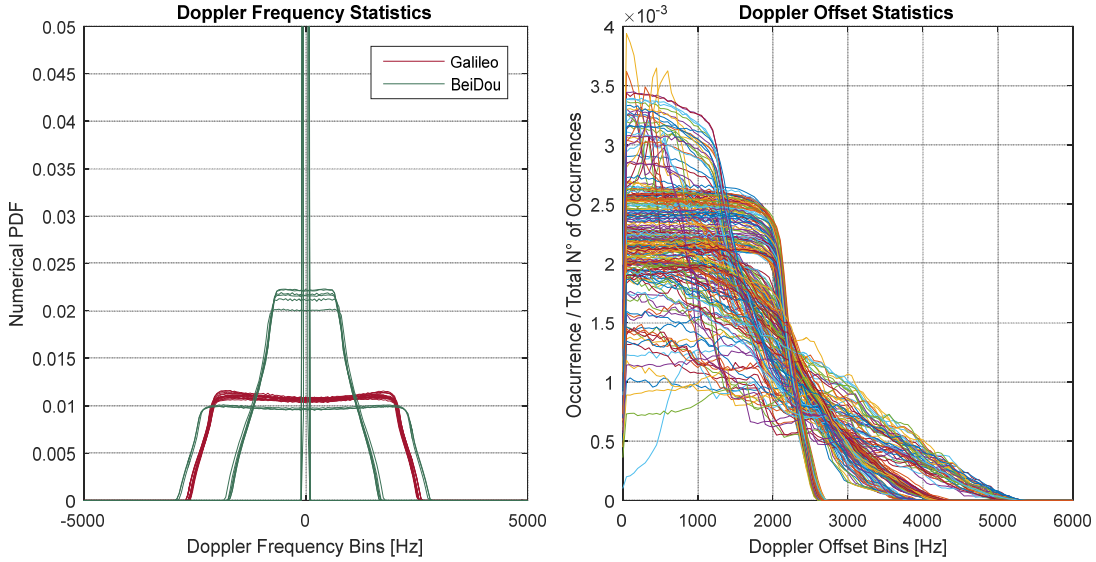

Figure 4–39: BeiDou B2-I and Galileo E5b-I Doppler Frequency Statistics, Open Sky.

5. Conclusions and Recommendations

This chapter presents the conclusions from the results obtained in the previous chapters and draws recommendations for future work.

5.1 Conclusions

This thesis has provided a complete overview on Pseudo-Random Noise (PRN) codes and their performance figures in the context of satellite navigation.

First, Chapter 2 has provided a theoretical framework for understanding the role of spreading codes into GNSS signals' structure. Generalised expressions to describe nowadays navigation signals have been derived and the impact of PRN codes onto the signals' spectral content has been explained. The concept of short-code and long-code signals has been introduced to distinguish between signals respectively with line spectrum and continuous spectrum.

Later in Chapter 3 a complete review of the spreading code properties and the typical performance figures has been provided. Mathematical expressions for the auto- and cross-correlation between spreading codes have been given as a basis to understand the correlation histogram and correlation percentiles computation. Several examples have been presented in support to the description of the figures of merit and for proving the correct implementation with respect to referenced sources. The aforementioned expressions and figures have been extended to take into account for overlay codes, sub-carrier components, chip shape, and integration time.
From the analysis on PRN code set self-interference, the following conclusions on the CDMA isolation of tired codes (Section 3.4.1) have been drawn:

- The use of 'short' secondary codes, whether they are the same for all SVs or different ones, results in degraded auto-correlation properties. This represents a disadvantage on the receiver side for signal acquisition operations.
- When the transmitted secondary code is the same on all SVs, the cross-correlation properties do not show a significant improvement compared to the cross-correlation properties of the primary code set.

- The use of different secondary codes on the SVs improves significantly the cross-correlation properties compared to the cross-correlation properties of the primary code set.

From the investigation on the effects of chip shape (Section 3.4.2), the following observations have been made:

- Multi-level coded symbols, such as BOC(1,1) CBOC(6,1,1/11) modulations, do not lead to a significant improvement of the spreading codes CDMA isolation in terms of cross-correlation properties;
- On the other hand, the analysed chip shapes introduce undesired high peaks in the auto-correlation function that can lead to false acquisition or tracking. Being the position of secondary lobes deterministic w.r.t. the main peak, several techniques have been proposed in literature for ensuring the correct code phase lock.

To conclude on the integration time and Doppler frequency aspects, the following has been demonstrated:

- The effect of multiple integrations onto auto- and cross-correlation performance is investigated taking as reference case the GPS L1-C/A signal. As expected, the even ACF and CCF are left unvaried by multiple integrations. On the other hand, odd auto-correlation over multiple sequences shows high peaks in correspondence of the PRN codes periodicity. This result was expected and it does not represent any impairment for acquisition/tracking operations, as the receiver can lock on the code phase of any PRN sequence within the integration time. It is up to the bit synchronization algorithm to detect sign changes corresponding to data symbols' transitions.
- The analysis between correlation values and integration window is further extended to the Doppler frequency offset. For short codes it is shown that the worst cross-correlation interference results from the shortest integration time. The curve of correlation percentiles versus Doppler frequency offset obtained with the smallest integration window represents an envelope for the other cases.

- Long-code signals with a 'continuous spectrum', smoothed by the presence of data bits or secondary code chips transmitted with relatively high rate, do not present sensitivity to particular values of the Doppler frequency offset.

The analysis on PRN code set cross-interference (Section 3.5) has provided a generalised expression for the cross-correlation between PRN code sets that encompasses all cases of desired and interfering code periods. Three computational examples have been provided, namely Galileo E1-OS versus GPS L1-C, GPS L1-C/A versus SBAS L1, and Galileo E5b-I versus BeiDou B2-I. The results have shown the validity of the mathematical model and provide cross-interference values for navigation signals of interest.

Chapter 4 has presented a new methodology for assessing spreading codes interference within and between satellite navigation systems based on CDMA technology.

First, the context of ITU radio frequency compatibility assessments has been described to the best knowledge of the author. The motivation for introducing a new methodology has been justified by highlighting the shortfalls of current methods that focus solely on the interfering power levels. As a starting point for the new proposed methodology, Rec. ITU-R M.1831 has been explained. The concept of self-interference and cross-interference has been introduced and the computation of the assessment criteria with the simulation model and the analytical model has been described. Finally a long section of simulation results has proven the effectiveness of the methodology and has highlighted relevant aspects related to the PRN codes compatibility among signals.

The main considerations on the RFC methodology with respect to the two proposed models are summarised in Table 5-1.

Table 5-1: Conclusions on the PRN Codes based RFC Methodology.

	PRN Code based RFC Methodology	
	Simulation Model	***Analytical Model***
Self-Interference	Results from the two approaches match perfectly. Therefore the analytical model can be adopted instead of the simulation model for a reduced computational load.	
	Computed examples: GPS L1-C/A in Section 4.4.1 Galileo E1-OS in Section 4.4.3	
Cross-Interference	Results obtained with the	Results obtained with the

	simulation model are representative for the whole correlation percentile statistics.	analytical model are representative of the average CI behaviour but cannot capture the values at the edge of the distribution. This approach is more suitable for reflecting the 1-σ, 2-σ and 3-σ statistics. The assumption of taking the average power offset between the two PRN code sets instead of the full distribution represents a limitation of the methodology.
	Computed examples: EGNOS L1→GPS L1-C/A in Section 4.4.2 GPS L1-C→Galileo E1-OS in Section 4.4.4 BeiDou B2-I→Galileo E5b-I in Section 4.4.5	

The major outcomes regarding the simulation results in Section 4.4 are listed below for each case considered:

- GPS L1-C/A Self-Interference: By comparing the CPs for 1 ms integration time (worst-case) in Table 4-19 with those obtained in Table 3-10 (0 Hz Doppler offset) and in Table 3-11 (uniform Doppler offset), the increase of L1-C/A self-interference measured by the new RFC methodology is enormous. The values obtained for even and odd cross-correlation (maximum peaks at -15.8 dB and -13.1 dB) are significantly higher because of the method takes into account for the real power levels and Doppler frequency offset distribution.
- EGNOS L1→GPS L1-C/A Cross-Interference: The levels or cross-interference computed with the simulation model are extremely high: the maximum correlation value over the coverage is measured on the equatorial region below Europe and it is about -10.0 dB. Again, the proposed methodology reveals an inter-system interference scenario more severe than what can be observed by computing the simple cross-correlation figure (see percentiles in Table 3-16).
- Galileo E1-OS Self-Interference: Simulation results show that the self-interference of Galileo E1-OS spreading codes computed with the new method is about 4 dB higher than the one obtained with cross-correlation performance figure in Chapter 3 (compare Table 4-27 with Table 3-9). This case has revealed that the spreading codes RFC analysis can be relevant also for long-code signals and not only for shot-code ones.

- GPS L1-C→Galileo E1-OS Cross-Interference: The difference in CI between analytical model and simulation model for the RIMS sites scenario is huge. This case demonstrates the limitations of the analytical model as the assumption to take the average power offset is only representative for the average performance. Additionally, the highly directive antenna of the RIMS sites is responsible for the big variation in received power levels that explains why percentile 100% computed with the RFC methodology is about 11 dB above the ones computed with cross-correlation performance figure (compare Table 4-30 with Table 3-13).
- BeiDou B2-I→Galileo E5b-I Cross-Interference: By comparing the CP results in Table 4-33 with those in Table 3-19 (0 Hz Doppler offset) an increase of about 5 dB is observed. Again, the RFC methodology here proposed is shown to be relevant also for long-code signals and not only for shot-code ones.

Additionally, some considerations regarding the influence of reference assumptions onto the PRN codes self- and cross-interference assessment are summarised in Table 5-2.

Table 5-2: Considerations on the Impact of RFC Reference Assumptions.

	Self-Interference	***Cross-Interference***
Power Level	Absolute power levels are not relevant. Only the offset between the best-case and worst-case link budget is important.	Absolute power levels are not relevant. Only the offset between the desired signal worst-case link budget and the interfering signal best-case link budget is important.
Antenna Pattern	The satellite transmit antenna and the reference receiver antenna gain patterns have a negligible impact.	The transmit antenna gain patterns from the desired and the interfering systems are relevant. The reference receiver antenna pattern has a significant impact only when RNSS systems with non-uniform coverage are involved.
Doppler Frequency Offset	The Doppler frequency offset is relevant for short-codes for which the correlation values distribution varies w.r.t. the Doppler offset value.	
Elevation Angle	When RNSS systems with non-uniform coverage are involved, the elevation angle determines the coverage area. However its impact on the CP values is negligible.	

To conclude, this thesis has provided new means to support future analysis in the field of radio-frequency compatibility. In view of extending Rec. ITU-R M.1831 by including the PRN codes based RFC methodology proposed in this thesis, the

following information should be specified in addition to the classical reference assumptions:

- PRN codes, available from public SIS ICDs.
- Association between spreading codes and SVs. Depending on the satellites constellation and the goodness of the PRN codes family, this information might not play a significant role for the RFC assessment.
- Minimum integration time for the desired signal (worst-case assessment).

Finally, note that Rec. ITU-R M.1831 does not provide 'acceptable' levels of Effective C/N_0 and C/N_0 Degradation as it is the task of service providers to reach a common agreement. Similarly, the PRN codes RFC methodology here proposed does not set a threshold for the cross-correlation interference generated by satellite navigation systems onto each other. However a detailed analysis should be carried out by each system provider to determine what is a tolerable figure.

5.2 Recommendations for Future Work

In order to guarantee the right coexistence of all current, planned, and future signals a complete understanding of all radio frequency compatibility aspects is fundamental. The PRN codes based RFC methodology presented in this thesis should be further investigated and consolidated though more self- and cross-interference assessments.

An extension to allow for multi-constellation PRN codes analysis is necessary to fully assess nowadays GNSS interference scenario. The aggregate level of cross-interference cannot be computed by a simple addition of the correlation percentiles. The spatial and temporal information is needed for correctly considering the correlation peaks originating from PRN codes transmitted by different navigation systems. The simulation model seems to be the only approach suitable for a multi-constellation assessment.

The analytical model proposed for the PRN codes based RFC methodology could be improved by making use of the received power distribution instead of only the average power offset. This information should be carefully combined with the Doppler offset statistics in order not to lose the spatial-temporal correlation.

Moreover the impact of PRN codes self- and cross-interference onto the receiver signal processing has not been discussed in this thesis. In particular, the effects

caused by the cross-correlation peaks onto the signal acquisition process should be investigated. Classical navigation literature always refers to the single cell detection approach in AWGN, but it would be of interest to modify the noise model by assuming self- and cross-interference contributions for the detection hypothesis.

Additionally, temporary effects are produced on the tracking operations when interfering PRN codes slide into the correlator. As discussed in [35], for the case of GPS L1-C/A self-interference this happens when the Doppler offset between two spreading codes is a multiple of 1 kHz. In [37] a model for predicting C/A-code self-interference is proposed.

A final recommendation goes to the GNSS system providers with reference to the on-going discussions on GPS L1-C/A signal evolution ([38]) and on a future Galileo E1-D acquisition aiding component: spreading codes aggregate cross-interference should be carefully assessed on a global scale. It is dangerous to design new CDMA navigation services neglecting the complex radio-frequency interference scenario where they should coexist.

A. Spectral Line Analysis for Galileo Signals

The content of Appendix A is partly based on the author's work in [51].

In this Appendix power spectral densities of the Galileo signals baseline (E1 OS, E6 CS, and E5) are computed according to the spectral line model presented in Chapter 2.

Table A–1 provides the list of Galileo signals together with the relative carrier frequency, modulation, and receiver reference bandwidth as described in [8]. The following analysis considers, for each of the selected signals, the normalized PSD (unit area over an infinite bandwidth) filtered within the reference bandwidth. A brick-wall filter is assumed to avoid the introduction of distortions related to the specific band-limiting filter.

Table A–1: Galileo Signals Overview.

Signal Name	***Carrier Frequency***	***Modulation***	***Ref. Bandwidth***
Galileo E1 OS	1575.420 MHz	CBOC(6,1,1/11)	$24\,f_0$
Galileo E5	1191.795 MHz	AltBOC(15,10)	$50\,f_0$
Galileo E6 CS	1278.750 MHz	BPSK(5)	$40\,f_0$

Information regarding the primary code, secondary code, and data rate characteristics for each signal is available in [8] and summarised in Table 3-2. The only exception is represented by the primary codes of Galileo E6 CS which are currently not in the public domain.

It is out of the scope of this Appendix to describe the Galileo signals modulations. Well-renowned references are provided for further details.

A.1 Galileo E1 OS

The E1 Open Service (OS) modulation receives the name of CBOC which stands for Combined Binary Offset Carrier. According to [18], CBOC(6,1,1/11) is the result of multiplexing a wideband signal - $BOC_s(6,1)$ - with a narrow-band signal - $BOC_s(1,1)$ - in a way that 1/11 of the power is allocated in average to the high frequency component. The transmitted Galileo E1 OS signal consists of the following components:

- The E1 OS data channel, or E1-B, which results from the combination of the navigation data stream, the ranging code, and the in-phase CBOC component.
- The E1 OS pilot channel, or E1-C, resulting from the combination of primary code, secondary code, and the anti-phase CBOC component.

The two channels E1-B and E1-C are generated independently and then summed up, as explained in [8]. The normalized PSD of the combined E1 OS service, without the effect of band-limiting filters and payload imperfections, is given by:

$$G_{E1-OS}(f) = \frac{1}{2}\left(G_{E1-B}(f) + G_{E1-C}(f)\right) \tag{A.1}$$

being the two channels statistically uncorrelated.

Figure A–1 shows the normalized PSD of respectively Galileo E1-B (left) and E1-C (right) components as transmitted by SVID 19. The PSD is constructed following the spectral line model explained in Chapter 2. The real spectra are overlapped by the ideal smooth spectrum corresponding to the CBOC modulation (black dashed line).Note how spectral lines are far above the power level of the smooth spectrum especially in the case of the pilot component, where there are no navigation symbols to smooth the spectrum.

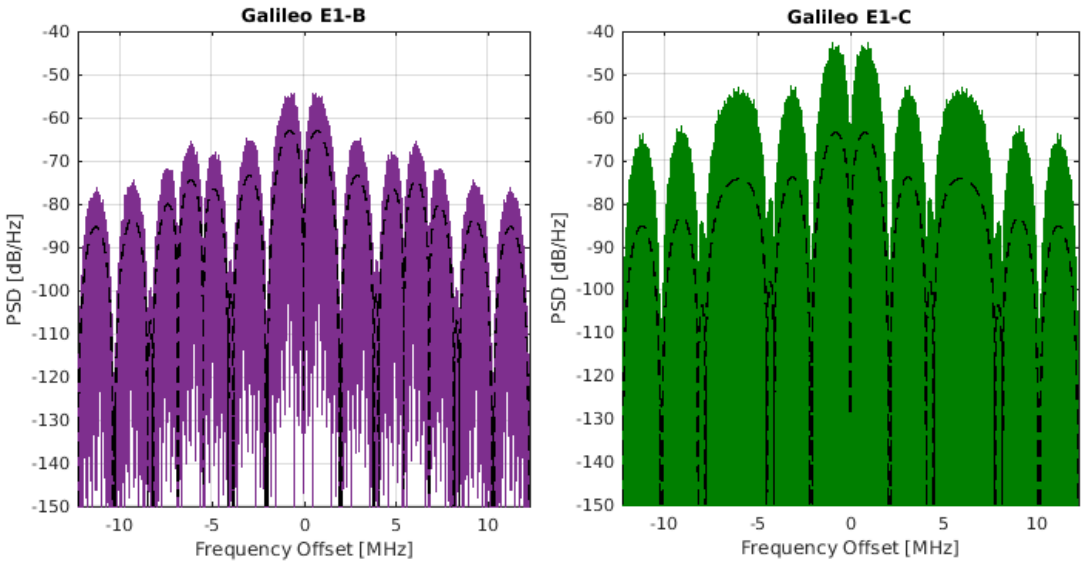

Figure A–1: Galileo E1-B/C PSD trasmitted by SVID 19.

Figure A–2 shows the combined Galileo E1 OS spectrum.

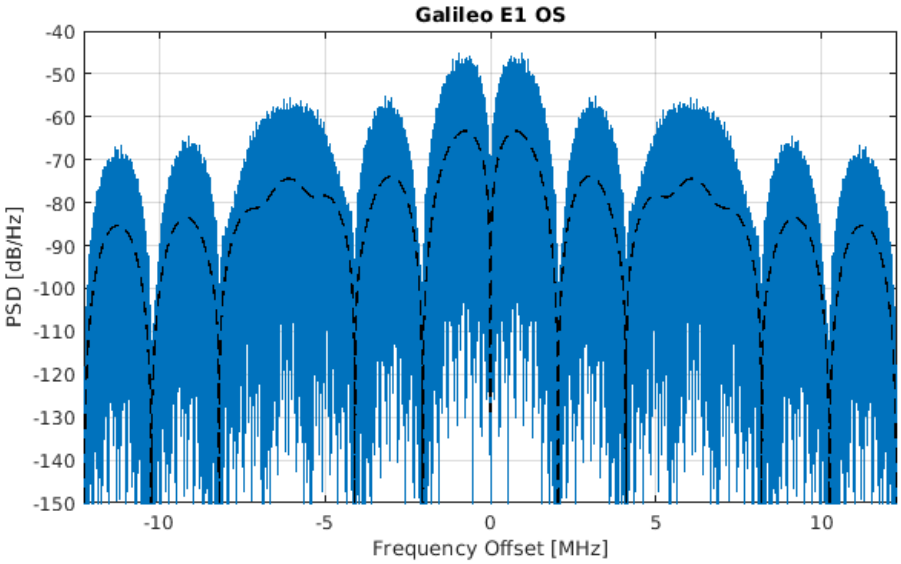

Figure A–2: PSD of Galileo E1 OS trasmitted by SVID 19.

Figure A–3 represents the fine structure of the normalized PSDs displayed in Figure A–1, and the combined E1 OS spectrum (blue) obtained as the linear sum of E1-B (purple) and E1-C (green) components.

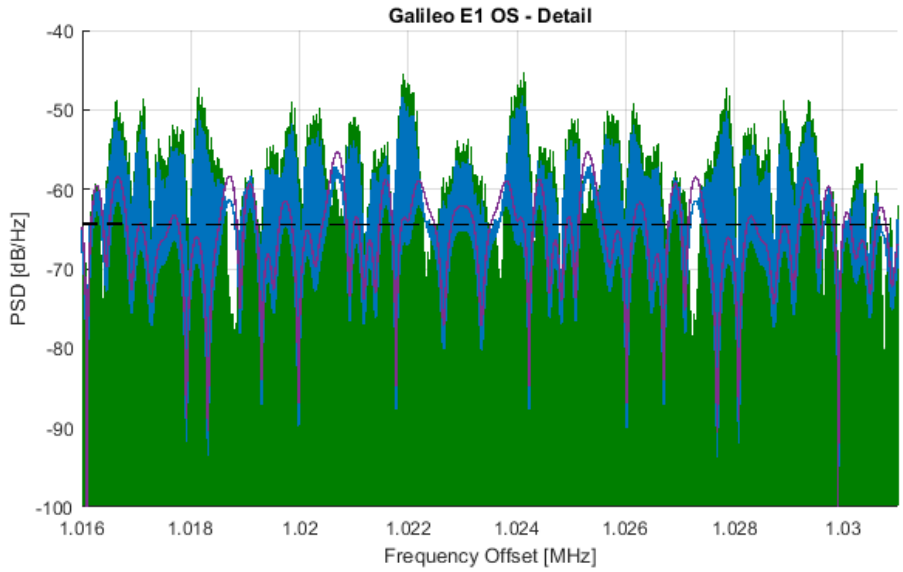

Figure A–3: PSD of Galileo E1 OS (detail) trasmitted by SVID 19.

A.2 Galileo E6 CS

The E6 Commercial Service (CS) modulation is a Binary Offset Phase Shift Keying BPSK(5) at 5.115MHz. The Galileo E6 CS signal consists of the following two components:

- The E6 CS data channel, or E6-B, that is the combination of the navigation data stream with the primary code sequence.

- The E6 CS pilot channel, or E6-C, which results from the combination of the primary code with the secondary code sequence.

For E6 CS as for E1 OS the two channels E6-B and E6-C are generated independently and then summed up [8]. The normalized PSD of the combined E6 CS service is given by:

$$G_{E6-CS}(f) = \frac{1}{2}\left(G_{E6-B}(f) + G_{E6-C}(f)\right) \quad \text{(A.2)}$$

being the two channels statistically uncorrelated.

Figure A–4 shows the normalized PSD of respectively Galileo E6-B (left) and 6-C (right) components as transmitted by SVID 19.

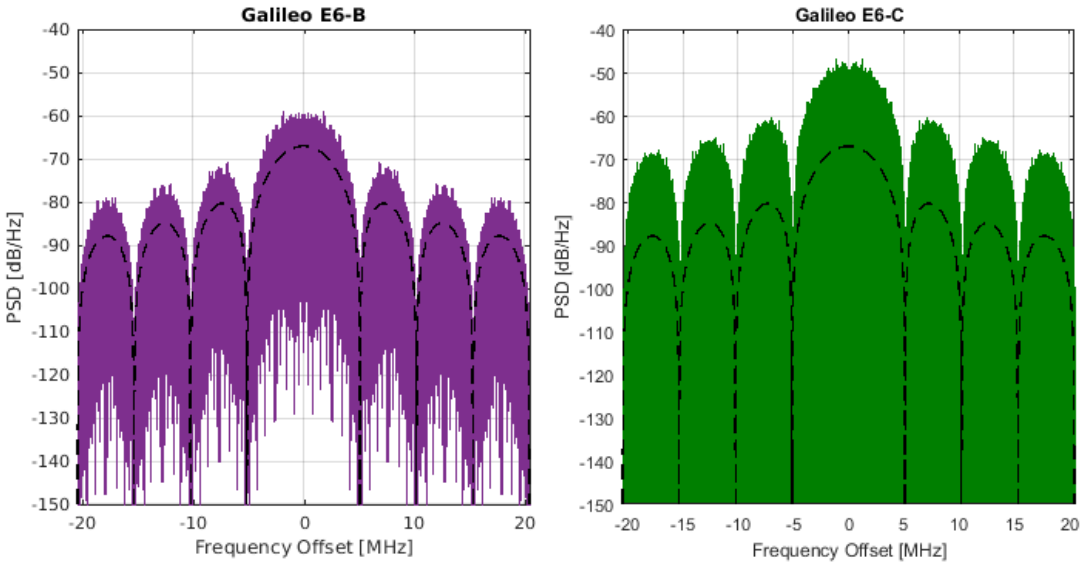

Figure A–4: Galileo E6-B/C PSD trasmitted by SVID 19.

Figure A–5 displays the normalized PSD of the Galileo E6 CS (blue) for SVID 19. The ideal smooth spectrum corresponding to the BPSK modulation is drawn with a black dashed line.

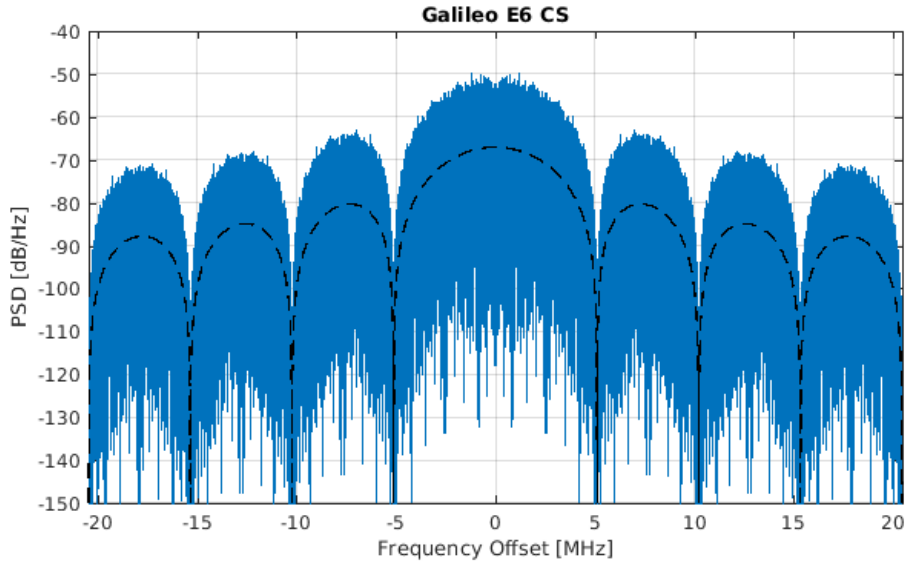

Figure A–5: PSD of Galileo E6 CS trasmitted by SVID 19.

Figure A–6 represents the fine structure of the normalized PSD displayed in Figure A–5 together with the two components E6-B (purple) and E6-C (green).

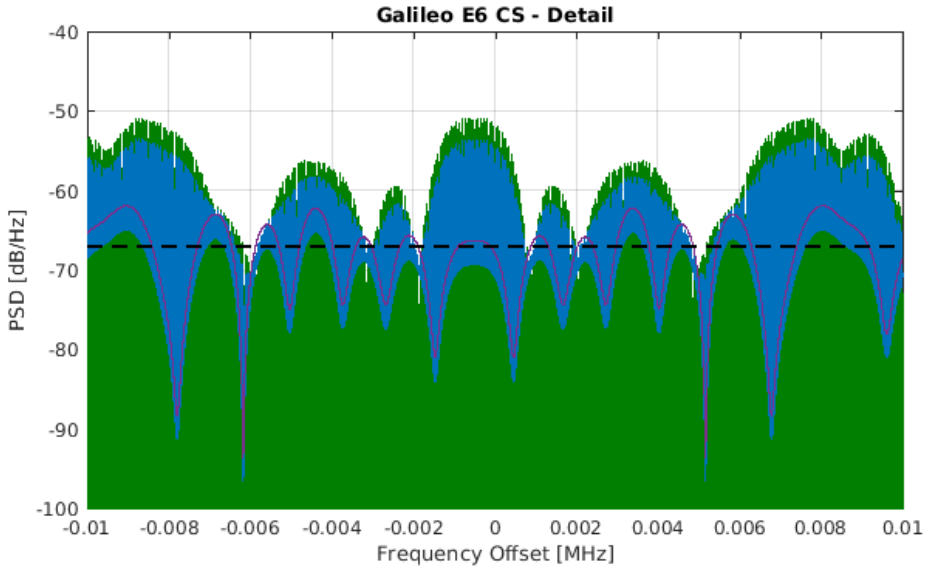

Figure A–6: PSD of Galileo E6 CS (detail) trasmitted by SVID 19.

A.3 Galileo E5

The Galileo E5 modulation receives the name of AltBOC and is a modified version of a BOC with code rate of 10.23 MHz and a sub-carrier frequency of 15.345 MHz [8]. The AltBOC multiplexing combines the E5a and E5b services in a composite constant envelope signal which is then injected through a very wideband channel. The different Galileo E5 signal components are generated according to the following scheme:

- The E5a data channel, or E5a-I: this channel is the combination of the E5a data stream with the E5a-I primary code sequence and the secondary code $CS20_1$.
- The E5a pilot channel, or E5a-Q: this channel is the combination of the E5a-I primary code sequence and the secondary code $CS100_{1\text{-}50}$.
- The E5b data channel, or E5b-I: this channel is the combination of the E5b data stream with the E5b-I primary code sequence and the secondary code $CS4_1$.
- The E5b pilot channel, or E5b-Q: this channel is the combination of the E5a-Q primary code sequence and the secondary code $CS100_{51\text{-}100}$.

The AltBOC multiplexing of the aforementioned signals is slightly more complex with respect to the previous cases where the components are simply summed up. To keep the envelope constant, four additional signals are constructed as a combination of the four single components e_{E5a-I}, e_{E5a-Q}, e_{E5b-I}, e_{E5b-Q}. These 'product components' are defined in [8] as:

$$\begin{aligned}
\bar{e}_{E5a-I} &= e_{E5a-Q} \cdot e_{E5b-I} \cdot e_{E5b-Q} \\
\bar{e}_{E5a-Q} &= e_{E5a-I} \cdot e_{E5b-I} \cdot e_{E5b-Q} \\
\bar{e}_{E5b-I} &= e_{E5a-I} \cdot e_{E5a-Q} \cdot e_{E5b-Q} \\
\bar{e}_{E5b-Q} &= e_{E5a-I} \cdot e_{E5a-Q} \cdot e_{E5b-I}
\end{aligned} \tag{A.3}$$

Following the signal description proposed in Section 2.1, it is possible to define the primary codes, secondary codes, and data rate for each of the product components as in Table A–2.

Table A–2: AltBOC product components.

	Primary Code	***Secondary Code***	***Data Rate [sps]***
$\bar{e}_{E5a-I}$	Length: 10230 $\{c_P\}_{E5a-Q} \cdot \{c_P\}_{E5b-I} \cdot \{c_P\}_{E5b-Q}$	Length: 100 $\{c_S\}_{CS100} \cdot \{c_S\}_{CS4} \cdot \{c_S\}_{CS100}$	250
$\bar{e}_{E5a-Q}$	Length: 10230 $\{c_P\}_{E5a-I} \cdot \{c_P\}_{E5b-I} \cdot \{c_P\}_{E5b-Q}$	Length: 100 $\{c_S\}_{CS20} \cdot \{c_S\}_{CS4} \cdot \{c_S\}_{CS100}$	250
$\bar{e}_{E5b-I}$	Length: 10230 $\{c_P\}_{E5a-I} \cdot \{c_P\}_{E5a-Q} \cdot \{c_P\}_{E5b-Q}$	Length: 100 $\{c_S\}_{CS20} \cdot \{c_S\}_{CS100} \cdot \{c_S\}_{CS100}$	50
$\bar{e}_{E5b-Q}$	Length: 10230 $\{c_P\}_{E5a-I} \cdot \{c_P\}_{E5a-Q} \cdot \{c_P\}_{E5b-I}$	Length: 100 $\{c_S\}_{CS20} \cdot \{c_S\}_{CS100} \cdot \{c_S\}_{CS4}$	250

The eight components are then modulated with two complex subcarriers to result in the Galileo E5 signal bi-modal spectrum.

From the analysis of the AltBOC constant envelope modulation provided in [20], it is known that the statistical autocorrelation function of the total signal is the sum of sixteen terms, i.e. four single components plus four product components, each of them modulated by the sub-carrier function in quadrature with a delayed version of it. The cross-terms cancel out under the hypothesis that the codes are ideally orthogonal with each other, that the cross correlation between the two subcarriers is zero, and that the cross-correlation between a sub-carrier and its delayed version is zero.

Thus, the normalized PSD of the combined E5 service is computed as:

$$\begin{aligned} G_{E5}(f) = \frac{1}{8}\big(&G^{S}_{E5a-I}(f) + G^{\tilde{S}}_{E5a-I}(f) + G^{S}_{E5a-Q}(f) + G^{\tilde{S}}_{E5a-Q}(f) + \\ &G^{S}_{E5b-I}(f) + G^{\tilde{S}}_{E5b-I}(f) + G^{S}_{E5b-Q}(f) + G^{\tilde{S}}_{E5b-Q}(f) + \\ &G^{P}_{E5a-I}(f) + G^{\tilde{P}}_{E5a-I}(f) + G^{P}_{E5a-Q}(f) + G^{\tilde{P}}_{E5a-Q}(f) + \\ &G^{P}_{E5b-I}(f) + G^{\tilde{P}}_{E5b-I}(f) + G^{P}_{E5b-Q}(f) + G^{\tilde{P}}_{E5b-Q}(f)\big) \end{aligned} \tag{A.4}$$

where the superscript S refers to the sub-carrier function for the single components and the superscript P refers to the sub-carrier function for the product components; the sign '$\tilde{}$' is used to indicate the delayed version (or quadrature component) of the sub-carrier function.

Figure A–7 and Figure A–8 show the normalized PSD of the Galileo E5a-I and E5a-Q single components transmitted by SVID 19 and their ideal smooth spectrum (black dashed line). As a convention, data components with a continuous spectrum are represented in purple, while line spectra are drawn in green.

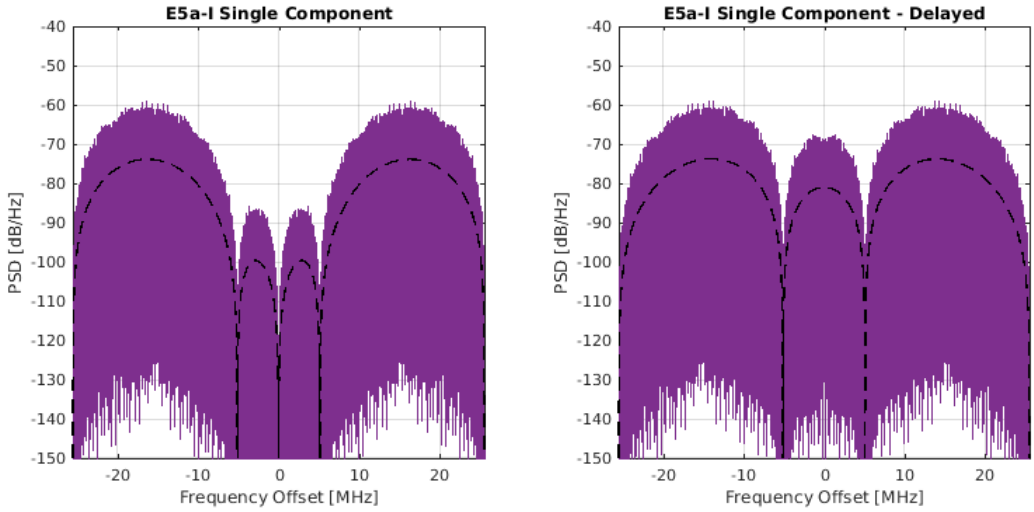

Figure A–7: PSD of Galileo E5a-I single component trasmitted by SVID 19.

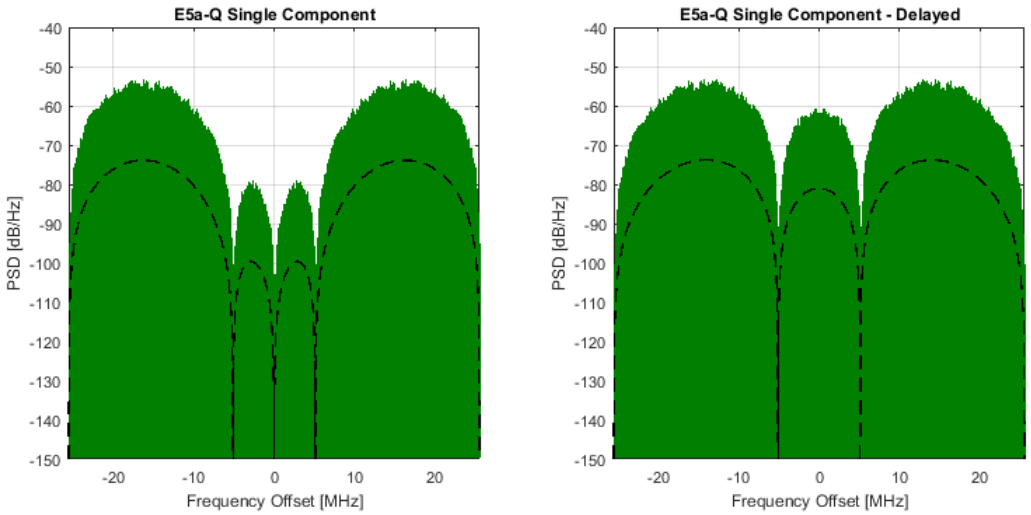

Figure A–8: PSD of Galileo E5a-Q single component trasmitted by SVID 19.

In the same way, Figure A–9 and Figure A–10 show the normalized PSD of the Galileo E5b-I and E5b-Q single components transmitted by SVID 19 and their ideal smooth spectrum (black dashed line).

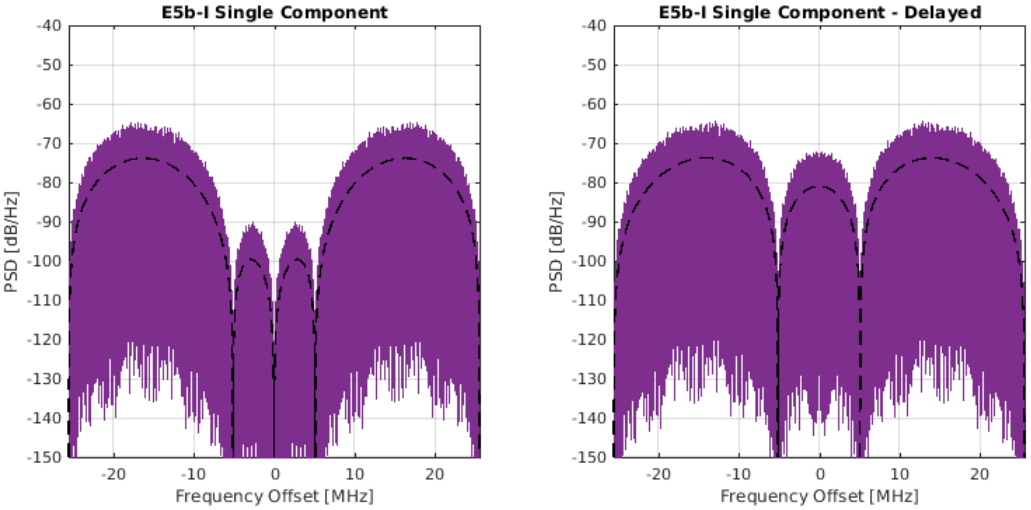

Figure A–9: PSD of Galileo E5b-I single component trasmitted by SVID 19.

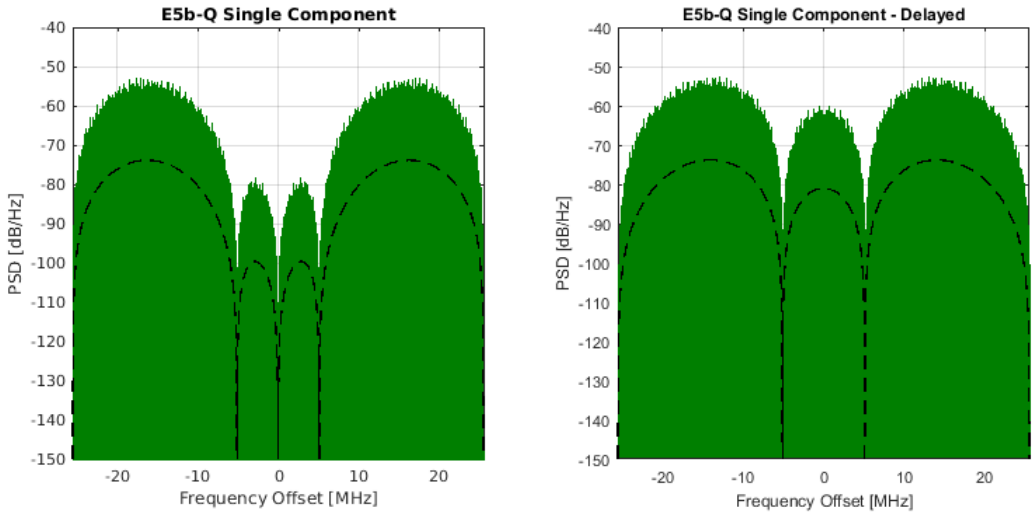

Figure A–10: PSD of Galileo E5b-Q single component trasmitted by SVID 19.

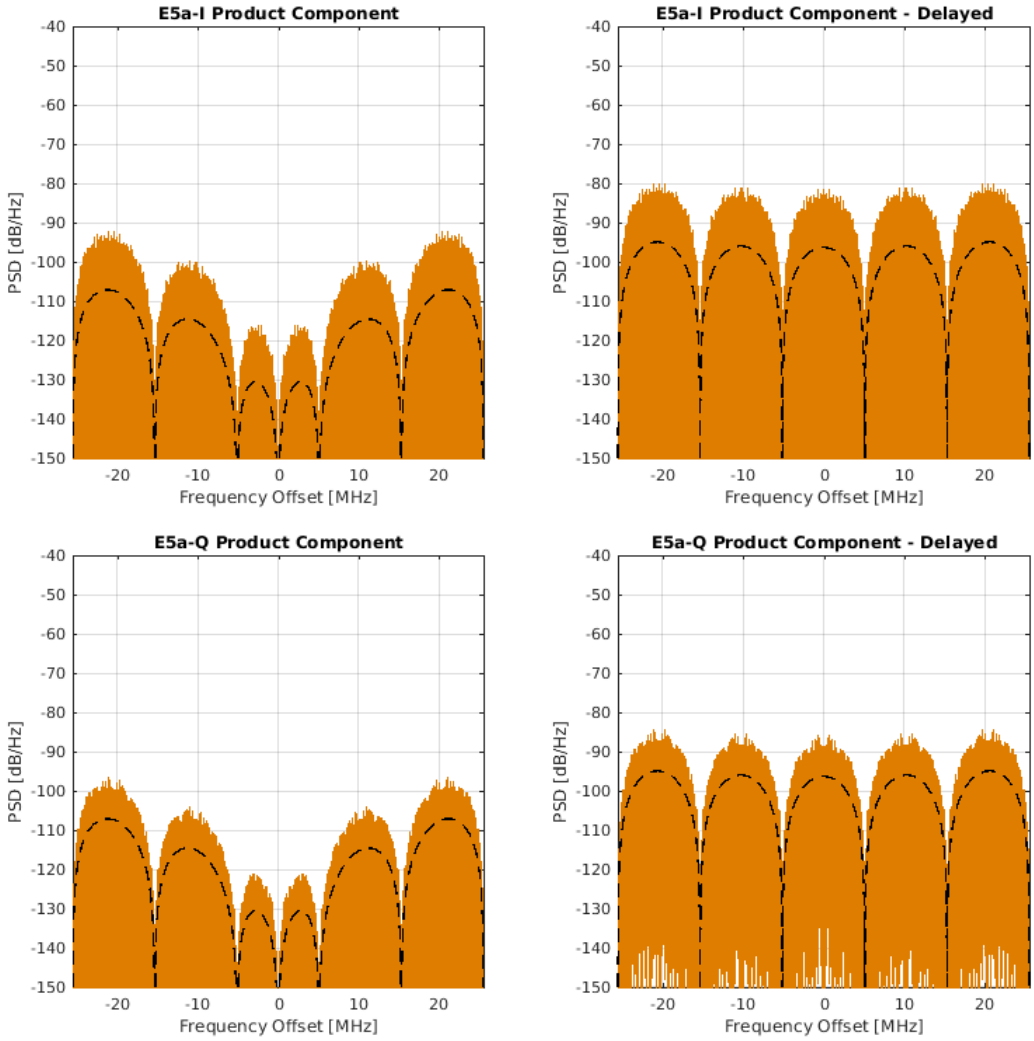

Figure A–11: PSD of Galileo E5a product components trasmitted by SVID 19.

Figure A–11 and Figure A–12 represent the 8 product components generated by multiplying the primary and secondary code sequences as reported in Table A–2.

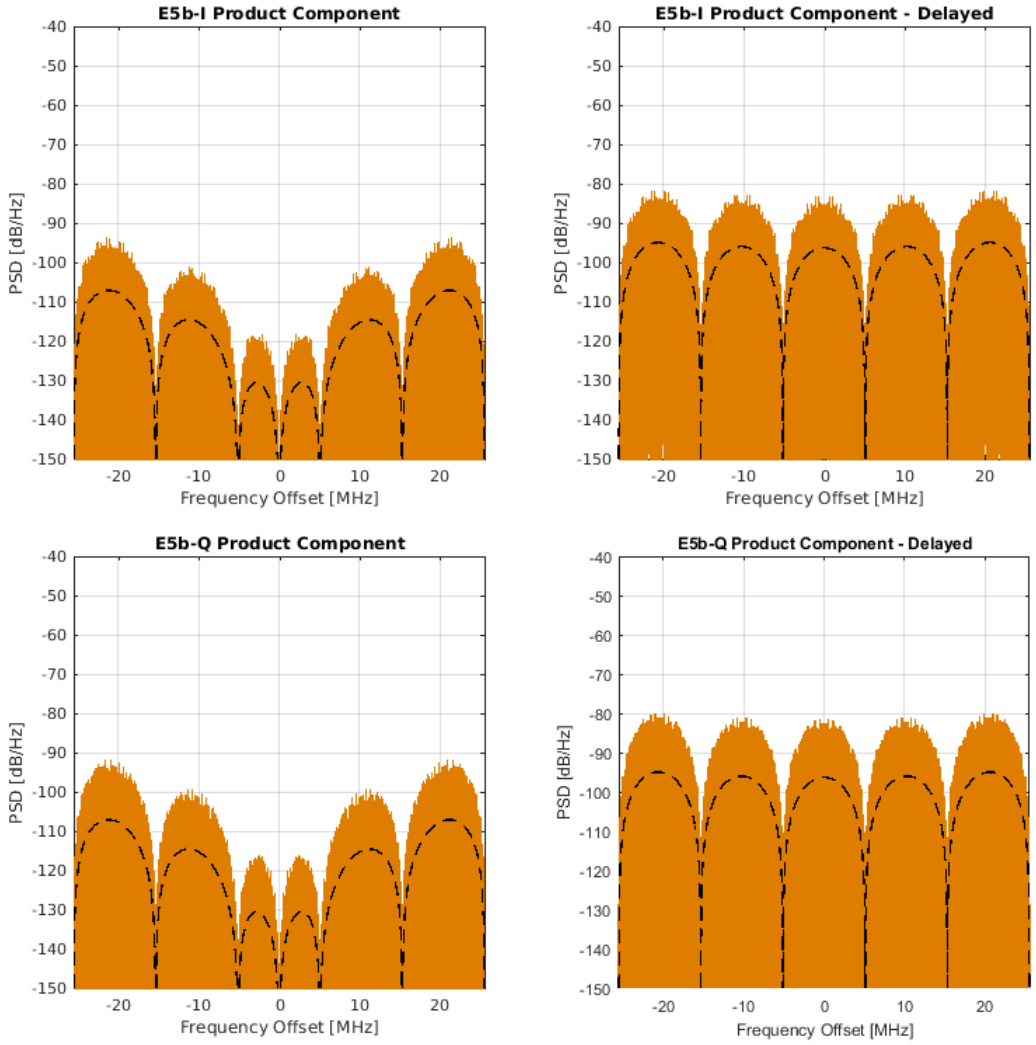

Figure A–12: PSD of Galileo E5b product components trasmitted by SVID 19.

Finally, the Galileo E5 signal resulting from the sum of the 16 components is represented in Figure A–13.

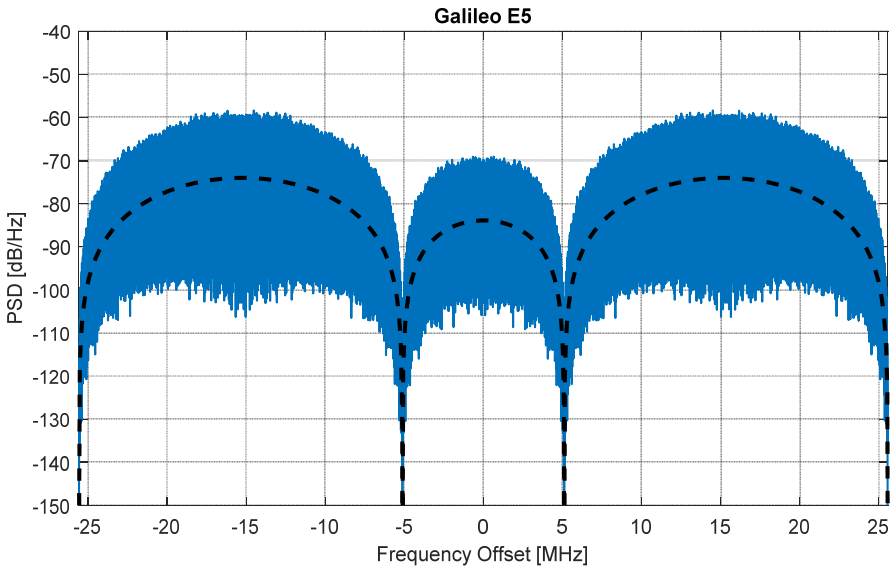

Figure A–13: PSD of Galileo E5 trasmitted by SVID 19.

B. Galileo Signals Distortions

The content of Appendix A is partly based on the author's work in [52].

With the advent of Galileo, Satellite Based Augmentation Systems (SBAS) such as EGNOS will rely also on the new signals to provide higher position accuracy and integrity of service.

SBAS users need to be protected against potential signal distortions causing 'unideal' correlation peak shapes that introduce biases into the position solution. Although differential corrections transmitted by the SBAS service, users generally do not have identical receiver characteristics as the reference receiver of the monitoring network. Therefore differential corrections cannot completely remove errors for all users and signal deformations limit user ranging accuracy.

Waveform distortions may result from imperfections in the signal generation chain and in particular in the clock unit, transmission filters, and antenna characteristics. Depending on the specific payload design, imperfections of the reference timing may cause variations in the chip widths of the spreading codes (digital distortion). Filtering effects may also introduce analog distortions onto the transmitted codes and signal modulation. In the literature some authors identify as sources of waveform imperfections also multipath effects and receiver front-end characteristics. These aspects are here not included in the definition of signal distortions even if they do cause ranging errors. Both propagation effects and receiver components behaviour are specific either of the user location or of the user equipment, and therefore they are considered limitations of the measurement means.

There is a fine line between nominal and non-nominal signal distortions. From a logical point of view, nominal distortions can be defined as 'natural' imperfections of the signal resulting from unideal payload elements that still behave within the design specifications; on the other hand, non-nominal distortions are caused by a failure of one or more payload elements resulting in a user ranging error far above mission requirements. From a user perspective however this distinction is not so clear. It is up to the SBAS systems to characterise the augmented navigation signals in order to discriminate between nominal and non-nominal distortions and to promptly alert the users.

For this purpose, SBAS systems implement the so-called Signal Quality Monitoring (SQM) algorithms which are capable of recognizing distorted navigation signals and thus discarding the corrupted information. The advent of new GNSS signals introduces the necessity to perform a new characterisation for nominal/non-nominal signal distortions and to extend already accepted failure models to the new modulations techniques.

Several models have been proposed to describe payload imperfections and non-ideal effects affecting a radio navigation signal, so as to recognize and discard the corrupted information. Appendix A investigates the concept of nominal and non-nominal signal distortions for Galileo signals. This topic is complex and quite controversial. Substantial literature is available on the subject but no common understanding has been reached up to now in the navigation community. Galileo system provider is still investigating the nature, effects, modelling, and detectability of such distortions. The content of this Appendix reflects only the author's view.

B.1 Nominal Signal Distortions

Nominal distortions are defined as imperfections of the navigation signal resulting from unideal payload elements behaviour. A performance indicator commonly used for measuring nominal signal distortions is represented by the S-Curve Bias (SCB). The expression below defines the SCB as:

$$SCB = \left| \max_{\delta \epsilon [0,\delta_{max}]} CD(\delta) - \min_{\delta \epsilon [0,\delta_{max}]} CD(\delta) \right| \tag{B.1}$$

where the parameter δ is the early-late spacing of the code tracking loop defined in the range $[0, \delta_{max}]$; the Code Delay (CD) is a function of the correlator spacing and is equal to the zero-crossing point of any unbiased DLL discriminator:

$$CD(\delta) = \arg\min_{\varepsilon} |SC(\varepsilon, \delta)| \tag{B.2}$$

For a non-coherent DLL discriminator, the S-Curve (SC) is computed as:

$$SC(\varepsilon, \delta) = \left| CCF\left(\varepsilon - \frac{\delta}{2}\right) \right|^2 - \left| CCF\left(\varepsilon + \frac{\delta}{2}\right) \right|^2 \tag{B.3}$$

being CCF the Cross-Correlation Function between the received signal and the local replica as defined by Eq. (2.33).

The ideal case is represented by an SCB equal to zero. However filtering effects and amplifier non-linearities may cause significant distortions of the SCB.

A measure of filter imperfections is represented by the Differential Group Delay (DGD) characteristics. In general the DGD is associated to the ranging function of

the navigation signal: for the ranging to be as accurate as possible, both GNSS system providers and user receiver manufacturers need to ensure an in-band Group Delay (GD) as flat as possible. For this purpose, GNSS satellites and SBAS navigation payloads are tested at different manufacturing stages to ensure that the resulting group delay characteristics satisfy a certain specification mask. Figure B–1 provides an example of test results for group delay in-orbit measurements.

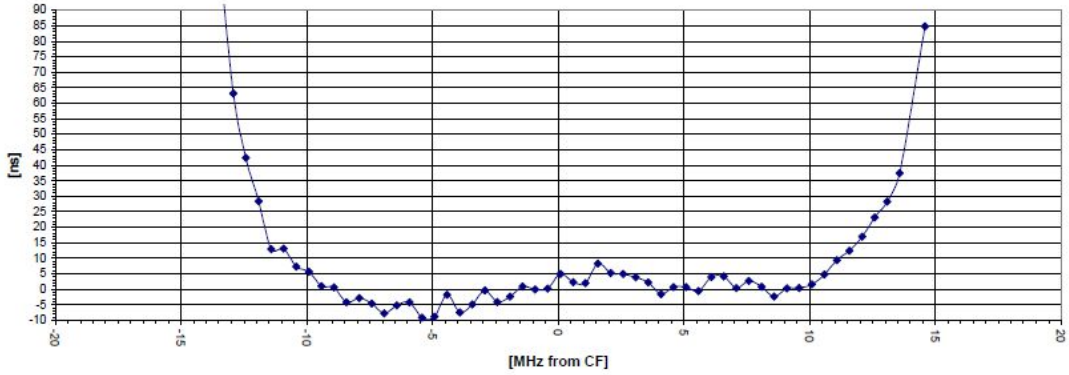

Figure B–1: Example of E1 Group Delay In-Orbit Test Measurements.

Also on the receiver side, group delay variations and asymmetries are typically introduced by user antennas and front-end filters whose behaviour fluctuate with environmental conditions.

In order to protect aviation users from undesired range biases, the approach followed by the standardisation community in MOPS DO-229D [17] is to constrain the equipment contribution to the correlation distortions through a maximum DGD. This value changes according to the different services and user receiver types.. The DGD definition from [17] is reported in Figure B–2.

The equipment differential group delay in seconds is defined as:

$$\frac{1}{360}\cdot\left|\frac{d[\Phi(f_1)]}{df}-\frac{d[\Phi(f_2)]}{df}\right| \text{ where:}$$

f_1 and f_2 are any frequencies within the 3 dB bandwidth of the pre-correlation filter.

$\Phi(f)$ is the combined phase response of the equipment in degrees (excluding the antenna).

f is the frequency in Hz.

Figure B–2: Extract from MOPS DO-229D [17].

The approach adopted in MOPS DO-229D [17] shows some criticalities that raise concerns in the standardisation community currently in the process of defining future Dual-Frequency Multi-Constellation (DFMC) MOPS.

First, there is only one maximum DGD value for each transfer function but there are infinite filter realisations with the same maximum DGD. Each of these filter realisations has a different impact on the correlation shape: the distortion caused can be none as well as severe, resulting in a ranging bias of several meters. This means that limiting the maximum DGD does not constrain the correlation distortions with a one-to-one relationship. As a result, starting from a maximum DGD value (e.g. 150 ns) and few other filter requirements (e.g. bandwidth, minimum attenuation per octave) it is not possible to define the 'worst-case' filter, i.e. the filter resulting in the worst correlation distortions.

Additionally, non-linear effects do not sum up linearly. Thus distortions introduced by the equipment DGD cannot be separated in principle from signal distortions characterising the SIS. In other words, the correlation distortions need to be constrained considering the complete chain from generation to reception and the worst correlation distortions result from a combination of the SIS and the equipment characteristics.

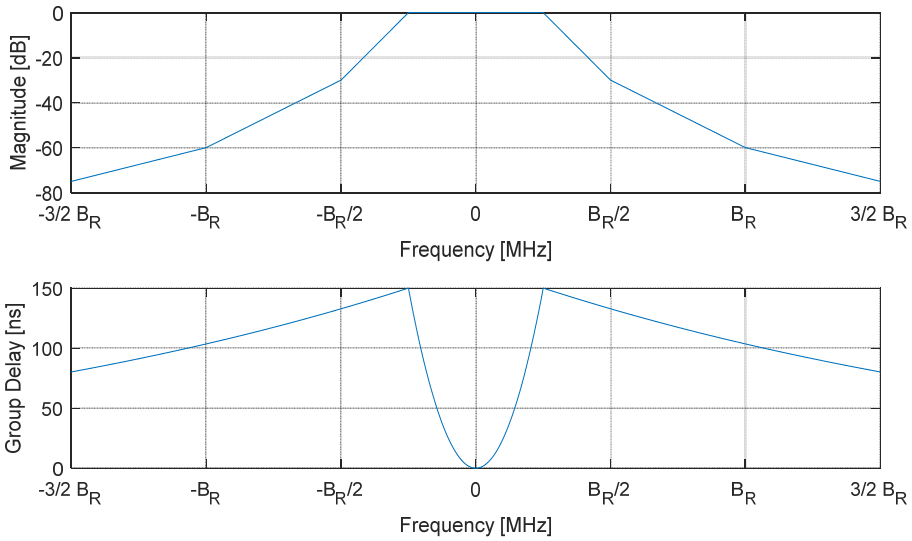

Figure B–3: Illustration of the Stanford Filter Model.

To overcome the issue of the definition of a worst-case filter, a theoretical model for the filter transfer function has been proposed by the Stanford community with the following constraints:

- the nominal filter group delay profile should be of a 'typical' type (e.g., resonator or SAW) that, in general, magnifies the errors from signal distortion faults;

- the filter model should not create additional fault modes in and of itself. In other words, the filter is assumed to behave nominally.

The Stanford filter model is illustrated in Figure B–3 for a generic bilateral receiver bandwidth B_R.

In the context of defining future DFMC MOPS specifications, several studies have been carried out concerning the characterisation of nominal signal distortions for GPS and Galileo new signals ([47], [48]).
Focussing on the Galileo system and on the signals that will be supported by EGNOS evolution (V3), nominal signal distortion analyses are based on the computation of user bias maps that provide an upper bound of ranging errors obtained by users with different receiver parameters than for the ground reference receivers.
The bias maps are calculated using the code delay expression in Eq. (B.2) and depend on a set of key parameters:

- receiver front-end bandwidth
- receiver front-end characteristics (magnitude, group delay)
- DLL discriminator type
- correlation spacing

The computation of worst-case user bias maps for Galileo satellites starts from recorded I/Q-sample-files measured via high gain antenna in E1/L1 and E5/L5 frequency-bands. It is assumed that the measurement system is very well calibrated and that continuous signal recordings over satellite passes are available for post-processing. For each sample-file the methodology described below can be adopted:

- For each receiver bandwidth, the selected receiver filter is applied to the sample-file.
- The filtered sample-file is processed with the selected DLL discriminator providing the code delay.
- The obtained CD values are normalised by subtracting the reference receiver CD values.
- The user bias map represents the worst-case CD value over time for each combination of receiver bandwidth and correlator spacing.

Note that the methodology described implies a very high computation load but the efficiency can be increased by inverting some of the implementation steps.

Finally, as only the differential biases between different satellites are relevant for positioning errors, the average user biases over all satellites and time can be further subtracted for each value set of user receiver parameters in an additional optional step. This subtraction has the very important advantage that the results become independent from the absolute measurement system calibration accuracy. However this makes only sense if sufficient representative satellites and measurements are available.

Figure B–4 provides an example of user bias map for Galileo E1-C component over the user space (correlator spacing, receiver bandwidth).

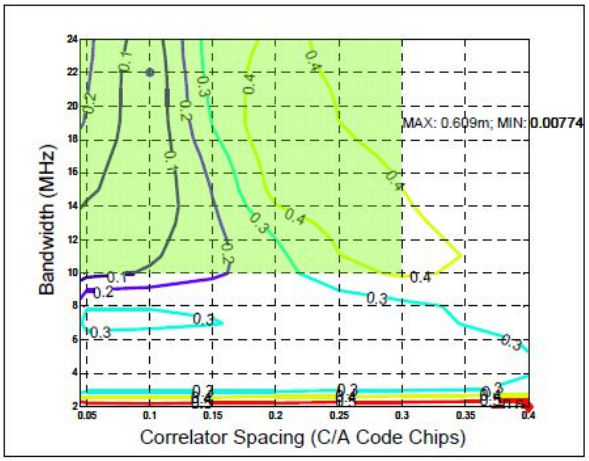

Figure B–4: Example of User Bias Map Computation from [47].

The current proposal for the user space is summarised in Table B–5.

Table B–1: Proposed User Space for future DFMC MOPS.

		Receiver Bandwidth [MHz]	*Correlator Spacing [chip]*
	GPS L1-C/A, Galileo E1-OS	12, 24	0.08, 0.12
	GPS L5, Galileo E5a	12, 24	0.9, 1.1

Additionally the following assumptions are under consideration:

- Group Delay for both L1/E1 and L5/E5a less than 150 ns (including antenna);
- DLL discriminator: only early minus late (E-L)

By taking into account the assumptions above, the maximum impact of nominal signal distortions onto GPS and Galileo signals is expected not to exceed 15 cm. The assessment is based on Stanford approach to define arbitrarily a worst-case filter. However this does not prevent a receiver manufacturer to design a receiver with transfer function characteristics respecting the maximum DGD value and resulting in correlation distortions worse than those obtained with the Stanford worst-case filter.
A revised requirement on the Differential Group Delay seems to be needed for future DFMC MOPS.

B.2 Non-nominal Signal Distortions

The ICAO 2nd-Order Step (2OS) threat model defines a class of signal deformations that represent potential integrity threat to GPS-based aircraft landing systems. This model, as introduced in [44] and [45], consists of three possible failure modes: digital, analog, and combined. The names Threat Model A (TM-A), Threat Model B (TM-B) and Threat Model C (TM-C) refer to each of the respective failure modes. In particular the anomalous waveform, or Evil WaveForm (EWF), results from the combination of second-order ringing (analog failure mode) and lead/lag of the pseudorandom noise code (PRN) chips (digital failure mode). The effect of such deformations is described in the time domain and consists of dead zones, distortions, and false peaks on the receiver correlation shape.
Always according to this model, the digital and analog distortions are defined by means of three parameters: the lead/lag for the digital distortion; the damped natural frequency and the damping factor for the analog one. Bounds for the three parameters are also provided (Table B–2). Note that T_c is the chip period for GPS L1-C/A signal, i.e. $T_c = 1/(1.023\ \text{MHz})$.

Table B–2: ICAO Threat Model Parameters Space.

Threat Model	***GPS L1-C/A Parameters***		
	Δ ***[s]***	f_d ***[MHz]***	σ_d ***[MNep/s]***
TM-A	$-0.12T_c, 0.12T_c$	-	-
TM-B	-	$4, 17$	$0.8, 8.8$
TM-C	$-0.12T_c, 0.12T_c$	$7.3, 13$	$0.8, 8.8$

An illustration of the digital and analog distortions is provided respectively in Figure B–5 and Figure B–6.

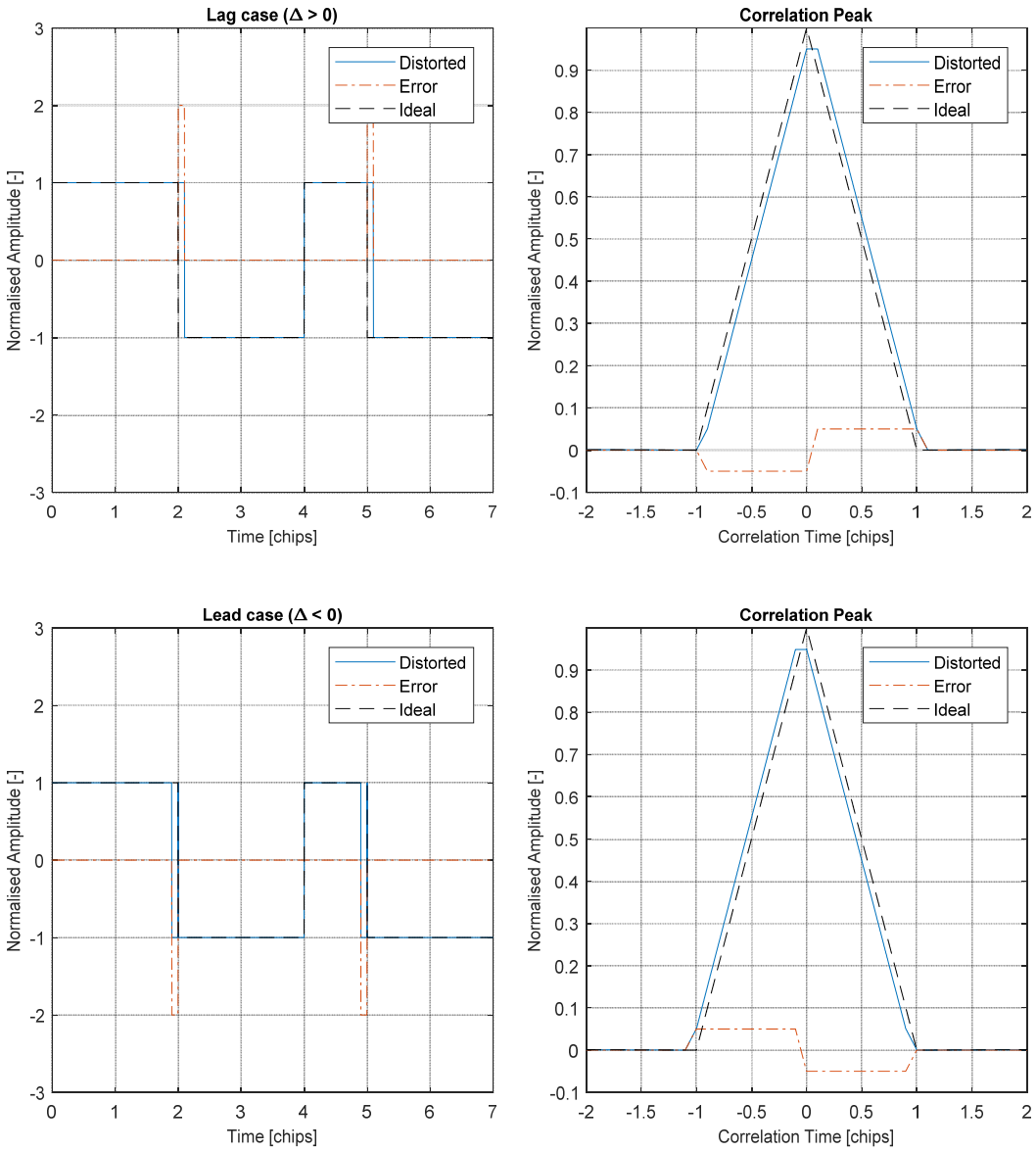

Figure B–5: Illustration of TM-A as defined for GPS L1-C/A signal.

Although this model has been adopted by ICAO as the standard threat scenario for GPS L1-C/A signal, there is still no agreement for new signals such as GPS L5/Galileo E5a and GPS L1/Galileo E1. In this context, some assumptions are made in B.2.1 in order to extend the ICAO model to the signal modulations described in B.2.1.

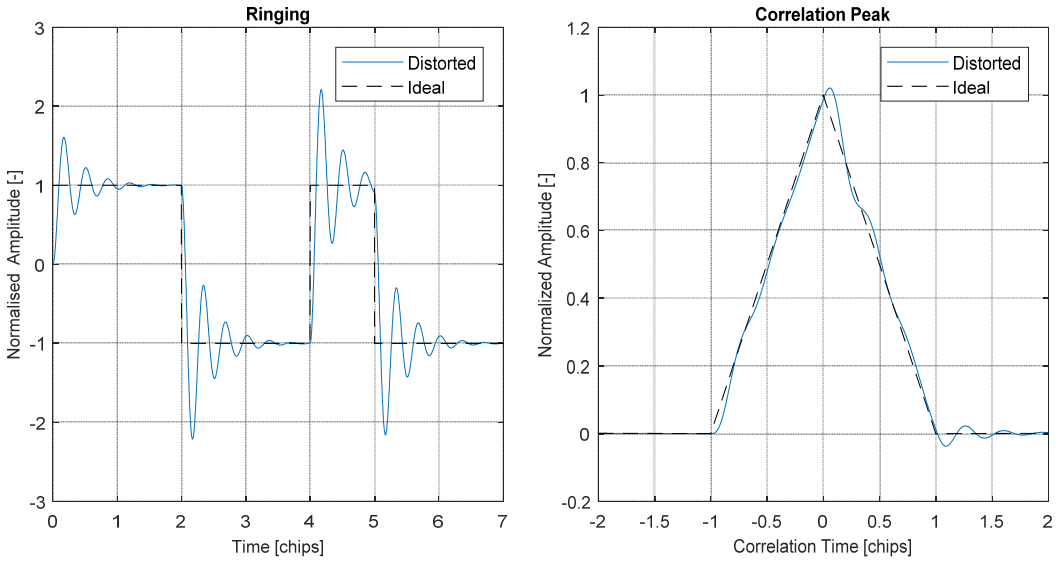

Figure B–6: Illustration of TM-B as defined for GPS L1-C/A signal.

B.2.1 Threat Model Formulation

Unlike for the GPS constellation, Galileo satellites are relatively recent and no signal anomalies have been recorded up to now. For this reason, it is quite difficult to predict how potential payload failures could affect the navigation signal shape and even more to tell how the distortions could be modelled. It is no surprise that the Galileo system provider struggles in taking an official position on this matter in front of the aviation community that pushes to have realistic assumptions for the EGNOS V3 standardisation process.

A lot of effort has been done by the scientific community to extend the ICAO threat model to the new modulations, but the payload architecture of Galileo satellites is in general different from the GPS one(s). This information, that is not in the public domain, would certainly help formulating the assumption at the basis of the threat model. Still, even with that knowledge, there is no guarantee that signal distortions will be as predicted.

The main assumption taken here is to consider that the NSGU generates a code sequence already spread by the sub-carrier, thus both the digital and analog failures affect directly the sub-chip generation. A similar approach is adopted in [45], where the digital deformation is assumed to occur on the squared wave generator. Starting from the hypothesis to consider the sub-chip autocorrelation peak instead of the chip autocorrelation peak, some modifications have to be done to the mathematical description of the EWF threat model.

First, a particular representation of the navigation signals needs to be introduced before the derivation of the threat model expressions. As described in Section 2.1, each navigation component can be written as the product of symbols (or chips) times a sequence of pulses. The pulse shape or waveform can be in general a rectangle, a Square Root Raised Cosine, a Gaussian shape, or any number of equal-length deterministic segments. The name Multilevel Coded Symbol (MCS) is used to designate a generic symbol which can adopt in principle any value or shape. The expression for the chip waveform is given by:

$$p^{chip}(t) = \sum_{i=0}^{N_{sub}-1} a_i p^{sub}\left(t - i\frac{T_c}{N_{sub}}\right) \tag{B.4}$$

where N_{sub} is the number of equal-length segments, or sub-chips, within one chip, $\{a_i\}$ is the deterministic sequence of sub-chip amplitudes and $p^{sub}(t)$ is a function representing the sub-chip shape.

Assume that $s(t)$ is the received DSSS signal as it is defined in base-band. It is possible to represent $s(t)$ as a MSC sequence:

$$s(t) = \sum_{n=-\infty}^{+\infty} c_n p^{chip}(t - nT_c) \tag{B.5}$$

being $\{c_n\}$ the amplitude of the PRN code sequence and $p^{chip}(t)$ the chip shape defined in Eq. (B.4). Under the hypothesis ideal PRN codes, the power spectral density (PSD) of $s(t)$ simplifies to $G_s(f) = |S(f)|/T_c$, which can be written as (see [40] for the derivation):

$$G_s(f) = \frac{sin^2\left(\frac{\pi f T_c}{N^{sub}}\right)}{T_c(\pi f)^2} \cdot \left|\sum_{i=1}^{N^{sub}} a_i e^{-\frac{2\pi j f i T_c}{N^{sub}}}\right|^2 \tag{B.6}$$

Being the sub-chip function $p^{sub}(t)$ a rectangular shape. From this formulation it is possible to identify a first term corresponding to the PSD of a Binary Phase Shift Keying (BPSK) with chip rate $N^{sub} \cdot f_c$, being $f_c = 1/T_c$, and a second term which represents the modulation:

$$G_s(f) = G_s^{sub}(f) G_s^{mod}(f) \tag{B.7}$$

Starting from the navigation signal formulation in Eq. (B.7), the expressions of the threat model A, B and C are derived in the following.

TM-A

The digital failure mode is described as a variation in the timing of the individual PRN chip transition with respect to ideal. This error is modelled as an advance or

delay (Δ) of the falling edge of the code chip and is assumed to be introduced in the generation of the digital sequence. As demonstrated in [45], the correlation function for the distorted signal at the receiver can be written as:

$$R_{\tilde{s},s}^{TM-A}(t) = \tilde{s}(t) * s(t) = R_{d,s}(t) + R_s\ (t) \tag{B.8}$$

being:

$$\tilde{s}(t) = s(t) + d(t) \tag{B.9}$$

the distorted signal, resulting from the sum of the ideal signal $s(t)$, defined in Eq. (B.5), and the deformation $d(t)$.

Taking into account of the aforementioned payload generation scheme, the lead/lag applies directly to the sub-chip generation. Since the ICAO model is described in terms of correlation functions, the signal PSD formulation given in Eq. (B.7) is written in the time domain as:

$$R_s(t) = R_s^{sub}(t) * R_s^{mod}(t) \tag{B.10}$$

Applying now Eq. (B.8) to $R_s^{sub}(t)$ in Eq. (B.10), a new expression for the distorted correlation peak is obtained:

$$R_{\tilde{s},s}^{TM-A}(t) = \left[R_{d,s}^{sub}(t) + R_s^{sub}(t)\right] * R_s^{mod}(t) = \left[R_{d,s}^{sub}(t) * R_s^{mod}(t)\right] + R_s\ (t) \tag{B.11}$$

This formulation applies to all the signal modulations described in Section B.2.2. Figure B–7 shows the correlation peak and the PSD of a distorted $BOC_s(1,1)$ signal, obtained by applying Eq. (B.11).

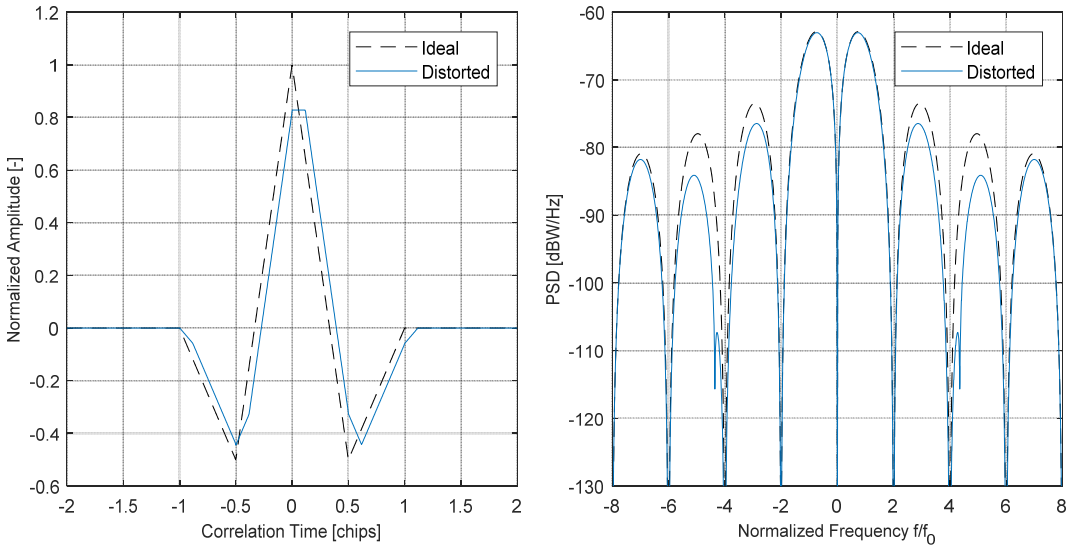

Figure B–7: Illustration of TM-A for a $BOC_s(1,1)$ signal.

TM-B

The analog failure mode is described as an amplitude modulation or ringing that occurs at every PRN chip transition independently of a digital failure. This error is modelled as a second order system with a pair of complex conjugate poles at $\zeta\omega_n \pm j\omega_n\sqrt{1-\zeta^2}$, being ω_n the undamped natural frequency and ζ the damping ratio. The impulse response of this system is described as:

$$h(t) = \begin{cases} 0 & t < 0 \\ \frac{\omega_n}{\sqrt{1-\zeta^2}} e^{-\zeta\omega_n t} sin(\omega_d\, t) & t \geq 0 \end{cases} \quad \text{(B.12)}$$

where $\omega_d = \omega_n\sqrt{1-\zeta^2}$ is the damping natural frequency and the damping factor is $\sigma_d = \zeta\omega_n$. The classical formulation of the model is given by:

$$R_{\tilde{s},s}^{TM-B}(t) = h(t) * R_s\ (t) \quad \text{(B.13)}$$

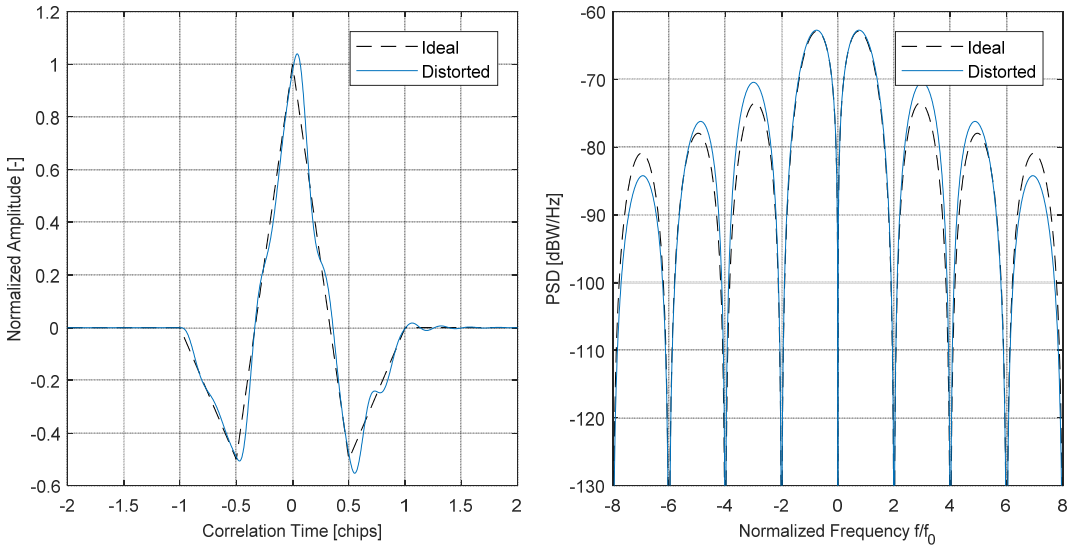

Figure B–8: Illustration of TM-B for a BOC$_s$(1,1) signal.

Again, taking into account that the deformation applies on the sub-chip generation, Eq. (B.13) can be substituted in Eq. (B.10) giving:

$$R_{\tilde{s},s}^{TM-B}(t) = [h(t) * R_s^{sub}(t)] * R_s^{mod}(t) = h(t) * R_s\ (t) \quad \text{(B.14)}$$

It is evident that for TM-B nothing changes with respect to the formulation in [45]. Figure B–8 illustrates the effect of the analog distortion on the correlation peak a BOC$_s$(1,1) signal.

TM-C

Threat Model C describes the EWF as the combination of the digital and analog failure modes. As reported in Table B–2, the parameters space for TM-C are slightly different from the one characterizing TM-A and TM-B, thus it can't be defined as the direct combination of both of them. Keeping in mind the underlying hypothesis that the deformation applies to the sub-chip autocorrelation peak, the combined threat model can be described from a mathematical point of view as follows:

$$R_{\tilde{s},s}^{TM-C}(t) = h(t) * \left[R_{d,s}^{sub}(t) + R_s^{sub}(t)\right] * R_s^{mod}(t) \tag{B.15}$$

B.2.2 Signals Description

All Galileo signals can be written according to Eq. (B.7), as a generalisation of Eq. (B.6). Table B–3 gives the sub-chip and the modulation components characterizing the PSDs for the Galileo signals generic formulation.

Table B–3: PSDs for GNSS Signal Modulations.

Modulations	***Power Spectral Densities***	
	$\boldsymbol{G^{sub}(f)}$	$\boldsymbol{G^{mod}(f)}$
BPSK(n)	$\frac{1}{T_c}\frac{sin^2(\pi f T_c)}{(\pi f)^2}$	-
BOC$_s$(p,q) $\boldsymbol{N^{sub} = 2 \cdot p/q}$	$\frac{N^{sub}}{T_c}\frac{sin^2\left(\frac{\pi f T_c}{N^{sub}}\right)}{(\pi f)^2}$	$N^{sub} + 2\sum_{i=1}^{N_{sub}-1}(-1)^i(N^{sub}-i)cos\left(\frac{2\pi f i T_c}{N_{sub}}\right)$
BOC$_c$(p,q) $\boldsymbol{N^{sub} = 4 \cdot p/q}$	$\frac{N^{sub}}{T_c}\frac{sin^2\left(\frac{\pi f T_c}{N^{sub}}\right)}{(\pi f)^2}$	$N^{sub} + 2\left[\sum_{i=1}^{\frac{N_{sub}}{2}}(-1)^i cos\left(\frac{2\pi f(2i-1)T_c}{N_{sub}}\right) + \sum_{i=1}^{\frac{N_{sub}}{2}-1} 2(-1)^i\left(\frac{N_{sub}}{2}-i\right)cos\left(\frac{2\pi f(2i)T_c}{N_{sub}}\right)\right]$
MBOC(6,1,1/11)	$G_{BOC(1,1)}^{sub}(f) = \frac{2}{T_c}\frac{sin^2\left(\frac{\pi f T_c}{2}\right)}{T_c(\pi f)^2}$ $G_{BOC(6,1)}^{sub}(f) = \frac{12}{T_c}\frac{sin^2\left(\frac{\pi f T_c}{12}\right)}{(\pi f)^2}$	$G_{BOC(1,1)}^{mod}(f) = 2 - 2cos(\pi f T_c)$ $G_{BOC(6,1)}^{mod}(f) = 12 + 2\sum_{i=1}^{11}(-1)^i(12-n)cos\left(\frac{2\pi f i T_c}{12}\right)$
AltBOC(p,q) $\boldsymbol{N^{sub} = 4 \cdot (2p/q)}$	$\frac{N^{sub}}{T_c}\frac{sin^2\left(\frac{\pi f T_c}{N^{sub}}\right)}{(\pi f)^2}$	$\frac{1}{N^{sub}}\left\lvert\sum_{i=0}^{N^{sub}-1} a_i e^{-j\frac{2\pi f i T_c}{N^{sub}}}\right\rvert^2$

Referring to Table B–3, first the general expression for the BPSK modulation is given as a reference. The notation BPSK(n) is used to indicate a BPSK modulation with $f_c = nf_0$, being $f_0 = 1.023$ MHz the reference frequency, and f_c the chip rate. Then the expressions for Binary Offset Carrier (BOC) signals are given, as in [40], under the assumption that the PRN sequence with chip rate $f_c = qf_0$ is modulated by a sub-carrier that is a squared sine/cosine waveform with frequency $f_s = pf_0$. The formulation is also extended to the Multiplexed Binary Offset Carrier (MBOC), the modulation introduced in 2007 for the GPS/Galileo interoperable signal [18]. Since it is a composed signal, the total spectrum is expressed as:

$$G_{MBOC(6,1,1/11)}(f) = \frac{10}{11} G^{sub}_{BOC(1,1)}(f) \cdot G^{mod}_{BOC(1,1)}(f) + \frac{1}{11} G^{sub}_{BOC(6,1)} \cdot (f) G^{mod}_{BOC(6,1)} \quad \text{(B.16)}$$

A similar approach is used for the Alternate BOC, AltBOC(p,q) modulated signals. In particular p and q refers to the sub-carrier frequency and chip rate factors. With reference to the AltBOC modulation description provided in [20] and Section A.3, the expression of the constant envelope AltBOC spectrum under the hypothesis ideal PRN codes is given by:

$$G_{AltBOC(p,q)}(f) = \frac{1}{2} G^{sub}(f) \cdot \left[G^{mod}_{S}(f) + G^{mod}_{\tilde{S}}(f) + G^{mod}_{P}(f) + G^{mod}_{\tilde{P}}(f) \right] \quad \text{(B.17)}$$

where the four modulation spectra refers respectively to the four components: prompt or in-phase ‘single signal’ sub-carrier, delayed or quadrature ‘single signal’ sub-carrier, prompt or in-phase ‘product signal’ sub-carrier and delayed or quadrature ‘product signal’ sub-carrier. The modulation spectra of the four components are derived using the following sub-chip sequences:

Table B–4: AltBOC Sub-Chip Sequences.

Signal	***Sub-Chip Sequences***			
$\{a_i\}_S$	$\frac{(\sqrt{2}+1)}{2}$	$\frac{1}{2}$	$-\frac{1}{2}$	$-\frac{(\sqrt{2}+1)}{2}$
$\{a_i\}_{\tilde{S}}$	$\frac{1}{2}$	$\frac{(\sqrt{2}+1)}{2}$	$\frac{(\sqrt{2}+1)}{2}$	$\frac{1}{2}$
$\{a_i\}_P$	$-\frac{(\sqrt{2}-1)}{2}$	$\frac{1}{2}$	$-\frac{1}{2}$	$\frac{(\sqrt{2}-1)}{2}$
$\{a_i\}_{\tilde{P}}$	$\frac{1}{2}$	$-\frac{(\sqrt{2}-1)}{2}$	$-\frac{(\sqrt{2}-1)}{2}$	$\frac{1}{2}$

Note that each of these sequences is repeated $2 \cdot p/q$ times (with sign inversion) within one single chip.

B.2.3 Threat Model Parameters Space

As for the threat model formulation, the same difficulties apply for the definition of the parameters space applicable to each of the modulations defined in Table B–3. In particular, the Galileo signals of interest for this analysis are the Galileo E1 OS and the Galileo E5a. These two signals in fact are in the baseline for the future EGNOS V3 DFMC Service. In particular, the pilot components E1-C and E5a-Q are planned to be monitored by SQM algorithms for EWF detection.

By definition an evil waveform occurs when the signal is distorted but tracking and acquisition operations are still possible. This is the situation when the distortion is 'evil' as it causes an excessive ranging error and a faulty PVT. A severe deformation of the correlation shape on the other hand would cause the user receiver tracking loops to lose lock and the satellite pseudorange would be discarded from the PVT solution. The assumption of considering the sub-chip autocorrelation peak instead of the chip autocorrelation peak leads to the following observations:

- the lead/lag parameter describing the digital distortion should be 'scaled' to the sub-chip duration and not anymore to the chip duration;
- a damping natural frequency lower than the sub-chip frequency or a very high damping factor result in an excessive analog distortion.

Since no official threat bounds have been derived yet, for the simulations presented in Section B.2.4 these considerations are taken into account.

Table B–5 provides the parameters space used for the generation of the simulation results in Section B.2.4.

Table B–5: Assumption on Parameters Space for Galileo Signals.

Threat Model	***Galileo E1 OS Parameters***		
	Δ *[s]*	**f_d *[MHz]***	**σ_d *[MNep/s]***
TM-A	-0.24 T_{sub}, 0.24 T_{sub}	-	-
TM-B	-	4, 23	2.8, 8.8
TM-C	-0.24 T_{sub}, 0.24 T_{sub}	4, 23	2.8, 8.8
Threat Model	***Galileo E5a Parameters***		
	Δ *[s]*	**f_d *[MHz]***	**σ_d *[MNep/s]***
TM-A	-0.25 T_c , 0.25 T_c	-	-

Threat Model	*Galileo E1 OS Parameters*		
	Δ *[s]*	f_d *[MHz]*	σ_d *[MNep/s]*
TM-B	-	4, 23	8.8, 18.8
TM-C	-0.25 T_c, 0.25 T_c	4, 23	8.8, 18.8

It has to be underlined that a particular case is represented by the Galileo E1 OS modulation whose composed spectrum is characterized by two different sub-chip lengths (see [8]). Since the threat model here illustrated is purely theoretical, various are the possible assumptions on where the deformation is introduced in the signal generation chain: the distortion in fact could occur before or after the summing up the $BOC_s(1,1)$ and $BOC_s(6,1)$ components. From a formulation point of view the analog distortion is simulated simply by applying Eq. (B.11) to the two components separately: this corresponds to the assumption that the failure occurs before. In any case, as already said previously, remember that the advance or delay affecting the falling edges of the digital sequence can't be longer than the sub-chip duration itself. Also for the TM-B it is reasonable to assume that the deformation can occur on the two components independently or on both of them with the same characteristics. In the last case remember that the principle of superimposition holds for LTI systems, thus the distortion can be equally applied to the single components before summing or directly to the composed signal.

B.2.4 Performance Analysis

In order to evaluate the impact of the EWF threat model here proposed on new generation signals, the tracking error bias with respect to an ideal correlation peak is analysed. No measurements noise or multipath delay is taken into account. The tracking error is computed for two different correlators, Narrow Early-minus-Late (E-L) and Double Delta (DD), and for various correlator spacing. The two different discriminators are defined as:

$$SC_{EL}(\varepsilon,\delta) = R_{\tilde{s},s}^{TM}\left(\varepsilon-\frac{\delta}{2}\right) - R_{\tilde{s},s}^{TM}\left(\varepsilon+\frac{\delta}{2}\right) \tag{B.18}$$

$$SC_{DD}(\varepsilon,\delta) = \left[R_{\tilde{s},s}^{TM}\left(\varepsilon-\frac{\delta}{2}\right) - R_{\tilde{s},s}^{TM}\left(\varepsilon+\frac{\delta}{2}\right)\right] - \frac{1}{2}\left[R_{\tilde{s},s}^{TM}(\varepsilon-\delta) - R_{\tilde{s},s}^{TM}(\varepsilon+\delta)\right] \tag{B.19}$$

where δ is the correlator spacing and $R_{\tilde{s},s}^{TM}$ is the filtered distorted correlation peak, computed according to Eq. (B.11) and (B.14) for respectively TM-A and TM-B. The selection of the correlators is done according to the current standard for aviation receivers in MOPS DO-229D [17]. The same holds for the applied filtering that is

modelled according to Stanford assumptions (Figure B–3). Regarding the range of correlator spacing values and receiver bandwidth, the user space reported in Table B–1 is taken as a reference.

In the following analysis of the Galileo signals user bias maps are computed for TM-A and TM-B. As introduced in Section B.1, a user bias map represents the maximum code delay suffered by the user receiver as a function of its filter bandwidth and correlator spacing. First, the code delay is computed by applying Eq. (B.2) to the S-curve expressions in (B.18) and (B.19); the worst-case value is then obtained by normalising the code delay with respect to a reference receiver value. It is here assumed for the reference receiver a filter bandwidth $\bar{B}_{RX}$ of 24 MHz and correlator spacing $\bar{\delta}$ of 0.1 chips. Being Π the set of parameters identified for each threat model, it is possible to express the maximum code delay or worst-case user bias as:

$$Bias(\delta, B_{RX}) = \max_{\Pi} \left| CD^{User}(\delta, B_{RX}, \Pi) - CD^{Ref}\left(\bar{\delta}, \bar{B}_{RX}, \Pi\right) \right| \tag{B.20}$$

$$\Pi = \begin{cases} \Delta & \text{TM-A} \\ f_d, \sigma_d & \text{TM-B} \\ \Delta, f_d, \sigma_d & \text{TM-C} \end{cases}$$

Galileo E1 OS

The first signal under analysis is the Galileo E1 OS. The latest standardization plan foresees that future aviation receivers will process E1 signals by correlating with the $BOC_s(1,1)$ component and neglecting the $BOC_s(6,1)$ component; further, of the two E1-B and E1-C components, only the pilot would be subject to signal quality monitoring. Figure B–9 shows the ideal and filtered S-curve bias for the Early-Late and Double-Delta correlators.

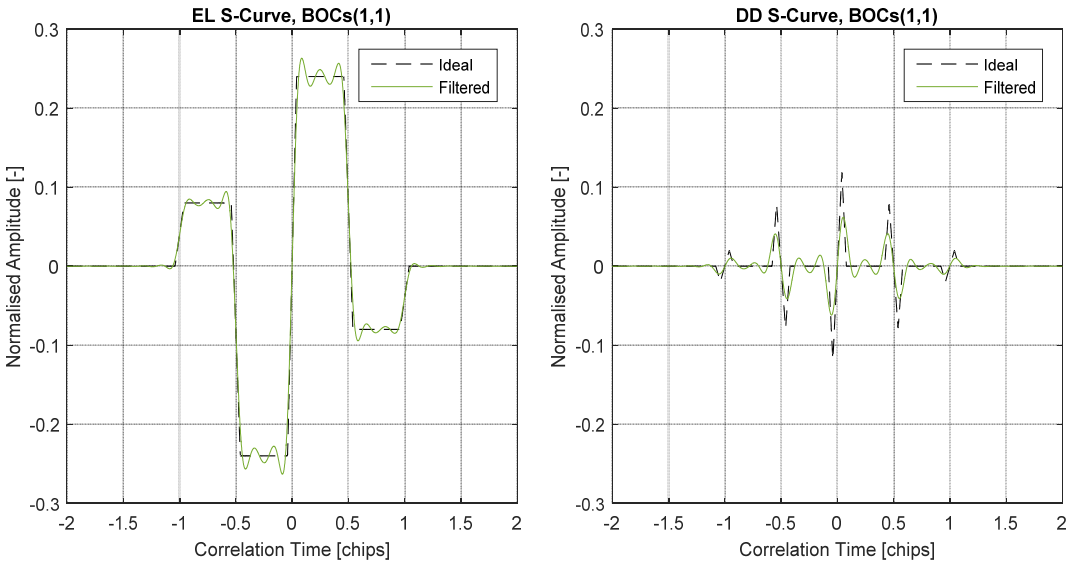

Figure B–9: Galileo E1 OS: Ideal and Filtered S-Curve for EL and DD correlators.

Note the ringing effect introduced by the filtering and bandwidth limitation. By comparing the two S-curves, the DD correlator is expected to be less robust against signal distortions than the EL. This is further confirmed by Figure B–10 that shows the TM-A user bias maps for respectively the EL (left) and DD discriminators (right).

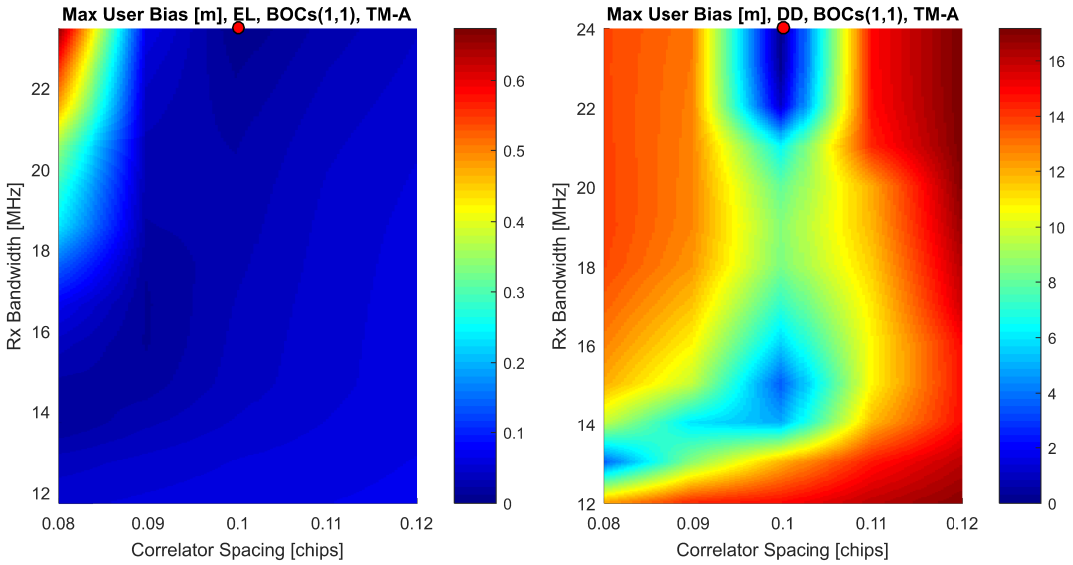

Figure B–10: Galileo E1 OS: TM-A User Bias Maps.

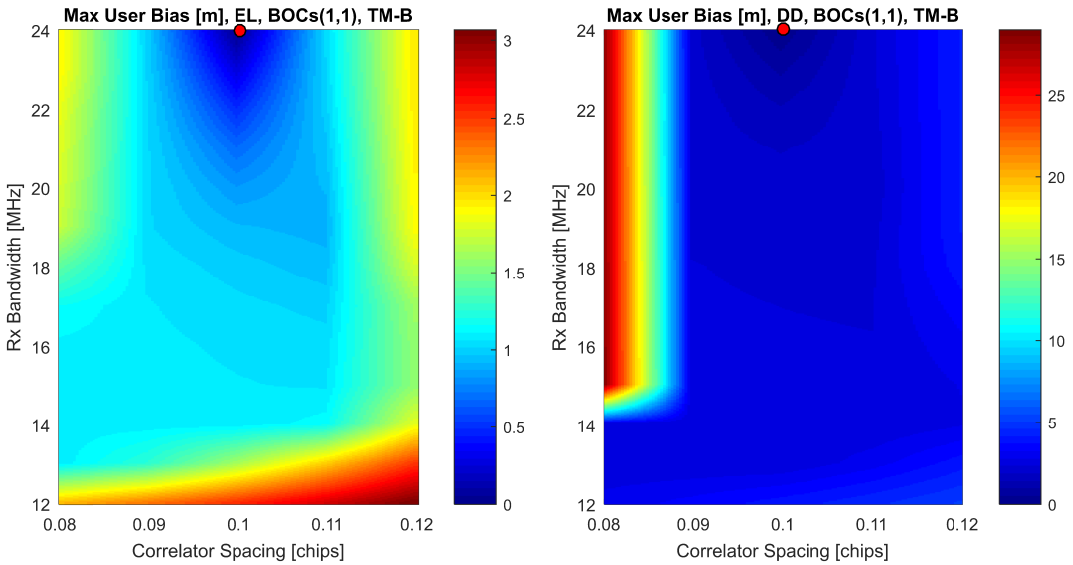

Figure B–11: Galileo E1 OS: TM-B User Bias Maps.

The user bias maps for the TM-B distortion are provided in Figure B–11. Again the EL discriminator proves to be more robust against distortions than the DD. It seems reasonable that the DD discriminator is planned to be excluded from the future DFMC MOPS.Note also that the analog distortions have a much higher impact than

the digital ones. By comparing the maximum impact of nominal signal distortions (15 cm) with the TM-A user bias map for the EL discriminator, it is clear that most of the user space is below that threshold. Only the up-left portion (0.08 – 0.09 chips, 16 – 24 MHz) is above 15 cm. By further reducing the allowed user space, or by slightly increasing the nominal distortions assumption, the TM-A could be excluded from the signal quality threats or feared events.

Galileo E5a

The second signal under analysis is the Galileo E5a. This service is composed by two components, E5a-I and E5a-Q, that are multiplexed with other components to form the Galileo E5 AltBOC(15,10) signal. The latest standardization plan foresees that future aviation receivers will process E5a components as a BPSK(10) modulation and that only the pilot will be under signal quality monitoring. Figure B–12 shows the ideal and filtered S-curve bias for the Early-Late and Double-Delta correlators.

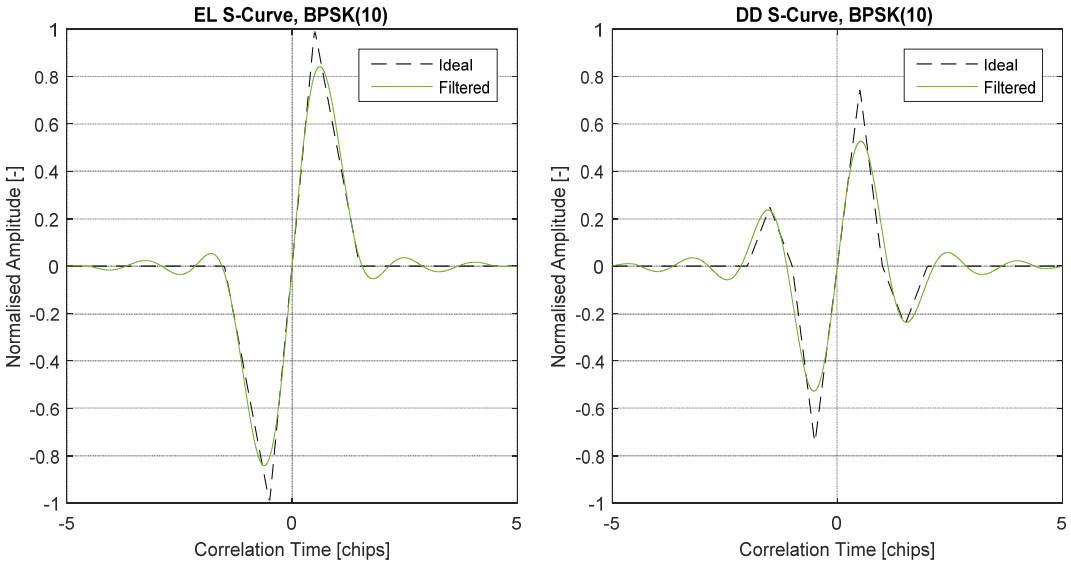

Figure B–12: Galileo E5a: Ideal and Filtered S-Curve for EL and DD correlators.

Figure B–13 and Figure B–14 below provide the user bias maps for respectively the TM-A and TM-B. The results for Galileo E5a confirm the worse performance of the DD discriminator in presence of non-nominal signal distortions. On the other hand, the EL user bias map for the TM-A scenario is below the nominal signal threshold of 15 cm. In other words, by keeping the current assumption on the TM-A parameters space, analog distortions would be hidden by the Galileo E5a signal nominal behaviour.

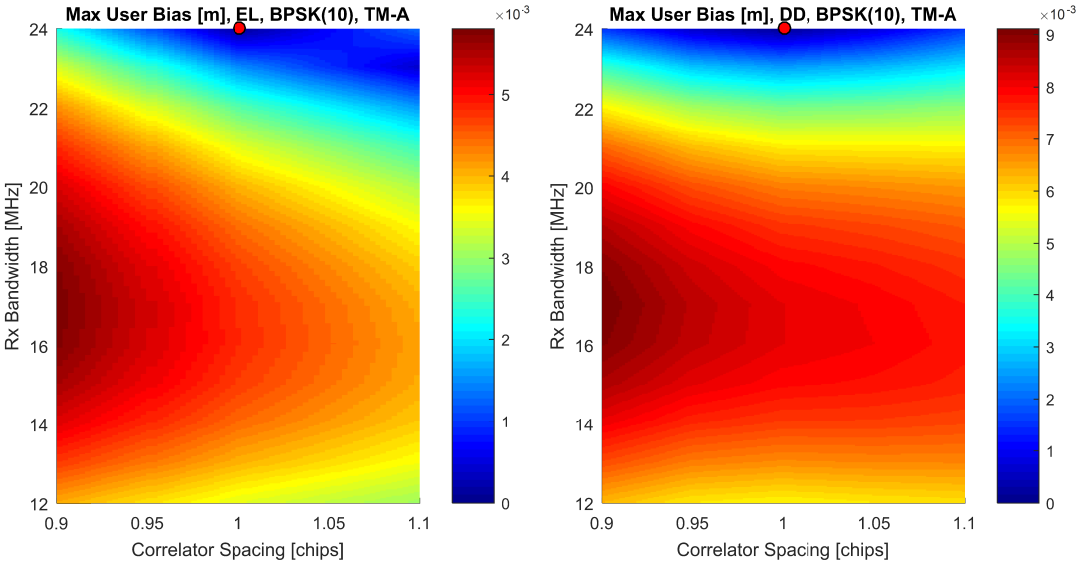

Figure B–13: Galileo E5a: TM-A User Bias Maps.

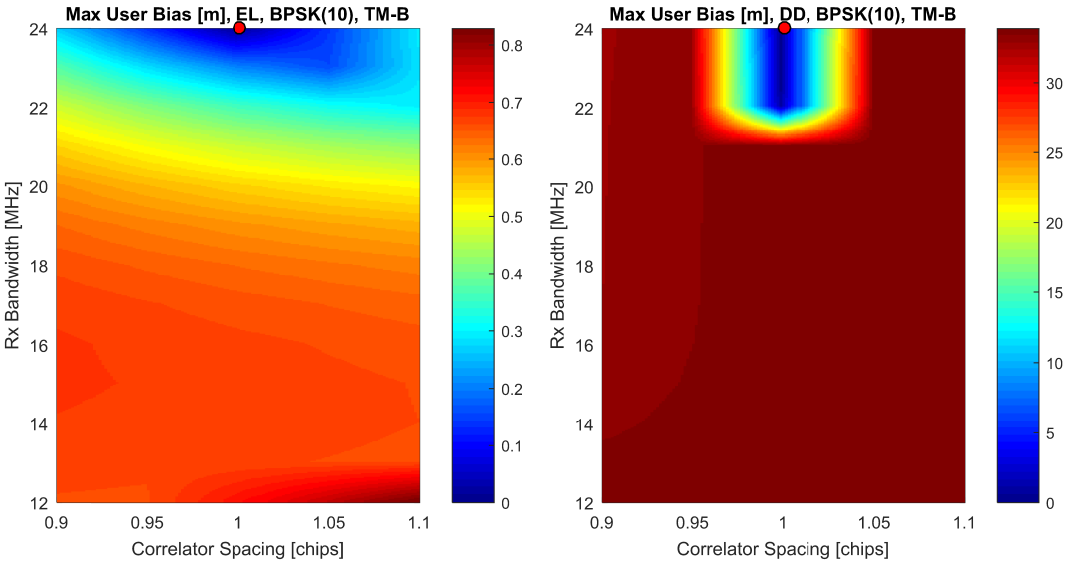

Figure B–14: Galileo E5a: TM-B User Bias Maps.

Bibliography

[1] Elliott D. Kaplan, Christopher J. Hegarty, “Understanding GPS: principles and applications”, Second Edition, Artech House Publishers, Boston, 2006

[2] Bradford W. Parkinson, James J. Spilker Jr., “Global Positioning System: Theory and Applications”, Vol. I and Vol. II, AIAA, Washington DC, 1996

[3] Pratap Mistra, Per Enge, “Global Positioning System: Signals, Measurements and Performance”, Revised Second Edition, Ganga-Jamuna Press, Lincoln, 2012

[4] Jack K. Holmes, “Spread Spectrum Systems for GNSS and Wireless Communications”, Artech House Publishers, Norwood, 2007

[5] Jhong Sam Lee, Leonard E. Miller, “CDMA Systems Engineering Handbook”, Artech House Publishers, Boston, 1998

[6] T. Koryu Ishii, “Handbook of microwave technology”, Vol. 2, Components and devices, Aca-demic Press, 1995

[7] Gerard Maral, Michel Bousquet, “Satellite Communications Systems: Systems, Techniques and Technology”, 4th edition, Wiley, May 2002

[8] European GNSS (Galileo) Open Service, Signal-In-Space Interface Control Document, Issue 1.3, December 2016

[9] IS-GPS-200, Navstar GPS Space Segment/Navigation User Segment Interfaces, IRN-IS-200H-003, 9 December 2015

[10] IS-GPS-800, Navstar GPS Space Segment/User Segment L1C Interfaces, IRN-IS-800D-002, 9 December 2015

[11] IS-GPS-705, Navstar GPS Space Segment/User Segment L5 Interfaces, IRN-IS-705D-003A, 27 October 2016

[12] BeiDou Navigation Satellite System Signal In Space ICD, Open Service Signal, Version 2.0, December 2013

[13] Indian Regional Navigation Satellite System, Signal In Space ICD for Standard Positioning Service, Version 1.0, June 2014

[14] Quasi-Zenith Satellite System Navigation Service, Interface Specification for QZSS, Version 1.6, November 2014

[15] ED-134 Signal Specification for SBAS L1/L5, Draft v.3, EUROCAE, May 2008

[16] Draft IWG SBAS L5 DFMC Interface Control Document (SBAS L5 DFMC ICD), GNSS-EV3-ST-ESA-X-00120, Issue 1 Revision 1, IWG, 13/04/2015

[17] SC-159, Minimum Operational Performance Standards for Global Positioning System/Wide Area Augmentation System Airborn Equipment, RTCA DO-229D, Washington D.C., 13 December 2006

[18] Avila-Rodriguez, Jose-Angel, Hein, Guenter W., Wallner, Stefan, Issler, Jean-Luc, Ries, Lionel, Lestarquit, Laurent, de Latour, Antoine, Godet, Jeremie, Bastide, Frederic, Pratt, Tony, Owen, John, "The MBOC Modulation: The Final Touch to the Galileo Frequency and Signal Plan", NAVIGATION, Journal of The Institute of Navigation,

Vol. 55, No. 1, Spring 2008, pp. 14-28

[19] Rebeyrol, Emilie, Macabiau, Christophe, Lestarquit, Laurent, Ries, Lionel, Issler, Jean-Luc, Boucheret, Marie-Laure, Bousquet, Michel, "BOC Power Spectrum Densities," Proceedings of the 2005 National Technical Meeting of The Institute of Navigation, San Diego, CA, January 2005, pp. 769-778

[20] Lestarquit, Laurent, Artaud, Géraldine, Issler, Jean-Luc, "AltBOC for Dummies or Everything You Always Wanted To Know About AltBOC," Proceedings of the 21st International Technical Meeting of the Satellite Division of The Institute of Navigation (ION GNSS 2008), Savannah, GA, September 2008, pp. 961-970

[21] Betz, John W., "On the Power Spectral Density of GNSS Signals, with Applications," Proceedings of the 2010 International Technical Meeting of The Institute of Navigation, San Diego, CA, January 2010, pp. 859-871

[22] Soualle, F., Burger, T.B., "Impact of Galileo Spreading Code Selection and Data Rate onto Navigation Signal Interference," Proceedings of the 16th International Technical Meeting of the Satellite Division of The Institute of Navigation (ION GPS/GNSS 2003), Portland, OR, September 2003, pp. 1035-1043

[23] F. Soualle, M. Soellner, Stefan Wallner, J.-A. Avila-Rodriguez,G. W. Hein, B. Barnes, T. Pratt, L. Ries, J. Winkel, C. Lemenager, P. Erhard, “Spreading Code Selection Criteria for the future GNSS Galileo”, GNSS 2005, Munich, Germany, 19-22 July 2005

[24] Wallner, Stefan, Avila-Rodriguez, Jose-Angel, Hein, Guenter W., Rushanan, Joseph J., "Galileo E1 OS and GPS L1C Pseudo Random Noise Codes - Requirements, Generation, Optimization and Comparison -," Proceedings of the 20th International Technical Meeting of the Satellite Division of The Institute of Navigation (ION GNSS 2007), Fort Worth, TX, September 2007, pp. 1549-1563

[25] F. Soualle, “Correlation and Randomness Properties of the Spreading Coding Families for the Current and Future GNSSs”, Fourth European Workshop on GNSS Signals and Signal Processing, GNSS SIGNALS 2009, Oberpfaffenhofen, Germany, December 2009

[26] M. Foucras, J. Leclère, C. Botteron, O. Julien, C. Macabiau, et al.. “Study on the cross-correlation of GNSS signals and typical approximations”, GPS Solutions, Springer Verlag, 2016

[27] L. Welch, “Lower bounds on the maximum cross correlation of signals”, in IEEE Transactions on Information Theory, vol. 20, no. 3, pp. 397-399, May 1974

[28] Hein, G.W., and J.-A. Ávila-Rodríguez and S. Wallner, “The Galileo Codes and Others,” Inside GNSS, Volume 1, September 2006

[29] S. Wallner, J.-A. Ávila-Rodríguez, “Codes: The PRN Code Family Grows Again”, InsideGNSS, September 2011

[30] Report of the First Meeting of the International Committee on Global Navigation Satellite Systems (ICG) Providers Forum, Bangalore, September 4th, 2007

[31] Models and Methodology For GPS/Galileo Radio Frequency Compatibility Analyses, Issue1.2, June 2004

[32] RECCOMENDATION ITU-R M.1831, A coordination methodology for RNSS inter-system interference estimation, 2007

[33] M. Paonni, D. Fontanella, M. Anghileri, B. Eissfeller “MBOC Multi-constellation

Interoperable Signal: Consequences on the Noise Floor". Presentation at the Fifth Meeting of the International Committee on Global Navigation Satellite Systems (ICG) WG-A, Turin, Italy, 18 - 22 October 2010

[34] Paonni, M., Fontanella, D., Eissfeller, B., Pratt, A.R., "Multi-Constellation Interoperability Interference Assessment in the Framework of GNSS Modernization: An Evaluation of the Impact on the Receiver Performance," Proceedings of the 2011 International Technical Meeting of The Institute of Navigation, San Diego, CA, January 2011, pp. 1207-1217

[35] Van Dierendonck, A.J., Erlandson, R.J., Shallberg, K., Ericson, S., "The Inadequacy of the Spectral Separation Coefficient and Aggregate Gain Factor for Quantifying the Effects of GPS C/A Code Self Interference," Proceedings of the 26th International Technical Meeting of The Satellite Division of the Institute of Navigation (ION GNSS+ 2013), Nashville, TN, September 2013, pp. 1435-1444

[36] Cerruti, A.P., Betz, J.W., Rushanan, J., "Further Investigations into C/A-to-C/A Interference," Proceedings of the 2014 International Technical Meeting of The Institute of Navigation, San Diego, California, January 2014, pp. 349-361

[37] Hegarty, Christopher J., "A Simple Model for C/A-Code Self-Interference," Proceedings of the 27th International Technical Meeting of The Satellite Division of the Institute of Navigation (ION GNSS+ 2014), Tampa, Florida, September 2014, pp. 3484-3494

[38] T.A. Stansell, J.W. Betz, F. van Diggelen, S. Kogure, "Proposed Evolution of the C/A Signal," Proceedings of the 28th International Technical Meeting of The Satellite Division of the Institute of Navigation (ION GNSS+ 2015), Tampa, Florida, September 2015

[39] http://www.celestrak.com/NORAD/elements/

[40] J.A. Avila-Rodriguez, "On Generalized Signal Waveforms for Satellite Navigation", Ph.D. Thesis, University FAF Munich, Germany, 2008

[41] Emilie Rebeyrol, "Galileo signals and payload optimization", École Nationale Supérieure des Télécommunications, France, 2007

[42] Daniele Borio, "A Statistical Theory for GNSS Signal Acquisition", Ph.D. Thesis, Politecnico di Torino, Italy, 2008

[43] R.E. Phelts, Multicorrelator Techniques for Robust Mitigation of Threats to GPS Signal Quality, Ph.D. Thesis, Stanford University, USA, 2001

[44] Phelts, R. Eric, Akos, Dennis M., Enge, Per, "Robust Signal Quality Monitoring and Detection of Evil Waveforms," Proceedings of the 13th International Technical Meeting of the Satellite Division of The Institute of Navigation (ION GPS 2000), Salt Lake City, UT, September 2000, pp. 1180-1190.

[45] Phelts, R. Eric, Akos, Dennis M., "Effects of Signal Deformations on Modernized GNSS Signals", Journal of Global Positioning Systems, Vol. 5 No. 1-2, Hong Kong, China, 2006.

[46] Phelts, R.E., Walter, T., Enge, P., "Characterizing Nominal Analog Signal Deformation on GNSS Signals," Proceedings of the 22nd International Technical Meeting of The Satellite Division of the Institute of Navigation (ION GNSS 2009), Savannah, GA, September 2009, pp. 1343-1350

[47] Phelts, R.E., Blanch, J., Walter, T., Enge, P., "The Effect of Nominal Signal Deformation

Biases on ARAIM Users," Proceedings of the 2014 International Technical Meeting of The Institute of Navigation, San Diego, California, January 2014, pp. 56-67

[48] Thoelert, S., Vergara, M., Sgammini, M., Enneking, C., Antreich, F., Meurer, M., Brocard, D., Rodriguez, C., "Characterization of Nominal Signal Distortions and Impact on Receiver Performance for GPS (IIF) L1/L5 and Galileo (IOV) E1 /E5a Signals," Proceedings of the 27th International Technical Meeting of The Satellite Division of the Institute of Navigation (ION GNSS+ 2014), Tampa, Florida, September 2014, pp. 3113-3128

[49] Wong, G., Phelts, R.E., Walter, T., Enge, P., "Characterization of Signal Deformations for GPS and WAAS Satellites," Proceedings of the 23rd International Technical Meeting of The Satellite Division of the Institute of Navigation (ION GNSS 2010), Portland, OR, September 2010, pp. 3143-3151

[50] Wong, G., Phelts, R.E., Walter, T., Enge, P., "Alternative Characterization of Analog Signal Deformation for GNSS-GPS Satellites," Proceedings of the 2011 International Technical Meeting of The Institute of Navigation, San Diego, CA, January 2011, pp. 497-507

[51] D. Fontanella, B. Eissfeller, “Spectral Line Analysis for Accurate Interference Assessment on GNSS Signals”, 5th European Workshop on GNSS Signals and Signal Processing, Toulouse, December 2011

[52] D. Fontanella, M. Paonni and B. Eissfeller, "A novel evil waveforms threat model for new generation GNSS signals: Theoretical analysis and performance," 2010 5th ESA Workshop on Satellite Navigation Technologies and European Workshop on GNSS Signals and Signal Processing (NAVITEC), Noordwijk, December 2010